

25043149

LIBRARY Michigan State University

They a



This is to certify that the

dissertation entitled

MODAL ANALYSIS OF VIBRATIONS
IN
LIQUID-FILLED PIPING SYSTEMS
presented by

Marlio William Lesmez

has been accepted towards fulfillment of the requirements for

DCWegger Major professor

Doctor of Philosophy degree in Civil Engineering

Date Feb 21, 1989

MSU is an Affirmative Action/Equal Opportunity Institution

0-12771

PLACE IN RETURN BOX to remove this checkout from your record. TO AVOID FINES return on or before date due.

DATE DUE	DATE DUE	DATE DUE

MSU Is An Affirmative Action/Equal Opportunity Institution

MODAL ANALYSIS OF VIBRATIONS

IN

LIQUID-FILLED PIPING SYSTEMS

Ву

Marlio William Lesmez

A DISSERTATION

Submitted to

Michigan State University

in partial fulfillment of the requirements

for the degree of

DOCTOR OF PHILOSOPHY

Department of Civil and Environmental Engineering

ABSTRACT

MODAL ANALYSIS OF VIBRATIONS IN LIQUID-FILLED PIPING SYSTEMS

Ву

Marlio William Lesmez

The vibration of liquid-filled piping systems is formulated using one-dimensional wave theory in both the liquid reaches and the pipe wall. Five families of waves and fourteen variables are considered and the effects of shear deformation and rotary inertia on the lateral vibration of the pipe reaches are included. A numerical model is described which includes both Poisson and junction coupling, thereby providing comprehensive interaction between the fluid reaches and the piping.

The transfer matrix method is used to study the motion of these systems. The motion is represented by an overall transfer matrix. This matrix is assembled by combining field transfer matrices representing the motion of single pipe reaches with point matrices describing specified boundary conditions.

A one-inch (25 mm) diameter variable length piping system with a U-type bend is used to obtain the experimental data. Various fluid and structural frequencies are excited by using a crank mechanism which vibrates the piping. Fluid pressure and pipe displacement responses for various forcing frequencies are obtained and compared with analytical results. Larger fluid pressure responses occur at higher harmonics than at the first fundamental frequency. Mode shapes for the liquid pressure and pipe motion are also presented. Good agreement of natural frequencies is found between predictions and observations.

A mi familia y mi esposa Becky

ACKNOWLEDGEMENTS

I would like to thank Professor David Wiggert, chairman of my graduate committee and the other members Frank Hatfield, Clark Radcliffe, Reinier Boumeester, and David Yen. My sincere appreciation goes to Professor Hatfield for his suggestions, assistance and discussion related to my research.

I am indebted to Dr. Robert Otwell and Dr. Sidney Stuckenbruck for their work in this area which constitutes the basis of my research. My gratitude is also extended to Dr. Dan Budny for his assistance in the construction and design of the experimental apparatus and data acquisition system. I found valuable the suggestions of my fellow graduate student David Fanson in the design of the crank mechanism. A word of gratitude is extended to Mr. Conan Doyle for his assistance with the graphics. The financial support provided by the National Science Foundation is also greatly appreciated.

Finally, I am especially indebted to my family for their support and understanding during this time. I express my deepest gratitude to my wife Becky for her encouragement, inspiration, and support during this research. Her suggestions and patience during the preparation of the manuscript were invaluable. Her help and dedication made possible the completion of this project.

TABLE OF CONTENTS

LIST	OF TABLES	xii
LIST	OF FIGURES	xv
NOME	NCLATURE	xix
CHAP.	TER	
1	OBJECTIVE AND SCOPE	1
	1.1 Introduction	1
	1.2 Objective	5
	1.3 Scope	5
2	LITERATURE REVIEW	8
	2.1 Introduction	8
	2.2 Unsteady Flow in Pipelines	9
	2.3 Fluid-Structure Interaction	10
	2.3.1 Poisson Coupling	11
	2.3.2 Junction Coupling	13
	2.4 Oscillatory Motion	18
	2.4.1 Impedance Method	19
	2 4 2 Transfer Matrix Mathod	20

3	ANALYTICAL DEVELOPMENT	23
	3.1 Introduction	23
	3.2 Governing Differential Equations	24
	3.2.1 Axial Waves - Liquid and Pipe Wall	24
	3.2.2 Transverse Waves - Shear and Bending	38
	3.2.2.1 Shear and Bending in x-z Plane	39
	3.2.2.2 Shear and Bending in y-z Plane	45
	3.2.3 Torsion About z-axis	48
4	NUMERICAL SIMULATION	56
	4.1 Introduction	56
	4.2 Transfer Matrix Method	57
	4.2.1 Description of Transfer Matrix Approach	58
	4.2.2 Field Transfer Matrices	63
	4.2.2.1 Liquid and Axial Pipe Wall	
	Vibration	65
	4.2.2.2 Transverse Vibration in x-z Plane	67
	4.2.2.3 Transverse Vibration in y-z Plane	69
	4.2.2.4 Torsional Vibration About z-Axis	71
	4.2.2.5 General Field Transfer Matrix	72
	4.2.3 Point Matrices	73
	4.2.3.1 Bend Point Matrix	73
	4.2.3.2 Spring Point Matrix	75
	4.2.3.3 Mass Point Matrix	77

	4.2.4 Overall Transfer Matrix	/9
	4.2.4.1 Overall Transfer Matrix	
	Rearrangement	80
	4.2.4.2 Coordinate Transformation	83
	4.2.5 Boundary and Intermediate Conditions	86
	4.2.5.1 Boundary Conditions	87
	4.2.5.2 Intermediate Conditions	88
	4.2.6 Natural Frequencies	92
	4.2.7 Mode Shapes	93
	4.2.8 Frequency Response	94
	4.3 Comparison with Other Methods	95
	4.3.1 Method of Characteristics	96
	4.3.2 Component Synthesis Method and	
	Experimental Data	98
5	EXPERIMENTAL APPARATUS	111
	5.1 Introduction	111
	5.2 Description of Experimental Apparatus	112
	5.2.1 Liquid Components	112
	5.2.1.1 Liquid	112
	5.2.1.2 Constant Pressure Reservoirs	113
	5.2.1.3 Valve	114
	5.2.2 Pipe Components	114
	5.2.2.1 Pipe Material	114

	5.2.2.2 Pipe Supports	115
	5.2.2.3 External Shaker	116
	5.2.2.4 Spring	117
	5.2.3 Experimental Configurations	120
	5.2.4 Transducers	121
	5.2.5 Dynamic Forces and Natural Frequencies	
	of Shaker	123
	5.2.5.1 Shaker Loads	123
	5.2.5.2 Spring Loads	125
	5.2.5.3 Natural Frequencies of Shaker	
	Components	127
	5.3 Experimental Procedure and Analysis	127
	5.3.1 Frequency Range of Excitation	128
	5.3.1.1 Liquid Frequencies	128
	5.3.1.2 U-Bend Frequencies	129
	5.3.2 Sampling Frequency and Sampling Time	131
	5.3.3 Sampling Procedure	131
	5.3.4 Analysis Procedure	132
	5.4 Experimental Uncertainty	133
•		
6	EXPERIMENTAL RESULTS AND COMPARISONS	142
	6.1 Introduction	142
	6.2 Transient Tests	143
	6.2.1 Snap-Back Test	143

	6.2.2 Valve Closure Test	144
	6.2.2.1 Fixed U-Bend	145
	6.2.2.2 Free U-Bend	146
	6.2.2.3 U-Bend with Spring	148
	6.3 Harmonic Tests	148
	6.3.1 U-Bend Response	150
	6.3.2 Spectral Response of Liquid-Filled Piping	151
	6.3.3 Liquid Mode Shapes	152
	6.3.3.1 Liquid Mode Shapes at Liquid	
	Natural Frequencies	153
	6.3.3.2 Liquid Mode Shapes at U-Bend	
	Natural Frequencies	154
7	SUMMARY AND CONCLUSIONS	190
A	LIQUID-AXIAL PIPE WALL TRANSFER MATRIX	193
	A.1 Introduction	193
	A.2 Uncoupled Analysis	194
	A.3 Coupled Analysis	194
В	DATA ACQUISITION	206
_	B.1 Introduction	206

B.2 Sy	stem Components	206
В.	2.1 Piezoelectric Pressure Transducers	207
В.	2.2 Quartz Accelerometers	208
В.	2.3 Computer Hardware and Accessories	210
	B.2.3.1 Analog-to-Digital Converter	211
	B.2.3.2 Programmable Real-Time Clock	212
	B.2.3.3 Patch Panel	212
В.	2.4 Data Acquisition Software	213
LIST OF REFER	ENCES	214

LIST OF TABLES

4.1	Properties of Straight Liquid-Filled Pipe	97
4.2	Natural Frequencies for Straight Pipe	98
4.3	Properties of L-Shaped Liquid-Filled Pipe	99
5.1	Physical Properties of Liquid	113
5.2	Physical Properties of Piping System	115
5.3	Shaker Components	118
5.4	Spring Properties	118
5.5	Piping System Configurations	120
5.6	Location of Transducers and U-Bend Relative to	
	Valve	122
5.7	Fluid Harmonics for Pipe Configurations	129
5.8	Natural Frequencies of U-Bend	130
6.1	Experimental and Computed U-Bend Response to	
	Snap-Back Test	144
6.2	Experimental and Computed Frequencies of	
	Liquid for Fixed Condition	145
6.3	Experimental and Computed Frequencies of	
	liquid for Free Condition	1/16

6.4	Experimental and Computed Frequencies of	
	Liquid for Spring Condition	149
6.5	Natural Frequencies of U-Bend to Harmonic	
	Excitation	151
6.6	Liquid Pressure Mode Shapes at Liquid Natural	
	Frequencies	154
6.7	Liquid Pressure Mode Shapes at U-Bend Natural	
	Frequencies	156
6.8	Experimental and Computed Results for	
	Configuration 1	157
6.9	Experimental and Computed Results for	
	Configuration 2	158
6.10	Experimental and Computed Results for	
	Configuration 3	159
6.11	Experimental and Computed Results for	
	Configuration 4	160
6.12	Experimental and Computed Results for	
	Configuration 5	161
6.13	Experimental and Computed Results for	
	Configuration 6	162
6.14	Experimental and Computed Results for	
	Configuration 7	163
6.15	Experimental and Computed Results for	
	Configuration 8	164
6.16	Experimental and Computed Results for	
	Configuration 9	165

A.1	Pipe Material Properties	194
A.2	Transfer Matrix Parameters	196
B.1	Properties of Pressure Transducers	205
B.2	Properties of Accelerometer Transducers	208

LIST OF FIGURES

1.1	Liquid-Filled Piping System	7
3.1	Sign Convention for Internal Forces	51
3.2	Axial Pipe Element	52
3.3	Radial Pipe Element	52
3.4	Deformations for Transverse Vibration in x-z Plane	53
3.5	Internal Forces for Transverse Vibration in	
	x-z Plane	53
3.6	Deformations for Transverse Vibration in y-x Plane	54
3.7	Internal Forces for Transverse Vibration in	
	y-z Plane	54
3.8	Pipe Reach Subjected to Torsion	55
4.1	Generalized Spring-Mass System	101
4.2	Free Body Diagrams of Spring and Mass Systems	101
4.3	Simple Spring-Mass System	101
4.4	General Piping System	102
4.5	General Straight Liquid-Filled Pipe Reach	102
4.6	Forces and Displacements at Bend	103
4.7	Forces at Spring	104
4.8	Forces at Concentrated Mass	104

4.9	Definition of Local and Global Axes	105
4.10	Coordinate Transformation of Straight Pipe Reach	105
4.11	Boundary Conditions	106
4.12	Intermediate Boundary Conditions	106
4.13	Pressure Amplitude Response for Straight	
	Pipe Reach	107
4.14	L-Shaped Liquid-Filled Pipe	108
4.15	Mobility Diagrams for L-Shaped Pipe	109
5.1	Experimental Liquid-Filled Pipe Set-Up	136
5.2	Liquid Boundaries	137
5.3	Crank Mechanism	138
5.4	Crank Diagram	139
5.5	Transducers and U-Bend Locations	139
5.6	One Degree-of-Freedom Representation of U-Bend	139
5.7	Experimental and Analysis Procedures	140
5.8	Input and Output Displacements	141
5.9	Input and Rated Torque at Shaft of Motor	141
5.10	Low-Pass Filter	141
6.1	Experimental Results of Snap-Back Test, U-Bend	
	Empty, Frequency of Free Bend is 4.4 Hz	166
6.2	Experimental Results of Snap-Back Test, U-Bend	
	Filled, Frequency of Free Bend is 3.9 Hz	167
6.3	Experimental Time Pressure Response to Sudden	
	Valve Closure at Closed End, U-Bend Fixed	168
6 4	FFT for Sudden Valve Closure II-Rend Fixed	169

6.5	Experimental Time Responses to Sudden Valve	
	Closure at Closed End, U-Bend Free	170
6.6	FFT for Sudden Valve Closure, U-Bend Free	171
6.7	Experimental Time Responses to Sudden Valve	
	Closure at Closed End, U-Bend with Spring	172
6.8	FFT For Sudden Valve Closure, U-Bend with Spring	173
6.9	Experimental U-Bend Displacements for Harmonic	
	Excitation	174
6.10	Computed U-Bend Mode Shapes, Free Bend	175
6.11	Computed U-Bend Mode Shapes, Bend Attached to	
	Spring	176
6.12	Liquid Mode Shapes at Liquid Natural Frequencies	177
6.13	Liquid Mode Shapes at U-Bend Natural Frequencies,	
	Configuration 1	179
6.14	Liquid Mode Shapes at U-Bend Natural Frequencies,	
	Configuration 2	180
6.15	Liquid Mode Shapes at U-Bend Natural Frequencies,	
	Configuration 3	181
6.16	Liquid Mode Shapes at U-Bend Natural Frequencies,	
	Configurations 4 and 5	182
6.17	Liquid Mode Shapes at U-Bend Natural Frequencies,	
	Configuration 6	183
6.18	Liquid Mode Shapes at U-Bend Natural Frequencies,	
	Configurations 7 and 8	184
6.19	Liquid Mode Shapes at U-Bend Natural Frequencies,	
	Configuration 9	185

A.1	Liquid and Axial Pipe Wall Wave Speeds Versus	
	Pipe Cross Sectional Ratio	. 198
A.2	Parameters for Liquid and Aixal Pipe Wall	
	Transfer Matrix	199
A.3	Elements of Field Transfer Matrix in Axial Pipe	
	Wall Submatrix .	200
A.4	Elements of Field Transfer Matrix in Upper	
	Coupling Submatrix	201
A.5	Elements of Field Transfer Matrix in Lower	
	Coupling Submatrix	202
A.6	Elements of Field Transfer Matrix in Liquid	
	Submatrix	203
B.1	Displacement Calibration Curve for PCB	
	Accelerometers	213

NOMENCLATURE

Symbols	Description	Units
		2
A	Cross-sectional area (pipe, fluid)	m
A	Coefficients of integration	
a	Wave speed	m/s
В	Matrix coefficients	
ь	Ratio of pipe radius to pipe wall	
	thickness	
С	Field transfer matrix coefficients	
c	Coupled wave speed ratio	
D	Mean spring diameter	mm
d	Wire spring diameter	mm
d	Ratio of pipe density to fluid density	y
E	Young's modulus of elasticity	Pa
e	Pipe wall thickness	m
F	Force amplitude	N
f	Force	N
f	Natural frequency	Hz
G	Shear modulus of rigidity	Pa
g	Bend point matrix coefficient	

h	Ratio of Young's modulus to modifie	d
	bulk modulus	
I	Moment of inertia	m 4
J	Polar moment of inertia	m 4
j	(-1) ¹ 2	
K	Fluid isothermal bulk modulus of	
	elasticity	Pa
k	Spring stiffness	N/m
L	Length of crank mechanism	m
l	Length of pipe reach	m
M	Moment amplitude	N - m
m	Moment	N-m
TO.	Mass	kg
N	Number of active coils in spring	
P	Fluid pressure amplitude	Pa
p	Fluid pressure	Pa
Q	External force amplitude	N
q	Ratio of fluid area to pipe area	
R	Crank radius	mm
r	Radius of pipe cross-section	mm
s	Coordinate along pipe axis	m
T	Torque	N-m
t	Time	s
U	Pipe displacement amplitude	m
u	Pipe displacement	m
v	Fluid displacement amplitude	m

v	Fluid displacement	m
w	Radial displacement	rad
z	Axial displacement	m
α	Angle between incident pipe reaches	rad
β	Angle of rotation due to shear	
Δ	Field transfer matrix coefficient	
Δ	Matrix determinant	
δ	Differential element	
5	Frequency parameter of a Bernoulli-	
	Euler beam	
7	Flexural stiffness correction factor	
	for a pipe bend	
0	Angular direction	
ĸ	Shape factor for shear	
λ	Eigenvalues	
ν	Poisson's ratio	
P	Mass density	kg/m
σ	Stress	Pa
Σ	Summation of forces	
φ	Angle between local and global axes	rad
¥	Rotation amplitude due to bending	
ψ	Rotation due to bending deformation	rad
Ω	Forcing frequency	rad/s
ω	Natural circular frequency.	rad/s
γ,σ,τ	Field transfer matrix coefficients	

Subscripts

В	U-bend
С	Columns
f	Fluid
G	Global coordinate system
i	Pipe end
L	Local coordinate system
p	Pipe
p	Local axis index
P	Global axis index
R	Rows
S	Spring
t	Time
z	Direction along pipe axis
fp	Fluid and axial pipe wall field transfer matrix
tz	Torsion vibration about z-axis field transfer matrix
xz	Transverse vibration in X-Z plane field transfer matrix
yz	Transverse vibration in Y-Z plane field transfer matrix
X,Y,Z	Global rectangular coordinate directions
x,y,z	Local rectangular coordinate directions
θ	Angular direction

Superscripts

В	Point matrix for a bend
L	Left of discontinuity
М	Point matrix for a lumped mass
R	Right of discontinuity
S	Point matrix for a spring
т	Matrix transposition
-1	Matrix inverse
*	Modified modulus

Matrices and Vectors

A	Vector, integration coefficients
В	Solution matrix
P	Point transfer matrix
T	Field transfer matrix
t	Transformation matrix
U	Global transfer matrix
Z	State vector

CHAPTER 1

OBJECTIVE AND SCOPE

1.1 Introduction

Vibrations that occur in liquid-filled piping systems are of interest in a variety of industrial, water supply, hydraulic, nuclear power, aircraft and automotive applications. The dynamic behavior of these systems includes both transient and steady-state vibrations caused by rapid valve closures and unbalanced rotating machinery. This dynamic behavior has usually been modeled by uncoupled analyses. The analyses of liquid columns contained in pipes are based in part on the assumptions that the piping system is sufficiently rigid to remain immobile and that it does not interact dynamically with either fluid oscillations or external loads. Possible sources of the external loads are machine vibrations and seismic motion. Analytical developments for free vibrations and resonance of liquid columns are presented by Jaeger [5], Wylie and Streeter [6] and Chaudhry [7]. On the other hand, well-known modal analysis techniques, such as those described by Clough and Penzien [52], can be used to analyze vibrations of piping structures if the motion of the contained liquid is neglected.

Recently, coupling analyses have been called to the attention of researchers. Experimental results in laboratories [19,24,25,64] have clearly shown that under certain conditions, vibrations of liquid columns and piping structural elements interact and respond differently than if the two components are treated independently. The interaction can be attributed in part to two coupling mechanisms, Poisson and junction coupling. Poisson coupling takes place along a pipe length. Axial strain of the pipe is induced by circumferential strain caused by a change in the fluid pressure. Junction coupling occurs at locations where the flow area and/or flow direction changes. At junctions, variations in fluid pressure create force resultants. It is necessary for these pressure forces to be balanced by axial forces in the pipe wall. The axial forces generate subsequent pipe motion that may excite flexural and torsional modes of vibration of the pipe.

Poisson and junction coupling generate forces and displacements in the fluid and in the pipe wall that are transmitted and reflected back and forth along the length of the pipe. Wilkinson [64] identified five families of waves: tension, torsion, and two families of transverse bending waves in the pipe wall and pressure waves in the liquid. A three-legged liquid-filled pipe in a three-dimensional space shown in Figure 1.1 is used to describe the transmission process of these waves. The pipes connect two reservoirs. A valve, location D, is located at the downstream reservoir where water is flowing at velocity V₀. Junctions B and C are unrestrained allowing displacements and rotations. The pipe is rigidly supported at the ends. An instantaneous valve

closure creates the system excitation. The following events take place as the valve begins to close. A pressure wave is generated and propagates in the fluid while an axial wave is transmitted along the pipe wall in leg 3, that is, Poisson coupling occurs. For most commercial pipe material, the axial wave (precursor wave) travels faster than the fluid pressure wave [21]. The precursor wave produces a displacement at junction C in the positive X direction. This motion, which is generated by Poisson coupling, induces a change in the fluid velocity and creates an unbalanced axial force at this location. The change in fluid velocity produces an increase in the fluid pressure that is transmitted towards the valve and location B. The unbalanced axial force is transmitted as a shear force and bending moment along leg 2. The motion at junction C is maximum when the fluid pressure wave from the valve reaches this point. Junction coupling is present at this point due to the unbalanced axial force produced by the change in pressure. Moreover, the motion at junction C and moment in leg 2 produce a rotation at junction B about the Y-axis. This generates a torsional moment that is transmitted along leg 1. The boundary conditions at D reflect the five waves described above.

The study of liquid-filled pipes becomes more complicated when several factors are taken into account. The five families of waves, tees and bends, supports of various stiffnesses, structural restraints and hydraulic devices such as pumps, orifices and valves must be considered. The speed of the wave components depends on the pipe material and fluid properties. The frequencies at which the liquid and pipe are

vibrating are influenced by the structural support configurations of the pipe and the hydraulic elements of the system.

The frequencies of the system may also be affected by the interaction between the fluid and the structure due to Poisson and junction coupling. Some incidents of hydraulic resonance at various pumped storage sites and power plants are presented by Jaeger [5], Wylie and Streeter [6] and Chaudrhy [7]. Jaeger [41] also reported several of these incidents and points out the importance and danger of vibrations from higher fluid harmonics. These harmonics may be excited by the motion of structural components of the system.

The analysis and design of piping systems can be performed in either the time or the frequency domain. The method of characteristics has been used to model the propagation of acoustic waves in liquids [5,6,7], beams as described by the Timoshenko's theory [89] and in fluid-structure interaction systems [17,19,20,21,22]. Unfortunately, numerical limitations have thwarted the evolution of a generalized solution methodology. In the frequency domain the transfer matrix method has been used to model distributed parameter systems [50]. Wilkinson [64] and Wiggert, Lesmez and Hatfield [65] use this method to model liquid-filled piping systems. Wilkinson's model uses the Bernoulli-Euler beam theory to describe the piping flexure, but does not include Poisson's coupling. His model then, does not account for the axial liquid pipe wall coupling.

The transfer matrix method is appropriate to model piping systems because it directly relates the force and displacement variables in the pipe wall and in the fluid at one end of the system to the corresponding variables at the other end. As a designing model, the method may be used to compute the natural frequencies, mode shapes and frequency responses of the system including the structural supports and hydraulic devices. It can also be used to compute the response of the system for free or forced vibration analysis. The variables are related by using a global transfer matrix. Elastic liquid-filled pipe reaches can be analyzed with an appropriate transfer matrix. Point matrices describe joints, such as tees, bends, point masses, and hydraulic elements.

1.2 Objective

The objective of the present research is to incorporate the flexural and torsional modes of vibration in an existing coupled liquid-axial pipe wall model. The proposed model accounts for Poisson and junction coupling and allows the inclusion of structural and hydraulic devices. The model represents an improvement over the previous model by Wilkinson [64]. In addition, an experimental apparatus was designed and built to provide experimental data collection to verify the analytical model.

1.3 <u>Scope</u>

This report is organized into two sections. Chapters 3 and 4 are included in the first section which is concerned with the development and

verification of the numerical analysis technique. Chapter 3 presents the equations of motion that describe the coupled liquid and axial pipe wall model and the equations that describe the transverse and torsional modes of vibrations. Chapter 4 describes the numerical technique that accounts for the five families of waves propagating in the pipe and the liquid. The modeling of bends, masses, springs and rigid supports is also presented. Forced vibration is also incorporated into the model. The proposed model is compared with two numerical techniques and with experimental data available in the literature.

The second part of the research is an experimental study of a piping system of variable pipe length and with a U-type bend that is excited by an external shaker. The variable pipe length allows changes in fluid frequency. The U-bend is free to move in one plane. The shaker excites the piping over a range of frequencies that includes the first natural frequencies of both the fluid and the U-bend. Chapter 5 describes the experimental apparatus and procedures. The experimental results and comparison with the analytical model are presented in Chapter 6.

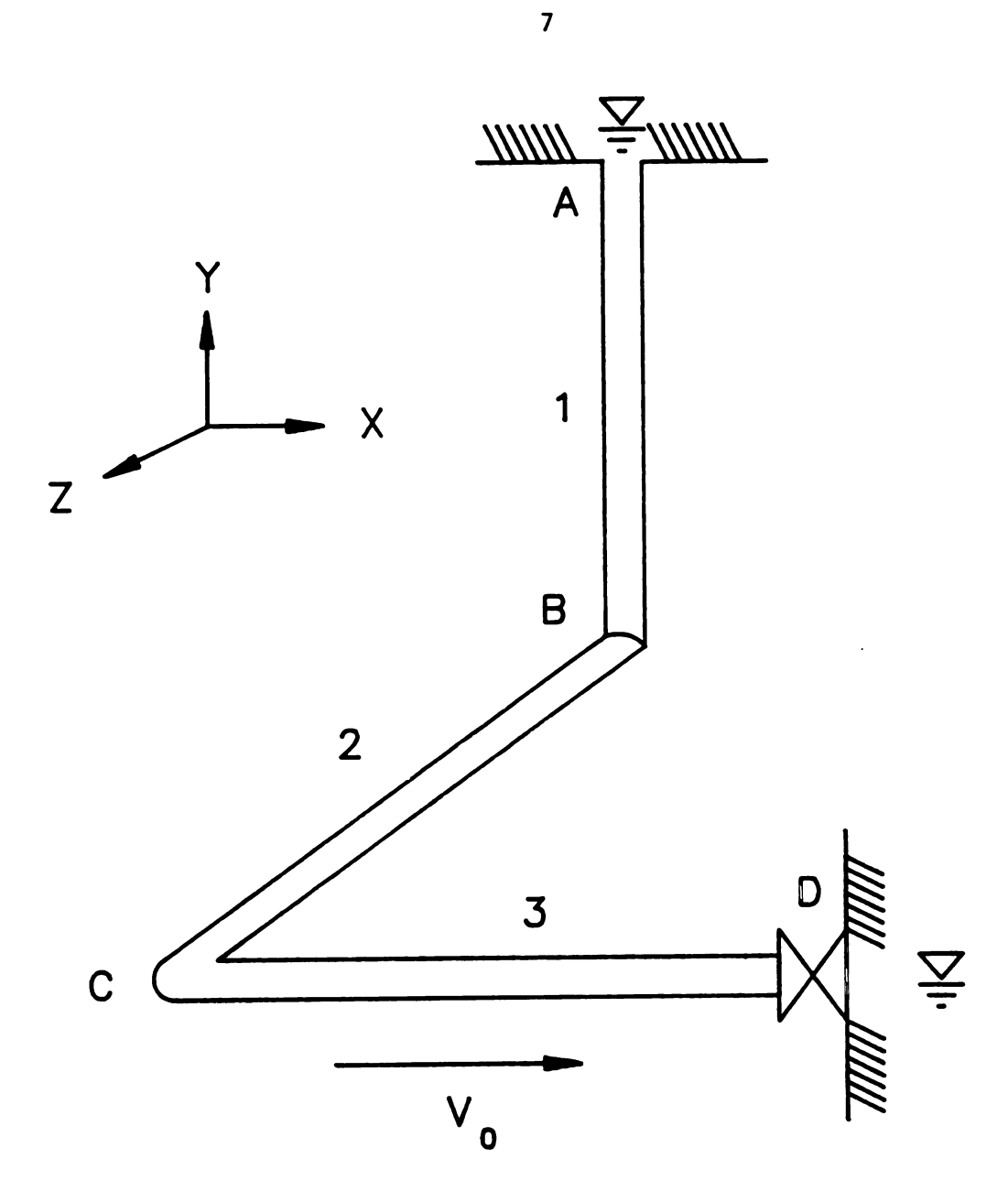


Figure 1.1 Liquid-Filled Piping System

Chapter 2 Literature Review

CHAPTER 2

LITERATURE REVIEW

2.1 Introduction

The objective of this study is to incorporate the flexural and torsional modes of vibration in an existing coupled axial pipe wall and liquid model. A review of the evolution of the axial model and these modes of vibration is necessary to incorporate the appropriate coupling mechanisms. This section is devoted to a review of the previous works in these areas. This review will be divided into three sections. The first section reviews the studies of unsteady flow in closed pipes. The second one relates the works on the interaction between fluid and structure in liquid-filled piping systems. The last section relates the studies of oscillatory motion in piping systems and the applications of the transfer matrix method to solve these problems.

2.2 Unsteady Flow in Pipelines

The study of unsteady flow in pipelines, or waterhammer as this phenomenon is more commonly known, has been of interest since the middle of the 1800's [1]. Among the early significant contributions to the solution of waterhammer problems are those of Joukowsky [2], Lamb [3], and Allievi [4]. Their findings predicted with accurately predicted the liquid wave speed and its associated pressure rise. With the exception of Lamb, who included the effect of longitudinal stresses in the pipe wall by considering the pipe an elastic membrane, the others predicted the existence of only one wave propagation. Joukowsky conducted extensive experiments and found that the speed at which disturbances propagates in the water is related to the relative circumferential stiffness of the pipe. His study concluded that the speed of propagation for the liquid in pipelines is less than the propagation speed in an infinite liquid. In his research, Joukowsky assumed that pressure is uniform across any given pipe section. He also neglected the mass of the pipe wall, the radial inertia of the liquid and the axial and bending stresses in the pipe wall. Based on these assumptions he derived a modified wave speed for the fluid in which the liquid bulk modulus is adjusted by the structural properties of the pipe wall.

The analysis of the waterhammer problem has produced much research after these early works. Some analytical solutions of unsteady flow problems with various boundary conditions are outlined in textbooks by Jaeger [5], Wylie and Streeter [6] and Chaudhry [7]. Waterhammer problems are

still being researched today. The basic equations are being investigated [8] and new numerical techniques are being developed [9,10].

2.3 Fluid-Structure Interaction

Research in the area of fluid-structure interaction has identified four main forms of dynamic liquid-pipe forces:

- 1. Lateral momentum forces. Blevins [11] reported some of the research into this mechanism which has been extensively investigated. The lateral momentum forces induced by high, steady flow rates through curved pipes can reduce flexural stiffness and may produce buckling of initially straight pipes.
- 2. Transverse pressure variation. This phenomenon occurs in cases where the inside diameter of the pipe is a multiple of the length of the transverse acoustic wave in the liquid. This may result in the excitation of higher symmetric lobar modes of the pipe cross section. Leissa [12] presented estimates of natural frequencies of lobar modes for infinitely long cylindrical shells.
- 3. Dilation pressures. This mechanism is related to the Poisson ratio [13] in which an axial elongation of a straight pipe causes a decrease of its inside diameter or , conversely, an axial contraction of the pipe causes a dilation of the inside diameter. This axial elongation or contraction of the pipe wall may be caused by a rapid change in the

fluid velocity creating a decrease or increase in the fluid pressure. This pressure change gives rise to an axial stress wave in the pipe. For most piping systems the propagation of the stress wave in the pipe wall is faster than that of the acoustic wave in the fluid. The result of this wave interaction is called the "precursor wave" and the mechanism by which it occurs is termed Poisson coupling.

4. Axial resultants at fittings. Variations in fluid pressure create pressure resultants that act at locations where flow changes area or direction, such as at bends, tees and orifices. These differential pressure forces have to be balanced by axial forces in the pipe wall to maintain equilibrium conditions. The axial forces generate subsequent pipe motion that may excite the flexural and torsional modes of vibration of the pipe. This phenomenon is known as junction coupling.

Poisson coupling and junction coupling are the phenomena to be studied in this research. The literature review concerning these follows.

2.3.1 Poisson Coupling

In liquid-filled pipes, Poisson coupling results from the transformation of the circumferential strain, caused by internal pressure, to axial strain and is proportional to Poisson's ratio. Skalak [14] was among the first to extend Joukowski's method to include Poisson coupling. His results identified the precursor wave for a sudden valve closure. The analytical model that he developed treated the pipe wall as an elastic

membrane to include the axial stresses and axial inertia of the pipe. Thorley [1] conducted experimental validation of Skalak's theory. Williams [85] conducted a similar study. He found that structural damping caused by longitudinal and flexural motion of the pipe was greater than the viscous damping in the liquid. In fact, Williams states that "mechanical damping can be more important for water hammer decay than viscous friction". These researchers did not include the radial inertia of the liquid or the pipe wall. Lin and Morgan [15,16] included the pipe inertia term and the transverse shear in their equations of motion. Their study was restricted to waves which have axial symmetry and purely sinusoidal variation along the axis. Walker and Phillips [17] extended the study by Lin and Morgan to include both the radial inertia of the pipe wall in the fluid and the axial equations of motion. Their interest in short duration, transient events produced a one-dimensional, axisymmetric system of six equations. Wilkinson and Curtis [18] developed a non-linear, twenty-one equation model for the axial and radial pipe wall deformations in both elastic and plastic zones. Vardy and Fan [75] conducted experiments on a straight pipe, generating a pressure wave by dropping the pipe onto a massive base. Their results showed good agreement with the analytical model by Wilkinson and Curtis [18]. They concluded that the fluid friction does not influence the pressure response and that the axial waves in the straight pipe are non-dispersive for a first order accuracy. Otwell [19], Wiggert, Otwell and Hatfield [20] and Stuckenbruck, Wiggert and Otwell [21] neglected the radial acceleration in their studies using the six-equation model of Walker and Phillips [17]. This simplification reduced the mathematical model to four equations. They presented

numerical examples for various combinations of liquids and piping materials and for various coupling constraints. Budny [22] also reduced the six-equation model, but he included viscous damping and a fluid shear stress term to account for the structural and liquid energy dissipation. Experimental tests verified that the model satisfactorily predicts the wave speeds, fluid pressure, and structural velocity of a straight pipeline for several fluid periods after a transient has excited the fluid.

The aforementioned researchers have helped in the understanding of the Poisson coupling mechanism in fluid-structure interaction problems. They identified two important waves that propagate in a straight pipe reach, one in the liquid and one in the pipe wall. However, none of these studies, with the exception of Otwell [19] and Wiggert et al. [20], considered the possibility that a fitting, such as an elbow, may move in response to the precursor wave, thereby, altering the transient response of the liquid. The following section discusses the models that have included the junction coupling mechanism.

2.3.2 Junction Coupling

Piping systems can be thought of as straight pipes joined at localized points by elbows, reducers, tees, orifices and the like. Pressure resultants at these points act as localized forces on the pipe, generating the junction coupling mechanism. For pipes with only a few bends, a continuous representation of the piping was devised by Blade, Lewis

and Goodykoontz [23]. Experimental tests were conducted to analyze the response of an L-shaped pipe to harmonic loading. The experimental setup included a restricting orifice plate at the downstream end of the pipe. Their experimental results validated their model. They concluded that an uncoupled analysis does not produce accurate estimates of natural frequencies, and that the elbow, which provides coupling between the pipe motion and liquid motion, causes no appreciable reflection, attenuation, or phase shift in the fluid waves. Davidson and Smith [24] conducted a similar investigation. Their analytical model was based on a vibration transmission matrix and it showed good agreement with experimental results. As an extension of that work, Davidson and Samsury [25] developed a more accurate solution to analyze a pipe assembly comprised of straight sections and uniform bends arranged in a nonplanar configuration. Experimental results indicated a significant level of coupling between the plane compressional wave in the liquid and that in the pipe wall. Comparison of numerical and experimental results, however, indicated a need for further refinement. Wiggert, Hatfield and Stuckenbruck [26], and Wiggert, Hatfield and Lesmez [27] used a onedimensional wave formulation in both the liquid reaches and the piping structure resulting in five wave components and fourteen variables. The five families of waves are pressure waves in the liquid, axial tension waves in the pipe wall, two families of transverse shear and bending waves, and torsional waves. The method of characteristics was used to solve for the fourteen variables and to find the expressions for the wave speeds. The authors showed a comparison of the predicted fluid pressures and structural velocities with experimental data to provide a partial validation of the model. However, their model showed that

numerical errors are introduced by time-line interpolations and by numerical integration of the coupled transverse shear force and bending moment. Experimental validation of the transverse vibration was not included. Joung and Shin [28] developed a model that takes into account the shear and flexural waves of an elastic axisymmetric tube. The method of characteristics was used in the solution for four families of propagating waves: the extensional, transverse, and symmetric bending waves of the elastic tube and the acoustic wave of the fluid medium. Their results compared closely to Walker and Phillips' results [17] for relatively small pipe deformations.

The above models used a continuous representation of the piping system. Another approach for complicated geometric configurations is to approximate the system as a set of discrete connected masses. Several techniques have been applied to a variety of models. A basic technique uses spring and point masses to represent the pipe structure. Wood [29] studied a pipe structure loaded with a harmonic excitation. He found that the natural frequencies of liquid were shifted, especially when the frequency of the harmonic load is near one of the natural frequencies of the supporting structure. Ellis [30] reduced a piping structure to equivalent springs and masses by selectively lumping mass and stiffness at fittings and releasing specific force components at bends, valves and tees. His formulation of axial response was a modification of the method of characteristics and included pipe stresses and velocities. Otwell [19] and Wiggert et al., [20] modeled a pipe elbow as two orthogonal springs. The stiffness of the springs corresponded to the

flexural stiffness of the upstream and downstream pipe reaches connecting to the elbow. Their investigation also included experimental data for a rapid valve closure. Their results showed that the motion of the elbow, driven by the axial stress in the pipe and by the liquid pressure, caused appreciable alteration of the pressure. The pressure response was 33% greater than the response for an immobile elbow. Otwell [31] used a spring-mass oscillator to represent each mode of the structural response. This approach, however, is limited to simple, orthogonal configurations because it provides only one liquid-structure coupling point and only one degree of freedom for each mode.

A second method uses the finite element method to model the structure, treating each pipe element as a beam. Schwirian and Karabin [32] generalized this approach by using a finite element representation of the liquid and the piping. Their studies imposed coupling at fittings only. The effect of the supports and piping stiffness was shown to be significant. Wiggert and Hatfield [33] used the method of characteristics to model the fluid. They coupled the results at pipe junctions with a finite element code to solve for the structure. Hatfield, Wiggert and Otwell [34] used the modal synthesis technique [35,36] to analyze fluid-structure systems with harmonic loading. The modal responses of the supporting structure were obtained from an existing finite element program. These responses were then coupled to the liquid analyses. Hatfield, Wiggert and Davidson [37] presented a validation of this methodology based on comparison to earlier experiments.

These models, however, cannot represent the precursor wave because classic beam theory neglects deformations of cross sections. The reduction in flexural stiffness at bends is also inappropriately treated by these models. To avoid these difficulties, Quezon and Everstine [38] used shell elements to represent the pipe wall. While providing useful estimates of flexural stiffness of a single bend, this method is computationally feasible for only short lengths of pipe.

The investigation of these two coupling mechanisms, Poisson and junction, in liquid-filled piping systems is continuing. Wiggert [39] presented a survey of the latest work in this area. The study of piping systems in industrial plants and experimental testing of large scale models as well as the inclusion of non-linearities such as cavitation, structural damping and fluid friction is necessary to gain a better understanding of these systems. Rothe and Wiggert [40] outlined some of these considerations when modeling condensation-induced waterhammer in power plant systems. Jaeger [41] reported incidents of hydraulic resonance caused by structural vibration at various pumped storage sites and power plants. The understanding of these mechanisms has been useful also in the study of seismic motion of pipelines. Hatfield and Wiggert [42] applied a response spectrum analysis to an elastically-supported, liquid-filled pipe aligned in the direction of ground motion. The same authors [43] described a technique for determining pressure and displacement responses of liquid-filled piping in the time domain. mathematical models included waves in the liquid and pipe wall coupled by the Poisson effect. Ogawa [44] conducted experiments on the dynamic

response of a real-scale piping system using a large scale shaking table to investigate earthquake induced hydraulic transient effects. The system was excited by a harmonic motion in the axial direction of pipe and showed a sharp resonance for a closed, liquid-filled pipeline. The system was analyzed using a simple model of a rigidly supported pipewater column system. The analytical and experimental results suggested that the coupling of a closed low pressurized liquid contained in a piping system is an important factor for seismic response estimations of liquid-filled pipelines.

2.4 Oscillatory Motion

Resonance in power conduits has been the cause of many severe and spectacular accidents as mentioned by Jaeger [41] in his remarkable discussion of incidents in hydropower systems. His discussion points out the importance and danger of vibrations from higher fluid harmonics. Jaeger [5], Wylie and Streeter [6] and Chaudhry [7] included extensive discussions of this phenomenon in their textbooks. Resonance, which is an oscillating condition that leads to a pressure amplification in the piping system, develops when there is an exciter present at some point in the system. The piping can be excited in two ways. First, a device may act as a forcing function, exciting the system at one of its natural frequencies. Second, self-excited oscillations occur when a component of the system acts as an exciter. These two actions may occur simultaneously or independently. Resonance, due to a forcing function, takes place when the interactive response occurs at or near one of the natural

19

periods of the system. A forcing excitation will be used in the current research to find the resonant frequencies of a liquid-filled pipe. Self-excited oscillations are caused by certain features of the piping system. Some of these features include a malfunctioning valve seal [45], cavitating pump [41] or interactive structural and fluid components [46,47,22].

The analysis of resonating conditions in liquid-filled piping systems can be studied in either the time domain, by the method of characteristics, or the frequency domain, by the impedance method or transfer matrix method. The frequency domain method of analysis will be the focus of this research.

2.4.1 Impedance Method

The impedance method was systemized for the analysis of complex liquid systems by Wylie [48]. The method computes the ratio of the oscillatory pressure and the discharge, known as the terminal impedance, by using known boundary conditions. Then, the terminal impedance is plotted as a function of frequency to find the natural frequencies of the system and the extreme terminal impedances. This method has been used by Zielke and Hack [49] for the frequency response analysis of pumped storage systems.

2.4.2 Transfer Matrix Method

The transfer matrix method has been widely used for analyzing structural and mechanical vibrations [50,51,52,53,54] and for analyzing electrical systems [55]. This method is an extension of Miklesta's and Holzer's methods [52,53,54]. Dawson and Davies [56] improved these methods by giving them an automatic natural frequency search capability for idealized lumped property models. Pestel and Leckie [50] detailed the work of many authors dealing with lumped and distributed property models.

The transfer matrix method was used by Chaudhry [57,58] for analysis of steady-oscillatory flows and for determining the frequency responses of hydraulic systems. Classic fluid transient textbooks such as those by Wylie and Streeter [6] and Chaudhry [7] describe the application of this methodology to hydraulic systems. To [59,60] used this method to simulate and analyze complicated reciprocating compressor piping systems. He developed nineteen parameter matrices for acoustic elements [59] and presented a description of a digital computer program and its applications [60]. The method has also been used in solving fluid-structure interaction problems. Keskinen [61], To and Kaladi [62] and Dupuis and Rousselet [63] developed methodologies to study non-conservative systems involving fluid flow in pipes. Keskinen's method [61] involved numerically solving a system of differential equations, expressed in matrix form, to obtain the transfer matrix for a pipe element which is treated as a discrete parameter model. To and Kaladi's model [62] differed from the previous work in that the transfer matrix was derived from a direct solution of the differential equation of motion of the pipe, which was considered a distributed parameter model. They presented a method of analysis for complicated piping networks with moving mediums involving bends, piping components of various diameter and lumped masses such as valves. Experimental validation of their model was presented. Dupuis and Rousselet [63] formulated the transfer matrix by using equations of motion that included shear and extensional deformations, rotatory inertia and variable pipe curvature. They applied the method to straight and curved cantilevered pipes containing a flowing fluid.

Another application of this method has been in the study of liquidfilled piping systems such as is the topic of this research. Wilkinson [64] showed that under certain conditions the vibrations of the liquid column and that of the supporting structure can interact. This causes the coupled system to respond dynamically in a manner different from the response of either of the independent components. He used the transfer matrix approach with the vibration state at a point described by a fourteen element vector representing five wave families. These five families are: pressure waves in the liquid, tension waves in the pipe wall, two families of transverse bending waves and a torsion wave. The Poisson effect between the liquid pressure and the axial tension wave in the pipe wall was not included. The equation of motion for the transverse vibration was based on the Bernoulli-Euler beam theory. results were compared with the experimental results for an L-shaped pipe. They indicated good agreement, but the author concluded that further study of this topic is needed. Wiggert, Lesmez and Hatfield [65] extended Wilkinson's work by including the Poisson effect and by using the Timoshenko beam theory to model the transverse vibration in the piping. The Timoshenko beam accounted for the secondary effects of rotatory inertia and shear deformation. Experimental results with an L-shaped pipe showed good agreement with the numerical model. Lesmez, Wiggert and Hatfield [66] used the same model with a U-shaped bend for a variable length piping system. The variation of the pipe length allowed for different acoustic natural frequencies in the liquid. Excellent agreement in the natural frequencies for both experimental and computed results indicated that the method accounted for the appropriate coupling mechanisms. This dissertation describes in a more detailed fashion the work reported in the two previous studies.

CHAPTER 3

ANALYTICAL DEVELOPMENT

3.1 Introduction

The equations of motion for the vibration of a liquid and the axial, transverse and torsional vibrations of the pipe wall in a liquid-filled piping system are presented in this chapter. The development includes simplifications of the radial properties of the fluid and pipe wall in the axial direction. Although these equations are well documented [17,19,20,21,22], they will be described below since they constitute the starting point of this research.

The major contribution of this study is the incorporation of the transverse and torsional vibrations of the pipe wall to an existing axial model that couples the liquid and pipe wall. This model includes Poisson and junction coupling and accounts for the effects of rotary inertia and shear deformation of the pipe wall. The addition of these mechanisms provides an improvement in accuracy over the previous axial-coupled models such as those by Otwell [19], Wiggert et al., [20] and Budny [22] and the junction coupled model described by Wilkinson [64]. The Timoshenko beam equation is used to represent the transverse

vibration of the pipe. The solution for the constants of integration constitute the connecting point between this chapter and Chapter 4.

3.2 Governing Differential Equations

This study is concerned with piping systems in which the inside diameter of the pipe is much smaller than the pipe length, limiting the equations of motion that describe the system to a one-dimensional wave approach [67,68]. The junction mechanism guarantees that a pipe element can transmit axial, torsion and transverse shear and bending waves in the pipe wall. Therefore, the inclusion of these waves is necessary to more realistically represent the motion of the piping system. The next section considers the axial liquid and axial pipe wall wave equations. The equations that describe the transverse vibration of the piping in the in-plane and out-of-plane modes are then developed. Finally, the equations describing the torsional pipe waves are presented. Figure 3.1 shows a general pipe reach with the sign convention used in this study. The z-axis is considered coincident with the centerline of the pipe reach.

3.2.1 Axial Waves - Liquid and Pipe Wall

The six-equation model by Walker and Phillips [17], which consists of one-dimensional continuity and momentum equations for the liquid, axial and radial momentum equations and two constitutive equations for the

pipe wall, constitutes the basis for the axial coupled model. Otwell [19], Wiggert et al., [20], Stuckenbruck et al., [21], and Budny [22] reduced the six-equation model to a four-equation model by neglecting the radial inertia of the pipe wall. The fluid in the model is assumed to be one-dimensional, linear, homogeneous, with isotropic flow and uniform pressure and fluid velocity over the cross section. The pipe wall is assumed to be linearly elastic, isotropic, prismatic, circular and thin-walled.

Two equations represent the axial continuity and momentum relations for the liquid:

$$\frac{\partial \mathbf{p}}{\partial \mathbf{t}} + \mathbf{K} \left[\frac{2}{\mathbf{r}} \frac{\partial \mathbf{w}}{\partial \mathbf{t}} + \frac{\partial^2 \mathbf{v}}{\partial \mathbf{t} \partial \mathbf{z}} \right] = 0 \tag{3.1}$$

$$\frac{\partial \mathbf{p}}{\partial \mathbf{z}} + \rho_{\mathbf{f}} \frac{\partial^2 \mathbf{v}}{\partial \mathbf{z}^2} + \frac{2\tau_0}{\mathbf{r}} = 0$$
 (3.2a)

in which p = p(z,t) is the fluid pressure, v = v(z,t) is the fluid displacement and w = w(z,t) is the pipe wall displacement. K and ρ_f are the fluid bulk modulus and density, r is the inside radius of the pipe, and the shear stress along the pipe wall is represented by τ_0 [22].

Previous authors arrived at these equations by making a number of standard assumptions [17,19,20,21,22]. First, the convective terms are ignored by assuming low Mach numbers, where the fluid wave speed is much greater than the fluid velocity. This implies that the fluid density in Equation 3.2a is constant. Second, the one-dimensional flow assumption implies that the radial component of the fluid velocity is zero and that the flow is developed in only the radial direction. The fluid friction term in the momentum equation can be neglected for forced vibrations [5,6] as is the case in this study. However, as noted by Williams [85] and Budny [22] the damping terms in both the liquid and the axial pipe wall equations of motion should be considered for transient events. Equation 3.2a reduces to:

$$\frac{\partial \mathbf{p}}{\partial z} + \rho_{\mathbf{f}} \frac{\partial^2 \mathbf{v}}{\partial z^2} = 0 \tag{3.2b}$$

Assuming an axisymmetric, linear elastic pipe wall and small deformations, the axial and circumferential stress-strain relationships for the pipe wall are:

$$\sigma_{\mathbf{z}} - \mathbf{E}^{\star} \left[\frac{\partial \mathbf{u}_{\mathbf{z}}}{\partial \mathbf{z}} + \nu \, \underline{\mathbf{w}} \, \right] = 0 \tag{3.3}$$

$$\sigma_{\theta} - E^{\star} \left[\frac{W}{r} + \nu \frac{\partial u_{z}}{\partial z} \right] = 0$$
 (3.4a)

where

$$E^* - \frac{E}{(1 - \nu^2)}$$
 (3.4b)

in which $\sigma_z = \sigma_z(z,t)$ and $\sigma_\theta = \sigma_\theta(z,t)$ are the stresses in the axial and radial direction, $u_z = u_z(z,t)$ is the pipe wall displacement in the axial direction, and E and ν are the Young's modulus and Poisson's ratio

of the pipe wall. Figures 3.2 and 3.3 show a section of a pipe with stresses and displacements in the axial and radial direction. The equations of motion for the pipe wall are:

$$\frac{\partial \sigma_{\mathbf{z}}}{\partial \mathbf{z}} - \rho_{\mathbf{p}} \frac{\partial^{2} \mathbf{u}_{\mathbf{z}}}{\partial \mathbf{r}^{2}} = 0 \tag{3.5}$$

$$pr - \sigma_{\theta} e - \left[\rho_{p} re + \rho_{f} \frac{r^{2}}{2} \right] \frac{\partial^{2} w}{\partial r^{2}} = 0$$
 (3.6)

in which $\rho_{\rm p}$ is the pipe wall density and e is the pipe wall thickness. The effect of the radial fluid acceleration appears as an added mass in the last term of Equation 3.6.

Equations 3.1 through 3.6 constitute the six-equation model. The radial inertia term is important when an excitation is approaching the first lobar mode of the cross section. Everstine, Marcus and Quezon [86] compared a one-dimensional finite element formulation with a three-dimensional one. The study showed that a one-dimensional finite element formulation of coupled pipe and liquid accurately predicts the dynamic responses up to the frequency of the first lobar mode. Therefore, neglecting the radial inertia term is accurate for frequencies below this mode. The expression for this lobar mode frequency is:

$$\omega_{\theta} = \frac{e}{r} \left[\frac{3E}{5\rho_{p}(1-\nu^{2})(1+\rho_{f}r/2\rho_{p}e)} \right]^{\frac{1}{2}}$$
 (3.7)

By neglecting the radial inertia term in Equation 3.6 the radial stress, σ_{g} , can be evaluated in terms of the fluid pressure:

$$\sigma_{\theta} = \frac{\text{pr}}{e} \tag{3.8}$$

The radial stress can be eliminated by combining Equations 3.4 and 3.8 and solving for the radial strain w/r

$$\frac{\mathbf{w}}{\mathbf{r}} = \frac{\mathbf{pr}}{\mathbf{E}^*} - \nu \frac{\partial \mathbf{u}_{\mathbf{z}}}{\partial \mathbf{z}} \tag{3.9}$$

Combining Equations 3.9 and 3.3 give the expression for the axial stress

$$\sigma_{z} - \nu \frac{\mathbf{r}}{\mathbf{e}} \mathbf{p} - \mathbf{E} \frac{\partial \mathbf{u}_{z}}{\partial z} = 0 \tag{3.10a}$$

Multiply the above equation by the pipe cross-sectional area $\mathbf{A}_{\mathbf{p}}$, to obtain the axial force, $\mathbf{f}_{\mathbf{z}}$

$$f_z - \nu A_p = p - EA_p \frac{\partial u_z}{\partial z} = 0$$
 (3.10b)

Differentiating Equation 3.9 with respect to time and combining it with Equation 3.1 produces the expression for the fluid pressure

$$\frac{\partial \mathbf{p}}{\partial \mathbf{z}} - 2\nu \mathbf{K}^* \frac{\partial^2 \mathbf{u}_z}{\partial \mathbf{t} \partial \mathbf{z}} + \mathbf{K}^* \frac{\partial^2 \mathbf{v}}{\partial \mathbf{t} \partial \mathbf{z}} = 0$$
 (3.11a)

where

$$K^* - \frac{K}{1 + \frac{2 K r}{E^* e}}$$
 (3.11b)

Equations 3.2b, 3.5, 3.10b and 3.11 constitute the four-equation model presented by Otwell [19], Wiggert et al., [20], Stuckenbruck et al., [21] and Budny [22]. These equations can be further reduced by differentiating Equations 3.2b and 3.5 with respect to the axial direction z, then differentiating Equations 3.10b and 3.11 with respect to time and combining them to solve for the axial force and fluid pressure.

$$a_{p}^{2} \frac{\partial^{2} f_{z}}{\partial z^{2}} - \frac{\partial^{2} f_{z}}{\partial z^{2}} + A_{p} \nu b \frac{\partial^{2} D}{\partial z^{2}} = 0$$
 (3.12)

$$a_{f}^{2} \frac{\partial^{2} p}{\partial z^{2}} - \frac{\partial^{2} p}{\partial t^{2}} + \frac{2\nu a_{f}^{2}}{A_{p} d} \frac{\partial^{2} f}{\partial z^{2}} = 0$$
 (3.13a)

where

$$a_f^2 - \frac{K^*}{\rho_f} \tag{3.13b}$$

$$a_p^2 - \frac{E}{\rho_p} \tag{3.13c}$$

$$b - \frac{r}{e} \tag{3.13d}$$

$$d = \frac{\rho_{\rm p}}{\rho_{\rm f}} \tag{3.13e}$$

In Equations 3.13b and 3.13c, af and a are the non-coupled fluid and axial pipe wall wave speeds, respectively, b is the pipe radius to wall thickness ratio and d is the density ratio. Equations 3.12 and 3.13a are second order partial differential equations in the fluid pressure and axial pipe wall force. They may be expressed in matrix form as:

$$\begin{bmatrix} \mathbf{a}_{\mathbf{p}}^{2} & 0 \\ \frac{2\nu}{d\mathbf{A}_{\mathbf{p}}} \mathbf{a}_{\mathbf{f}}^{2} & \mathbf{a}_{\mathbf{f}}^{2} \end{bmatrix} \frac{\partial^{2}}{\partial z^{2}} \begin{Bmatrix} \mathbf{f}_{\mathbf{z}} \\ \mathbf{p} \end{Bmatrix} - \begin{bmatrix} 1 & -\nu b \mathbf{A}_{\mathbf{p}} \\ 0 & 1 \end{bmatrix} \frac{\partial^{2}}{\partial \mathbf{t}^{2}} \begin{Bmatrix} \mathbf{f}_{\mathbf{z}} \\ \mathbf{p} \end{Bmatrix} = 0$$
 (3.14a)

A similar equation can be obtained for the axial pipe wall and fluid displacements by combining and solving Equations 3.2b, 3.5, 3.10b and 3.11.

$$\begin{bmatrix} 2\nu^{2}\frac{b}{d}a_{f}^{2} + a_{p}^{2} & -\nu\frac{b}{d}a_{f}^{2} \\ -\nu\frac{b}{d}a_{f}^{2} & \frac{b}{2d}a_{f}^{2} \end{bmatrix} \quad \frac{\partial^{2}}{\partial z^{2}} \left\{ \begin{array}{c} u_{z} \\ v \end{array} \right\} - \begin{bmatrix} 1 & 0 \\ 0 & \frac{b}{2d} \end{array} \right] \quad \frac{\partial^{2}}{\partial z^{2}} \left\{ \begin{array}{c} u_{z} \\ v \end{array} \right\} = 0 \quad (3.14b)$$

Poisson terms couple Equations 3.12 and 3.13a as shown by the off-diagonal elements of the matrices in Equations 3.14a and 3.14b.

The separation of variables technique [76] is used to solve for the force f_z and fluid pressure p in Equation 3.14a. Three steps are necessary to solve for the dependent variables in the above equation: 1) convert the partial differential equation into ordinary differential equation, 2) find solutions for the ordinary differential equation, and 3) find the constants of integration of the differential equation. The solution for the constants of integration will be postponed to the next chapter since they depend on the boundary conditions imposed on the piping system.

1) Separation of Variables

Assuming a harmonic oscillation for the time dependence, which is appropriate for oscillatory flow [41,71] and oscillatory structural motion in the axial direction [68], we can write:

$$f_z(z,t) = F_z(z) e^{j\omega t}$$
 (3.15)

$$p(z,t) - P(z) e^{j\omega t}$$
 (3.16)

where $F_z(z)$ and P(z) are functions of z only, ω is the oscillatory frequency and $j=(-1)^{\frac{1}{2}}$. Substituting the above equations into Equation 3.14 yields the ordinary differential equation in F_z and P:

$$\begin{bmatrix} \mathbf{a}_{\mathbf{p}}^{2} & 0 \\ \frac{2\nu}{d\mathbf{A}_{\mathbf{p}}} \mathbf{a}_{\mathbf{f}}^{2} & \mathbf{a}_{\mathbf{f}}^{2} \end{bmatrix} \begin{Bmatrix} \mathbf{F}_{\mathbf{z}}^{\mathbf{r}} \\ \mathbf{p}^{\mathbf{r}} \end{Bmatrix} + \omega^{2} \begin{bmatrix} 1 & -\nu b \mathbf{A}_{\mathbf{p}} \\ 0 & 1 \end{bmatrix} \begin{Bmatrix} \mathbf{F}_{\mathbf{z}} \\ \mathbf{p} \end{Bmatrix} - 0$$
 (3.17)

where $F_Z^{"}$ and $P^{"}$ are the derivatives with respect to the axial direction z. The elimination method [92] can be used to reduce Equation 3.17 to a single dependent variable. This procedure yields

$$F_z^{iv} + \frac{(\tau + \sigma + \gamma)}{\rho^4} F'' + \frac{\tau\sigma}{\rho^2} = 0$$
 (3.18a)

where ℓ is the length of a pipe reach and

$$\tau = \frac{\omega^2 \ell^2}{a_f^2}$$
 (3.18b)

$$\sigma = \frac{\omega^2 \ell^2}{a_p^2}$$
 (3.18c)

$$\gamma = 2\nu^2 \frac{b \omega^2 \ell^2}{d a_p^2}$$
 (3.18d)

Equation 3.18a is a fourth-order, ordinary differential equation with constant coefficients.

2) Solution of the Ordinary Differential Equation

The solutions for $\mathbf{F}_{\mathbf{z}}$ in Equation 3.18a is of the form

$$F_{z}(z) - \overline{A} e^{\lambda \ell}$$
 (3.19)

where \overline{A} is a constant.

Substitution of Equation 3.19 into 3.18a produces the characteristic equation in λ :

$$\lambda^{4} + (\tau + \sigma + \gamma) \lambda^{2} + \sigma \tau = 0 \tag{3.20}$$

where λ is the characteristic value. The roots of this equation are $\pm j\lambda_1$ and $\pm j\lambda_2$, where

$$\lambda_{1,2}^{2} = \frac{1}{2} \left\{ (\tau + \sigma + \gamma) \right\} \left[(\tau + \sigma + \gamma)^{2} - 4\sigma\tau \right]^{\frac{1}{2}}$$
 (3.21)

This equation can also be expressed as:

$$c_{f}^{2} = \frac{\omega^{2} \ell^{2}}{\lambda_{1}^{2}} = \frac{1}{2} \left\{ \left[a_{f}^{2} + a_{p}^{2} + 2\nu^{2} \frac{b}{d} a_{f}^{2} \right] - \left[\left[a_{f}^{2} + a_{p}^{2} + 2\nu^{2} \frac{b}{d} a_{f}^{2} \right]^{2} - 4a_{f}^{2} a_{p}^{2} \right]^{\frac{1}{2}} \right\}$$
(3.22)

$$c_{p}^{2} = \frac{\omega^{2} \ell^{2}}{\lambda_{2}^{2}} = \frac{1}{2} \left\{ \left[a_{f}^{2} + a_{p}^{2} + 2\nu^{2} \frac{b}{d} a_{f}^{2} \right] + \left[\left[a_{f}^{2} + a_{p}^{2} + 2\nu^{2} \frac{b}{d} a_{f}^{2} \right]^{2} - 4a_{f}^{2} a_{p}^{2} \right]^{\frac{1}{2}} \right\}$$
(3.23)

The above equations give the expressions for the coupled wave speeds. These coupled speeds are the same as those derived by Budny [22] using the method of characteristics. An inspection of Equations 3.22 and 3.23, assuming no coupling between liquid and pipe wall by neglecting the second order Poisson terms, yields

$$\left(\frac{\omega \ell}{\lambda_1}\right)^2 - a_f^2 \tag{3.24a}$$

$$\left(\frac{\omega \ell}{\lambda_2}\right)^2 - a_p^2 \tag{3.24b}$$

As noted by Stuckenbruck, et al., [21], Equation 3.24a is the classical fluid wave speed prediction [6] for a pipe anchored throughout against axial motion.

Placing Equation 3.21 into 3.19, the solution for $F_{7}(z)$ is:

$$F_{z}(z) = \overline{A}_{1} e^{j\lambda_{1} \frac{Z}{\ell}} + \overline{A}_{2} e^{-j\lambda_{1} \frac{Z}{\ell}} + \overline{A}_{3} e^{-j\lambda_{2} \frac{Z}{\ell}} + \overline{A}_{4} e^{-j\lambda_{2} \frac{Z}{\ell}}$$
 (3.25)

and using the relation

$$\begin{array}{cccc}
\pm j \left(\lambda_{\ell}^{Z}\right) \\
e & -\cos(\lambda_{\ell}^{Z}) \pm j\sin(\lambda_{\ell}^{Z})
\end{array} (3.26)$$

Equation 3.25 can be written in the following form

$$F_{z}(z) = A_{1}\cos(\lambda_{1}\frac{z}{\ell}) + A_{2}\sin(\lambda_{1}\frac{z}{\ell}) + A_{3}\cos(\lambda_{2}\frac{z}{\ell}) + A_{4}\sin(\lambda_{2}\frac{z}{\ell})$$
(3.27a)

where

$$A_1 = \overline{A}_1 + \overline{A}_2 \tag{3.27b}$$

$$A_2 = j(\overline{A}_1 - \overline{A}_2) \tag{3.27c}$$

$$A_3 = \overline{A}_3 + \overline{A}_4 \tag{3.27d}$$

$$A_4 = j(\overline{A}_3 - \overline{A}_4) \tag{3.27e}$$

3) Solution for the Constants of Integration

The solutions for the pipe wall and fluid displacements and the fluid pressure are of the same form as Equation 3.27a. To solve for the four dependent variables, the constants of integration A_1 , A_2 , A_3 and A_4 must have known values.

Expressing the axial and fluid displacements in similar forms as the force and fluid pressure in Equations 3.15 and 3.16 gives

$$u_z(z,t) = U_z(z) e^{j\omega t}$$
 (3.28)

$$v(z,t) = V(z) e^{j\omega t}$$
 (3.29)

Placing Equation 3.28 into 3.5 and combining with Equation 3.27a we obtain the solution for the axial displacement:

$$U_{Z}(z) = \frac{\ell}{A_{p}E\sigma} \left\{ \lambda_{1} \left[A_{1}\sin(\lambda_{1}\frac{Z}{\ell}) - A_{2}\cos(\lambda_{1}\frac{Z}{\ell}) \right] + \lambda_{2} \left[A_{3}\sin(\lambda_{2}\frac{Z}{\ell}) - A_{4}\cos(\lambda_{2}\frac{Z}{\ell}) \right] \right\}$$
(3.30)

The fluid pressure is obtained by placing Equations 3.27a and 3.30 into 3.10b

$$P(z) = \frac{1}{A_{p}\nu b\sigma} \left\{ (\sigma - \lambda_{1}^{2}) \left[A_{1}\cos(\lambda_{1}\frac{Z}{\ell}) + A_{2}\sin(\lambda_{1}\frac{Z}{\ell}) \right] + (\sigma - \lambda_{2}^{2}) \left[A_{3}\cos(\lambda_{2}\frac{Z}{\ell}) + A_{4}\sin(\lambda_{2}\frac{Z}{\ell}) \right] \right\}$$
(3.31)

Finally, the fluid displacement is obtained by placing Equations 3.29 and 3.31 into 3.2b

$$V(z) = \frac{-\ell}{A_{p}\nu b K^{*} \tau \sigma} \left\{ (\sigma - \lambda_{1}^{2}) \lambda_{1} \left[A_{1} \sin(\lambda_{1} \frac{Z}{\ell}) - A_{2} \cos(\lambda_{1} \frac{Z}{\ell}) \right] + (\sigma - \lambda_{2}^{2}) \lambda_{2} \left[A_{3} \sin(\lambda_{2} \frac{Z}{\ell}) - A_{4} \cos(\lambda_{2} \frac{Z}{\ell}) \right] \right\}$$
(3.32)

Arranging Equations 3.27a, 3.30, 3.31 and 3.32 into matrix form we obtain

$$\begin{cases}
U_{Z} \\
P \\
V \\
F_{Z}
\end{cases} =
\begin{bmatrix}
B_{1}\sin(\lambda_{1}\frac{Z}{\ell}) & -B_{1}\cos(\lambda_{1}\frac{Z}{\ell}) & B_{2}\sin(\lambda_{2}\frac{Z}{\ell}) & -B_{2}\cos(\lambda_{2}\frac{Z}{\ell}) \\
B_{3}\cos(\lambda_{1}\frac{Z}{\ell}) & B_{3}\sin(\lambda_{1}\frac{Z}{\ell}) & B_{4}\cos(\lambda_{2}\frac{Z}{\ell}) & B_{4}\sin(\lambda_{2}\frac{Z}{\ell}) \\
-B_{5}\sin(\lambda_{1}\frac{Z}{\ell}) & B_{5}\cos(\lambda_{1}\frac{Z}{\ell}) & -B_{6}\sin(\lambda_{2}\frac{Z}{\ell}) & B_{6}\cos(\lambda_{2}\frac{Z}{\ell}) \\
\cos(\lambda_{1}\frac{Z}{\ell}) & \sin(\lambda_{1}\frac{Z}{\ell}) & \cos(\lambda_{2}\frac{Z}{\ell}) & \sin(\lambda_{2}\frac{Z}{\ell})
\end{bmatrix}
\begin{cases}
A_{1} \\
A_{2} \\
A_{3} \\
A_{4}
\end{cases}$$
(3.33a)

where

$$B_1 = \frac{\ell \lambda_1}{A_p E \sigma} \tag{3.33b}$$

$$B_2 = \frac{\ell \lambda_2}{A_p E \sigma} \tag{3.33c}$$

$$B_{3} = \frac{\sigma - \lambda_{1}^{2}}{A_{p}\nu b\sigma}$$
 (3.33d)

$$B_4 = \frac{\sigma - \lambda_2^2}{A_D \nu b \sigma}$$
 (3.33e)

$$B_{\delta} = \frac{(\sigma - \lambda_1^2) \ell \lambda_1}{A_p \nu b K^* \tau \sigma}$$
 (3.33f)

$$B_6 = \frac{(\sigma - \lambda_2^2) \ell \lambda_2}{A_p \nu b K^* \tau \sigma}$$
 (3.33g)

Equation 3.33a will be the starting point of the next chapter. Solutions for the constants of integration of the axial waves equations will be derived.

3.2.2 Transverse Waves - Shear and Bending

The classical one-dimensional Bernoulli-Euler theory of flexural motions in elastic beams is inadequate to describe vibrations of higher modes as well as those beams where the effect of the cross-sectional dimensions on frequencies cannot be neglected [69]. Rayleigh [70] introduced the effect of rotatory inertia and Timoshenko [68,71,72] extended it to include the effect of transverse shear deformation. The equations that include these effects are generally referred to as the Timoshenko beam equations. The derivation of the equations for transverse vibrations in the x-z and y-z planes are presented following the sign convention in Figures 3.4 through 3.7.

3.2.2.1 Shear and Bending in x-z Plane

The derivation of the Timoshenko equations for the pipe reach in Figure 3.1, vibrating in the x-z plane, are based on the diagrams shown in Figures 3.4 and 3.5. Figure 3.4 shows that the slope of the center line of the pipe reach, $\frac{\partial u_x}{\partial z}$ is affected by both the bending moment and the shear force [50]. The action of the internal bending moment, m_y , rotates the face of the cross section through angle ψ_y . From there, the internal shearing force, f_x , turns the center line to adopt the slope $\frac{\partial u_x}{\partial z}$. The angle of the face of the pipe element remains unchanged. Inspection of Figure 3.4 shows that the angle between the line perpendicular to the face and the center line of the pipe element which is caused by the shear force is the shear angle, β_y :

$$\beta_{y} = \frac{\partial u_{z}}{\partial z} - \psi_{y} \tag{3.34}$$

The relation between this angle and the shear force causing it is:

$$f_x - GA_p \kappa_s \left[\frac{\partial u_x}{\partial z} - \psi_y \right] = 0$$
 (3.35a)

where

$$G = \frac{E}{2(1+\nu)} \tag{3.35b}$$

The shear modulus is G, the product $A_p \kappa_s$ represents the effective shear area of the section and κ_s is a factor depending on the shape of the cross section [73,74]. For a thin-walled tube κ_s is given by

$$\kappa_{\rm s} = \frac{2(1+\nu)}{4+3\nu} \tag{3.36}$$

The relation between the bending moment and cross-sectional rotation is given by elementary beam theory as:

$$\mathbf{m}_{\mathbf{y}} - \mathbf{E}\mathbf{I} \mathbf{p} \frac{\partial \psi_{\mathbf{y}}}{\partial z} = 0 \tag{3.37}$$

in which I_p is the second moment of inertia about the y-axis for the pipe wall. Equations 3.35a and 3.37 constitute elastic laws relating the deformations to the internal loading. Equilibrium considerations (Fig. 3.5) give the equations

$$\frac{\partial f_{x}}{\partial z} - (\rho_{p} A_{p} + \rho_{f} A_{f}) \frac{\partial^{2} u_{x}}{\partial t^{2}} = 0$$
 (3.38)

$$\frac{\partial \mathbf{m}_{\mathbf{y}}}{\partial \mathbf{z}} + \mathbf{f}_{\mathbf{x}} - (\rho_{\mathbf{p}} \mathbf{I}_{\mathbf{p}} + \rho_{\mathbf{f}} \mathbf{I}_{\mathbf{f}}) \frac{\partial^{2} \psi_{\mathbf{y}}}{\partial \mathbf{z}^{2}} = 0$$
 (3.39)

in which I is the second moment of inertia about the y-axis for the fluid. Equations 3.38 and 3.39 describe the translation and rotational

equilibrium, respectively. Solving for ψ_y and u_x in Equations 3.35a and 3.38, substituting the results in Equation 3.37 and eliminating m_y from Equation 3.39, we obtain a fourth-order partial differential equation in $f_y(z,t)$:

$$EI_{p} \frac{\partial^{4} f_{x}}{\partial z^{4}} + (\rho_{p} A_{p}^{+} \rho_{f} A_{f}) \frac{\partial^{2} f_{x}}{\partial z^{2}} - (\rho_{p} I_{p}^{+} \rho_{f} I_{f}) \frac{\partial^{4} f_{x}}{\partial z^{2}} + \frac{EI_{p}}{GA_{p} \kappa_{s}} \frac{\partial^{2}}{\partial z^{2}} \left[(\rho_{p} A_{p}^{+} \rho_{f} A_{f}) \frac{\partial^{2} f_{x}}{\partial z^{2}} \right] + \frac{(\rho_{p} A_{p}^{+} \rho_{f} A_{f})}{GA_{p} \kappa_{s}} \frac{\partial^{2} f_{x}}{\partial z^{2}} \left[(\rho_{p} A_{p}^{+} \rho_{f} A_{f}) \frac{\partial^{2} f_{x}}{\partial z^{2}} \right] - 0$$

$$(3.40)$$

The third term in the above equation corresponds to rotatory inertia, the fourth to shear deformation and the last term represents the combined influence of shear deformation and rotatory inertia [52]. By neglecting these three terms, we obtain the Bernoulli-Euler beam equation in the shear force $f_{\mathbf{y}}$,

$$EI_{p} \frac{\partial^{4} f_{x}}{\partial z^{4}} + (\rho_{p} A_{p} + \rho_{f} A_{f}) \frac{\partial^{2} f_{x}}{\partial t^{2}} = 0$$
(3.41)

The separation of variables technique is used to solve for the dependent variable f_x , in time, t, and axial direction z [50].

$$f_{x}(z,t) = F_{x}(z) e^{j\omega t}$$
 (3.42)

Substitution of the above equation into Equation 3.40 we obtain

$$\mathbf{F}_{\mathbf{X}}^{\mathbf{i}\mathbf{v}} + \frac{\sigma + \tau}{2} \mathbf{F}_{\mathbf{X}}^{\mathbf{n}} - \left[\frac{\gamma - \sigma \tau}{2} \right] \mathbf{F}_{\mathbf{X}} = 0$$
 (3.43a)

where

$$\sigma = \frac{(\rho_{\mathbf{p}} \mathbf{A}_{\mathbf{p}} + \rho_{\mathbf{f}} \mathbf{A}_{\mathbf{f}})}{G \mathbf{A}_{\mathbf{p}} \kappa_{\mathbf{s}}} \omega^{2} \ell^{2}$$
(3.43b)

$$\tau = \frac{(\rho_{\mathbf{p}} \mathbf{I}_{\mathbf{p}} + \rho_{\mathbf{f}} \mathbf{I}_{\mathbf{f}})}{\mathbf{E} \mathbf{I}_{\mathbf{p}}} \omega^{2} \ell^{2}$$
 (3.43c)

$$\gamma = \frac{(\rho_{\mathbf{p}} A_{\mathbf{p}} + \rho_{\mathbf{f}} A_{\mathbf{f}})}{\text{EI}_{\mathbf{p}}} \omega^{2} \ell^{4}$$
 (3.43d)

and ℓ is the length of the pipe reach.

Equation 3.43a is a fourth-order ordinary differential equation with constant coefficients whose solution is of the form

$$F_{x}(z) = \overline{A} e^{\lambda \frac{Z}{\ell}}$$
 (3.44)

where A is a constant.

Substitution of Equation 3.44 into 3.43a produces the characteristic equation in λ :

$$\lambda^{4} + (\sigma + \tau) \lambda^{2} - (\gamma - \sigma\tau) = 0 \tag{3.45}$$

The roots of this equation are $\pm \lambda_1$ and $\pm j \lambda_2$, where

$$\lambda_{1,2}^{2} = \left(\gamma + \frac{1}{4}(\sigma - \tau)^{2}\right)^{\frac{1}{2}} + \frac{1}{2}(\sigma + \tau)$$
 (3.46)

The solution of Equation 3.43a is

$$F_{x}(z) = \overline{A}_{1} e^{\lambda_{1} \frac{Z}{\ell}} + \overline{A}_{2} e^{-\lambda_{1} \frac{Z}{\ell}} + \overline{A}_{3} e^{-j\lambda_{2} \frac{Z}{\ell}} + \overline{A}_{4} e^{-j\lambda_{2} \frac{Z}{\ell}}$$
(3.47)

and using the relations

Equation 3.47 can be written in the following form

$$F_{\mathbf{X}}(z) = A_1 \cosh(\lambda_1 \frac{z}{\ell}) + A_2 \sinh(\lambda_1 \frac{z}{\ell}) + A_3 \cos(\lambda_2 \frac{z}{\ell}) + A_4 \sin(\lambda_2 \frac{z}{\ell}) \quad (3.49a)$$

where

$$A_1 = \overline{A}_1 + \overline{A}_2$$
 (3.49b)

$$A_2 = \overline{A}_1 - \overline{A}_2 \tag{3.49c}$$

$$A_3 = \overline{A}_3 + \overline{A}_4 \tag{3.49d}$$

$$A_4 = j(\bar{A}_3 - \bar{A}_4)$$
 (3.49e)

The solution for the other three dependent variables, My, ψ_y and Ux is based on the solution for Fy.

The solution for $U_{\chi}(z)$ can be found by substituting Equation 3.49a in Equation 3.38

$$U_{X}(z) = -\frac{\ell^{4}}{EI_{p}^{\gamma}} \left[A_{1} \frac{\lambda_{1}}{\ell} \sinh(\lambda_{1} \frac{z}{\ell}) + A_{2} \frac{\lambda_{1}}{\ell} \cosh(\lambda_{1} \frac{z}{\ell}) - A_{3} \frac{\lambda_{2}}{\ell} \sin(\lambda_{2} \frac{z}{\ell}) + A_{4} \frac{\lambda_{2}}{\ell} \cos(\lambda_{2} \frac{z}{\ell}) \right]$$

$$(3.50)$$

The solution for $\Psi_y(z)$ is obtained by placing Equations 3.49a and 3.50 into 3.35a

$$\Psi_{y}(z) = -\frac{\ell^{2}}{EI_{p}\gamma} \left\{ (\sigma + \lambda_{1}^{2}) \left[A_{1} \cosh(\lambda_{1} \frac{z}{\ell}) + A_{2} \sinh(\lambda_{1} \frac{z}{\ell}) \right] + (\sigma - \lambda_{2}^{2}) \left[A_{3} \cos(\lambda_{2} \frac{z}{\ell}) + A_{4} \sin(\lambda_{2} \frac{z}{\ell}) \right] \right\}$$

$$(3.51)$$

The expression for $M_y(z)$ is found placing Equation 3.51 into 3.37

$$M_{y}(z) = -\frac{\ell}{\gamma} \left\{ (\sigma + \lambda_{1}^{2}) \lambda_{1} \left[A_{1} \sinh(\lambda_{1} \frac{Z}{\ell}) + A_{2} \cosh(\lambda_{1} \frac{Z}{\ell}) \right] + (\lambda_{2}^{2} - \sigma) \lambda_{2} \left[A_{3} \sin(\lambda_{2} \frac{Z}{\ell}) - A_{4} \cos(\lambda_{2} \frac{Z}{\ell}) \right] \right\}$$

$$(3.52)$$

Arranging equations 3.49a through 3.52 into matrix form we obtain

$$\begin{bmatrix} \mathbf{U}_{\mathbf{X}} \\ \mathbf{\Psi}_{\mathbf{y}} \\ \mathbf{M}_{\mathbf{y}} \\ \mathbf{F}_{\mathbf{X}} \end{bmatrix} = \begin{bmatrix} -\mathbf{B}_{1} \sinh(\lambda_{1} \frac{\mathbf{Z}}{\ell}) & -\mathbf{B}_{1} \cosh(\lambda_{1} \frac{\mathbf{Z}}{\ell}) & \mathbf{B}_{2} \sin(\lambda_{2} \frac{\mathbf{Z}}{\ell}) & -\mathbf{B}_{2} \cos(\lambda_{2} \frac{\mathbf{Z}}{\ell}) \\ -\mathbf{B}_{3} \cosh(\lambda_{1} \frac{\mathbf{Z}}{\ell}) & -\mathbf{B}_{3} \sinh(\lambda_{1} \frac{\mathbf{Z}}{\ell}) & -\mathbf{B}_{4} \cos(\lambda_{2} \frac{\mathbf{Z}}{\ell}) & -\mathbf{B}_{4} \sin(\lambda_{2} \frac{\mathbf{Z}}{\ell}) \\ -\mathbf{B}_{5} \sinh(\lambda_{1} \frac{\mathbf{Z}}{\ell}) & -\mathbf{B}_{5} \cosh(\lambda_{1} \frac{\mathbf{Z}}{\ell}) & -\mathbf{B}_{6} \sin(\lambda_{2} \frac{\mathbf{Z}}{\ell}) & \mathbf{B}_{6} \cos(\lambda_{2} \frac{\mathbf{Z}}{\ell}) \\ \cos(\lambda_{1} \frac{\mathbf{Z}}{\ell}) & \sin(\lambda_{1} \frac{\mathbf{Z}}{\ell}) & \sin(\lambda_{2} \frac{\mathbf{Z}}{\ell}) \end{bmatrix} \begin{bmatrix} \mathbf{A}_{1} \\ \mathbf{A}_{2} \\ \mathbf{A}_{3} \\ \mathbf{A}_{4} \end{bmatrix}$$

$$(3.53a)$$

where

$$B_1 = \frac{\ell^3}{EI_p \gamma} \lambda_1 \tag{3.53b}$$

$$B_2 = \frac{\ell^3}{EI_p \gamma} \lambda_2 \tag{3.53c}$$

$$B_3 = \frac{\ell^2}{EI_p \gamma} (\sigma + \lambda_1^2)$$
 (3.53d)

$$B_4 = \frac{\ell^2}{EI_{p\gamma}} (\sigma - \lambda_2^2)$$
 (3.53e)

$$B_{\delta} = \frac{\ell}{\gamma} \left(\sigma + \lambda_1^2 \right) \lambda_1 \tag{3.53f}$$

$$B_6 = \frac{\ell}{\gamma} (\lambda_2^2 - \sigma) \lambda_2 \qquad (3.53g)$$

The solution for the constants of integration is given in the next chapter.

3.2.2.2 Shear and Bending in y-z Plane

The procedure to derive Timoshenko's beam equation in the y-z plane for the pipe element shown in Figures 3.6 and 3.7 is the same as described in the previous section. The only differences arise in the sign convention.

The shear angle is given by:

$$\beta_{x} - \frac{\partial u_{y}}{\partial z} + \psi_{x} \tag{3.54}$$

The relation between this angle and the shear force is:

$$f_y - GA_p \kappa_s \left[\frac{\partial u_y}{\partial z} + \psi_x \right] = 0$$
 (3.55)

The bending relation is:

$$m_{x} - EI_{p} \frac{\partial \psi_{x}}{\partial z} = 0 \tag{3.56}$$

Equilibrium considerations (Fig 3.7) give the equations

$$\frac{\partial \mathbf{f}_{\mathbf{y}}}{\partial \mathbf{z}} - (\rho_{\mathbf{p}} \mathbf{A}_{\mathbf{p}} + \rho_{\mathbf{f}} \mathbf{A}_{\mathbf{f}}) \frac{\partial^{2} \mathbf{u}_{\mathbf{y}}}{\partial \mathbf{z}^{2}} = 0$$
 (3.57)

$$\frac{\partial \mathbf{m}_{\mathbf{x}}}{\partial \mathbf{z}} - \mathbf{f}_{\mathbf{y}} - (\rho_{\mathbf{p}} \mathbf{I}_{\mathbf{p}} + \rho_{\mathbf{f}} \mathbf{I}_{\mathbf{f}}) \frac{\partial^{2} \psi_{\mathbf{x}}}{\partial \mathbf{t}^{2}} - 0$$
 (3.58)

Combining Equations 3.55 through 3.58 gives the fourth-order partial differential equation in the lateral displacement $f_v(z,t)$:

$$\mathrm{EI}_{p} \frac{\partial^{4} \mathbf{f}_{y}}{\partial z^{4}} + (\rho_{p} \mathbf{A}_{p} + \rho_{\mathbf{f}} \mathbf{A}_{\mathbf{f}}) \frac{\partial^{2} \mathbf{f}_{y}}{\partial z^{2}} - (\rho_{p} \mathbf{I}_{p} + \rho_{\mathbf{f}} \mathbf{I}_{\mathbf{f}}) \frac{\partial^{4} \mathbf{f}_{y}}{\partial z^{2}} + \frac{\mathrm{EI}_{p}}{G \mathbf{A}_{p} \kappa_{s}} \frac{\partial^{2}}{\partial z^{2}} \left[(\rho_{p} \mathbf{A}_{p} + \rho_{\mathbf{f}} \mathbf{A}_{\mathbf{f}}) \frac{\partial^{2} \mathbf{f}_{y}}{\partial z^{2}} \right]$$

$$+\frac{(\rho_{\mathbf{p}}^{\mathbf{A}}\mathbf{p}^{+\rho}\mathbf{f}^{\mathbf{A}}\mathbf{f})}{G\mathbf{A}_{\mathbf{p}}\kappa_{\mathbf{s}}}\frac{\partial^{2}}{\partial t^{2}}\left[(\rho_{\mathbf{p}}^{\mathbf{A}}\mathbf{p}^{+\rho}\mathbf{f}^{\mathbf{A}}\mathbf{f})\frac{\partial^{2}\mathbf{f}_{\mathbf{y}}}{\partial t^{2}}\right]-0$$
(3.59)

The solution for the constants of integration is of the same form as for the shear and bending in the x-z plane. The change in the sign of the shear angle $\beta_{\rm X}$ determines sign changes in the rotation and bending moment, whereas the shear force and lateral displacement remain the same. Equation 3.53a becomes:

$$\begin{bmatrix} \mathbf{U}_{\mathbf{y}} \\ \mathbf{\Psi}_{\mathbf{x}} \\ \mathbf{H}_{\mathbf{x}} \\ \mathbf{F}_{\mathbf{y}} \end{bmatrix} = \begin{bmatrix} -\mathbf{B}_{1} \sinh(\lambda_{1} \frac{\mathbf{Z}}{\ell}) & -\mathbf{B}_{1} \cosh(\lambda_{1} \frac{\mathbf{Z}}{\ell}) & \mathbf{B}_{2} \sin(\lambda_{2} \frac{\mathbf{Z}}{\ell}) & -\mathbf{B}_{2} \cos(\lambda_{2} \frac{\mathbf{Z}}{\ell}) \\ \mathbf{B}_{3} \cosh(\lambda_{1} \frac{\mathbf{Z}}{\ell}) & \mathbf{B}_{3} \sinh(\lambda_{1} \frac{\mathbf{Z}}{\ell}) & \mathbf{B}_{4} \cos(\lambda_{2} \frac{\mathbf{Z}}{\ell}) & \mathbf{B}_{4} \sin(\lambda_{2} \frac{\mathbf{Z}}{\ell}) \\ \mathbf{B}_{5} \sinh(\lambda_{1} \frac{\mathbf{Z}}{\ell}) & \mathbf{B}_{5} \cosh(\lambda_{1} \frac{\mathbf{Z}}{\ell}) & \mathbf{B}_{6} \sin(\lambda_{2} \frac{\mathbf{Z}}{\ell}) & -\mathbf{B}_{6} \cos(\lambda_{2} \frac{\mathbf{Z}}{\ell}) \\ \cos(\lambda_{1} \frac{\mathbf{Z}}{\ell}) & \sinh(\lambda_{1} \frac{\mathbf{Z}}{\ell}) & \sin(\lambda_{2} \frac{\mathbf{Z}}{\ell}) & \sin(\lambda_{2} \frac{\mathbf{Z}}{\ell}) \end{bmatrix} \begin{bmatrix} \mathbf{A}_{1} \\ \mathbf{A}_{2} \\ \mathbf{A}_{3} \\ \mathbf{A}_{4} \end{bmatrix}$$

$$(3.60)$$

where the coefficients of the matrix are given in Equations 3.53b through 3.53g.

3.2.3 Torsion About z-axis

Figure 3.8 illustrates the internal moment, m_Z , acting on the pipe section and the rotation about the z-axis ψ_Z . The equilibrium condition is given by:

$$\frac{\partial \mathbf{m}_{\mathbf{z}}}{\partial \mathbf{z}} - \rho_{\mathbf{p}} J_{\mathbf{p}} \frac{\partial^{2} \psi_{\mathbf{z}}}{\partial \mathbf{t}^{2}} = 0 \tag{3.61}$$

From the elastic properties we obtain

$$\mathbf{m}_{\mathbf{z}} - \mathbf{GJ}_{\mathbf{p}} \frac{\partial \psi_{\mathbf{z}}}{\partial \mathbf{z}} = 0 \tag{3.62}$$

in which J_p is the polar moment of inertia for the pipe wall. Combining Equations 3.61 and 3.62 the wave equation for the moment $m_z(z,t)$ is:

$$\frac{\partial^2 \mathbf{m}_{\mathbf{z}}}{\partial z^2} - \frac{\rho_{\mathbf{D}}}{G} \frac{\partial^2 \mathbf{m}_{\mathbf{z}}}{\partial z^2} = 0 \tag{3.63}$$

The separation of variables can be used to solve for $\mathbf{m}_{\mathbf{Z}}$ in the above equation.

$$m_z(z,t) - M_z(z)e^{j\omega t}$$
 (3.64)

Substitution of the above equation into 3.63 yields

$$M_{Z}^{"} + \frac{\gamma}{2} M_{Z} = 0$$
 (3.65a)

where

$$\gamma = \frac{\rho_{\rm D}}{G} \omega^2 \ell^2 \tag{3.65b}$$

The solution of Equation 3.65a is of the form

$$M_{z}(z) - \bar{A} e^{\lambda \bar{l}}$$
 (3.66)

Placing the above equation into 3.65a yields the characteristic equation in λ :

$$\lambda^2 + \gamma = 0 \tag{3.67}$$

The roots of this equation are $\pm j\lambda$ where

$$\lambda = \pm \left[\gamma \right]^{1_2} = \pm \omega \ell \left[\frac{\rho_{\mathbf{p}}}{G} \right]^{1_2} \tag{3.68}$$

Placing the characteristic value λ in Equation 3.66, the solution for $M_{_{\hbox{\scriptsize Z}}}$ is

$$M_{z}(z) - \bar{A}_{1}e^{j\lambda_{\ell}^{z}} + \bar{A}_{2}e^{-j\lambda_{\ell}^{z}}$$
(3.69)

using the relation in Equation 3.26, the above equation becomes

$$M_{z}(z) = A_{1}\cos(\lambda_{g}^{Z}) + A_{2}\sin(\lambda_{g}^{Z})$$
 (3.70)

Where A_1 and A_2 are given in Equations 3.27b and 3.27c.

The solution of the rotation Ψ_{Z} about the z-axis is found by placing Equation 3.70 into 3.61 and using

$$\psi_{z}(z,t) = \Psi_{z}(z)e^{j\omega t}$$
 (3.71)

we obtain

$$\Psi_{\mathbf{Z}}(z) = \frac{\lambda}{\rho_{\mathbf{p}} J_{\mathbf{p}} \ell} \left[A_{1} \sin(\lambda \frac{\mathbf{Z}}{\ell}) - A_{2} \cos(\lambda \frac{\mathbf{Z}}{\ell}) \right]$$
(3.72)

Equation 3.70 and 3.72 can be arranged in matrix form as

The matrix Equations 3.33a, 3.53a, 3.60 and 3.73 constitute the starting point to derive the field transfer matrices in the next chapter.

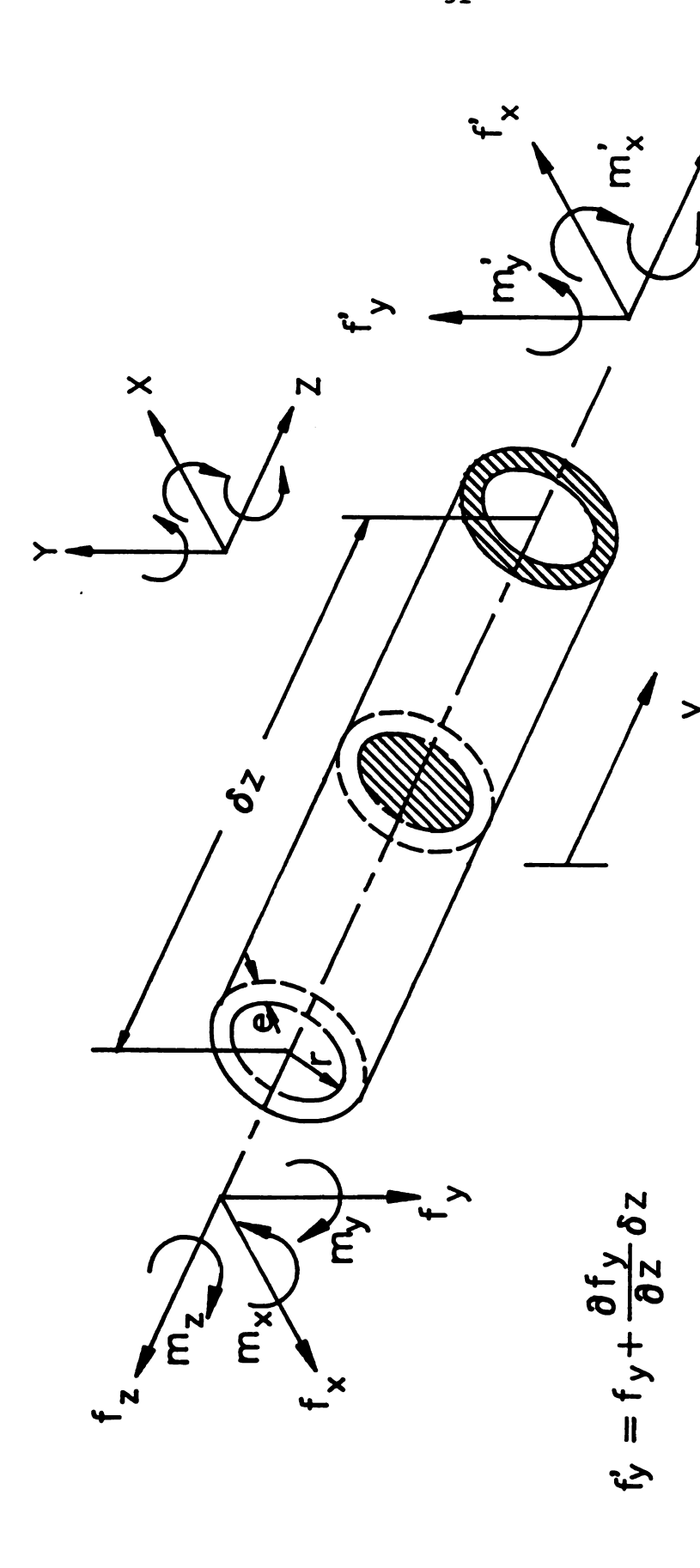


Figure 3.1 Sign Convention for Internal Forces

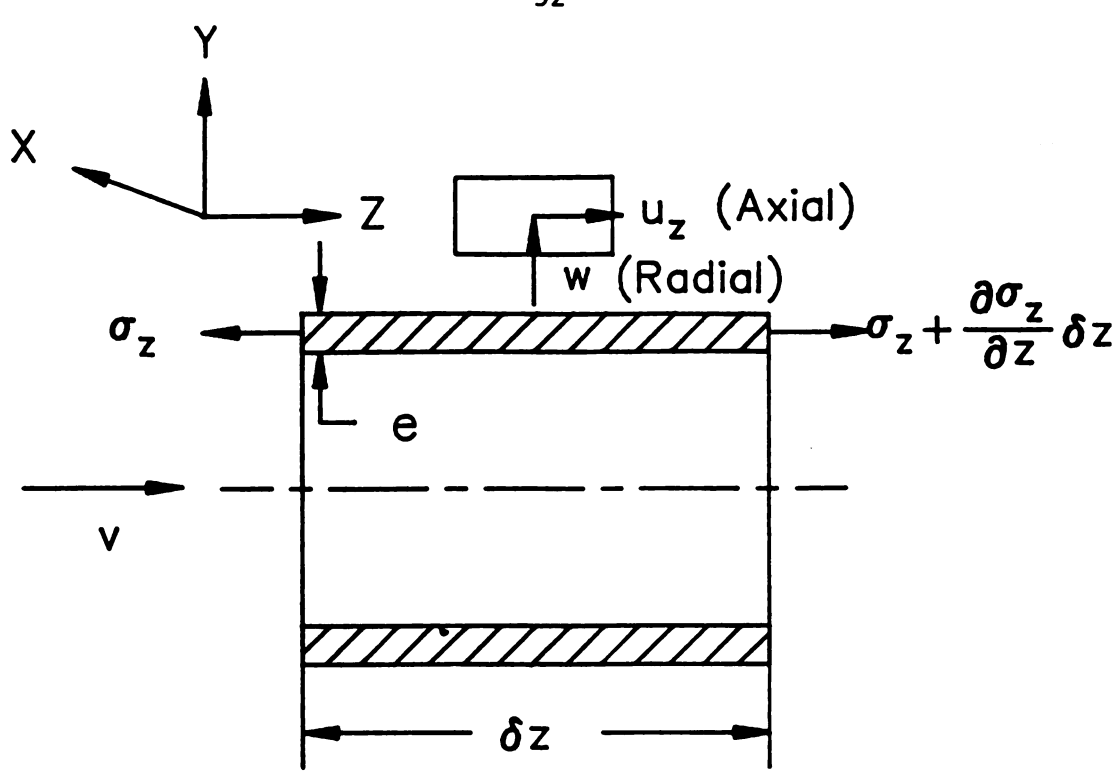


Figure 3.2 Axial Pipe Element

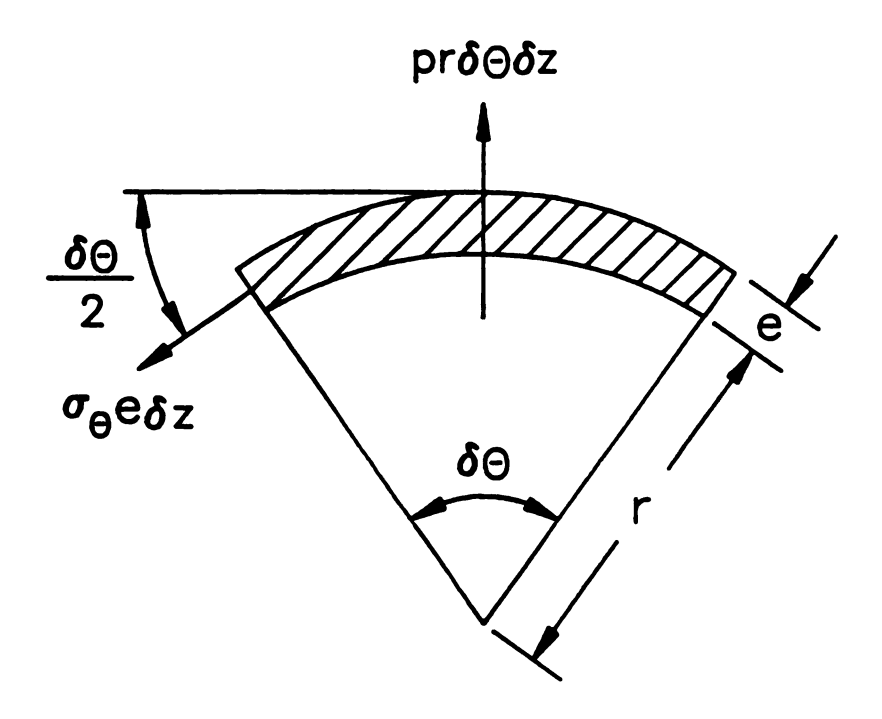


Figure 3.3 Radial Pipe Element

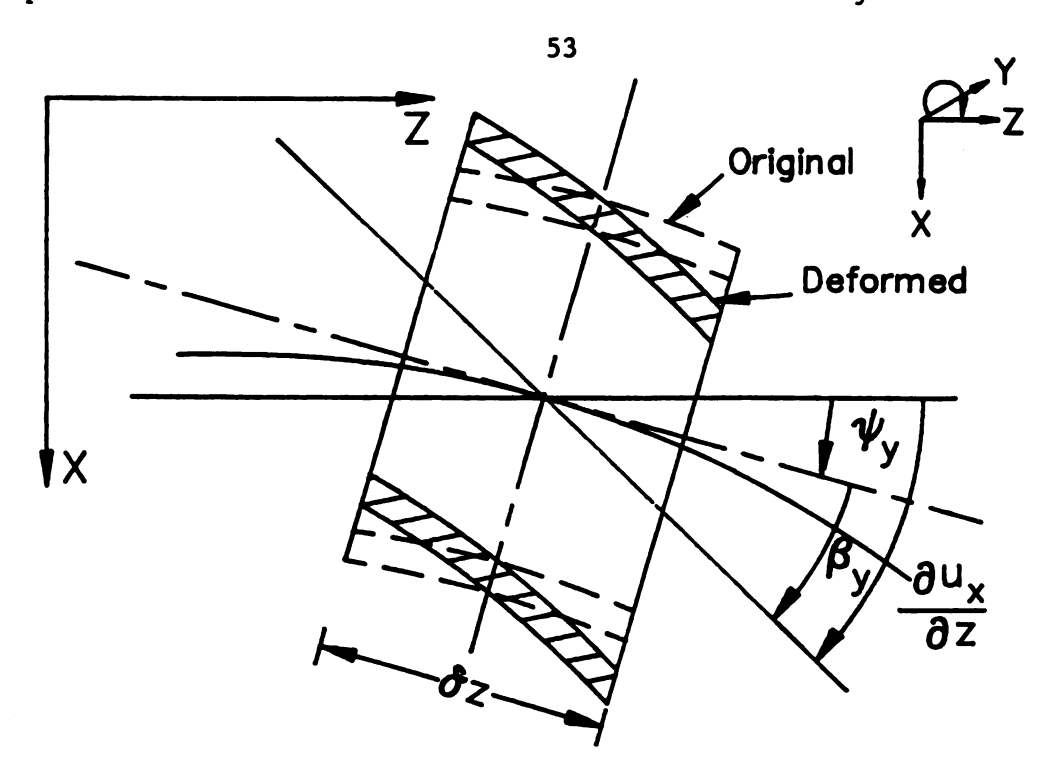


Figure 3.4 Deformations for Transverse Vibration in x-z Plane

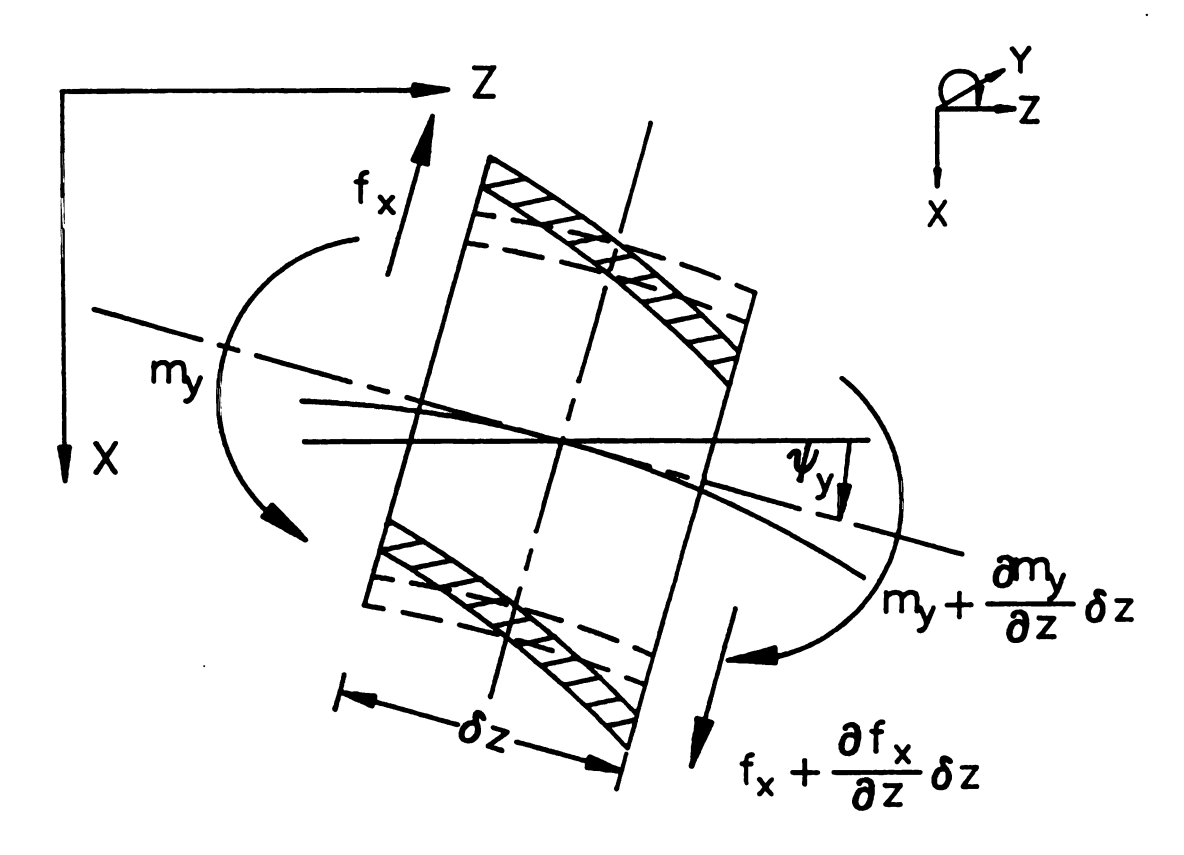


Figure 3.5 Internal Forces for Transverse Vibration in x-z Plane

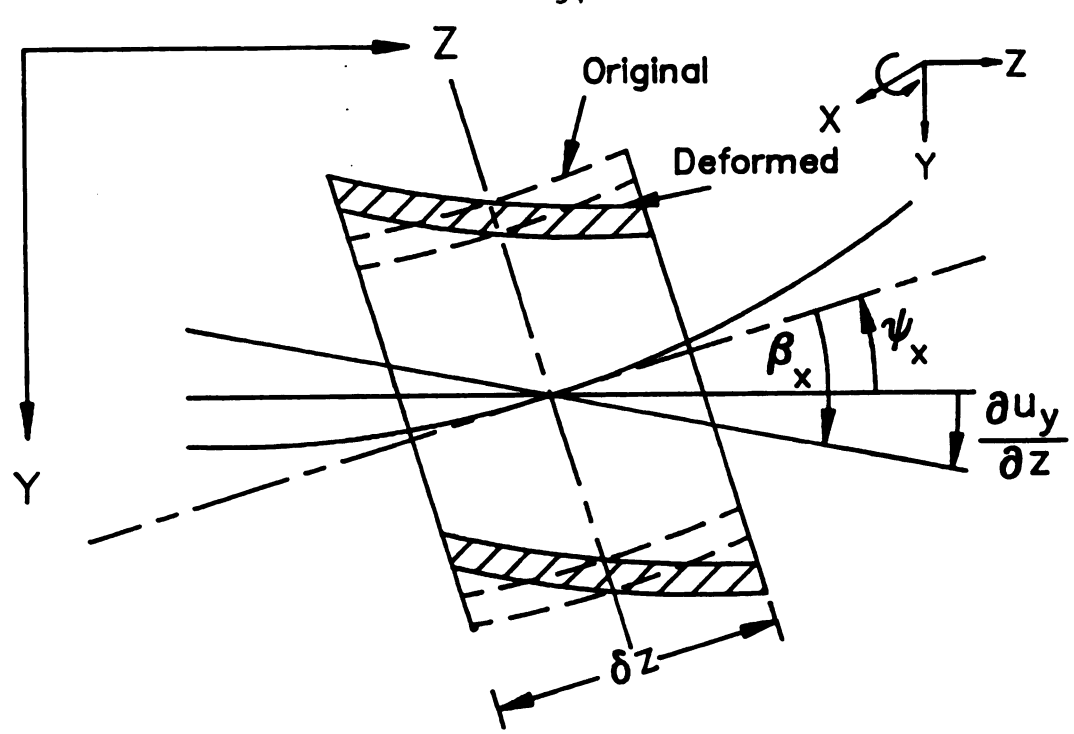


Figure 3.6 Deformations for Transverse Vibration in y-x Plane

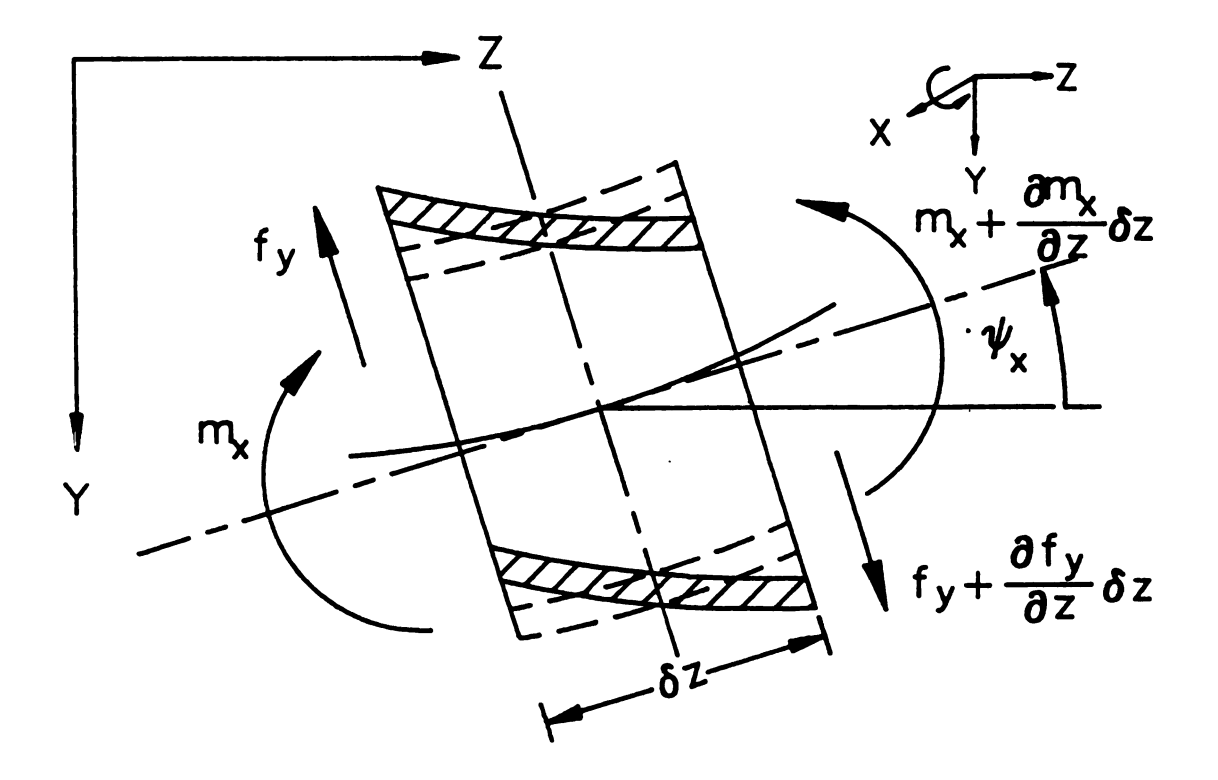


Figure 3.7 Internal Forces for Transverse Vibration in y-z Plane

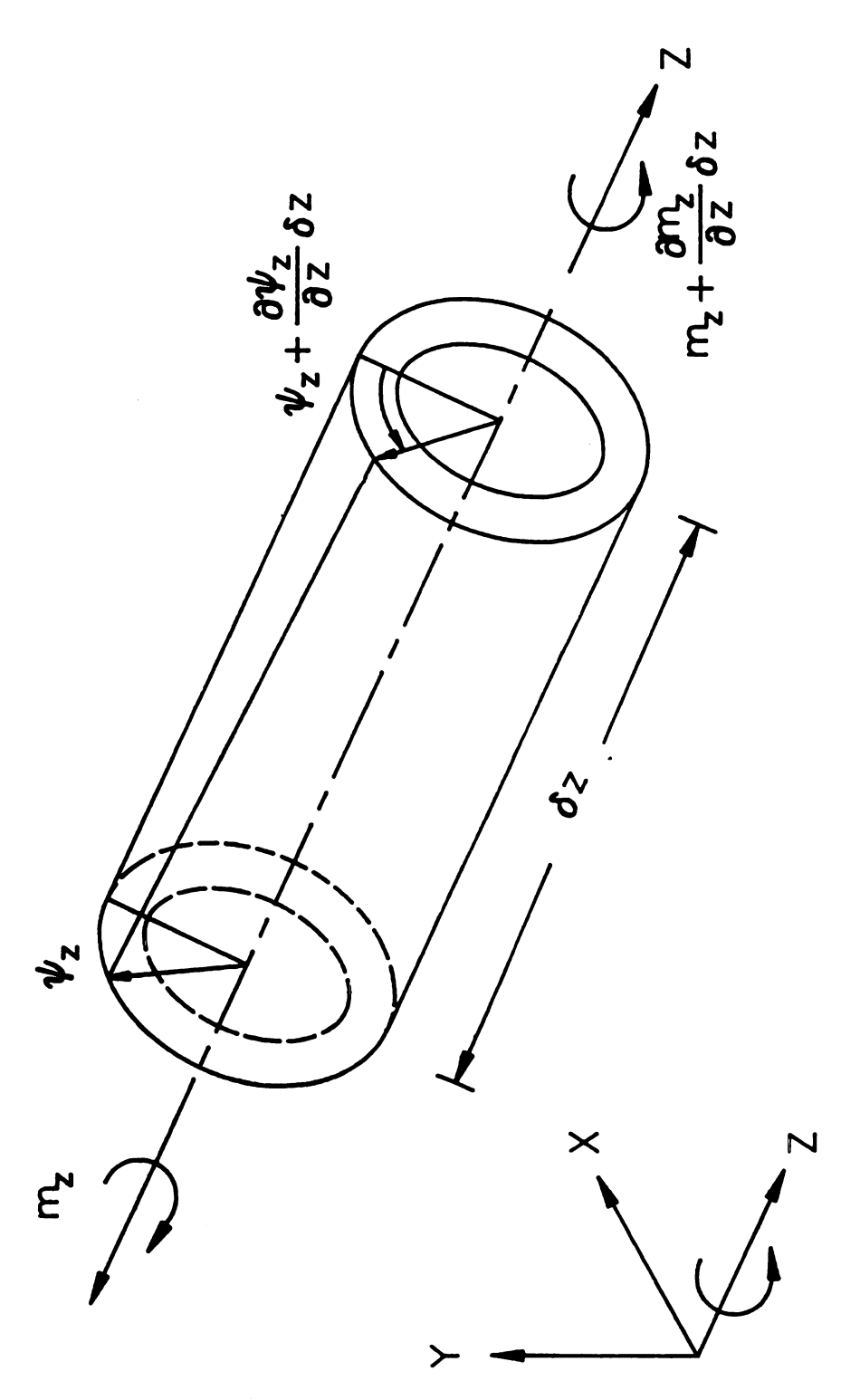


Figure 3.8 Pipe Reach Subjected to Torsion

CHAPTER 4

NUMERICAL SIMULATION

4.1 Introduction

The equations that describe the motion of five families of waves were derived in the previous chapter. The separation of variables technique was used to solve for forces and displacements. The solutions for the constants of integration of the equations of motion are the connecting point between this chapter and the previous one. The solution for the constants of integration are derived in a general form based on the end points of a pipe reach. Once these constants are known for each family of waves, the transfer matrix is assembled. The transfer matrix method is used to find the frequency response of liquid-filled pipe systems. This chapter gives a description of this method and presents comparisons with other numerical methods such as the method of characteristics and the component synthesis method.

4.2 Transfer Matrix Method

The transfer matrix method is the systemization of the Holzer and Myklestad procedures [50,52,53,54]. Holzer applied the method to torsional systems, whereas Myklestad applied it to bending vibrations of bars. Both methods calculate the natural frequencies and mode shapes of the system. This is done by assuming a frequency and starting with a unit amplitude at one end of the system and systematically calculating the responses at the other end. The frequencies that satisfy the required boundary condition at the other end are the natural frequencies of the system. Their findings are based on the fact that when an undamped system is vibrating freely at any one of its natural frequencies, no external force, torque or moment is necessary to maintain the vibration. Also, the amplitude of the mode shape is immaterial to the vibration [53]. These two methods have been applied to lumped mass systems. The masses are lumped at discrete points of the system called stations and the portion between the lumped masses is assumed massless and of uniform stiffness.

The transfer matrix method is suitable for the analysis of large liquid-filled piping systems made up of subsystems such as pipe links, snubbers, springs, concentrated masses, rigid supports, valves, pumps, orifices, and the like. Each subsystem is modeled as simple elastic and dynamic elements described by a field matrix and a point matrix. At the stations, the displacements and internal forces of the systems are arranged in a state vector. The overall transfer matrix is assembled by the systematic multiplication of the field and point matrices.

The advantages of this method are:

- 1. The assembly of complex, branched, parallel, and series systems is suitable for digital computation,
- Boundary conditions at the ends and at intermediate points in a system are easy to identify and model,
- 3. The method can be applied to piping systems of non-uniform cross sections.
- 4. The stability of a system can be checked by the root locus technique [7],
- 5. Systems with more than two dependent variables can be analyzed, since the size of the matrices does not depend on the number of subsystems but rather on the order of the differential equations governing the systems behavior,
- 6. The method can be extended to stability problems such as flow induced vibrations and damped vibrations,
- 7. External excitation of the system can be modeled by the extended field, point, and global matrix and extended state vector, and
- 8. The method can be used to model systems as discrete parameter or distributed parameter systems.

4.2.1 Description of Transfer Matrix Approach

The procedure to implement the transfer matrix method is illustrated using a spring-mass system [50] in Figure 4.1. The state vector at point i is a column vector whose elements are the various displacements, linear or rotary, of the point i and the corresponding internal forces.

In the system shown in Figure 4.1, the state vector $\{Z\}_i$ at point i is comprised of the linear displacement z_i and the spring force f_i :

A field transfer matrix relates the state vectors at two locations in a system. Equilibrium conditions can be used to obtain the field matrix of the system. Thus, the displacements and forces to the left of mass $\mathbf{m_i}$ denoted as $\{\mathbf{Z}\}_{\mathbf{i}}^{\mathbf{L}}$ are related to the forces and displacements to the right of mass $\mathbf{m_{i-1}}$ denoted as $\{\mathbf{Z}\}_{\mathbf{i-1}}^{\mathbf{R}}$ by means of the matrix $[\mathbf{T}]_{\mathbf{i}}$, called the field matrix.

Equilibrium of the massless spring (Figure 4.2a) is expressed

$$\mathbf{f}_{i-1}^{R} - \mathbf{f}_{i}^{L} \tag{4.2}$$

Also,

$$z_{i} = z_{i-1} + \frac{f_{i-1}^{R}}{k_{i}}$$
 (4.3)

The above equations can be expressed in matrix form as:

$$\left\{ \begin{array}{l} z \\ f \end{array} \right\}_{i}^{L} - \left[\begin{array}{cc} 1 & \frac{1}{k_{i}} \\ 0 & 1^{i} \end{array} \right] \left\{ \begin{array}{c} z \\ f \end{array} \right\}_{i-1}^{R}$$
 (4.4a)

$$(Z)_{i}^{L} - [T]_{i}(Z)_{i-1}^{R}$$
 (4.4b)

In the same form, the state vectors to the left and right of mass m_i are related by matrix $[P]_i$ called the point matrix. This is possible because the transfer between the two adjacent state vectors is over a point. Assuming the system is vibrating with a frequency ω the following equation of motion is obtained, (Fig. 4.2b).

$$f_i^R - f_i^L - m_i \omega^2 z_i \tag{4.5}$$

Also, by continuity and since the mass is rigid,

$$z_i^R - z_i^L \tag{4.6}$$

The last two equations can be expressed in matrix notation as:

$$\left\{ \begin{array}{c} \mathbf{z} \\ \mathbf{f} \end{array} \right\}_{\mathbf{i}}^{\mathbf{R}} - \left[\begin{array}{cc} 1 & \mathbf{z} & 0 \\ -\mathbf{m}_{\mathbf{i}} \boldsymbol{\omega} & 1 \end{array} \right] \left\{ \begin{array}{c} \mathbf{z} \\ \mathbf{f} \end{array} \right\}_{\mathbf{i}}^{\mathbf{L}}$$
 (4.7a)

or

$$(\mathbf{Z})_{i}^{R} - [\mathbf{P}]_{i} (\mathbf{Z})_{i}^{L}$$
 (4.7b)

Combining Equations 4.4b and 4.7b renders

$$\{z\}_{i}^{R} - [P]_{i}[T]_{i}\{z\}_{i-1}^{R}$$
 (4.8)

Following a similar procedure, the state vector at the end of a system (Figure 4.1) consisting of n number of springs and masses, joined end-to-end can be related by multiplying together the various field and point matrices in the proper order. Thus,

$$\{Z\}_{n}^{R} - [P]_{n}[T]_{n}[P]_{n-1}[T]_{n-1}...[P]_{1}[T]_{1}\{Z\}_{0}^{R} - [U]\{Z\}_{0}^{R}$$
 (4.9a)

where [U] is the overall transfer matrix of the system

$$[\mathbf{U}] - \mathbf{I}[\mathbf{P}]_{\mathbf{i}}[\mathbf{T}]_{\mathbf{i}} \tag{4.9b}$$

Once the overall transfer matrix of the system is obtained, the natural frequencies can be found by applying the boundary conditions. This is shown for a simple spring-mass system in Figure 4.3. The global transfer matrix of this system is:

$$[\mathbf{U}] = [\mathbf{P}]_{1}[\mathbf{T}]_{1} = \begin{bmatrix} 1 & 0 \\ -m_{1}\omega^{2} & 1 \end{bmatrix} \begin{bmatrix} 1 & \frac{1}{k_{1}} \\ 0 & 1 \end{bmatrix} = \begin{bmatrix} 1 & 1/k_{1} \\ -m_{1}\omega^{2} & (1-m\omega^{2}/k_{1}) \end{bmatrix}$$
(4.10)

The boundary conditions, $f_1 = 0$ and $z_0 = 0$ and the overall transfer matrix form the general equation for the system:

$$\left\{ \begin{array}{c} \mathbf{z} \\ \mathbf{0} \end{array} \right\}_{\mathbf{1}} - \left[\mathbf{v} \right] \left\{ \begin{array}{c} \mathbf{0} \\ \mathbf{f} \end{array} \right\}_{\mathbf{0}} \tag{4.11}$$

which gives the frequency equation

$$0 - 0 + (1 - \frac{m\omega}{k}) f_0$$
 (4.12)

The well-known frequency of a single spring-mass system is, thus, derived as:

$$\omega = \left(\frac{k}{m}\right)^{k_2} \tag{4.13}$$

This procedure can be used for more complicated systems providing the field and point matrices for each subsystem are known.

Figure 4.4 shows a liquid-filled piping system composed of straight links and subsystems such as point masses, springs, and supports that suppress the pipe motion partially or totally. These subsystems connect to and have an effect on the response of the pipe wall. A constant-pressure reservoir and a closed valve affect the behavior of the liquid. To find the natural frequencies of this system, the field matrices for straight pipe links, and the point matrices defined where there are bends, springs, point masses, and supports, must be known. The following sections will explain the derivation of these matrices.

The field matrix for a straight pipe reach is composed of four submatrices representing the vibrations of the liquid and axial pipe wall, shear and bending in the x-z plane and in the y-z plane and torsion about the z-axis. Expressions for each submatrix are given. The field transfer matrix derivation for the liquid and axial pipe wall vibration is presented in detail. The field matrices for the transverse and torsional vibrations were obtained by Pestel and Leckie [50]. Their derivation is presented for completeness. Point matrices for springs, concentrated masses and bends are also presented. Point and field matrices for each subsystem are derived with respect to a local rectangular coordinate system, x,y,z. Transformation matrices to express these matrices in a global coordinate system, X,Y,Z are also presented. Supports, reservoirs and closed valves are treated as boundary conditions.

4.2.2 Field Transfer Matrices

As mentioned earlier, the field transfer matrix expresses the forces and displacements at one section of a chain-type structure in terms of the corresponding forces and displacements at an adjacent section. For a discrete system, field matrices provide for transfer across the elastic segments between the masses [52,53,54]. To and Kaladi [62] and Wilkinson [64] use a distributed parameter approach to derive the field transfer matrices for fluid-structure interaction problems. Wylie and Streeter [8], and Chaudhry [7] use this approach for oscillatory flow problems.

The derivation of the field matrices for a distributed parameter model involves three steps: 1) converting the partial differential equations of motion into one ordinary differential equation, 2) finding solutions for the differential equation, and 3) finding the constants of integration of the differential equation. Steps one and two are developed in Chapter 3. The constants of integration are left in matrix form for each family of waves in section 3.2. These constants are solved as function of the state vector at the end points of the pipe reach of length & shown in Figure 4.5. A general procedure that can be applied to any of the matrices of the previous chapter is presented. Either one of the matrix Equations 3.33a, 3.53a, 3.60 or 3.73 can be represented as:

$$Z(z) = [B(z)] A$$
 (4.14)

where Z(z) is the state vector representing the dependent variables of any one of the above equations, B(z) is a matrix that depends on the geometry of the pipe wall and material properties, and A is a vector containing the constants of integration.

At point z = 0 in Fig. 4.5, $Z(z) = Z_{i-1}$, the matrix Equation 4.14 becomes

$$Z_{i-1} - [B(0)] A$$
 (4.15)

Solving for the column vector A in the above equation

$$A - [B(0)]^{-1} Z_{i-1}$$
 (4.16)

Substituting Equation 4.16 into Equation 4.14 yields

$$Z(z) = [B(z)] [B(0)]^{-1} Z_{i-1}$$
 (4.17)

At point z - l, $Z(z) - Z_i$, so Equation 4.17 becomes

$$Z_{i} - [B(l)] [B(0)]^{-1} Z_{i-1} - [T] Z_{i-1}$$
 (4.18)

where [T] is the field transfer matrix. The field transfer matrix for each one of the family of waves is presented next.

4.2.2.1 Liquid and Axial Pipe Wall Vibration

Equation 4.18 for the liquid and axial pipe wall vibration becomes

$$\mathbf{Z_{i}} - [\mathbf{T_{fp}}]_{i}\mathbf{Z_{i-1}} \tag{4.19a}$$

where

$$[T_{fp}] - [B(l)] [B(0)]^{-1}$$
 (4.19b)

The matrices [B(0)] and [B(l)] are obtained from the matrix of Equation 3.33a evaluated at locations i-1 and i in Figure 4.5, respectively. The non-dimensional representation of the field transfer matrix and state vector are

$$\begin{bmatrix} \sigma C_2 - C_0 & \frac{\nu b}{h} [C_1 - (\sigma + \tau + \gamma) C_3] & \frac{\nu b}{h} \tau C_2 & -C_1 + (\sigma + \gamma) C_3 \\ 2\nu \sigma \tau C_3 & (\tau + \gamma) C_2 - C_0 & \tau [(\tau + \gamma) C_3 - C_1] & -2\nu \tau C_2 \\ 2\nu \sigma C_2 & \frac{1}{\tau} \Big[(\tau + \gamma) C_1 - [(\tau + \gamma)^2 + \sigma \gamma] C_3 \Big] & (\tau + \gamma) C_2 - C_0 & 2\nu [(\sigma + \tau + \gamma) C_3 - C_1] \\ \sigma (C_1 - \sigma C_3) & -\frac{\nu b}{h} \sigma C_2 & -\frac{\nu b}{h} \sigma \tau C_3 & \sigma C_2 - C_0 \end{bmatrix}$$

$$(4.20)$$

where

$$\tau = \frac{\omega^2 \ell^2}{a_f^2} \tag{4.21a}$$

$$\sigma = \frac{\omega^2 \ell^2}{a_p^2} \tag{4.21b}$$

$$\gamma = 2\nu^2 \frac{b\sigma}{d} \tag{4.21c}$$

$$b = \frac{r}{e} \tag{4.21d}$$

$$d = \frac{\rho_{D}}{\rho_{E}} \tag{4.21e}$$

$$h = \frac{E}{\kappa^*} \tag{4.21f}$$

$$C_0 = \Delta \left[\lambda_2^2 \cos(\lambda_1) - \lambda_1^2 \cos(\lambda_2) \right]$$
 (4.21g)

$$C_1 = \Delta \left[\frac{\lambda_2^2}{\lambda_1} \sin(\lambda_1) - \frac{\lambda_1^2}{\lambda_2} \sin(\lambda_2) \right]$$
 (4.21h)

$$C_2 = \Delta \left[\cos(\lambda_1) - \cos(\lambda_2) \right] \tag{4.21i}$$

$$C_3 = \Delta \left[\frac{1}{\lambda_1} \sin(\lambda_1) - \frac{1}{\lambda_2} \sin(\lambda_2) \right]$$
 (4.21j)

$$\Delta = \left(\lambda_1^2 - \lambda_2^2\right)^{-1} \tag{4.21k}$$

$$\lambda_1^2 = \frac{1}{2} \left\{ (\tau + \sigma + \gamma) - \left[(\tau + \sigma + \gamma)^2 - 4\sigma\tau \right]^{\frac{1}{2}} \right\} \qquad (4.21\ell)$$

$$\lambda_2^2 = \frac{1}{2} \left\{ (\tau + \sigma + \gamma) + \left[(\tau + \sigma + \gamma)^2 - 4\sigma\tau \right]^{\frac{1}{2}} \right\} \qquad (4.21\text{m})$$

and the non-dimensional state vector at location i in Figure 4.5 is:

$$\mathbf{z_{i}} - \left\{ \begin{array}{ccc} \frac{\mathbf{U}_{\mathbf{Z}}}{\ell} & \frac{\mathbf{P}}{K^{\star}} & \frac{\mathbf{V}}{\ell} & \frac{\mathbf{F}_{\mathbf{Z}}}{\mathbf{A}_{\mathbf{P}}\mathbf{E}} \end{array} \right\}_{\mathbf{I}}^{\mathbf{T}} \tag{4.22}$$

The matrix in Equation 4.20 is valid providing that the coupled wave speeds ratio are different from one another. This condition guarantees that the eigen values in Equations 4.212 and 4.21m are different from one another, therefore, avoiding the undeterminate form of Equation 4.21k.

4.2.2.2 Transverse Vibration in x-z Plane

Equation 4.18 for the transverse vibration of a pipe reach in the x-z plane becomes

$$\mathbf{Z}_{i} = [\mathbf{T}_{xz}]_{i} \mathbf{Z}_{i-1} \tag{4.23a}$$

where

$$[T_{xz}] = [B(l)] [B(0)]^{-1}$$
 (4.23b)

The matrices [B(0)] and [B(l)] are obtained from the matrix of Equation 3.53a evaluated at locations i-1 and i in Figure 4.5, respectively. The non-dimensional representation of the field transfer matrix [50] and state vector are

$$\begin{bmatrix} C_0 - \sigma C_2 & C_1 - (\sigma + \tau)C_3 & C_2 & -\frac{1}{\gamma} [-\sigma C_1 + (\gamma + \sigma^2)C_3] \\ \gamma C_3 & C_0 - \tau C_2 & C_1 - \tau C_3 & -C_2 \\ \gamma C_2 & (\gamma + \tau^2)C_3 - \tau C_1 & C_0 - \tau C_2 & -[C_1 - (\sigma + \tau)C_3] \\ -\gamma (C_1 - \sigma C_3) & -\gamma C_2 & -\gamma C_3 & C_0 - \sigma C_2 \end{bmatrix}$$
(4.24)

where

$$\sigma = \frac{(\rho_{\mathbf{p}} \mathbf{A}_{\mathbf{p}} + \rho_{\mathbf{f}} \mathbf{A}_{\mathbf{f}})}{G \mathbf{A}_{\mathbf{p}} \kappa_{\mathbf{s}}} \omega^{2} \ell^{2}$$
 (4.25a)

$$\tau = \frac{(\rho_{\mathbf{p}} \mathbf{I}_{\mathbf{p}} + \rho_{\mathbf{f}} \mathbf{I}_{\mathbf{f}})}{\mathbf{E} \mathbf{I}_{\mathbf{p}}} \omega^{2} \ell^{2}$$
 (4.25b)

$$\gamma = \frac{(\rho_{\mathbf{p}} \mathbf{A}_{\mathbf{p}} + \rho_{\mathbf{f}} \mathbf{A}_{\mathbf{f}})}{\text{EI}_{\mathbf{p}}} \omega^{2} \ell^{4}$$
 (4.25c)

$$C_0 = \Delta \left[\lambda_2^2 \cosh(\lambda_1) + \lambda_1^2 \cos(\lambda_2) \right]$$
 (4.25d)

$$C_1 - \Delta \left[\frac{\lambda_2^2}{\lambda_1} \sinh(\lambda_1) + \frac{\lambda_1^2}{\lambda_2} \sin(\lambda_2) \right]$$
 (4.25e)

$$C_2 = \Delta \left[\cosh(\lambda_1) - \cos(\lambda_2) \right]$$
 (4.25f)

$$C_3 = \Delta \left[\frac{1}{\lambda_1} \sinh(\lambda_1) - \frac{1}{\lambda_2} \sin(\lambda_2) \right]$$
 (4.25g)

$$\Delta = \left(\lambda_1^2 + \lambda_2^2\right)^{-1} \tag{4.25h}$$

$$\lambda_1^2 = \left(\gamma + \frac{1}{4} (\sigma - \tau)^2 \right)^{\frac{1}{2}} - \frac{1}{2} (\sigma + \tau)$$
 (4.251)

$$\lambda_2^2 = \left(\gamma + \frac{1}{4} (\sigma - \tau)^2 \right)^{\frac{1}{2}} + \frac{1}{2} (\sigma + \tau)$$
 (4.25j)

and the state vector in the x-z plane at location i in Figure 4.5 is given by

$$\mathbf{z_{i}} - \left\{ \begin{array}{ccc} \frac{\mathbf{U_{X}}}{\ell} & \Psi_{\mathbf{y}} & \frac{\mathbf{M_{y}}\ell}{\mathbf{EI_{p}}} & \frac{\mathbf{F_{X}}\ell^{2}}{\mathbf{EI_{p}}} \end{array} \right\}_{i}^{T}$$
 (4.26)

The matrix in Equation 4.24 differs from the one by Pestel and Lackie [50] in that the mass of the contained liquid is included in the parameters σ , τ and γ .

4.2.2.3 Transverse Vibration in y-z Plane

Equation 4.18 for the transverse vibration of a pipe reach in the y-z plane can be represented by

$$\mathbf{Z_{i}} - [\mathbf{T_{vz}}]_{i} \mathbf{Z_{i-1}} \tag{4.27a}$$

where

$$[T_{yz}] - [B(\ell)] [B(0)]^{-1}$$
 (4.27b)

The matrices [B(0)] and [B(l)] are obtained from the matrix of Equation 3.60 evaluated at locations i-1 and i in Figure 4.5, respectively. The non-dimensional representation of the field transfer matrix and state vector are

$$\begin{bmatrix} C_0 - \sigma C_2 & -[C_1 - (\sigma + \tau)C_3] & -C_2 & -\frac{1}{\gamma}[-\sigma C_1 + (\gamma + \sigma^2)C_3] \\ -\gamma C_3 & C_0 - \tau C_2 & C_1 - \tau C_3 & C_2 \\ -\gamma C_2 & (\gamma + \tau^2)C_3 - \tau C_1 & C_0 - \tau C_2 & [C_1 - (\sigma + \tau)C_3] \\ -\gamma (C_1 - \sigma C_3) & \gamma C_2 & \gamma C_3 & C_0 - \sigma C_2 \end{bmatrix}$$

$$(4.28)$$

where the coefficients are given in Equations 4.25a through 4.25j. The state vector in the y-z plane at location i in Figure 4.5 is

$$\mathbf{Z}_{i} - \left\{ \begin{array}{ccc} \frac{\mathbf{U}_{y}}{\ell} & \Psi_{x} & \frac{\mathbf{M}_{x}\ell}{\mathbf{E}\mathbf{I}_{p}} & \frac{\mathbf{F}_{y}\ell}{\mathbf{E}\mathbf{I}_{p}} \end{array} \right\}_{i}^{T}$$
 (4.29)

4.2.2.4 Torsional Vibration About z-Axis

Equation 4.18 for the torsion about the z-axis is

$$\mathbf{Z}_{i} - \left[\mathbf{T}_{rz}\right]_{i} \mathbf{Z}_{i-1} \tag{4.30a}$$

where

$$[T_{LZ}] = [B(\ell)] [B(0)]^{-1}$$
 (4.30b)

The matrices [B(0)] and $[B(\ell)]$ are obtained from the matrix of Equation 3.73 evaluated at locations i-1 and i in Figure 4.5, respectively. The non-dimensional representation of the field transfer matrix and state vector are

$$\begin{bmatrix} \mathbf{T}_{\mathsf{tz}} \end{bmatrix}_{\mathbf{i}} = \begin{bmatrix} -\cos(\lambda) & -\frac{1}{\lambda}\sin(\lambda) \\ \lambda & \sin(\lambda) & -\cos(\lambda) \end{bmatrix} \tag{4.31}$$

where

$$\lambda^2 - \omega^2 \ell^2 \frac{\rho_{\rm p}}{G} \tag{4.32}$$

and the state vector, $\mathbf{Z_i}$ in Equation 4.30a is

$$\mathbf{z_{i}} - \left\{ \Psi_{\mathbf{z}} \quad \frac{M_{\mathbf{z}}\ell}{GJ_{\mathbf{p}}} \right\}_{\mathbf{i}}^{\mathbf{T}} \tag{4.33}$$

4.2.2.5 General Field Transfer Matrix

The field transfer matrix for a single straight pipe reach shown in Figure 4.5 is composed of four submatrices: longitudinal vibration of the liquid and pipe wall, transverse vibration in the x-z as well as in the y-z planes and torsional vibration about the z-axis. Their expressions were given in Equations 4.20, 4.24, 4.28 and 4.31, respectively. The state vectors have fourteen dependent variables: three for each of forces, moments, displacements and rotations of the pipe wall and pressure and displacement of the liquid. The equation below shows these arrangements:

$$\mathbf{Z_{i}} - [\mathbf{T_{L}}] \ \mathbf{Z_{i-1}} \tag{4.34}$$

where $[T_L]$ is the field transfer matrix for a pipe reach of length ℓ in the local coordinate system. The fourteen by fourteen element matrix is given below:

$$[\mathbf{T}_{L}] - \begin{bmatrix} [\mathbf{T}_{fp}] & [\mathbf{T}_{xz}] \\ [\mathbf{T}_{yz}] & [\mathbf{T}_{tz}] \end{bmatrix}$$
(4.35)

The state vector at location i in Figure 4.5 is:

$$\mathbf{Z}_{1} = \left\{ \frac{\mathbf{U}_{z}}{\ell} \quad \frac{\mathbf{P}}{\mathbf{K}^{\star}} \quad \frac{\mathbf{V}}{\ell} \quad \frac{\mathbf{F}_{z}}{\mathbf{A}_{p}E} \quad \frac{\mathbf{U}_{x}}{\ell} \quad \Psi_{y} \quad \frac{\mathbf{M}_{y}\ell}{EI_{p}} \quad \frac{\mathbf{F}_{x}\ell^{2}}{EI_{p}} \quad \frac{\mathbf{U}_{y}}{\ell} \quad \Psi_{x} \quad \frac{\mathbf{M}_{x}\ell}{EI_{p}} \quad \frac{\mathbf{F}_{y}\ell^{2}}{EI_{p}} \quad \Psi_{z} \quad \frac{\mathbf{M}_{z}\ell}{GJ_{p}} \right\}_{1}^{T} \quad (4.36)$$

4.2.3 Point Matrices

Three types of point matrices for the pipe wall will be discussed: bends, springs and point masses. Point matrices for structures that affect the liquid directly, such as orifices, accumulators and oscillatory valves were developed by Chaudhry [7], and Wylie and Streeter [8]. Wilkinson [64] developed point matrices for T-junctions, curved bends and pumps as sources of excitation.

4.2.3.1 Bend Point Matrix

A piping system in two or three dimensional space can be treated as a collection of straight pipe reaches, differing in orientation and joined end-to-end. The difference in orientation generates junction coupling of the fluid pressure and of the pipe wall moments and forces between the reaches. The junction itself is treated as a discontinuity with negligible mass and length. Equilibrium and continuity relationships constitute the basis for point matrices at bends.

The point matrix is derived for two reaches in a two-dimensional space and is shown in Figure 4.6. The reaches are connected so that α is the angle between the axis of each pipe. Figure 4.6a shows the internal forces in the local coordinate system and Figure 4.6b shows the displacements. The equilibrium and continuity conditions that relate the

state vector, \mathbf{Z}_{i}^{R} to the right and the state vector, \mathbf{Z}_{i}^{L} to the left of point i are as follows [26,27]:

Equilibrium of fluid displacement, pipe moments and forces (Figure 4.6a):

$$\Sigma M_{x}: M_{x}^{R} - M_{x}^{L} = 0$$
 (4.37a)

$$\Sigma F_y$$
: $P^R A_f \cos \alpha - F_z^R \cos \alpha + F_y^R \sin \alpha - P^L A_f + F_z^L = 0$ (4.37b)

$$\Sigma F_z: -P^R A_f \sin\alpha + F_z^R \sin\alpha + F_y^R \cos\alpha - F_y^L = 0$$
 (4.37c)

Displacements:
$$-(V^{L} - U_{z}^{L}) + (V^{R} - U_{z}^{R}) = 0$$
 (4.37d)

Continuity of fluid pressure, pipe displacements and rotations (Figure 4.6b):

Rotations:
$$\Psi_{\mathbf{v}}^{\mathbf{L}} = \Psi_{\mathbf{v}}^{\mathbf{R}}$$
 (4.37e)

Displacements:
$$U_y^L = U_y^R \cos\alpha + U_z^R \sin\alpha$$
 (4.37f)

$$-U_{z}^{L} - U_{y}^{R} \sin\alpha - U_{z}^{R} \cos\alpha \qquad (4.37g)$$

Pressures:
$$P^{L} = P^{R}$$
 (4.37h)

These equations are assembled in matrix form as:

or

$$\mathbf{z_i^R - [P_L^B]_i z_i^L} \tag{4.39a}$$

and

$$g = \frac{A_{p}\ell^{2}}{I_{p}}$$
 (4.39b)

$$q - \frac{A_f}{A_p} \tag{4.39c}$$

4.2.3.2 Spring Point Matrix

Piping systems generally are supported at several locations, restricting motion partially or totally, or they may be placed on an elastic foundation. The elastic foundation can be represented by springs. Each spring can be modeled as a point matrix.

Suppose the pipe reach in Figure 4.7a has a spring support and is vibrating in the y-z plane and in the axial direction z. The state vectors to the right and left of point i, $\mathbf{Z}_{\mathbf{i}}^{R}$ and $\mathbf{Z}_{\mathbf{i}}^{L}$, can again be related by a point matrix. The lateral displacement, rotation, moment and axial variables are continuous over point i. But because of the spring restoring force, a discontinuity occurs in the shear force. When the spring is deflected by an amount $\mathbf{U}_{\mathbf{y}}$, the restoring force is $\mathbf{k}_{\mathbf{i}}\mathbf{U}_{\mathbf{y}}$, where $\mathbf{k}_{\mathbf{i}}$ is the stiffness of the spring (Fig. 4.7b). The relations between the state vector elements to the left and right of the spring are then

$$U_z^R - U_z^L \tag{4.40a}$$

$$P^{R} - P^{L} \tag{4.40b}$$

$$(v^R - U_z^R) - (v^L - U_z^L)$$
 (4.40c)

$$\mathbf{F}_{\mathbf{z}}^{\mathbf{R}} = \mathbf{F}_{\mathbf{z}}^{\mathbf{L}} \tag{4.40d}$$

$$\mathbf{U}_{\mathbf{v}}^{\mathbf{R}} - \mathbf{U}_{\mathbf{v}}^{\mathbf{L}} \tag{4.40e}$$

$$\Psi_{\mathbf{x}}^{\mathbf{R}} - \Psi_{\mathbf{x}}^{\mathbf{L}} \tag{4.40f}$$

$$M_{x}^{R} - M_{x}^{L} \tag{4.40g}$$

$$\mathbf{F}_{\mathbf{y}}^{\mathbf{R}} - \mathbf{F}_{\mathbf{y}}^{\mathbf{L}} - \mathbf{k}_{\mathbf{i}} \mathbf{U}_{\mathbf{y}}^{\mathbf{L}} \tag{4.40h}$$

Here the subscript i of the dependent variables has been dropped for clarity. In matrix notation, and in non-dimensional form the equations become:

$$\begin{bmatrix}
\frac{U_{z}}{\ell} \\ \frac{P}{k^{*}} \\ \frac{V}{\ell} \\ \frac{V}{\ell} \\ \frac{I}{E_{p}} \\ \frac{I}{E_{p}} \\ \frac{I}{E_{p}} \\ \frac{I}{E_{p}} \end{bmatrix}_{i}
\begin{bmatrix}
1 & 0 & 0 & 0 & 0 & 0 & 0 & 0 & 0 \\
0 & 1 & 0 & 0 & 0 & 0 & 0 & 0 & 0 \\
0 & 0 & 1 & 0 & 0 & 0 & 0 & 0 & 0 \\
0 & 0 & 0 & 1 & 0 & 0 & 0 & 0 & 0 \\
0 & 0 & 0 & 0 & 1 & 0 & 0 & 0 & 0 \\
0 & 0 & 0 & 0 & 0 & 1 & 0 & 0 & 0 \\
0 & 0 & 0 & 0 & 0 & 0 & 1 & 0 & 0 \\
0 & 0 & 0 & 0 & 0 & 0 & 1 & 0 & 0 \\
0 & 0 & 0 & 0 & 0 & 0 & 1 & 0 & 0 \\
0 & 0 & 0 & 0 & 0 & 0 & 1 & 0 & 0 \\
0 & 0 & 0 & 0 & 0 & 0 & 1 & 0 & 0 \\
0 & 0 & 0 & 0 & 0 & 0 & 1 & 0 & 0 \\
0 & 0 & 0 & 0 & 0 & 0 & 1 & 0 & 0 \\
0 & 0 & 0 & 0 & 0 & 0 & 1 & 0 & 0 \\
0 & 0 & 0 & 0 & 0 & 0 & 1 & 0 & 0 \\
0 & 0 & 0 & 0 & 0 & 0 & 1 & 0 & 0 \\
0 & 0 & 0 & 0 & 0 & 0 & 1 & 0 & 0 \\
0 & 0 & 0 & 0 & 0 & 0 & 0 & 1 & 0 \\
0 & 0 & 0 & 0 & 0 & 0 & 1 & 0 & 1 \\
0 & 0 & 0 & 0 & 0 & 0 & 0 & 1 & 0 \\
0 & 0 & 0 & 0 & 0 & 0 & 0 & 1 & 0 \\
0 & 0 & 0 & 0 & 0 & 0 & 0 & 1 & 0 \\
0 & 0 & 0 & 0 & 0 & 0 & 0 & 1 & 0 \\
0 & 0 & 0 & 0 & 0 & 0 & 0 & 1 & 0 \\
0 & 0 & 0 & 0 & 0 & 0 & 0 & 1 & 0 \\
0 & 0 & 0 & 0 & 0 & 0 & 0 & 1 & 0 \\
0 & 0 & 0 & 0 & 0 & 0 & 0 & 1 & 0 \\
0 & 0 & 0 & 0 & 0 & 0 & 0 & 1 & 0 \\
0 & 0 & 0 & 0 & 0 & 0 & 0 & 1 & 0 \\
0 & 0 & 0 & 0 & 0 & 0 & 0 & 1 & 0 \\
0 & 0 & 0 & 0 & 0 & 0 & 0 & 1 & 0
\end{bmatrix}$$

or

$$\mathbf{z_i^R - [P_L^S]_i z_i^L} \tag{4.42}$$

4.2.3.3 Mass Point Matrix

Valves, accumulators and control instrumentation can be modeled as concentrated or point masses. For example, consider the pipe reach in Figure 4.8a which has a valve of mass $\mathbf{m_i}$ in the mid-span. Assume that the radius of gyration of the mass of the valve is zero about the x-axis and that the system is vibrating in the y-z plane as well as in the

axial direction z. The point mass matrix connecting $\mathbf{Z_i^R}$ and $\mathbf{Z_i^L}$ is found by noting that the lateral displacement, rotation and moment as well as the axial variables are continuous across $\mathbf{m_i}$, so that

$$U_z^R - U_z^L \tag{4.43a}$$

$$P^{R} = P^{L} \tag{4.43b}$$

$$(v^R - v_z^R) - (v^L - v_z^L)$$
 (4.43c)

$$U_{\mathbf{y}}^{\mathbf{R}} - U_{\mathbf{y}}^{\mathbf{L}} \tag{4.43d}$$

$$\Psi_{\mathbf{x}}^{\mathbf{R}} = \Psi_{\mathbf{x}}^{\mathbf{L}} \tag{4.43e}$$

$$M_{x}^{R} - M_{x}^{L} \tag{4.43f}$$

An inertia force causes a discontinuity in the shear and axial force due to the vibrating mass. Equilibrium considerations in the free-body diagram shown in Figure 4.8b yield

$$F_y^R - F_y^L - m_i \omega^2 U_y^L$$
 (4.43g)

$$\mathbf{F}_{z}^{R} - \mathbf{F}_{z}^{L} - \mathbf{m}_{i} \omega^{2} \mathbf{U}_{z}^{L} \tag{4.43h}$$

In non-dimensional matrix notation Equations 4.43a through 4.43h become

$$\begin{bmatrix}
\frac{\mathbf{U}_{\mathbf{Z}}}{2} \\
\frac{\mathbf{P}_{\mathbf{K}^{*}}}{\mathbf{X}^{*}} \\
\frac{\mathbf{F}_{\mathbf{Z}}}{\mathbf{A}_{\mathbf{P}}^{E}}
\end{bmatrix} =
\begin{bmatrix}
1 & 0 & 0 & 0 & 0 & 0 & 0 & 0 \\
0 & 1 & 0 & 0 & 0 & 0 & 0 & 0 \\
0 & 0 & 1 & 0 & 0 & 0 & 0 & 0
\end{bmatrix} \begin{bmatrix}
\frac{\mathbf{U}_{\mathbf{Z}}}{2} \\
\frac{\mathbf{P}_{\mathbf{K}^{*}}}{\mathbf{X}^{*}} \\
\frac{\mathbf{P}_{\mathbf{K}^{*}}}{2} \\
\frac{\mathbf{P}_{\mathbf{K}^{*}}}{2} \\
\frac{\mathbf{P}_{\mathbf{K}^{*}}}{2} \\
\frac{\mathbf{P}_{\mathbf{K}^{*}}}{2} \\
\frac{\mathbf{P}_{\mathbf{K}^{*}}}{2} \\
0 & 0 & 0 & 1 & 0 & 0 & 0 & 0
\end{bmatrix} \begin{bmatrix}
\frac{\mathbf{U}_{\mathbf{Z}}}{2} \\
\frac{\mathbf{P}_{\mathbf{K}^{*}}}{2} \\
\frac{\mathbf{P}_{\mathbf{K}^{*}}}{2} \\
\frac{\mathbf{P}_{\mathbf{K}^{*}}}{2} \\
\frac{\mathbf{P}_{\mathbf{K}^{*}}}{2} \\
0 & 0 & 0 & 1 & 0 & 0 & 0
\end{bmatrix} \begin{bmatrix}
\frac{\mathbf{U}_{\mathbf{Z}}}{2} \\
\frac{\mathbf{P}_{\mathbf{K}^{*}}}{2} \\
\frac{\mathbf{P}_{\mathbf{K}^{*}}}{$$

4.2.4 Overall Transfer Matrix

The overall transfer matrix relates the state vector at one end of a system to that at the other end. The matrix is obtained by an ordered multiplication of all the intermediate field and point matrices [7]. Once the field and point matrices for each subsystem have been obtained, three steps are necessary to form the overall transfer matrix. The first step consists of rearranging the terms of the matrices. The second step transforms the matrices from a local to a global coordinate system by using transformation matrices. The final step is the ordered multiplication of the transformed matrices. The first two steps are considered next.

4.2.4.1 Overall Transfer Matrix Rearrangement

The state vector in Equation 4.36 has fourteen elements corresponding to fourteen dependent variables that are necessary to describe a liquid-filled piping system in a three dimensional space. Assume that the piping system is in the y-z plane. This piping set-up allows motion in the axial direction, z and in the y-z plane. The state vectors and transfer matrix are given by:

$$\mathbf{z_{i}} - \begin{bmatrix} \mathbf{T_{fp}} \\ \mathbf{T_{yz}} \end{bmatrix} \mathbf{z_{i-1}}$$
 (4.46a)

or

$$\mathbf{Z}_{i} - [\mathbf{T}]_{i} \mathbf{Z}_{i-1} \tag{4.46b}$$

where $[T_{fp}]$ and $[T_{yz}]$ are given in Equations 4.20 and 4.28, respectively. The state vector $\mathbf{Z_i}$ is given by:

$$z_{i} - \left\{ \frac{U_{z}}{\ell} \quad \frac{P}{K^{*}} \quad \frac{V}{\ell} \quad \frac{F_{z}}{A_{p}E} \quad \frac{U_{y}}{\ell} \quad *x \quad \frac{M_{x}\ell}{EI_{p}} \quad \frac{F_{y}\ell^{2}}{EI_{p}} \right\}_{i}^{T}$$
(4.47)

In order to keep the variables subjected to continuity and equilibrium conditions separate from one another [26,27,50], the state vector is rearranged

$$\mathbf{z}_{\mathbf{i}} - \left\{ \begin{array}{ccc} \mathbf{P} & \Psi_{\mathbf{x}} & \frac{\mathbf{U}_{\mathbf{y}}}{\ell} & \frac{\mathbf{U}_{\mathbf{z}}}{\ell} & \frac{\mathbf{V}_{\mathbf{z}}}{\ell} & \frac{\mathbf{V}_{\mathbf{x}}}{\ell} & \frac{\mathbf{F}_{\mathbf{y}}}{\ell} & \frac{\mathbf{F}_{\mathbf{y}}}{\ell} & \frac{\mathbf{F}_{\mathbf{z}}}{\mathbf{A}_{\mathbf{p}}} \mathbf{E} \end{array} \right\}_{\mathbf{i}}^{\mathbf{T}} \tag{4.48}$$

To have the transfer matrix compatible with the state vector in Equation 4.48, the columns and rows of the matrix in Equation 4.46a must be rearranged. Comparing the state vectors in the two previous equations one can see, for example, that the second element, P/K^* , is now the first and the sixth element, $\Psi_{\rm X}$, is now the second. In a similar manner the transfer matrix is rearranged. Row and column shifting can be achieved in two steps. First, the columns are rearranged by postmultiplying the transfer matrix by a square matrix $[t_{\rm C}]$. Then, rearrangement of rows is accomplished by premultiplying by $[t_{\rm R}]$ so that:

$$[\mathbf{T}_{\mathsf{T}}] = [\mathsf{t}_{\mathsf{D}}] [\mathbf{T}] [\mathsf{t}_{\mathsf{C}}] \tag{4.49}$$

where $[t_R]$ is given by:

and
$$\left[t_{C}\right] - \left[t_{R}\right]^{t}$$
 (4.51)

The final field transfer matrix, in local coordinates, is given in the equation below:

$$\begin{bmatrix}
\frac{P}{K^{*}} \\
\frac{V}{K} \\
\frac{U}{V} \\
\frac{U}{V} \\
\frac{U}{V} \\
\frac{V}{V} \\
\frac{V}{V}$$

or

$$\{Z_L\}_i - [T_L]_i \{Z_L\}_{i-1}$$
 (4.53)

where the elements of the matrix $[T_L]$, T_{RC}^{fp} and T_{RC}^{yz} are given in Equations 4.20 and 4.28, respectively. The subscripts R and C in each element of $[T_L]$ refer to rows and columns. The procedure described can be generalized to a three-dimensional space. The size of the overall transfer matrix will be fourteen by fourteen. The state vector will be composed of three rotations, displacements, moments and forces, in addition to the liquid pressure and displacement.

4.2.4.2 Coordinate Transformation

State vectors and field and point matrices are developed based on the local coordinate system, x,y,z, associated with each particular subsystem. In order to relate the state vectors at the end of a pipe reach to those at the end of an adjacent pipe, the state vectors are expressed with respect to a set of global coordinates, X,Y,Z, fixed with respect to the piping system.

The state vector $\mathbf{Z}_{\mathbf{L}}$ with respect to the local coordinates, x,y,z, and the state vector $\mathbf{Z}_{\mathbf{G}}$ with respect to the global coordinates, X,Y,Z, are related by the transformation matrix [t]:

$$\mathbf{Z}_{L} = [\mathbf{t}]\mathbf{Z}_{G} \tag{4.54}$$

where

$$\mathbf{Z}_{L} = \left\{ \begin{array}{cccc} \mathbf{P} & \Psi_{\mathbf{X}} & \frac{\mathbf{U}_{\mathbf{Y}}}{\ell} & \frac{\mathbf{U}_{\mathbf{Z}}}{\ell} & \frac{\mathbf{V}}{\ell} & \frac{\mathbf{M}_{\mathbf{X}}\ell}{\mathrm{EI}_{\mathbf{p}}} & \frac{\mathbf{F}_{\mathbf{Y}}\ell^{2}}{\mathrm{EI}_{\mathbf{p}}} & \frac{\mathbf{F}_{\mathbf{Z}}}{\mathrm{A}_{\mathbf{p}}\mathrm{E}} \end{array} \right\}^{\mathrm{T}} \tag{4.55a}$$

$$\mathbf{Z}_{G} = \left\{ \begin{array}{cccc} \mathbf{P} & \Psi_{X} & \frac{\mathbf{U}_{Y}}{\ell} & \frac{\mathbf{U}_{Z}}{\ell} & \frac{\mathbf{V}}{\ell} & \frac{\mathbf{M}_{X}\ell}{\mathrm{EI}_{p}} & \frac{\mathbf{F}_{Y}\ell^{2}}{\mathrm{EI}_{p}} & \frac{\mathbf{F}_{Z}}{\mathrm{A}_{p}\mathrm{E}} \end{array} \right\}^{\mathrm{T}} \tag{4.55b}$$

To obtain the transformation matrix, the orientation of the pipe reach with respect to the global axis must be defined. The orientation is

defined by using the direction cosines of the local axis with respect to the global axis. This is expressed in matrix form as:

$$\left\{ \begin{array}{l} \mathbf{x} \\ \mathbf{y} \\ \mathbf{z} \end{array} \right\} = \left[\begin{array}{l} \cos(\varphi_{11}) & \cos(\varphi_{12}) & \cos(\varphi_{13}) \\ \cos(\varphi_{21}) & \cos(\varphi_{22}) & \cos(\varphi_{23}) \\ \cos(\varphi_{31}) & \cos(\varphi_{32}) & \cos(\varphi_{33}) \end{array} \right] \left\{ \begin{array}{l} \mathbf{X} \\ \mathbf{Y} \\ \mathbf{Z} \end{array} \right\}$$
(4.56)

where φ_{pq} is the angle between the local and global axes. The subscript p refers to the local axis, whereas q refers to the global axis. This is shown in Figure 4.9. As an example, Figure 4.10 shows a pipe reach in both the local and global coordinate systems. The local coordinates have been rotated about the X-axis, which is perpendicular to the plane of the paper. The local y-axis and global Z-axis coincide. The following relations can be observed:

or

$$\mathbf{Z}_{L} - [t] \mathbf{Z}_{G} \tag{4.58}$$

The transformation matrix for this example is:

$$\begin{bmatrix}
\frac{P}{K^{*}} \\
\frac{V}{V} \\
\frac{U}{V} \\
\frac{U}{V} \\
\frac{V}{\ell}
\end{bmatrix}$$

$$\begin{bmatrix}
0 & 1 & 0 & 0 & 0 & 0 & 0 & 0 & 0 \\
0 & 1 & 0 & 0 & 0 & 0 & 0 & 0
\end{bmatrix}$$

$$\begin{bmatrix}
\frac{P}{K^{*}} \\
\frac{V}{V} \\
\frac{V}{\ell} \\
\frac{U}{V} \\
\frac{V}{\ell}
\end{bmatrix}$$

$$\begin{bmatrix}
0 & 0 & 0 & 1 & 0 & 0 & 0 & 0 & 0 \\
0 & 0 & -1 & 0 & 0 & 0 & 0 & 0
\end{bmatrix}$$

$$\begin{bmatrix}
\frac{P}{K^{*}} \\
\frac{V}{V} \\
\frac{V}{\ell} \\
\frac{U}{V} \\
\frac{V}{\ell} \\
\frac{V}{\ell}$$

The relation between the local state vector at locations i and i-l is:

$$\{Z_L\}_i - [T_L]_i \{Z_L\}_{i-1}$$
 (4.60)

Combining Equations 4.54 and 4.60 and remembering that $[t]^{-1} - [t]^{t}$ the following relation is obtained

$$\{Z_G\}_i - [t]^t [T_L]_i [t] \{Z_G\}_{i-1}$$
 (4.61a)

or

$$\{\mathbf{Z}_{G}\}_{1}^{Z} - [\mathbf{T}_{G}]_{1}^{T} \{\mathbf{Z}_{G}\}_{1-1}^{Z}$$
 (4.61b)

and

$$\left[\mathbf{T}_{\mathbf{G}}\right]_{\mathbf{i}} - \left[\mathbf{t}\right]^{\mathbf{t}} \left[\mathbf{T}_{\mathbf{L}}\right]_{\mathbf{i}} \left[\mathbf{t}\right] \tag{4.61c}$$

where $[\mathbf{T}_G]_{\mathbf{i}}$ is the field transfer matrix in global coordinates relating the state vectors at the two ends of a pipe reach. The state vectors are defined with respect to the global coordinate system.

Similar procedures for rearranging and transforming the coordinates from local into global can be applied to the point matrices defined in Equations 4.38, 4.41 and 4.44. The overall transfer matrix for the system shown in Figure 4.4 between points 7 and 5 is given by:

$$[\mathbf{U}] - \dots [\mathbf{P}_{G}^{\mathbf{B}}]_{7} [\mathbf{T}_{G}]_{7} [\mathbf{P}_{G}^{\mathbf{S}}]_{6} [\mathbf{T}_{G}]_{6} [\mathbf{P}_{G}^{\mathbf{M}}]_{5} [\mathbf{T}_{G}]_{5} \dots$$
(4.62)

The number of columns of the overall matrix may be reduced according to the boundary conditions at one end of the system or increased, in the case of a rigid support, to account for the new unknown introduced by the intermediate boundary condition. These special conditions will be defined in the next section.

4.2.5 Boundary and Intermediate Conditions

Boundary and intermediate conditions are restrictions imposed on the system affecting the degrees of freedom of the pipe or liquid. The natural frequencies of the system are dependent upon these conditions.

4.2.5.1 Boundary Conditions

Figure 4.11 shows a piping system vibrating in both the axial direction Z and in the Y-Z plane. The boundary conditions at location 0 are a reservoir of constant pressure for the liquid and restrictions on rotations and displacements of the pipe. The reservoir represents an openend condition in the liquid, whereas the restriction of pipe motion is a fixed-end condition. Since the reservoir level is constant, a pressure node always exists at this end. This boundary will be referred to as an open-fixed end condition. The state vector, in global coordinates, at this end is given by:

$$\begin{pmatrix}
P \\
\Psi_X \\
U_Y \\
U_Z \\
V \\
M_X \\
F_Y \\
F_Z
\end{pmatrix}_0$$

$$\begin{pmatrix}
0 \\
0 \\
0 \\
0 \\
V \\
M_X \\
F_Y \\
F_Z
\end{pmatrix}_0$$
(4.63)

At location 1 in Fig. 4.13 there is a closed valve and a release (for example, a flexible hose of negligible length) that allow pipe motion. Moment and forces in the pipe vanish due to the release. A liquid pressure antinode exists at this end due to the presence of the closed valve. Assuming that the release does not affect the fluid pressure and that the valve is rigid so that fluid displacement is not allowed, the state vector at this closed-free end condition is given by:

$$\begin{pmatrix}
P \\
\Psi X \\
U_Y \\
U_Z \\
V \\
M_X \\
F_Y \\
F_Z
\end{pmatrix}_1$$

$$\begin{pmatrix}
P \\
\Psi X \\
U_Y \\
U_Z \\
0 \\
0 \\
0 \\
0
\end{pmatrix}_1$$
(4.64)

4.2.5.2 Intermediate Conditions

Rigid supports and external excitations of the piping are the intermediate conditions studied in this research. Figure 4.12 shows these two intermediate conditions. Lesmez, et al. [66] presented a description of these conditions.

1) Rigid Supports

A rigid support restricts all motion of piping at a given location. This support condition may be represented by increasing the number of columns of the transfer matrix. The increase in the number of columns accounts for the reaction at the location and increases the number of unknowns. This boundary condition can be illustrated by a simple example. The clamped-clamped beam in Figure 4.12a has a support at location 2. Let T1 and T2 be the field transfer matrices between points 1 and 2, and 2 and 3, respectively. The matrices T1 and T2 can be written as follows:

$$[T1] = \begin{bmatrix} T1_{11} & T1_{12} & T1_{13} & T1_{14} \\ T1_{21} & T1_{22} & T1_{23} & T1_{24} \\ T1_{31} & T1_{32} & T1_{33} & T1_{34} \\ T1_{41} & T1_{42} & T1_{43} & T1_{44} \end{bmatrix}, [T2] = \begin{bmatrix} T2_{11} & T2_{12} & T2_{13} & T2_{14} \\ T2_{21} & T2_{22} & T2_{23} & T2_{24} \\ T2_{31} & T2_{32} & T2_{33} & T2_{34} \\ T2_{41} & T2_{42} & T2_{43} & T2_{44} \end{bmatrix}$$
(4.65)

The state vector for shear and bending in the Y-Z plane is given by:

$$\mathbf{Z} - \left(\mathbf{U}_{\mathbf{Y}} \mathbf{\Psi}_{\mathbf{X}} \mathbf{M}_{\mathbf{X}} \mathbf{F}_{\mathbf{Y}} \right)^{\mathbf{T}} \tag{4.66}$$

Applying the fixed boundary conditions $U_Y = 0$, $\Psi_X = 0$ at 1, the first and second columns of the field transfer matrix [T1] are dropped and the state vector becomes $\{M_X, F_Y\}^T$. The rigid support at point 2 causes a discontinuity in the shear force according to the relation

$$F_{Y_2}^R - F_{Y_2}^L + Q$$
 (4.67)

This restraint also introduces the relation

$$U_{Y_2} = 0 - T1_{13}M_{X_1} + T1_{14}F_{Y_1}$$
 (4.68)

In order to introduce the reaction Q, a column is added in the field transfer matrix. It has unit value in the row corresponding to the discontinuity, as shown in the equation below.

$$\begin{bmatrix}
U_{Y} \\ \Psi_{X} \\ M_{X} \\ F_{Y} \end{bmatrix}_{2}^{R} = \begin{bmatrix}
T1_{13} & T1_{14} & 0 \\
T1_{23} & T1_{24} & 0 \\
T1_{33} & T1_{34} & 0 \\
T1_{43} & T1_{44} & 1
\end{bmatrix} \quad
\begin{cases}
M_{X} \\ F_{Y} \\ Q
\end{cases} 1$$
(4.69)

Point 3 is reached by multiplication of the modified matrix T1 by the field transfer matrix [T2]:

$$[T] = \begin{bmatrix} T2_{11} & T2_{12} & T2_{13} & T2_{14} \\ T2_{21} & T2_{22} & T2_{23} & T2_{24} \\ T2_{31} & T2_{32} & T2_{33} & T2_{34} \\ T2_{41} & T2_{42} & T2_{43} & T2_{44} \end{bmatrix} \begin{bmatrix} T1_{13} & T1_{14} & 0 \\ T1_{23} & T1_{24} & 0 \\ T1_{33} & T1_{34} & 0 \\ T1_{43} & T1_{44} & 1 \end{bmatrix}$$
(4.70)

Equation 4.66 can be added to the overall transfer matrix:

$$\begin{bmatrix} \mathbf{U}_{\mathbf{Y}} \\ \mathbf{\Psi}_{\mathbf{X}} \\ \mathbf{M}_{\mathbf{X}} \\ \mathbf{F}_{\mathbf{Y}} \\ \mathbf{0}^{\mathbf{Y}} \end{bmatrix}_{3} = \begin{bmatrix} \mathbf{U}_{11} & \mathbf{U}_{12} & \mathbf{U}_{13} \\ \mathbf{U}_{21} & \mathbf{U}_{22} & \mathbf{U}_{23} \\ \mathbf{U}_{31} & \mathbf{U}_{32} & \mathbf{U}_{33} \\ \mathbf{U}_{41} & \mathbf{U}_{42} & \mathbf{U}_{43} \\ \mathbf{T}\mathbf{1}_{13} & \mathbf{T}\mathbf{1}_{14} & \mathbf{0} \end{bmatrix} \begin{bmatrix} \mathbf{M}_{\mathbf{X}_{1}} \\ \mathbf{F}_{\mathbf{Y}_{1}} \\ \mathbf{Q} \end{bmatrix}$$
 (4.71)

or

$$\mathbf{Z_3} - [\mathbf{U}] \ \mathbf{Z_1} \tag{4.72}$$

where the state vector at location 1 includes the reaction at location 2 and the state vector at location 3 has now five elements.

2) External Force

A static or harmonic force can be represented by an extended state vector and an extended transfer matrix. Figure 4.12b shows the same beam as the previous figure, but now at point 2 a harmonic force of amplitude Q and frequency Ω is being applied. The force at location 2 is given by the relation

$$F_{Y_2}^R - F_{Y_2}^L + Q$$
 (4.73)

This equation is introduced in the transfer matrix by adding one row and one column to matrix [T1] in the following manner:

$$\begin{bmatrix}
U_{Y} \\
\Psi_{X} \\
M_{X} \\
F_{Y} \\
1
\end{bmatrix}^{R} = \begin{bmatrix}
T1_{13} & T1_{14} & 0 \\
T1_{23} & T1_{24} & 0 \\
T1_{33} & T1_{34} & 0 \\
T1_{43} & T1_{44} & Q \\
0 & 0 & 1
\end{bmatrix}
\begin{bmatrix}
M_{X} \\
F_{Y} \\
1
\end{bmatrix}^{1}$$
(4.74)

where one more equation has been added: 1 - 1.

The overall extended transfer matrix is given by the product of the matrix in Equation 4.74 and that in [T2]. The final matrix equation that expresses the state vector at 3 is:

$$\begin{pmatrix} \mathbf{U}_{\mathbf{Y}} \\ \mathbf{M}_{\mathbf{X}} \\ \mathbf{F}_{\mathbf{Y}} \\ \mathbf{1}^{\mathbf{Y}} \end{pmatrix}_{3} - \begin{pmatrix} \mathbf{U}_{11} & \mathbf{U}_{12} & \mathbf{Q}_{1} \\ \mathbf{U}_{21} & \mathbf{U}_{22} & \mathbf{Q}_{2} \\ \mathbf{U}_{31} & \mathbf{U}_{32} & \mathbf{Q}_{3} \\ \mathbf{U}_{41} & \mathbf{U}_{42} & \mathbf{Q}_{4} \\ \hline 0 & 0 & 1 \end{pmatrix} \begin{pmatrix} \mathbf{M}_{\mathbf{X}} \\ \mathbf{F}_{\mathbf{Y}} \\ \mathbf{1} \end{pmatrix}_{1}$$
(4.75)

or

$$\mathbf{Z_3} - [\mathbf{U}] \ \mathbf{Z_1} \tag{4.76}$$

where the Q_1 , Q_2 , Q_3 and Q_4 represent the forcing terms.

4.2.6 Natural Frequencies

The natural frequencies of liquid-filled piping systems are important in the design process. Let [U] and Z be the global transfer matrix and state vector of the single pipe reach vibrating in the Y-Z plane shown in Figure 4.11. The global transfer matrix relates the state vectors at the end points

$$\mathbf{Z}_{1} - [\mathbf{U}] \ \mathbf{Z}_{0} \tag{4.77}$$

The natural frequencies of this system depend on the boundary conditions described in Equations 4.63 and 4.64. Because some of the variables are zero at the boundaries, the number of elements of the state vectors at locations 0 and 1 is reduced. Therefore, the order of the global transfer matrix is also reduced. For example, the plane vibration of the pipe reach has eight variables. Four variables are known at each end reducing the number of elements of the state vector to four. This can be represented by

$$\begin{cases}
0 \\
0 \\
0 \\
0
\end{cases} - \begin{bmatrix}
U_{55} & U_{56} & U_{57} & U_{58} \\
U_{65} & U_{66} & U_{67} & U_{68} \\
U_{75} & U_{76} & U_{77} & U_{78} \\
U_{85} & U_{86} & U_{87} & U_{88}
\end{bmatrix} \quad
\begin{cases}
V \\
M_X \\
F_Y \\
F_Z
\end{cases} 0$$
(4.78)

or

$$\{0\}_{1}^{-} [\mathbf{U}] \{\mathbf{Z}_{0}^{-}\}$$
 (4.79)

where the vector Z represents the non-zero variables and the order of the matrix [U] has been reduced by the boundary conditions that are zero. To have a non-trivial solution the determinant of the reduced matrix must be zero

$$\Delta - \left| \left[\mathbf{U} \right] \right| \tag{4.80}$$

This generates an equation for the circular natural frequency ω . In practice [50], the procedure adopted is to choose certain values for ω and compute the corresponding values of the frequency determinant $\Delta(\omega)$. The values of the determinant are then plotted against the frequency ω . The values of ω at which the determinant equals zero are the natural frequencies of the system.

4.2.7 Mode Shapes

After the natural frequencies have been determined, the mode shapes of an elastic system can be found in terms of one variable. For example, assume that the fluid displacement at location 0 in Figure 4.11 has a unit amplitude. Equation 4.78 then becomes

$$\begin{cases}
0 \\
0 \\
0 \\
0
\end{cases} = \begin{bmatrix}
U_{55} & U_{56} & U_{57} & U_{58} \\
U_{65} & U_{66} & U_{67} & U_{68} \\
U_{75} & U_{76} & U_{77} & U_{78} \\
U_{85} & U_{86} & U_{87} & U_{88}
\end{bmatrix} = \begin{bmatrix}
1 \\
M_X \\
F_Y \\
F_Z
\end{bmatrix}_0$$
(4.81)

where the partitioning corresponds to the unknown variables. Once the variables at 0 are known, the variables at specified locations of the pipe reach may be found. This is accomplished by evaluating the transfer matrix at the natural frequency and at the given location. Then, the transfer matrix is multiplied by the state vector at the initial location. This is represented by

$$\begin{cases}
P \\
\Psi_{X} \\
U_{Y} \\
U_{Z} \\
V \\
M_{X} \\
F_{Y} \\
F_{Z}
\end{cases} =
\begin{bmatrix}
T_{15} & T_{16} & T_{17} & T_{18} \\
T_{25} & T_{26} & T_{27} & T_{28} \\
T_{35} & T_{36} & T_{37} & T_{38} \\
T_{45} & T_{46} & T_{47} & T_{48} \\
T_{55} & T_{56} & T_{57} & T_{58} \\
T_{65} & T_{66} & T_{67} & T_{68} \\
T_{75} & T_{76} & T_{77} & T_{78} \\
T_{85} & T_{86} & T_{87} & T_{88}
\end{bmatrix}$$

$$\begin{cases}
V \\
M_{X} \\
F_{Y} \\
F_{Z}
\end{cases} =$$

$$(4.82)$$

where i represents a location along the pipe reach. This procedure is followed until the other boundary is reached.

4.2.8 Frequency Response

The transfer matrix method can be used to determine the frequency response of systems having one or more periodic forcing functions. Chaudhry [7] describes a method to determine the frequency response of these systems. The extended matrix and state vector concepts and the method of superposition can be used to find the total response. The response of the system to each forcing function is evaluated and the results are then superimposed to determine the total response of the

system. Determining the response for a forcing function of frequency Ω involves evaluating the global transfer matrix at that frequency. Then, the response of the dependent variable such as forces and displacements at the starting point are found by following a similar procedure to the one used to compute the mode shapes. For example, the moment and force of the system shown in Figure 4.12b and represented in Equation 4.75, become

Once the conditions at location 1 (Figure 4.12b) are known the response at the desired locations can be found by evaluating the transfer matrix from the starting point up to that location. This procedure is followed for each frequency of the frequency range at a specified frequency interval.

4.3 Comparison with Other Methods

The transfer matrix method is compared in this section with the method of characteristics (MOC) [5,6,7], the component synthesis method (CSM) [34,35,36], and with experimental data available in the literature. Two piping systems are used to make the comparisons. The first system is a one-dimensional liquid-filled pipeline with a reservoir that has a closed end, either free or fixed. The second system is an L-shaped pipe

connected to a reservoir and free at the other end. The L-shaped pipe was tested at the David W. Taylor Naval Research and Development Center in Maryland [24]. This pipe has been extensively studied. The previous modeling efforts included direct analytical solution of simultaneous differential equations [24], component synthesis using finite element discretization (Nastran) for the structural elements [37] and finite element analysis in three dimensions [86].

4.3.1 Method of Characteristics

The method of characteristics has been widely used to estimate the response of liquid systems to transient events. A description of the method is presented by Wylie and Streeter [6] and Chaudhry [7]. The MOC has also been used to model waves propagating in beams including rotary inertia and shear deformation [89]. Numerical difficulties in modeling beams have made the MOC unattractive in modeling liquid-filled pipings for plane vibration [65]. This method was used by Otwell [19], Wiggert et al.[20], and Budny [22] to compare experimental data in which fluid-structure interaction was allowed. Budny [22] incorporated damping in both the pipe and the liquid. His model is used here to predict the pressure response of the one-dimensional pipe with no energy dissipation. Table 4.1 shows the characteristics of a straight copper pipe filled with water.

TABLE 4.1
PROPERTIES OF STRAIGHT LIQUID-FILLED PIPE

	Pipe				Liquid			
	Property Young's Modulus Density Poisson's Ratio Inside Radius Thickness Wave Speed		Value		Property	Value		
			117	GPa	Bulk Modulus	2.2 1000 1248	Gpa kg/m m/s	
			8940 0.45 13 1.2 3744	kg/m ³ mm mm m/s	Density Wave Speed			
Boundary	Conditions			_, _	opene		, 0	
	Case a Fixed-Fixed Case b Fixed-Free				Open-Closed Open-Closed			

The Poisson's ratio has been adjusted to 0.45 so that the ratio of the coupled wave speeds is three. Taking the pipe wave speed as a mutiple of the liquid avoids any interpolations that may introduce numerical errors in the MOC [6,90]. The relative displacement as well as the net force must be zero at the free end condition as described by Budny [22]. Inertia forces are not included at the free end. A sinusoidal function applied to the liquid at the open-end is the source of excitation in both cases. A fast Fourier transform (FFT) analysis of the time history generated by the MOC is performed to obtain the frequency response. The pressure amplitude response at the closed end is plotted in Figure 4.13. The natural frequencies are the same regardless of the method of computation. Table 4.2 shows the natural frequencies for both cases. The results for Case a are shown in Figure 4.13a. Case b shows that when the pipe wall is free in the axial direction, the third liquid and first pipe natural frequencies coincides at 12 Hz. The frequencies of both

the liquid and pipe are split apart to 9.0 and 14.4 Hz. The same result occurs at the ninth liquid harmonic which coincide with the second natural frequency of the axial pipe wall at 36 Hz. Figure 4.13b shows this result.

TABLE 4.2

NATURAL PREQUENCIES FOR STRAIGHT PIPE

	Case a		Case b			
Frequency	Type	Harmonic	Frequency	Туре	Harmonic	
· (Hz)			(Hz)			
4.0 11.7 19.4 23.4 27.4 35.1 42.8 46.8	F F P F F P	1 3 5 1 7 9 11 2	4.0 9.0 14.4 19.4 27.3 32.4 37.8 42.8	F P F F P F	1 1 3 5 7 2 9	
50.8	F	13	50.7	F	13	

F - Fluid, P - Pipe

4.3.2 Component Synthesis Method and Experimental Data

The second comparison of the transfer matrix method is with the component synthesis method and experimental data. Hatfield et al. [37] devised the component synthesis approach which is an extension of the modal synthesis technique [36] for dynamic analysis of structures. The L-shaped pipe in Figure 4.14 was used to validate the CSM. Table 4.3 describes the properties of the pipe, 70% copper and 30% nickel and filled with oil [24].

TABLE 4.3

PROPERTIES OF L-SHAPED LIQUID-FILLED PIPE

Pip	Pipe				Liquid			
Property	Value		Property	Value				
Young's Modulus	157	GPa	Bulk Modulus	2	Gpa			
Density Poisson's Ratio Outside Diameter Inside Diameter Radius of Bend	9000 kg/m 0.34 114 mm 102 mm 102 mm	Density	872 kg	kg/m				
Radius of Bend	102	mm	Sound Speed In-Situ	1372	m/s			
Boundary Conditions Fixed-	Clos	ed-Open						

A correction for the flexural stiffness, EI, of the bend was used for both numerical methods. A curved pipe subject to bending is less stiff than would be indicated by elementary theory of bending [87]. The correction formula developed by von Karman [88] is

$$\eta = \frac{1 + 12(eR/r^2)}{10 + 12(eR/r^2)}$$
 (4.84)

where η is the correction factor for the flexural stiffness, R is the radius of the bend, r is the inside radius of the pipe and e is the thickness of the pipe. The CSM does not include the Poisson's coupling because in the computation of the normal modes of vibration of the pipe the interaction with the liquid is not considered. However, the mass of the contained liquid is included as part of the total mass. The first lobar mode of the cross section is 850 Hz.

The pipe frequencies for the CSM are computed by using the finite element program Nastran. Ten modes and 25 elements are used in the computations. Seven pipe reaches are used to model the pipe by using the transfer matrix method. The 90 bend is modeled using three pipe reaches each with a relative change of 30 in orientation. The liquid in the pipe was excited by a harmonic oscillator. Neither structural nor fluid damping are considered in the computations. The liquid is free to move at the free end. The mobility (ratio of velocity over force) of the liquid at the excitation point and free end, as well as the mobility of the pipe in the Y and Z directions are shown in Figure 4.15. Discrepancies in predicted and measured responses in the vicinity of the amplitude peaks are because damping was not included in the computed analysis. In non-resonant frequency ranges, differences in the responses predicted by the two analyses are minor compared to the deviations of both predictions from observed responses, particularly in the structural responses (Figures 4.15c and 4.15d). The discrepancy in the structural mobility may be caused by the flexibility factor which is significant in accurately modeling elbows [86].

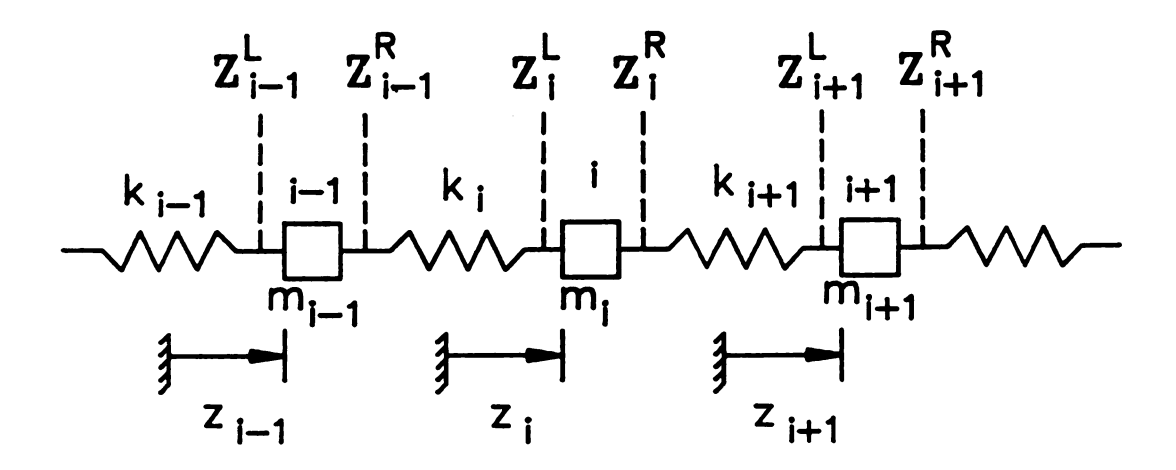


Figure 4.1 Generalized Spring-Mass System

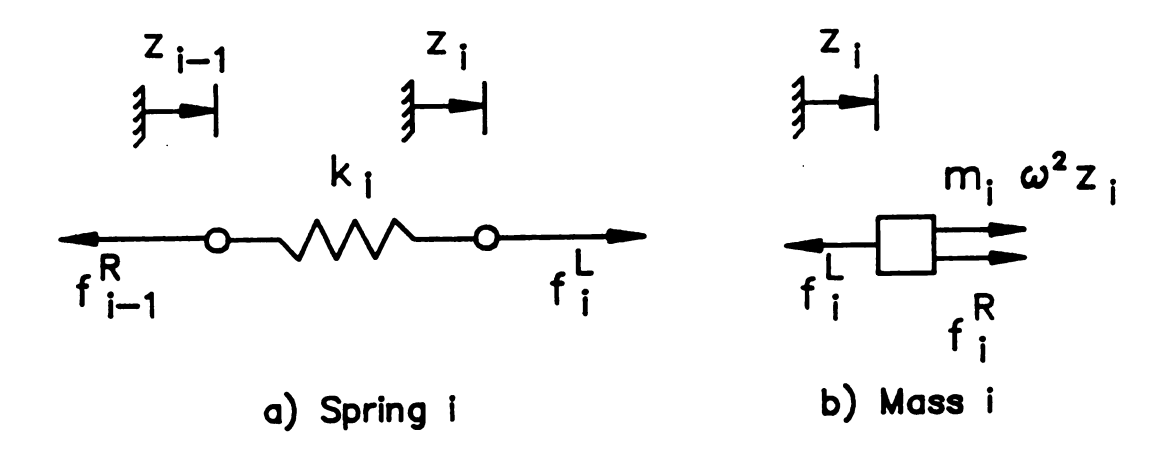


Figure 4.2 Free Body Diagrams of Spring and Mass Systems

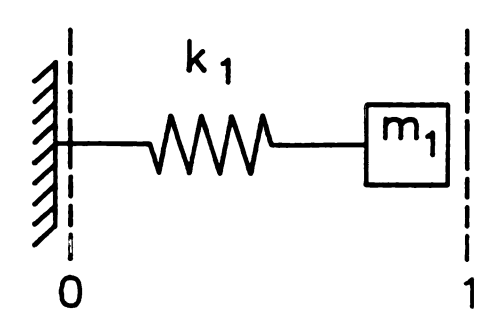


Figure 4.3 Simple Spring-Mass System

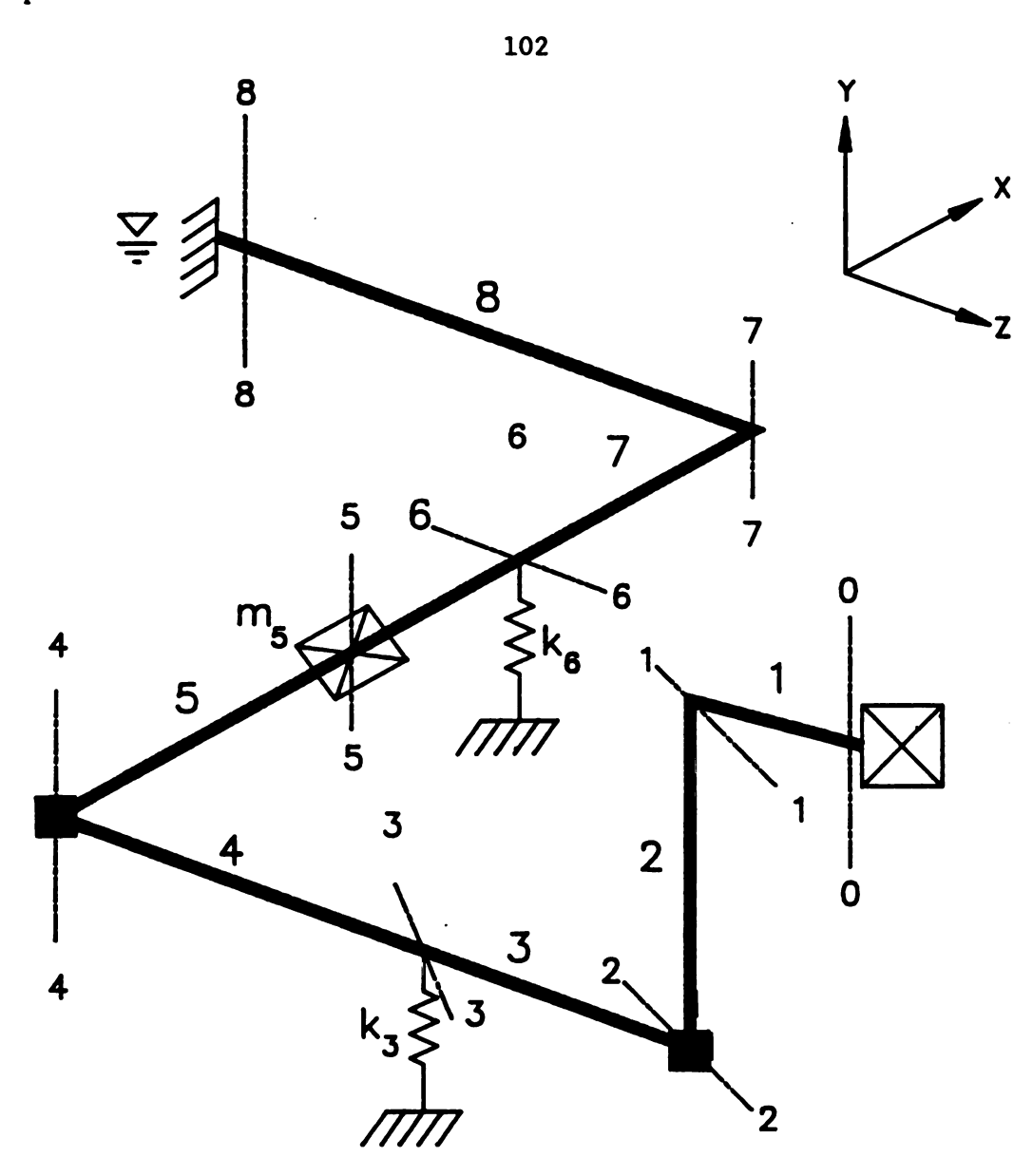


Figure 4.4 General Piping System

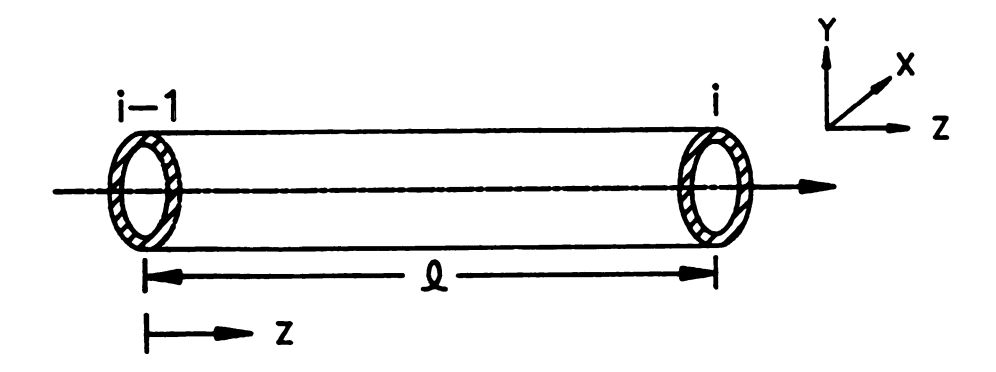
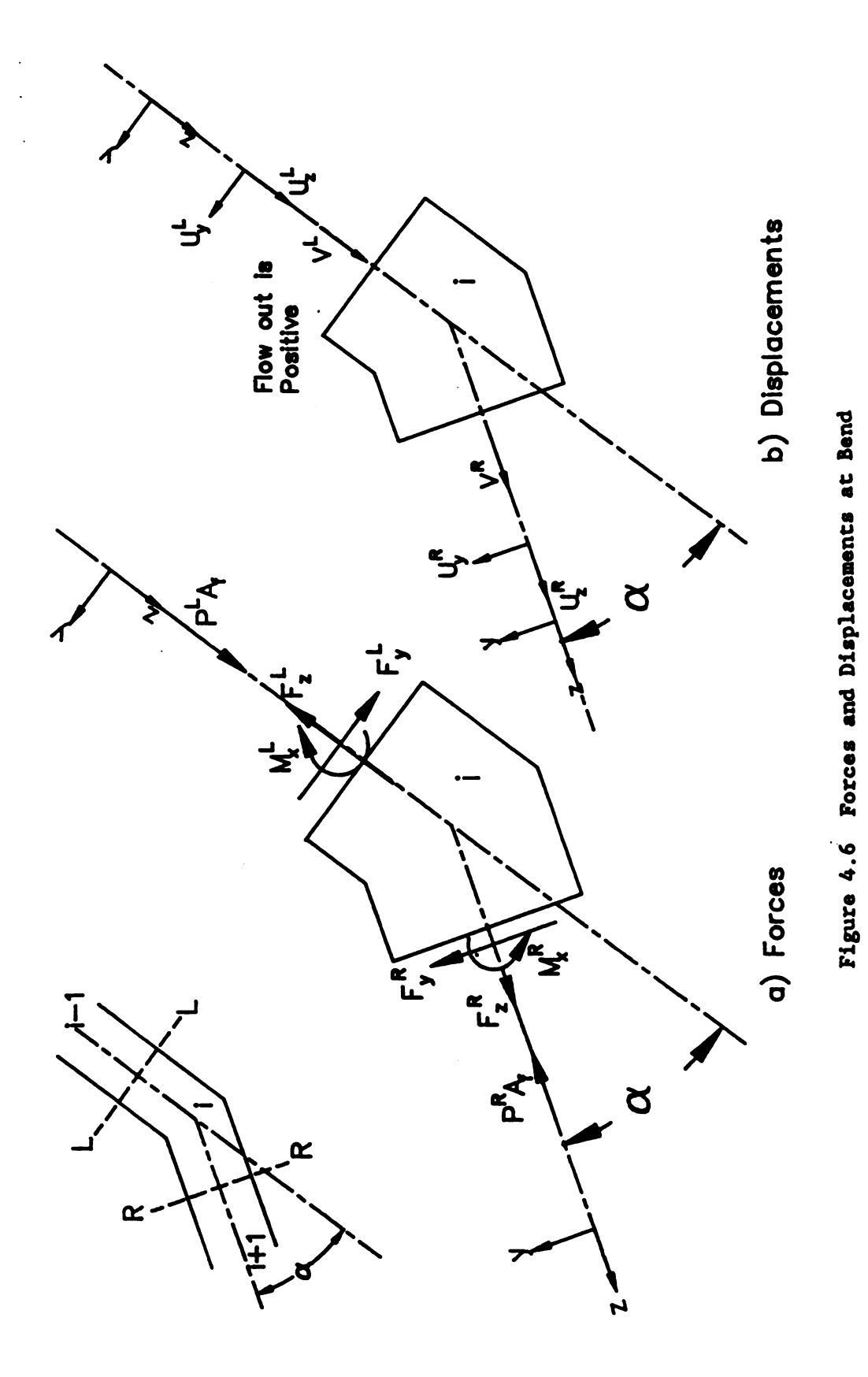
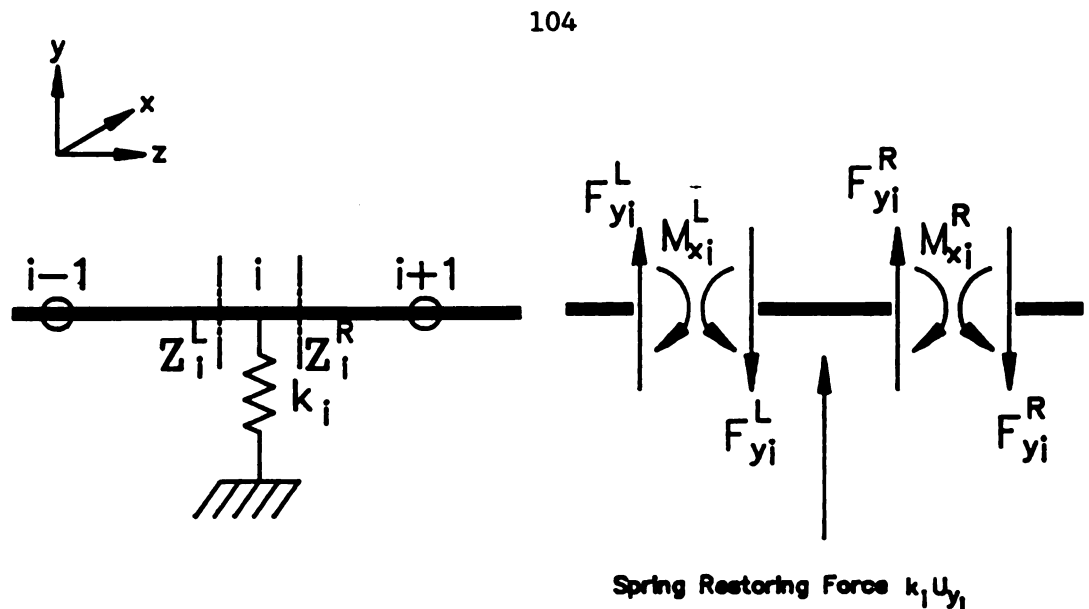


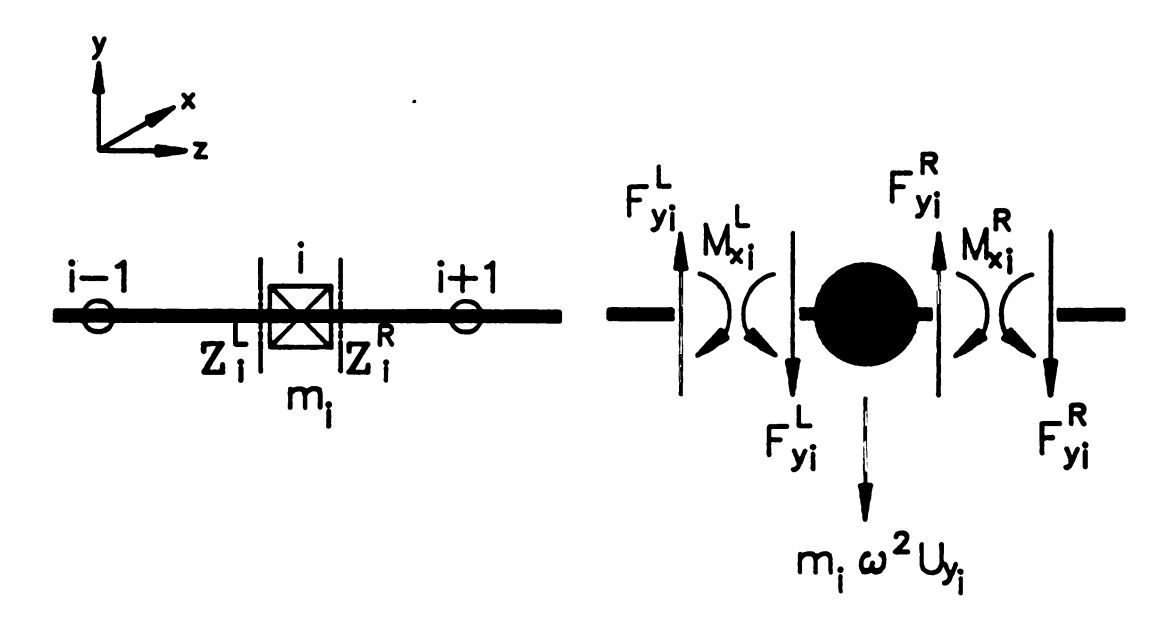
Figure 4.5 General Straight Liquid-Filled Pipe Reach





- a) Liquid-Filled Pipe With Spring
- b) Free Body Diagram

Figure 4.7 Forces at Spring



- a) Liquid-Filled Pipe With a Point Mass
- b) Free Body Diagram

Figure 4.8 Forces at Concentrated Mass

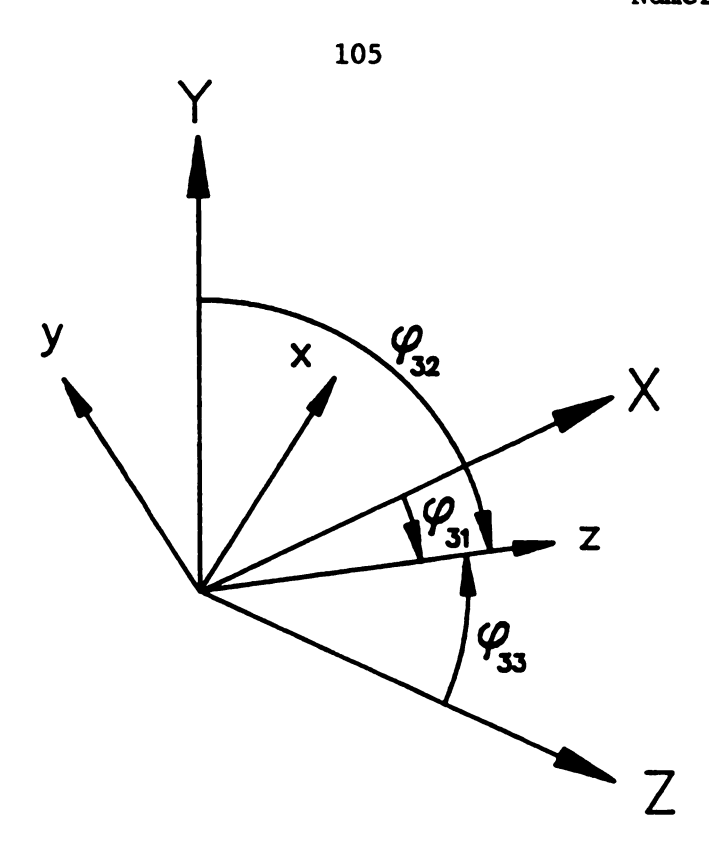


Figure 4.9 Definition of Local and Global Axes

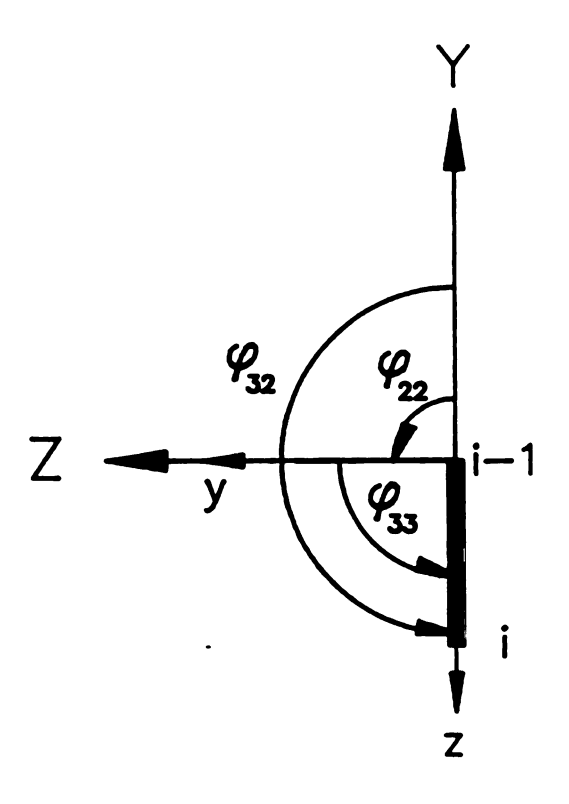


Figure 4.10 Coordinate Transformation of Straight Pipe Reach

Figure 4.11 Boundary Conditions

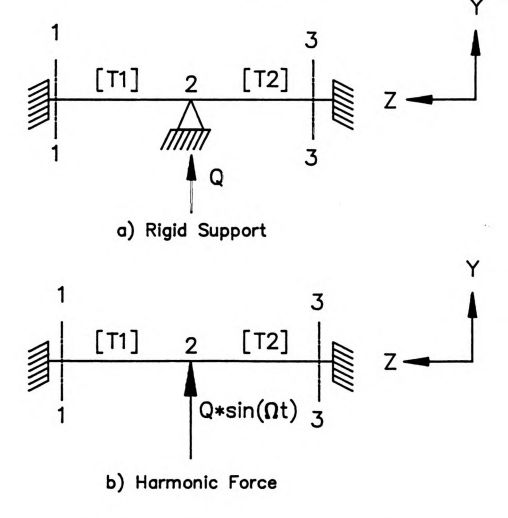
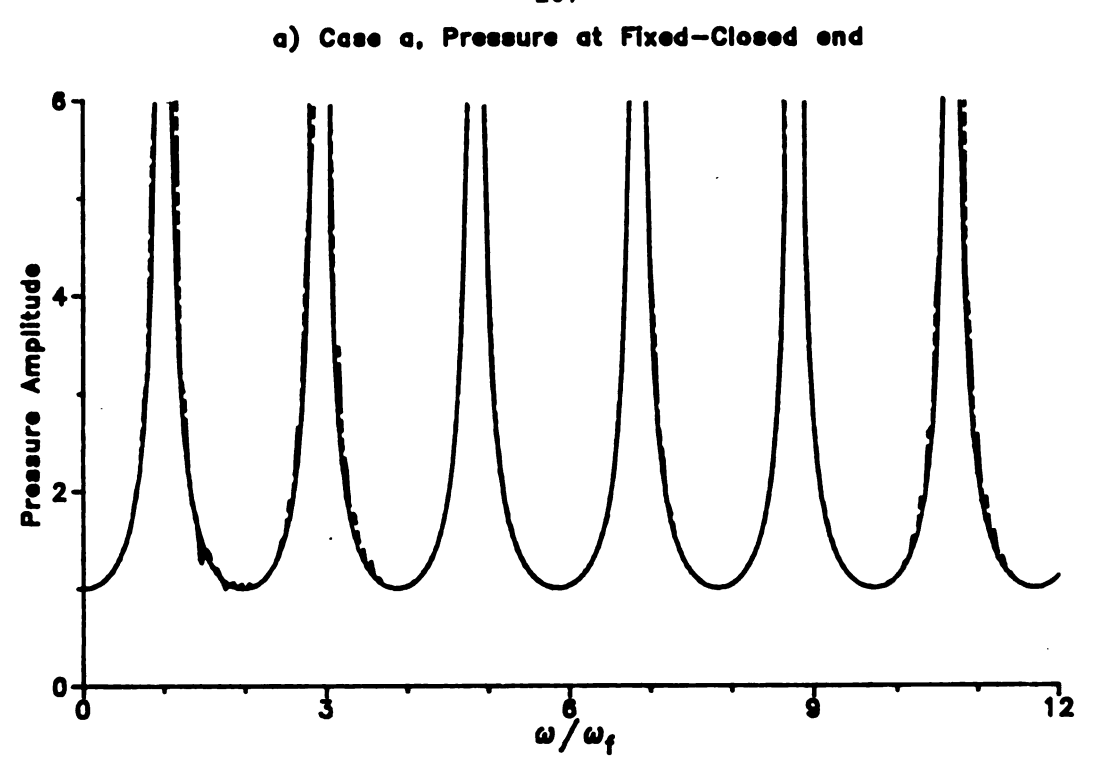


Figure 4.12 Intermediate Boundary Conditions



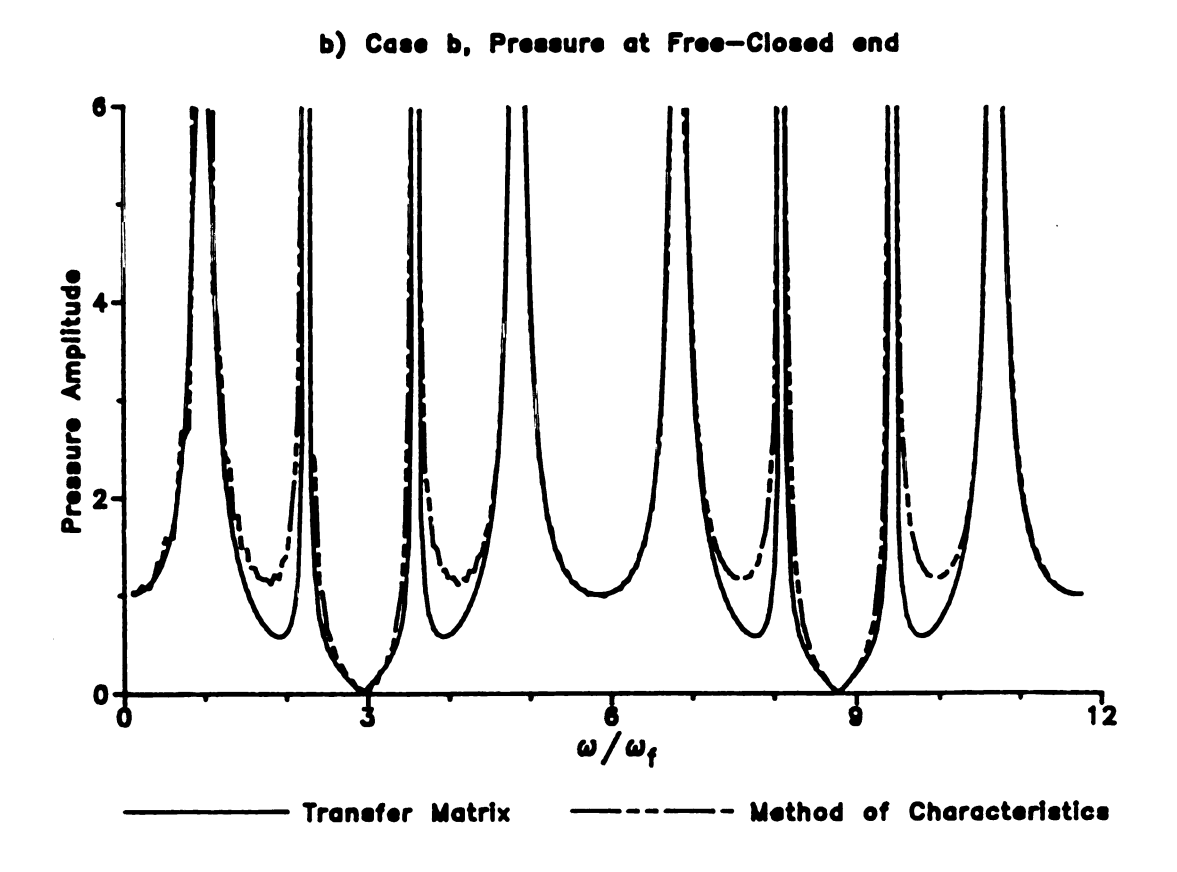


Figure 4.13 Pressure Amplitude Response for Straight Pipe Reach

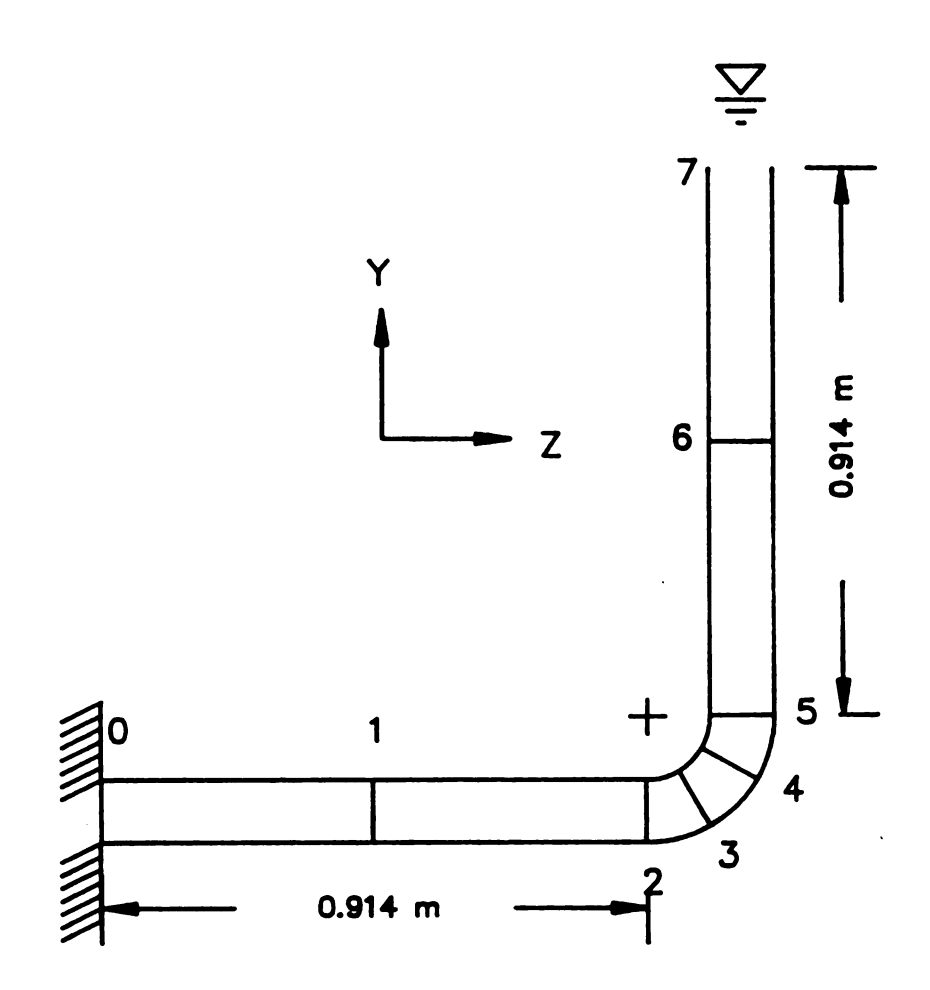
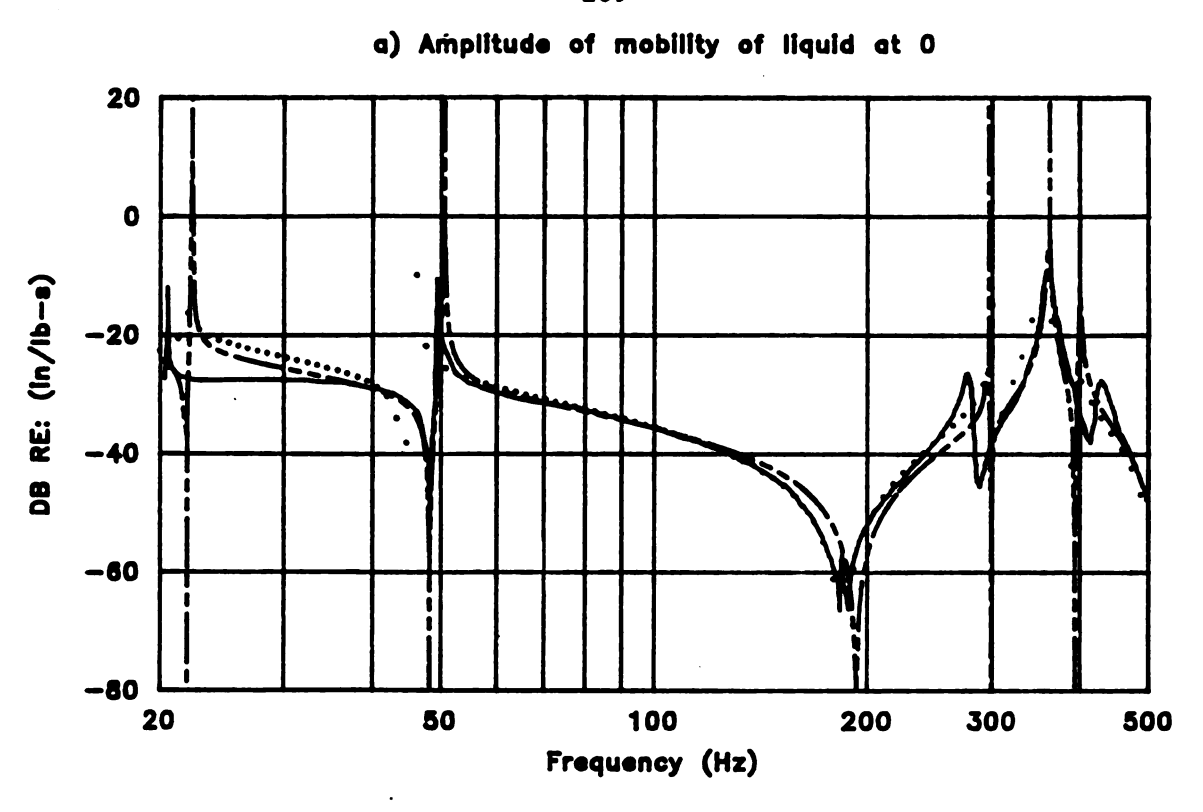


Figure 4.14 L-Shaped Liquid-Filled Pipe



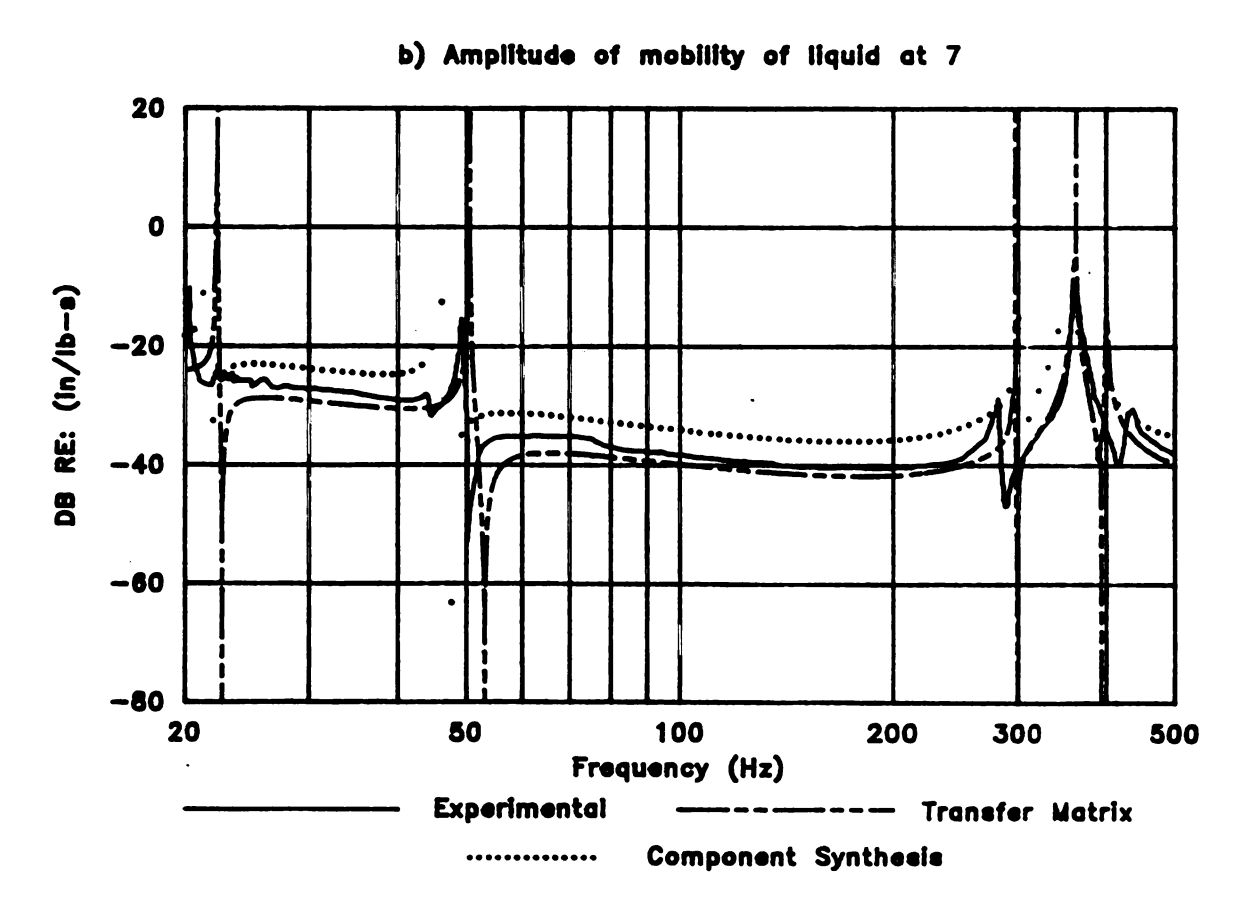
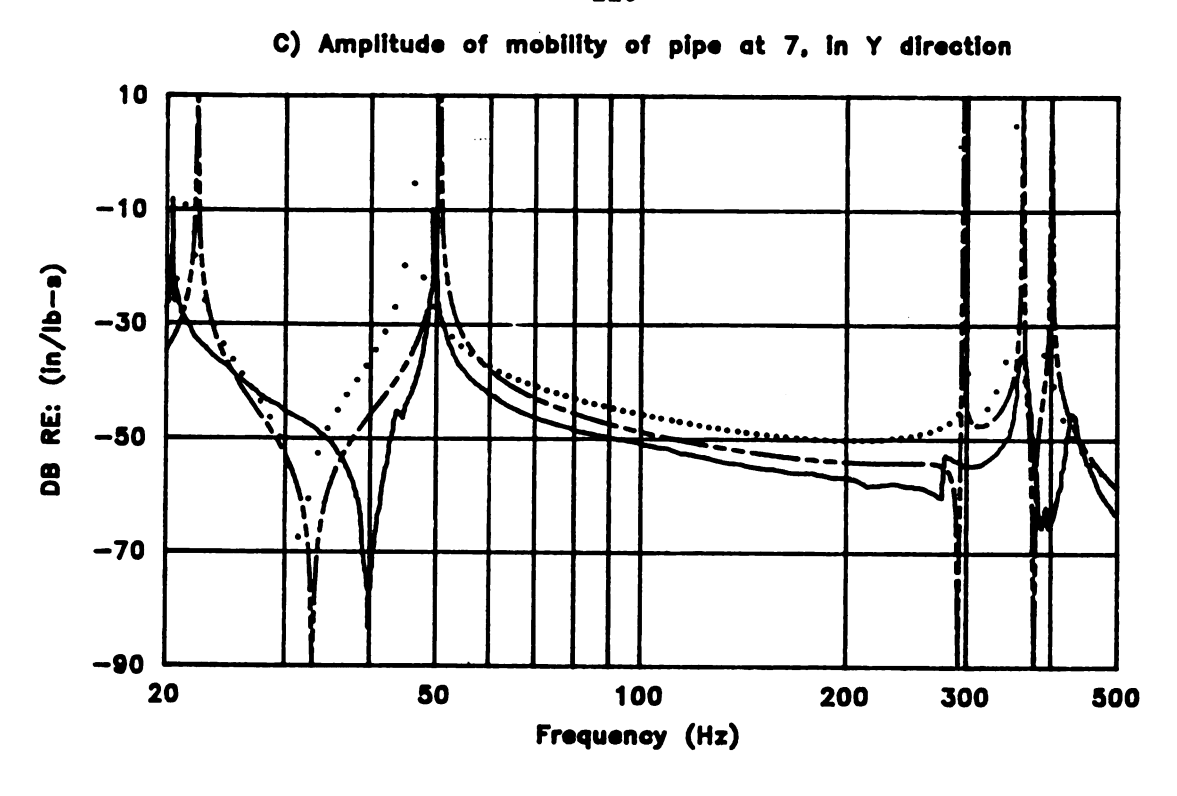


Figure 4.15 Mobility Diagrams for L-Shaped Pipe



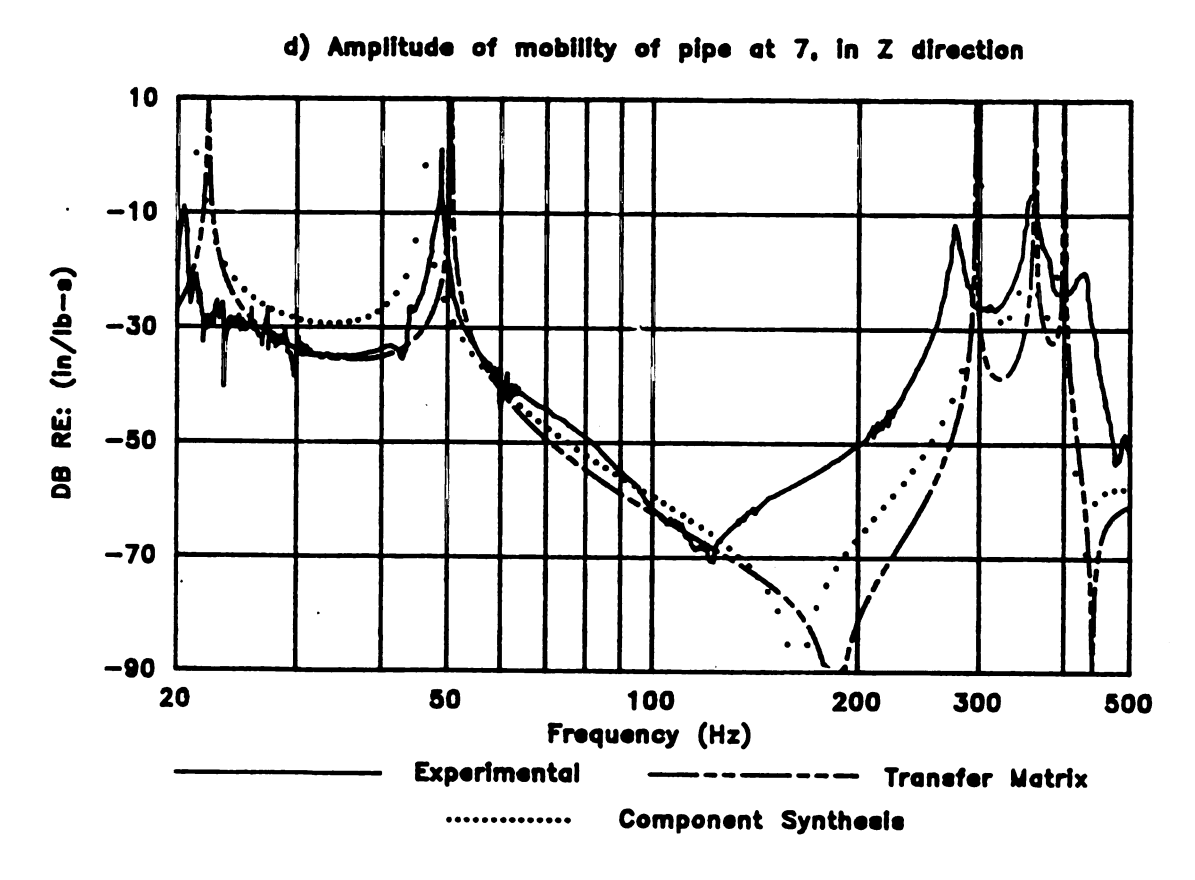


Figure 4.15 (Continuation)

CHAPTER 5

EXPERIMENTAL APPARATUS

5.1 Introduction

The analytical model derived in Chapter 3 and the methodology described in Chapter 4 incorporate the flexural and torsional modes of vibration into an existing coupled axial pipe wall and liquid model. This model represents five families of waves. Four of the waves propagate in the pipe wall and one in the liquid. The previous section compared the frequency responses of the proposed model to the method of characteristics and the component synthesis method. The model was also compared with experimental results available in the literature.

This chapter describes the experimental apparatus that was designed and built to validate the proposed model. The comparisons of the previous chapter validate the model only partially because the excitation was applied to the liquid column and the natural frequencies of the liquid were unchanged. The experimental apparatus is designed to excite the natural frequencies of a piping system. The excitation is harmonic.

The experimental apparatus was located in the basement of the Engineering Building on the campus of Michigan State University. The piping system, the experimental procedure and the sources of experimental error are described in this chapter. Appendix B describes the data acquisition equipment utilized, including the hardware and software.

5.2 Description of Experimental Apparatus

This section examines the components considered in the design of the apparatus. These components will be discussed in reference to either the pipe or the contained liquid. Liquid medium, constant pressure reservoirs and a valve are the components related to the liquid. Pipe material, pipe supports and the external shaker are associated with the pipe. The final component of the experimental apparatus is the data acquisition equipment. Figure 5.1 shows the piping system set-up.

5.2.1 Liquid Components

5.2.1.1 Liquid

The liquid used in the experiments was water from the university water supply system. Table 5.1 [78,79] lists the physical properties of the water.

TABLE 5.1
PHYSICAL PROPERTIES OF LIQUID

Property					
Temperature	(V)	25.0 2.2	°C GPa	77.	°F
Bulk Modulus	(K)	2.2	Gra	320.	kpsi
Density	(ρ)	997.0	kg/m	1.93	slugs/ft

5.2.1.2 Constant Pressure Reservoirs

The upstream and downstream reservoirs each consist of two 454 liter vertical F.E. Myers Model V120G 14800C8 well tanks. Each tank is rated for 517 kPa (75 Psi). The set-up of the tanks is shown in Figure 5.2a. A one inch U.S. nominal diameter pipe connects the bases of the pair of tanks, allowing them to act as a single reservoir.

The tanks are pressurized with Engineering Building air supply that has a maximum pressure of approximately 650 kPa (94 Psi). The air pressure allows a constant liquid pressure at point C as shown in Figure 5.1. The air supply passes through a Schrader Model 3564-2000 pressure regulator, and is directed through an orifice on top of the tanks with a common header. The header is used to maintain equal air pressure in both tanks.

The tanks are filled with water through a hose connection on the one inch nominal diameter transfer line at the base of the tanks. This transfer line is connected to the one inch diameter pipe at the base of each reservoir and has a shutoff valve at each end. In addition to

allowing filling and emptying of the tanks, this transfer line is used to transfer water between the reservoirs. Water level in the tank is monitored using a sight glass connected to the orifices on the side of one of the tanks in each reservoir. These tanks are also used to purge the air from the system. The purging procedure described by Budny [22] was used. The open boundary condition defined in section 4.2.5.1 is simulated by the set of tanks at one end of the piping system.

5.2.1.3 Valve

A fast closing valve, described by Budny [22], was placed at one end of the piping system, as shown at point A in Figure 5.1. Figure 5.2b shows two views of the valve. For the purposes of this study, the valve was kept in the closed position simulating a dead-end [6,7].

5.2.2 Pipe Components

5.2.2.1 Pipe Material

The pipeline used is a one inch U.S. nominal diameter type L copper pipe with standard soldered fittings. Unions are installed at intervals of approximately 7.3 meters (24 ft.) along the pipeline to allow for changes of the total pipe length. Figure 5.1 shows the pipeline setup. Table 5.2 [78,80,81] lists the physical properties of the piping system.

TABLE 5.2

PHYSICAL PROPERTIES OF PIPING SYSTEM

Property			Value		
Young's Modulus	(E)	117.0	GPa	17.00	Mpsi
Density*	(ρ)	8900.0	Kg/m	17.30	slugs/ft
Inside Radius	(r)	13.0	mm	0.51	in
Outside Radius		14.3	mm	0.56	in
Thickness	(e)	1.3	THE REAL PROPERTY.	0.05	in
Poisson's Ratio	(v)		0.35		

^{*} Determined by water displacement [22]

5.2.2.2 Pipe Supports

Unistrut model P2031 pipe clamps mounted approximately 3.7 meters (12 ft.) apart are used to provide support of the pipe to the wall. In addition, rigid supports are connected to the piping at each elbow to eliminate axial motion.

Each rigid support is an aluminum block bolted to the wall. Each block has a hole matching the OD of the pipe drilled in its center. Each block is cut in half through this hole and bolt holes are drilled through both sections. Bolts are then used to hold the two pieces together enabling the block to act as a vise, squeezing the pipe around its entire circumference. The entire support is then bolted to the wall, using 3/8 inch Red Head anchor bolts.

Rope hangers are used to hold the piping at locations where neither one of the above supports are placed. The locations of the supports are

displayed in Figure 5.1. The Unistrut supports may be replaced by rigid supports to vary the length of the piping. The procedure to change these supports is discussed in section 5.2.3.

5.2.2.3 External Shaker

The excitation of the pipe is induced by a reciprocating force produced by an external shaker. The shaker is a crank-slider mechanism that transfers rotary motion to reciprocating motion. Top and side views of the mechanism are shown in Figure 5.3. Figure 5.4 shows a sketch of the same mechanism. The mechanism consists of five major elements: a motor, crank, connecting rod, linear bearing structure and connecting spring. These elements will be described next.

The motor is a Dayton model 42140, permanent magnet DC variable-speed motor with a Dayton SCR control which allows changes of the rotational speed. The rated frequency and torque of the motor are 1800 RPM and 0.5 N-m (4.38 in-1b), respectively. The motor is mounted on a structure made of 102 mm (4 inch) L-shaped steel bars bolted to the wall. This structure prevents any vibration that may interfere with the experiments. A flywheel is attached to the end of the shaft of the motor. Bolted to the flywheel is an aluminum disk. A distance of 1.5 mm between the center of the aluminum disk and the center of the flywheel forms the crank of the slider mechanism. A 1/2 inch Heim Unibal Spherical Rod End Bearing is joined to the aluminum disk by a 6.4 mm screw. This joint is a pin-type connection, as shown at point C in

Figure 5.4. The pin connection, which follows a circular path, transfers the rotary motion of the crank to the spherical bearing. spherical bearing is screwed to a one inch diameter aluminum rod. At the other end of the rod there is a similar spherical bearing that connects to a linear bearing structure by a wrist-type connection. motion at point P in Figure 5.4 oscillates along a linear path. The transfer of rotary motion to reciprocating motion occurs along the aluminum rod, whose points follow elliptical paths. The total length of the link is 880 mm (Figure 5.3). Two pairs of 1/4 inch linear selfaligning, super-ball bushing bearings slide on two stainless steel rods, simulating piston-type motion of the linear bearing structure. static coefficient of friction is 0.2% [82]. These rods are supported on acrylic blocks which are glued to an acrylic base. The base is mounted on a L-shaped steel bar bolted to the wall. A 1/2 inch steel rod anchored to the bearing structure, in the same plane as the link, connects to the spring. Table 5.3 gives the technical information concerning these shaker components.

5.2.2.4 Spring

The reciprocating motion of the linear bearing structure is transmitted to the pipe by a round-wire helical compression spring. The spring allows a linear relationship between the reciprocating displacement at the bearing structure and the force that is transmitted to the pipe. The technical information regarding the spring is shown in Table 5.4 [13].

TABLE 5.3 SHAKER COMPONENTS

Component	Material	Diameter	Thickness	Length	Mass
		(mm)	(mm)	(mm)	(gm)
Motor Shaft		12.7			
Flywheel	Steel	127.0	32.0		2980
Disk	Aluminum	61.0	22.9		150
Crank Off-Center		6.4		1.5	
Heim Uniball Sphe	erical				
Rod End Bearing		12.7		76.2	
Rod	Aluminum	25.4		825.0	
Link				880.0*	1350
Linear Bearings		6.4		20.3	
Linear Bearing Structure					1510
Rod Connector	Steel	12.7		140.0	

^{*} Total distance between point C and P in Figure 5.4.

(See Figure 5.3)

TABLE 5.4 SPRING PROPERTIES

Property	Value					
Material	Hard-drawn steel wire, zinc plated*					
Mass (m _s)	20.3 gma					
Spring Constant	(k _g)	7.0	kN/m	40	lb/in*	
Modulus of Rigidity	(G)	79.3	Gpa	11.5	Mpsi	
Mean Spring Diameter	(D)	15.9	mm	0.63	in	
Wire Diameter	(d)	2.4	mm	0.09	in	
Active Coils	(N)			11*		
Natural Frequency	(f _e)		290	.0 Hz		
Spring Ends	3		Both end	s squared		

^{*} Obtained from the manufacturer

The spring is connected to the bearing structure by a 1/2 inch steel rod. A screw rigidly connects the spring to the rod. Another screw connects the other end of the spring to an acrylic collar that embraces the copper pipe, as shown in Figure 5.3. These connections reduce the number of active coils to seven, thereby increasing the stiffness of the spring to 11.7 kN/m (67 lb/in). This value was obtained from Equation 5.1 [13].

$$k_s = \frac{d^4G}{8D N}$$
 (5.1)

where k_s is the spring constant and D and d are the mean spring diameter and wire diameter, respectively. The modulus of rigidity is G and the number of active coils is represented by N. The reduction of the number of active coils also increases the natural frequency of the spring to 460 Hz. The natural frequency of the spring can be obtained from Equation 5.2, [13]

$$f_s - \frac{1}{2} \left(k_s / m_s \right)^{1/2} \tag{5.2}$$

where $\mathbf{m}_{\mathbf{s}}$ represents the active mass of the spring.

5.2.3 Experimental Configurations

The general piping set-up in Figure 5.1 will be used to describe the pipe configurations. Each pipe configuration varies in total length, therefore, the frequency of the liquid varies. A U-type bend is placed between the valve and the reservoir. The legs of the U-bend are 1.83 m (6 ft) each. The Unistrut and rigid supports restrict the motion of the pipe whereas the U-bend is free to move in the Y-Z plane. The external shaker is attached at the mid-point of the vertical leg of the U-bend, location D. The elbows of the U-bend are reinforced with a steel plate. Brass blocks are soldered to the copper pipe at both sides of each elbow. The steel plates then are screwed to the brass blocks. The steel plates, screws and the brass blocks add 0.5 Kg of mass to the U-bend, localized at each elbow.

TABLE 5.5
PIPING SYSTEM CONFIGURATIONS

Configuration	Location				Length		
	Valve		able Support	Reservoir	Meters	Feet	
1	В		4 4'	С	40.99	134.45	
2	В		5 5'	C	55.62	182.43	
3	Α	1 1'	4 4'	C	65.51	214.87	
4	A	1 1'	5 5'	C	80.14	262.93	
5	A	2 2'	4 4'	C	80.16	262.92	
6	В		6 6'	C	91.89	301.40	
7	A	3 3'	4 4'	C	94.77	310.85	
8	A	2 2'	5 5'	C	94.79	310.99	
9	A	3 3'	5 5'	С	109.40	358.92	
10	A	3 3'	6 6'	C	145.67	477.80	

(See Figure 5.1)

A total of 10 different pipe lengths can be obtained. The movable rigid supports are placed at locations where two pipe unions are aligned in the Y direction, as shown in Figure 5.1. Table 5.5 shows the total length of the system for each configuration. The change in pipe length allows variance of several parameters: frequency of the liquid, location of the U-bend, external excitation and data acquisition transducers.

5.2.4 Transducers

The responses of the liquid pressure and pipe motion to the harmonic excitation are recorded as functions of time. These recordings were accomplished using PCB pressure and acceleration transducers interfaced with either a Digital PDP-11/73 computer or a Tektronix D13 dual beam storage oscilloscope. A description of the components of the data acquisition equipment is presented in Appendix B. Two pressure transducers and two accelerometers were used in the recording. Another accelerometer monitored the motion of the linear bearing structure. Their locations are shown in Figures 5.1 and 5.5. One pressure transducer is located at the closed end where a liquid pressure antinode occurs. The other is located after the U-bend to monitor the effect of the motion of the pipe during the pressure response. The accelerometers are located at the spring and the elbow of each leg. At these locations, large displacements are expected to occur for the first and second natural frequencies of the U-bend [83].

TABLE 5.6 LOCATION OF TRANSDUCERS AND U-BEND RELATIVE TO VALVE

Location		Configuration								
	1	2	3	4	5					
$\begin{array}{c} {\tt Valve} \\ {\tt P_1} \end{array}$	0.0 0.3	0.0 0.3	0.0 0.2	0.0 0.2	0.0 0.2					
$\mathtt{B_1}$	1.2	0.9	38.2	31.2	49.5					
D_1	3.4	2.5	39.6	32.4	50.6					
$\mathtt{D_2}$	5.5	4.0	40.8	33.4	51.7					
\mathtt{B}_{2}	5.7	4.2	41.0	33.5	51.8					
Вз	10.1	7.5	43.8	35.8	54.1					
B ₄	14.6	10.8	46.6	38.1	56.3					
$\mathbf{P_2}$	16.1	11.9	47.5	38.8	57.1					
Reservoir	100.0	100.0	100.0	100.0	100.0					

Location		Configuration								
	6	7	8	9	10					
$\begin{array}{c} {\tt Valve} \\ {\tt P_1} \end{array}$	0.0 0.2	0.0 0.1	0.0 0.1	0.0 0.1	0.0 0.1					
$\mathtt{B_1}$	0.5	57.3	41.9	49.6	37.3					
$\mathtt{D_1}$	1.5	58.2	42.8	50.4	37.9					
\mathtt{D}_{2}	2.4	59.1	43.7	51.2	38.5					
B ₂	2.5	59.2	43.8	51.3	38.5					
B ₃	4.5	61.1	45.7	53.0	39.8					
B ₄	6.5	63.1	47.6	54.6	41.0					
P_2	7.2	63.7	48.3	55.2	41.4					
Reservoir	100.0	100.0	100.0	100.0	100.0					

- (See Figure 5.5) P = Pressure Transducer D = Accelerometer

 - B U-Bend

Table 5.6 shows the relative locations of the transducers, U-bend elbows and rigid supports with respect to the total length of each experimental configuration. Distances are measured from the closed end (valve) to the open end (reservoir).

5.2.5 Dynamic Forces and Natural Frequencies of Shaker

The magnitude and characteristics of the dynamic loads that the shaker puts into the spring and, therefore, into the pipe, must be known before experiments are performed. The dynamic forces are studied in the form of the reciprocating force induced by the crank mechanism and the force that the spring transmits to the pipe. Also, the shaker may introduce noise into the signals if a natural frequency of the component coincides with the frequency of excitation.

5.2.5.1 Shaker Loads

The reciprocating force at point P in Figure 5.4 can be defined when the acceleration at this point is known. Given that Ω is the frequency of oscillation in radians per second, then the displacement of the piston z_z^p measured from the dead-center position, at which Ω t is zero, is [84]:

$$z_z^p = \left(R + \frac{R^2}{4L}\right) - R\left(\cos(\Omega t) + \frac{R}{4L}\cos(2\Omega t)\right)$$
 (5.3)

The reciprocating force is:

$$f_z^p - (m_1 + m_b)R\Omega^2 \left[\cos(\Omega t) + \frac{R}{L}\cos(2\Omega t)\right]$$
 (5.4)

The inertia torque, $T_{_{\mathbf{Y}}}$ exerted by the motor on the crank is:

$$T_{x}^{o} = \frac{(m_{1}+m_{b})}{2}R^{2}\Omega^{2}\left[\sin(2\Omega t) - \frac{R}{2L}\left[\sin(\Omega t) - 3\sin(\Omega t)\right]\right]$$
(5.5)

where m₁ and m_b are the mass of the link and linear bearing structure, respectively. The first term in Equation 5.4 is called the primary term. Its frequency varies with the frequency of the motor. The other term is called the secondary term because its frequency varies with twice the frequency of the motor. The importance of the secondary term is established by the ratio R/L. In the case of an infinitely long connecting rod, the secondary term may be neglected and the piston follows a harmonic motion. For a connecting rod of finite length the motion of the piston is periodic but not harmonic. This ratio is less than 0.2% for the crank mechanism in Figures 5.3 and 5.4 (see Table 5.3). When the effect of the secondary term is neglected, the motion that the piston induces in the spring is harmonic. The reciprocating force and torque, then, depend on the mass of the link and linear bearing structure, the crank radius and the frequency of oscillation. Neglecting the secondary terms, Equations 5.3 through 5.5 become:

$$z_z^p = R \left(1 - \cos(\Omega t)\right) \tag{5.6}$$

$$f_z^p = (m_1 + m_b) R\Omega^2 \cos(\Omega t)$$
 (5.7)

$$T_{x}^{o} = \frac{(m_{1} + m_{b})}{2} R^{2} \Omega^{2} \sin(2\Omega t)$$
 (5.8)

Placing the values for the mass of the link and bearing structure in Equation 5.8 at the rated frequency shows that the torque on the motor shaft is 0.1 N-m, 20% of the rated torque of the motor. The torque induced by the reaction force of the spring on the shaft of the motor should also be included. This torque depends on the displacement at both sides of the spring, the stiffness of the spring and the crank radius. Because the displacement of the spring at the U-bend is frequency dependent the torque also depends on the frequency of oscillation. The curve that describes this relationship is presented in section 5.3.3.

5.2.5.2 Spring Loads

The shaker mechanism inputs a specified displacement at one end of the spring as given in Equation 5.6. The influence of the spring on the U-bend as shown in Figure 5.5 can be analyzed by studying a simplified structure. The U-bend can be considered a single mass-spring system connected to a spring with specified displacement U_0 and a force F as

shown in Figure 5.6. Let m_B and k_B be the mass and stiffness of the mass-spring system, and k_S the spring constant. A transfer matrix analysis of this system yields:

At location 2 the displacement $\mathbf{U}_{\mathbf{Z}}$ is zero, therefore, the frequency equation is

$$\left[1 - \frac{\Omega^2}{\omega^2}\right] U_0 + \left[\frac{1}{k_s} \left[1 - \frac{\Omega^2}{\omega^2}\right] + \frac{1}{k_B}\right] F = 0$$
 (5.10)

where ω is the frequency of the spring-mass system and Ω is the frequency at which the crank-slider mechanism is oscillating. This equation suggests that the dynamic loads from the shaker can be divided into two loads: one associated with the displacement, U_0 and one associated with the force, F. This force is the same as the spring force described in the previous section. Its description is also presented in Section 5.3.3.

5.2.5.3 Natural Frequencies of Shaker Components

The components that may induce high frequency vibration are the link, the spring and the steel rods on which the linear bearings slide. The link that connects the crank to the slider bearing may bend rather than having a purely rigid body motion, inducing lateral vibration to the mechanism. A transfer matrix analysis for a free-pinned solid beam (locations C and P in Figure 5.4) demonstrates that the first natural frequency occurs at 100 Hz which is 70 Hz above the rated frequency of the motor. The natural frequency of the spring is 460 Hz. The natural frequencies of the stainless-steel rods are 88 and 550 Hz for vibrations in the axial and transversal directions, respectively. The natural frequency of these components are higher than the rated frequency of the motor, therefore, the dynamic components of the shaker do not interfere with the harmonic motion induced onto the U-bend.

5.3 Experimental Procedure and Analysis

The objective of the experiments was to excite the natural frequencies of the U-bend and the liquid contained in the pipe and to record the pressure response and pipe motion. Several sampling parameters had to be determined before collecting data for each pipe configuration. These included the frequency range of excitation, the sampling frequency and the duration of the sampling process. Figure 5.7 is a diagram of the experimental procedure and analysis. Four transducers were used to collect the time series of the liquid pressure and pipe displacements.

These were compared with results from the analytical model developed in Chapters 3 and 4. This section describes the experimental procedures and analyses that were used for each pipe configuration.

5.3.1 Frequency Range of Excitation

The determination of the frequency range of excitation depends on the rated frequency of the motor and the natural frequencies of the liquid and the U-bend. The rated frequency of the motor is 30 Hz which is the upper bound of the range. The lower bound of the frequency range is determined by the frequency at which the inertia forces of the shaker mechanism are overcome producing a harmonic oscillation of the linear bearing structure. This lower bound frequency was found to be at 3.4 Hz. Several natural frequencies of the liquid and U-bend are excited over the frequency range.

5.3.1.1 Liquid Frequencies

The fundamental frequency of an open-closed liquid system is [5,6,7,41]

$$f_f = \frac{c_f}{4\ell} \tag{5.11}$$

Where f_f is the fundamental frequency of the liquid, c_f is the coupled wave speed and ℓ is the length of the pipe. A pressure node is formed at the open end and a pressure antinode is formed at the closed end.

The higher harmonics of the system are determined by the odd harmonics of the fundamental frequency computed from Equation 5.11. Table 5.7 lists the first through the ninth harmonic for the first nine pipe configurations. The coupled wave speed c_f , which was determined for this piping system by Budny [22], is 1265 m/s. The results in Table 5.7 show that the ninth harmonic of configurations 7, 8 and 9 can be excited. The first harmonic of configurations 7, 8 and 9 is periodic but not harmonic.

TABLE 5.7

FLUID HARMONICS FOR PIPE CONFIGURATIONS

Configuration					
			(Hz)		
	First	Third	Fifth	Seventh	Ninth
1	7.7	23.1			
2	5.7	17.1	28.4		
3	4.8	14.5	24.1		
4	3.9	11.8	19.7	27.6	
5	3.9	11.8	19.7	27.6	
6	3.4	10.3	17.2	24.1	
7	3.3	10.0	16.7	23.4	30.0
8	3.3	10.0	16.7	23.4	30.0
9	2.9	8.7	14.5	20.2	26.0

5.3.1.2 U-Bend Frequencies

The U-bend may be thought of as a plane frame clamped at the columns and having rigid joints at the elbows. Chang [83] developed frequency charts for identical columns and cross-beam plane frames. The frequency

equation, which is based on the Bernoulli-Euler beam theory, includes the effect of axial vibration. It is given by:

$$f_{p} = \frac{c^{2}}{2\pi \ell^{2}} \left[\frac{EI_{p}}{\rho_{p}A_{p}} \right]^{l_{2}}$$
 (5.12)

where ζ is the frequency parameter and ℓ is the length of a column. Table 5.8 shows the estimated frequencies, using Chang's development, for the U-bend shown in Figure 5.5 and the values presented in Tables 5.1 and 5.2. The mass of the liquid can be added to the denominator of the radical term as: $\rho_{\rm p} A_{\rm p} + \rho_{\rm f} A_{\rm f}$. The modes of vibration are asymmetrical and symmetrical. In the asymmetrical modes the elbows of the U-bend translates, simulating a rigid motion of the horizontal leg. The elbows in the symmetrical modes do not translate.

TABLE 5.8

NATURAL FREQUENCIES OF U-BEND

Frequency parameter	Natura	1 frequency	Mode of vibration		
5		(Hz)			
	Empty	Liquid-Filled			
1.790	5.1	4.1	asymmetrical		
3.553	21.0	16.9	symmetrical		
4.541	34.3	27.6	asymmetrical		
6.693	74.5	60.0	asymmetrical		

The frequency range of 3.4 Hz through 30 Hz excites two natural frequencies of the empty U-bend. The same frequency range also excites three natural frequencies of the liquid-filled U-bend.

5.3.2 Sampling Frequency and Sampling Time

The frequency range of 3.4 Hz to 30 Hz used for the experiments was determined as shown in the previous section. The sampling frequency is 1000 Hz and the duration of the sampling process is 4096 milliseconds. These parameters minimize the sampling errors due to aliasing and leakage. The upper limit of the frequency range is 30 Hz. This frequency is more than ten times less than the Nyquist frequency which is 500 Hz [93]. In the frequency range, the number of sinusoidal cycles for the duration of the sampling varies from 14 to 123. The error introduced, due to leakage when computing the frequencies, is less than 0.12 Hz, which is the resolution of the fast Fourier transform (FFT).

5.3.3 Sampling Procedure

The SCR motor control was calibrated to input the same frequency increments for all pipe configurations. The spacing between forcing frequencies was 0.41 Hz, yielding a total of 65 discrete frequencies. An input-output calibration curve for the frequency range was obtained between an accelerometer located at the linear bearing structure and another located at the spring. These displacements are presented in Figure 5.8. The input displacement at the bearing structure slightly

increases as the circular frequency of the motor increases, this was caused by a small bending of the shaft of the motor. This increase was 0.4 mm over the frequency range from 3.4 Hz to 30.0 Hz. The spring force at Dl in Figure 5.5 is of the same form as the displacement at this location. The torque described in Section 5.2.5.1 and the rated torque of the motor are shown in Figure 5.9. The reaction force of the spring onto the shaft of the motor was included.

The response spectra for the four transducers were obtained by sweeping through the frequency range. The signals from the pressure transducer located at the closed end and the accelerometer at the spring were monitored on an oscilloscope during the sweeping process. The oscilloscope monitoring had two purposes. First, before each sampling the system was allowed to reach a steady-state condition. Second, it allowed determination of the natural frequencies of the system. After the sweeping process was finished, the responses of the transducers at the natural frequencies were sampled.

5.3.4 Analysis Procedure

The time series for the 65 discrete frequencies and the natural frequencies were stored in a PDP 11/73 microcomputer. A fast Fourier transform FFT of these series was performed to obtain the magnitude and frequency. Before the FFT analysis, each time series was low pass filtered. The filter, which is shown in Figure 5.10, had a cut-off frequency of 80 Hz. This cut-off minimizes the noise introduced to the

signals by the shaker components. The sampling parameters described in the previous section determined that the resolution of the FFT was ± 0.12 Hz.

5.4 Experimental Uncertainty

The uncertainty of the experiments performed arises from three sources: the transducers, the A/D conversion and the pipe and fluid characteristics. Appendix B describes the characetristics of the data acquisition equipment used.

Tables B.1 and B.2 of Appendix B list the characteristics provided by the manufacturer for the two types of transducers used in the experiments and the error in the conversion of the analog voltage to digital format by the A/D converter. Pressure transducers models 111A26 and 113A24 were used. Both models have a linear error of 2%. The linearity of the error means the error is a constant 2% along the entire operating range of the transducer. Thus, a reading of 50 psi (345 kPa) would have an error of ±1.0 psi (±7.0 kPa). The resolution is a measure of the ability to distinguish between nearly equal values of a quantity. It is also referred to as "threshold", that is, the lowest level of valid measurement.

The accelerometers used were manufacturer model 302A. The error is based on the type of power unit that is connected to the transducer. Double integrator units were used in all the experiments to obtain

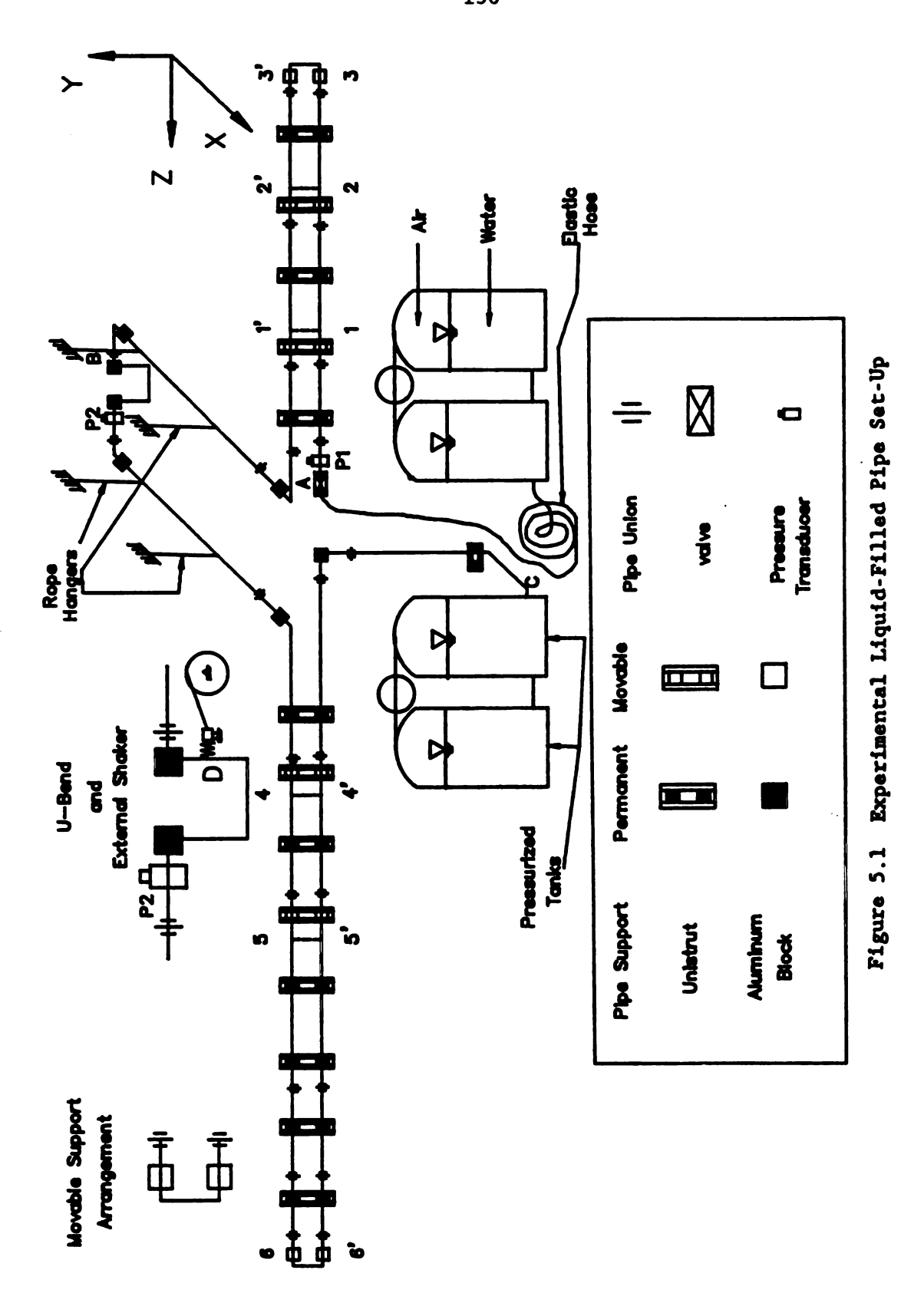
displacements. The error associated with this type of unit is 5%. Another source of error of the accelerometers is the nonlinearity of the response at frequencies less than 10 Hz. A calibration was necessary to find the conversion from volts to millimeters in the range from 3.4 Hz to 10 Hz. The procedure used is described in Appendix B.

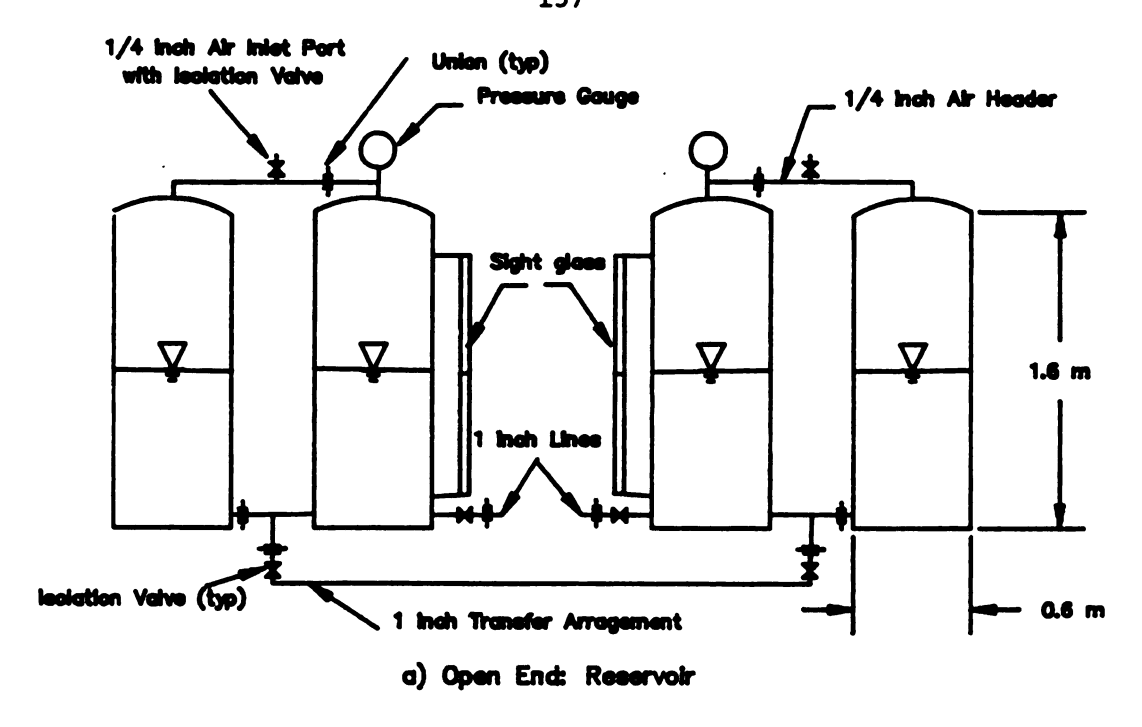
The error due to the A/D conversion is controlled by the 11 bit resolution of the input data. Because the A/D board is configured for bipolar inputs of ± 10.0 volts, the 11 bit resolution is equivalent to an error of ± 9.7 millivolts. The base frequency for the programmable realtime clock is 10 Mhz, thus the accuracy of the time measurement is ± 0.1 microseconds.

Thus, the maximum experimental error associated with the pressure readings due to the propagation of both the transducer and conversion error based on root mean square (rms) estimates for a 500 kPa reading is ± 12.0 kPa.

The sources of error that arise from the fluid and pipe properties come from the measurement of these properties. The copper pipe was manufactured by American Brass Company. The tolerances for the inside diameter and wall thickness of the pipe were 0.4% (0.1 mm) and 3% (0.04 mm), respectively. The fluid temperature was measured with an accuracy of 0.5 °C. The length of each pipe configuration was taken with a 100-foot tape with 100 divisions per foot. The error associated with the total pipe length depends on the number of measurements taken. For example, 17 measurements were taken for configuration 10 and 9 for configuration

1. Then, the error in pipe length measurement varies from ± 0.04 ft (0.01 m) to ± 0.03 ft (0.01 m). A 12 foot tape with 16 divisions per inch was used to measure pipe lengths less than 10 feet. For example, the legs of the U-bend were measured with this tape. The error in the measurement is ± 0.06 inch (2 mm). Possible errors due to temperature changes and sagging of the tape were not estimated.





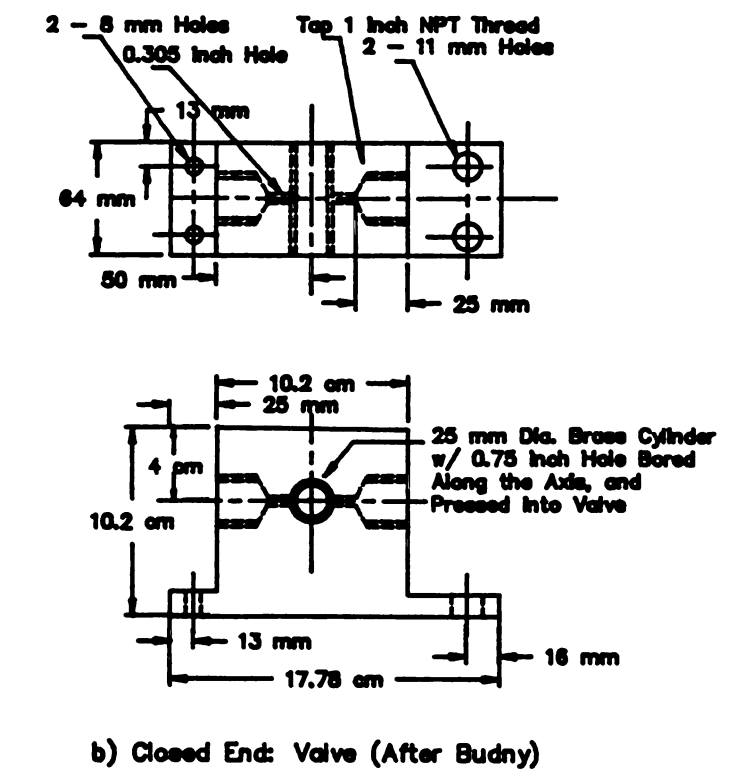
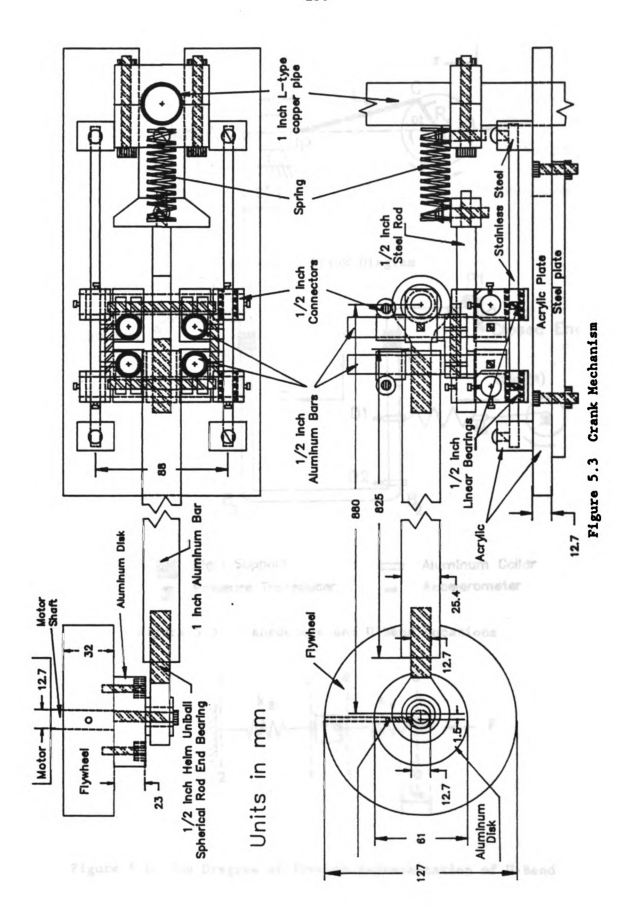
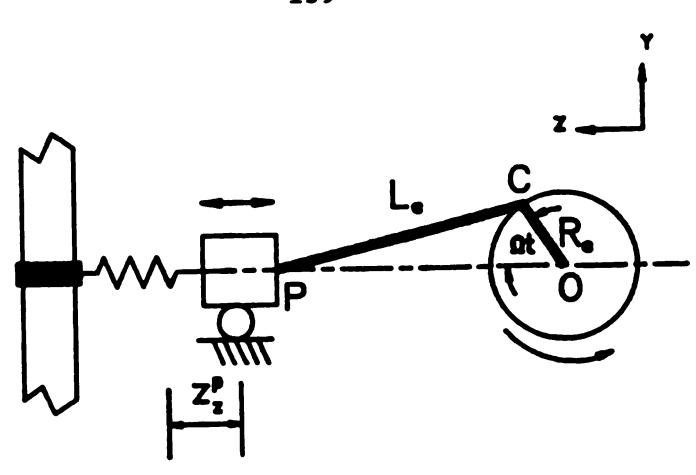


Figure 5.2 Liquid Boundaries





Open End

P2

P1

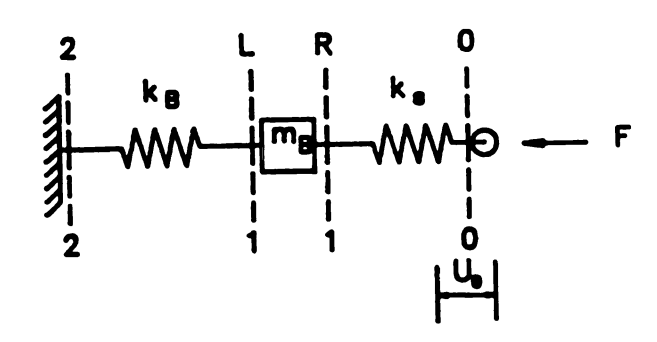
Qein(Ωt)

Rigid Support

Aluminum Collar

Figure 5.5 Transducers and U-Bend Locations

Pressure Transducer



Accelerometer

Figure 5.6 One Dregree-of-Freedom Representation of U-Bend

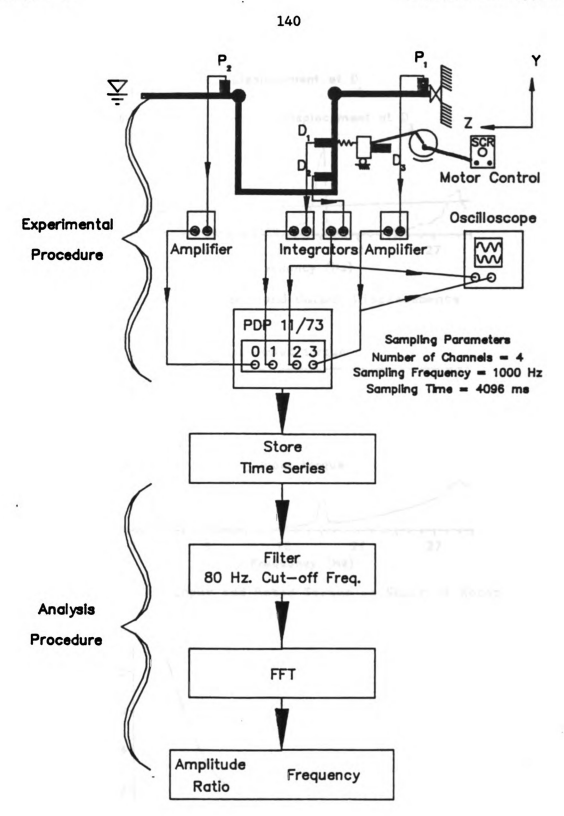


Figure 5.7 Experimental and Analysis Procedures

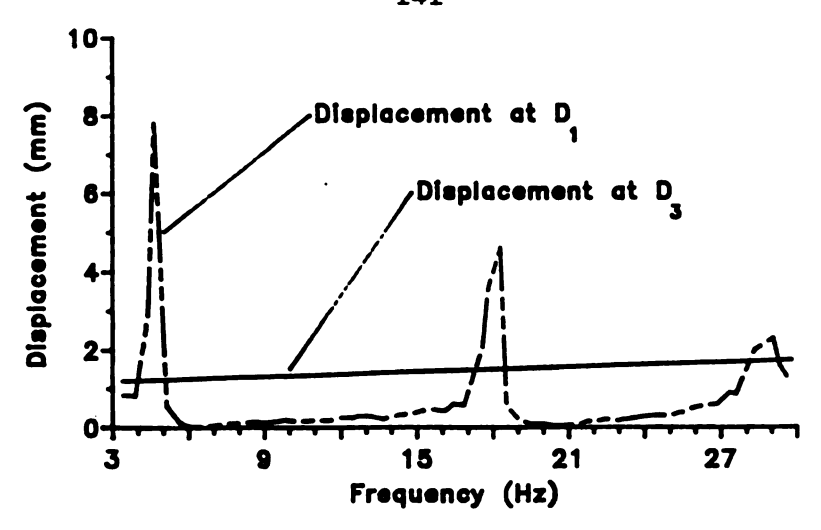


Figure 5.8 Input and Output Displacements

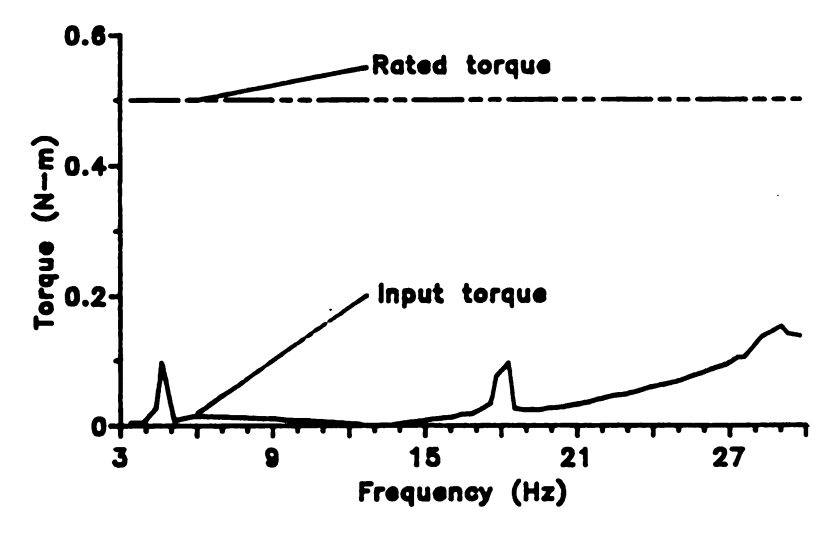


Figure 5.9 Input and Rated Torque at Shaft of Motor

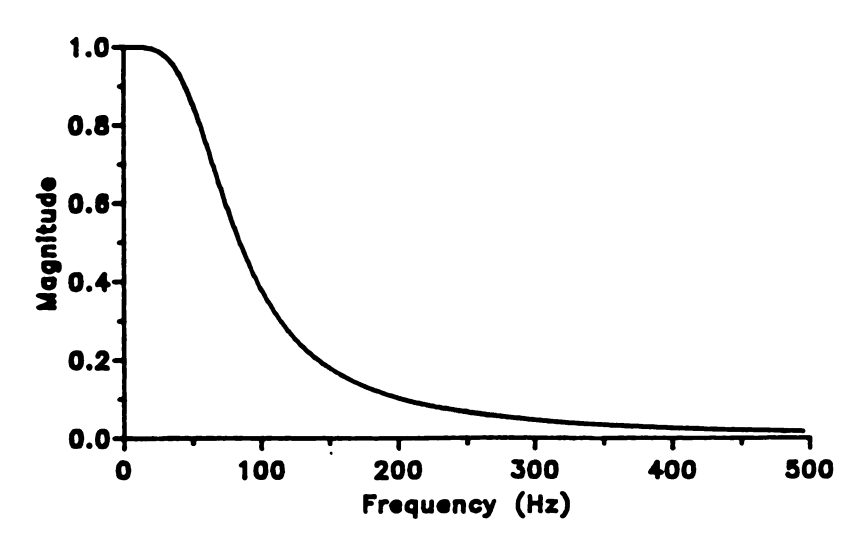


Figure 5.10 Low-Pass Filter

CHAPTER 6

EXPERIMENTAL RESULTS AND COMPARISONS

6.1 Introduction

The purpose of the experiments was to validate the analytical model derived in Chapters 3 and 4 and gain further physical understanding of the phenomena. Transient and harmonic tests were conducted to find the natural frequencies of the system. Fluid pressure and pipe displacement responses were monitored. Transient tests were used to calibrate the apparatus and measure the natural frequency of the U-bend and natural frequencies of the contained liquid. The transient tests were rapid valve closure and snap-back of the piping. The U-bend was excited harmonically by the crank mechanism that inputs a harmonic load to the pipe, as discussed in Chapter 5.

The first part of this chapter gives the results of the transient tests.

The second part presents the experimental results of the harmonic test and compares them with the computed results from the analytical model.

6.2 Transient Tests

Transient tests allow measurement of the natural frequencies of the system. Snap-back of the U-bend and rapid valve closure were the tests performed. The description of the tests and the results are presented.

6.2.1 Snap-Back Test

This test was used to measure the first natural frequency of the U-bend and calibrate the analytical model. The test consisted in displacing the elbows of the U-bend 12.7 mm (0.5 inch) from the equilibrium position and then releasing them. The calibration consisted of determining the effective stiffness of the spring between the linear bearing structure and the U-bend. Tests were conducted on an empty U-bend and a liquid-filled U-bend. The U-bend can be either free from or attached to a spring. Table 6.1 shows the results of the experimental tests and the computed results using either the transfer matrix method (TMM) or the Bernoulli-Euler beam theory developed by Chang [83] as shown in Table 5.8. Figures 6.1 and 6.2 show the time responses and the FFT's of the time series for the various U-bend conditions mentioned above. The added masses from the accelerometers, aluminum collar and steel bars at the elbows of the U-bend were included in the computed results for the The stiffness of the spring was found to be 8 KN/m which is greater than the stiffness provided by the manufacturer, as shown in Table 5.4. The results, in Table 6.1, show that the natural frequency

increases when the U-bend is attached to the spring. This result suggests that the stiffness of the U-bend - spring system increases. Including the mass of the liquid decreased the natural frequency of the U-bend, as expected.

TABLE 6.1

EXPERIMENTAL AND COMPUTED U-BEND RESPONSE TO SNAP-BACK TEST

	:	Free	Spring		
Condition	Experimental (Hz)	TMM (Hz)	Chang [83] (Hz)	Experimental (Hz)	TMM (Hz)
Empty Liquid-Filled	4.4 3.9	4.4 3.9	5.1 4.1	5.1 4.4	5.1 4.4

6.2.2 Valve Closure Test

A rapid valve closure induces excitement of the liquid pressure. The experimental procedures as well as the software and hardware used for these tests are described by Budny [22]. These tests also allow measurement of the liquid wave speed if the length of the pipe is known as shown in Equation 5.11. An open-closed system results upon closure of the valve and excites the odd harmonics of the liquid. The first harmonic corresponds to the first or fundamental frequency of the liquid. According to the state of the U-bend, three cases were studied for configurations 4, 8, 9 and 10: fixed, free and with spring. The total length of the pipe and relative location for each configuration are given in Tables 5.4 and 5.5.

6.2.2.1 Fixed U-Bend

A Unistrut was placed at each free elbow of the U-bend, locations B2 and B3 in Figure 5.5. The time series for the pressure at the closed-end for the four configurations are presented in Figure 6.3. The FFT's of the time series are shown in Figure 6.4. The FFT's were normalized with respect to the largest pressure or displacement response for all three cases. The natural frequencies from the experiment were compared with the frequencies computed by the TMM. A straight pipe of variable length with a harmonic oscillation at the open end was used to compute the natural frequencies of the system. The results, shown in Table 6.2 demonstrate the ability of the TMM to predict the natural frequencies of an axially coupled system. The computed wave speed is within 0.5% of the experimental.

TABLE 6.2

EXPERIMENTAL AND COMPUTED FREQUENCIES OF LIQUID FOR FIXED CONDITION

Configuration	Wave Speed (m/s)		Fi :	Harmonics (Hz) First Third				Fifth	
	E	С	E	C	E	С	E	C	
4	1267	1260	3.9	4.0	12.0	11.8	19.8	19.6	
8	1266	1260	3.4	3.4	10.0	10.0	16.6	16.5	
9	1265	1260	2.9	2.9	8.5	8.7	14.4	14.3	
10	1267	1260	2.2	2.2	6.6	6.5	11.0	10.8	

E - Experimental C - Computed

6.2.2.2 Free U-Bend

For this case, the U-bend is free to vibrate in the Y-Z plane, as shown in Figure 5.5. The time series of the liquid pressure at the closedend, P_1 , and the U-bend elbow displacement, D_2 , were recorded; the results are shown in Figure 6.5. The FFT's of the time series are shown in Figure 6.6. Table 6.3 shows the experimental and computed results for the natural frequencies of the liquid and the experimental compliance. Compliance [34] is defined as ratio of the elbow displacement over pressure at the closed-end, D_2/P_1 .

TABLE 6.3

EXPERIMENTAL AND COMPUTED FREQUENCIES OF LIQUID FOR FREE CONDITION

Fluid Harmonics

Configuration		First		Third		Fifth	
		E	C	E	C	E	C
4	Frequency (Hz) D_2/P_1 (mm/Pa)	3.9 69.4	4.0	12.0 1.8	12.0	19.8 0.4	19.7
8	Frequency (Hz) D ₂ /P ₁ (mm/Pa)		3.4	10.0 3.0	10.1	16.4 0.4	16.7
9	Frequency (Hz) D ₂ /P ₁ (mm/Pa)	2.9 1.1	2.9	8.5 3.1	8.8	14.4 1.2	14.5
10	Frequency (Hz) D ₂ /P ₁ (mm/Pa)	2.2 0.1	2.2	6.6 8.6	6.6	11.0 0.3	10.8

E - Experimental

C - Computed

D₂ - Accelerometer response at U-bend elbow

 P_1 - Pressure transducer response at closed end

The computed frequencies show good agreement with the experimental frequencies of the system. The following observations can be made concerning the experimental compliance:

- 1) Configuration 4 shows the largest magnitude. The frequency of the U-bend and the first natural frequency of the liquid nearly coincide. The proximity of the frequencies results in a beat as shown in Figure 6.5a.
- 2) The magnitude of the compliance at the first fluid frequency decreases as both the frequency of the fluid and the U-bend move apart from each other.
- 3) The opposite occurs at the third liquid harmonic. Configuration 10 shows a larger compliance than configuration 4. This phenomenon takes place because the third harmonic of configuration 10 (6.6 Hz) is closer to the natural frequency of the U-bend than the other configurations.
- 4) The compliance at the third liquid harmonic is greater than that at the first harmonic for configurations 8, 9 and 10. The third liquid harmonic for configuration 10 constitute the dominant frequency of the U-bend. The compliance is greater than the compliance at the natural frequency of the U-bend as shown in Figure 6.6d.

The pipe line from the closed-end to B_1 and from B_4 to the open-end, Figure 5.5, was treated as a straight pipe. Only the axial modes of vibration for the pipe and the liquid modes were included in these reaches. This simplification is based on the previous experimental results of this research. The pressure response at the closed-end is

affected by the status of the bend (as shown in Figure 6.5a for configuration 4). The reponse of the U-bend is affected by the closing of the valve. Only the liquid and U-bend frequencies were found to be of significance in the results. This simplification also reduces the numerical difficulties associated with the TMM as pointed out by Pestel and Leckie [50] and as described in Chapter 4.

6.2.2.3 U-bend with Spring

The U-bend was attached to the spring, as described in Chapter 5, at location D₁ in Figure 5.5. The experimental time series and FFT's are shown in Figures 6.7 and 6.8, respectively. The experimental and computed results are shown in Table 6.4. The same observations as for the previous case can be made. In the present situation the frequency of the U-bend is 0.5 Hz higher than the previous case, because of the additional stiffness provided by the spring. This causes the third fluid frequency for configuration 10 to be closer to the U-bend frequency, thus, resulting in a larger ratio than in the previous case.

6.3 <u>Harmonic Tests</u>

The harmonic tests consisted of obtaining the liquid pressure and pipe displacement responses of the liquid-filled pipe when a harmonic displacement is induced at the U-bend. Two liquid pressure readings at the

closed end and at the U-bend (locations P1 and P2 in Figure 5.5), and two displacement readings at the spring and at U-bend elbow (locations D_1 and D_2 in Figure 5.5) were collected at each frequency. The frequency range of excitation varied from 3.4 Hz to 30 Hz. A preliminary evaluation of the U-bend subjected to harmonic displacement is presented. Then, the response spectra and liquid mode shapes follow.

TABLE 6.4

EXPERIMENTAL AND COMPUTED FREQUENCIES OF LIQUID FOR SPRING CONDITION

Fluid Harmonics

Configuration	on	Fi E	rst C		ird C	Fi E	fth C
4	Frequency (Hz) D ₂ /P ₁ (mm/Pa)	3.9 10.1	4.0	12.0 2.2	12.0	19.8 0.4	19.7
8	Frequency (Hz) D ₂ /P ₁ (mm/Pa)		3.4	10.0 2.4	10.1	16.6 · 0.5	16.7
9	Frequency (Hz) D ₂ /P ₁ (mm/Pa)		2.9	8.6 3.4	8.8	14.4	14.5
10	Frequency (Hz) D ₂ /P ₁ (mm/Pa)	2.2 0.1	2.2	6.4 11.3	6.6	10.7 0.1	10.8

E - Experimental

C - Computed

D₂ - Accelerometer response at U-bend elbow

P₁ - Pressure transducer response at closed end

6.3.1 U-Bend Response

Displacements at locations D_1 and D_2 were recorded to find the natural frequencies of the U-bend. Two cases were considered, when the U-bend is empty and when it is liquid-filled. Figure 6.9 shows the responses at the spring and the elbow for the two cases. The added mass of the liquid reduces the natural frequencies of the U-bend. Table 6.5 shows the experimental and computed results at the natural frequencies. The computed mode shapes for the liquid-filled U-bend are displayed in Figures 6.10 and 6.11. Figure 6.10 shows the mode shapes of the U-bend without the spring. Figure 6.11 shows the mode shapes with the spring. The odd natural frequencies correspond to asymmetrical modes and the even frequencies to symmetrical modes of vibration. The inclusion of the spring affects the first and second modes of vibration. The other mode shapes do not show any appreciable change. It can be noted that the inclusion of the spring allows for larger displacements of the leg where the spring is attached. The largest discrepancy between the experimental and computed natural frequencies occurs at the second mode. The computed frequencies for this mode are 0.9 Hz and 0.6 Hz lower than the experimental when the U-bend is empty and liquid-filled respectively.

TABLE 6.5

NATURAL FREQUENCIES OF U-BEND TO HARMONIC EXCITATION

Natural Frequencies (Hz)

		:y	y Liquid-Filled						
Frequ	ency Mode of	Sp	ring	F	ree	Sp	ring	F	ree
Numb	er Vibration	E	Č	E*	С	E	Č	E*	С
1	Asymmetrical	5.1	5.1	4.4	4.4	4.4	4.4	3.9	3.9
2	Symmetrical	22.7	21.8		21.2	18.1	17.5		17.0
3	Asymmetrical		35.5		35.0	28.3	28.6		28.0
4	Symmetrical		44.4		41.4		34.3		32.1
5	Asymmetrical		73.3		73.1		58.9		58.8
6	Symmetrical		89.9		89.8		72.9		72.9

^{*} Results for the free case were obtained from the snap-back test, see Table 6.1.

6.3.2 Spectral Response of Liquid-Filled Piping

Tables 6.9 and 6.11, at the end of this chapter, show the results at the natural frequencies of the system. The largest experimental pressure response occurred at the fifth and seventh harmonic of configurations 2 (28.3 Hz and 521 kPa) and 4 (27.8 Hz and 290 kPa). The large pressure responses are associated with the third natural frequency of the U-bend. This frequency, 28.3 Hz, corresponds to an asymmetrical mode, in which the elbows show a small displacement, Figure 6.11. This small displacement generates the large liquid pressure responses through the junction coupling mechanism.

6.3.3 Liquid Mode Shapes

The first pressure mode shape of the liquid in an open-closed pipe corresponds to 1/4 of a sinusoidal wave [5,6,7]. The maximum response occurs at the closed-end (s/l = 0), where a pressure loop develops. A pressure node, where the pressure is zero, develops at the open-end (s/l = 1), where s is a coordinate along the pipe length l. The other mode shapes correspond to the odd multiples of the 1/4 sinusoidal wave.

The response of the pressure transducers P_1 and P_2 were used to obtain the mode shapes for each natural frequency of the system. The distance from these transducers to the closed end varies for each pipe configuration. In this way, a point of the liquid mode shape was obtained for each configuration. The relative location of P_1 and P_2 with respect to the closed-end is given in Table 5.6. Tables 6.8 through 6.16 show the experimental and computed results at the natural frequencies of the system for configurations 1 through 9. The behavior of the mode shapes of the liquid is different if the frequency of the harmonic excitation is oscillating at a natural frequency of the liquid or the U-bend. Thus, the liquid mode shapes will be studied at the liquid frequencies and at the natural frequencies of the U-bend. The pressure ratio P_2/P_1 will be used to compare the computed and experimental liquid mode shapes.

6.3.3.1 Liquid Mode Shapes at Liquid Natural Frequencies

Figure 6.12 shows the normalized pressure mode shapes at the natural frequencies of the liquid. The mode shapes were normalized with respect to the pressure at the closed end. The first through ninth odd harmonics are shown in this figure; the solid line represents the computed mode shape and the dots represent experimental points. The encircled numbers correspond to the pipe configuration. They are placed at the relative location of P2 with respect to the closed-end. Table 6.6 shows the experimental and computed results depicted in Figure 6.12. Good agreement between the experimental points and the computed mode shapes is noted in this figure. The correlation coefficient [92] between computed and experimental results is unity for all harmonics, except for the first. The first liquid mode shape, which is associated with the first harmonic, shows the largest discrepancies for configurations 1, 2, and 3. These configurations show that the first natural frequency of the liquid is higher than the first natural frequency of the U-bend. The minimal motion of the elbows of the U-bend at the liquid frequencies causes a minimal response of the pressure, increasing the experimental error. Pressure readings lower than 15 KPa are only four times greater than the resolution of the A/D converter board, as mentioned in the previous chapter.

TABLE 6.6

LIQUID PRESSURE MODE SHAPES AT LIQUID NATURAL FREQUENCIES

Harmonic Conf. First Fifth Seventh Third Ninth No. P2 C C E E E C E E 0.15 0.83 0.97 0.71 0.74 0.11 0.73 0.98 0.89 0.86 0.60 0.57 0.56 0.47 0.89 0.75 0.60 0.94 0.83 0.38 0.78 0.81 0.24 0.24 0.94 0.97 0.41 0.46 0.56 0.60 0.61 0.85 0.88 0.23 0.22 0.99 1.00 0.95 0.07 1.00 0.86 0.71 0.74 - -0.98 0.63 0.51 0.54 0.92 0.32 0.75 0.87 0.84 --0.69 0.72 0.80 0.52 0.54 0.89 8 0.48 0.60 0.63 - -0.89 9 0.55 0.63 0.65 0.82 0.84 0.90 0.99 0.35 0.36 0.00 0.09 Correlation 0.77 1.00 1.00 1.00 1.00

6.3.3.2 Liquid Mode Shapes at U-Bend Natural Frequencies

The experimental liquid mode shapes at the frequency of the U-bend were obtained as in the previous section. The behavior of the liquid pressure at the natural frequencies of the U-bend follows the same trend as the behavior at the natural frequencies of the liquid. However, an abrupt change of the mode shape at the location of the U-bend is produced due to the motion of the elbows. Three of the natural frequencies of the U-bend were excited by harmonic oscillation. The first and third, which correspond to asymmetrical modes, as shown in Figure 6.10, allow motion of the elbows in the Y-Z plane. The second natural frequency, which is a symmetrical mode, allows no motion at the elbows.

E - Experimental C - Computed

^{*} P2 is the relative location of the pressure transducer with respect to the closed-end, see Table 5.6.

This lack of motion at the elbows prohibits the development of junction coupling. Therefore, the liquid pressure response is minimum at this mode. Tables 6.8 through 6.16, at the end of this chapter, show the experimental and computed results at the natural frequencies of the system.

Figures 6.13 through 6.19 show the liquid mode shapes at the two asymmetrical U-bend frequencies for configurations 1 through 9. In addition to the features described in the previous section for Figure 6.12, the location of the horizontal leg of the U-bend is shown for each configuration (locations B_2 and B_3 in Figure 5.5). The location is marked by two parallel vertical lines. Figure 6.16 shows the liquid mode shapes for configurations 4 and 5 and Figure 6.18 for configurations 7 and 8.

Table 6.7 shows the results depicted in Figures 6.13 through 6.19. The experimental and computed results show good correlation at the first natural frequency of the U-bend. The largest discrepancies at the third U-bend frequency occur for configurations 4 and 9. The liquid is oscillating between the ninth and eleventh harmonic for both configurations. The pressure gradient at P₂ shown in Figures 6.16 and 6.19 are higher than for any other configuration. Thus, any change of the frequency of oscillation may cause considerable changes in the magnitude of the pressures.

TABLE 6.7

LIQUID PRESSURE MODE SHAPES AT U-BEND NATURAL FREQUENCIES

U-bend Frequency (Hz)

		4.	4	28.3 Third		
Configuration	P2*	Fir	st			
Number		E	C	E	С	
1	0.15	0.00	0.07	0.76	0.74	
2	0.11	0.16	0.14	0.94	0.97	
3	0.47	0.55	0.55	1.18	1.22	
4	0.38	1.20	1.18	0.94	1.53	
5	0.56	0.82	0.80	0.53	0.35	
6	0.07	0.00	0.19	0.22	0.20	
7	0.63	0.92	0.98	1.80	1.54	
8	0.48	1.66	1.65	0.28	0.43	
9	0.55	2.05	1.95	1.09	1.83	
Correlation		1.0	00	0.8	32	

E - Experimental C - Computed

^{*} P2 is the relative location of the pressure transducer with respect to the closed-end.

TABLE 6.8

EXPERIMENTAL AND COMPUTED RESULTS FOR CONFIGURATION 1

Freq. (Hz)			Disp	lacement (mm)	Pressure (kPa)			
	Туре	Location D1	Location D2	Ratio D2/D1	Location Pl	Location P2	Ratio P2/P1	
4.4 4.4	E C	S1	13.6	33.2	2.4 2.8	49	0	0.0 0.07
7.6 7.8	E C	F1	0.2	0.5	2.5 2.6	12	10	0.83 0.97
18.1 17.5	E C	S2	3.8	0.7	0.2 0.5	0	0	0.03
23.2 23.3	E C	F3	0.4	0.2	0.5 0.7	56	40	0.71 0.74
28.6 28.6	E C	S 3	6.0	1.3	0.2 0.2	59	45	0.76 0.74

TABLE 6.9

EXPERIMENTAL AND COMPUTED RESULTS FOR CONFIGURATION 2

			Disp	lacement (mm)	Pressure (kPa)			
Freq. (Hz)		Туре	Location D1	Location D2	Ratio D2/D1	Location P1	Location P2	Ratio P2/P1
4.4 4.4	E C	S1	11.8	30.2	2.1 2.8	49	8	0.16 0.14
5.6 5.7	E C	F1	0.3	1.8	6.0 2.8	11	8	0.73 0.98
17.1 17.1	E C	F3	1.2	0.1	0.1 0.0	18	16	0.89 0.86
18.1 17.5	E C	S2	3.9	0.7	0.2 0.5	0	0	3.94
28.3 28.1	E C	F5	3.1	0.6	0.2 0.4	521	310	0.60 0.57
28.8 28.7	E C	S 3	5.2	1.3	0.3 0.2	239	225	0.94 0.97

TABLE 6.10

EXPERIMENTAL AND COMPUTED RESULTS FOR CONFIGURATION 3

			Disp	lacement (mm)	Pressure (kPa)			
Freq. (Hz)		Туре	Location D1	Location D2	Ratio D2/D1	Location Pl	Location P2	Ratio P2/P1
4.4 4.4	E C	S1	13.4	39.2	2.9 2.8	214	117	0.55 0.55
5.1 4.9	E C	F1	0.5	2.1	4.4 2.7	16	14	0.89 0.75
14.6 14.7	E	F3	0.5	0.1	0.3 2.2	52	29	0.56 0.60
18.1 17.5	E C	S2	12.5	2.5	0.2 0.1	7	0	0.00 0.14
24.4 24.2	E C	F5	0.4	0.2	0.5 0.4	18	17	0.94 0.83
28.3 28.6	E C	S 3	4.9	1.1	0.2 0.2	43	50	1.18 1.22

TABLE 6.11

EXPERIMENTAL AND COMPUTED RESULTS FOR CONFIGURATION 4

			Disp	lacement (mm)	Pressure (kPa)			
Freq. (Hz)		Туре	Location D1	Location D2	Ratio D2/D1	Location P1	Location P2	Ratio P2/P1
3.9 4.0	E C	F1	1.7	3.5	2.1	102	80	0.78 0.81
4.4 4.4	E C	S1	12.9	38.5	3.0 2.8	99	119	1.20 1.18
12.0 12.0	E C	F3	0.4	0.1	0.3 2.3	41	10	0.24 0.24
18.1 17.5	E C	S2	9.3	2.0	0.2 0.5	0	7	18.53
19.8 19.7	E C	F5	0.3	0.2	0.7 0.8	36	34	0.94 0.97
27.8 27.4	E C	F9	1.7	0.3	0.2 0.2	290	118	0.41 0.46
28.6 28.6	E C	S 3	6.4	1.6	0.3 0.2	154	145	0.94 1.53

TABLE 6.12

EXPERIMENTAL AND COMPUTED RESULTS FOR CONFIGURATION 5

			Disp	lacement (mm)	Pressure (kPa)			
Freq. (Hz)		Туре	Location D1	Location D2	Ratio D2/D1	Location Pl	Location P2	Ratio P2/P1
3.9 4.0	E C	F1	1.7	3.5	2.1 2.8	144	87	0.60 0.61
4.4 4.4	E C	S1	13.8	40.5	2.9 2.8	160	131	0.82 0.80
12.0 12.0	E C	F3	0.3	0.1	0.3 2.3	26	22	0.85 0.88
18.1 17.5	E C	S2	12.6	2.5	0.2 0.1	10	0	0.00 0.08
19.8 19.7	E C	F5	0.2	0.2	1.0 0.8	39	9	0.23 0.22
27.6 27.5	E C	F9	1.9	0.4	0.2 0.2	231	228	0.99 1.00
28.3 28.6	E C	S3	5.4	1.3	0.2 0.2	188	100	0.53 0.35

TABLE 6.13

EXPERIMENTAL AND COMPUTED RESULTS FOR CONFIGURATION 6

			Disp	lacement (mm)	Pressure (kPa)			
Freq. (Hz)		Туре	Location D1	Location D2	Ratio D2/D1	Location Pl	Location P2	Ratio P2/P1
3.4 3.4	E C	F1	1.1	0.9	0.8	0	0	0.20
4.4 4.4	E C	S1	11.5	26.0	2.3 2.8	36	0	0.00 0.19
10.5 7.8	E C	F3	0.3	0.2	0.7 2.4	6	0	0.00 0.95
17.1 17.5	E C	F5	0.9	0.1	0.1 0.5	5	0	0.86
18.1 17.5	E C	S2	3.8	0.7	0.2 0.5	0	0	0.03
23.2 23.3	E C	F 7	0.4	0.2	0.5 0.7	56	40	0.71 0.74
28.6 28.6	E C	S3	6.0	1.3	0.2 0.2	59	45	0.76 0.74

TABLE 6.14

EXPERIMENTAL AND COMPUTED RESULTS FOR CONFIGURATION 7

			Disp	lacement (mm)	Pressure (kPa)			
Freq. (Hz)		Type	Location D1	Location D2	Ratio D2/D1	Location P1	Location P2	Ratio P2/P1
3.4 3.4	E	F1	0.9	1.6	1.9 2.8	39	20	0.51 0.54
4.4 4.4	E C	S1	13.2	38.5	2.9 2.8	65	60	0.92 0.98
10.0 10.1	E C	F3	0.2	0.2	0.8 2.5	12	11	0.92 0.98
16.8 16.8	E C	F5	0.7	0.1	0.1 10.8	22	0	0.00 0.32
18.1 17.5	E C	S 2	12.2	2.4	0.2 0.1	11	0	0.20
22.7 23.4	E C	F7	0.2	0.1	0.5 0.5	7	0	0.01 0.75
28.1 28.5	E C	S3	2.9	0.6	0.2 0.2	30	54	1.80 1.54
30.0 29.9	E	F9	1.2	0.4	0.3	263	228	0.87 0.84

164

TABLE 6.15

EXPERIMENTAL AND COMPUTED RESULTS FOR CONFIGURATION 8

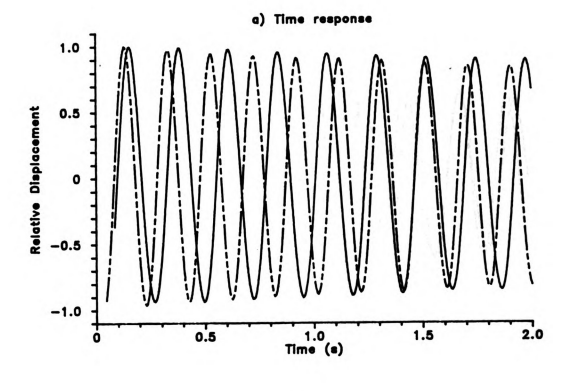
			Disp	lacement (mm)	Pressure (kPa)			
Freq. (Hz)		Туре	Location D1	Location D2	Ratio D2/D1	Location P1	Location P2	Ratio P2/P1
3.4 3.4	E C	F1	1.1	2.0	1.8 2.8	39	27	0.69 0.72
4.4 4.4	E C	S1	13.6	40.4	3.0 2.8	41	68	1.66 1.65
10.0 10.1	E C	F3	0.2	0.2	1.0 2.4	35	21	0.60 0.63
16.6 16.7	E	F5	0.8	0.0	0.0 2.7	6	0	0.00 0.80
18.1 17.5	E C	S2	11.2	2.3	0.2 0.5	0	0	
23.7 23.2	E C	F7	0.3	0.2	0.5 0.7	87	45	0.52 0.54
28.3 28.6	E C	S3	5.0	1.2	0.2 0.2	56	16	0.30 0.40
30.3 29.9	E C	F9	0.9	0.2	0.3 0.1	29	26	0.89 0.89

TABLE 6.16

EXPERIMENTAL AND COMPUTED RESULTS FOR CONFIGURATION 9

			Disp	lacement (mm)		Pressure (kPa)			
Freq. (Hz)		Туре	Location D1	Location D2	Ratio D2/D1	Location Pl	Location P2	Ratio P2/P1	
2.9 2.9	E	F1	0.2	0.0	0.0 2.8	22	14	0.63 0.65	
4.4 4.4	E C	S1	13.8	39.8	2.9 2.8	26	54	2.05 1.95	
8.5 8.8	E C	F3	0.1	0.2	2.0 2.5	14	11	0.82 0.84	
14.4 14.5	E C	F5	0.3	0.1	0.2	21	7	0.35 0.36	
18.1 17.5	E C	S2	10.5	2.1	0.2 0.5	0	0	••	
20.3 20.2	E C	F7	0.1	0.2	2.0 1.0	37	33	0.90 0.99	
26.1 25.8	E C	F9	0.6	0.1	0.2 0.2	99	0	0.00 0.09	
28.3 28.6	E C	S3	4.5	1.0	0.2 0.2	36	39	1.09 1.83	





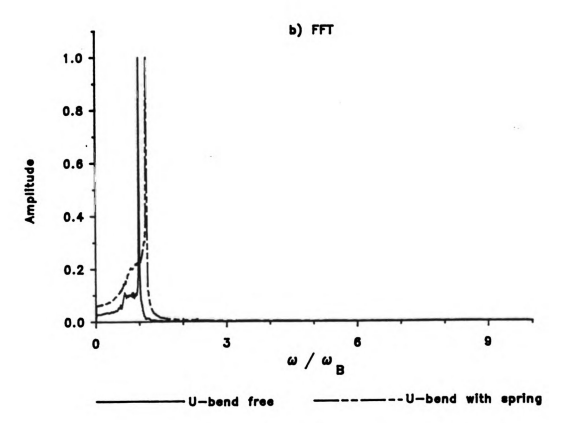
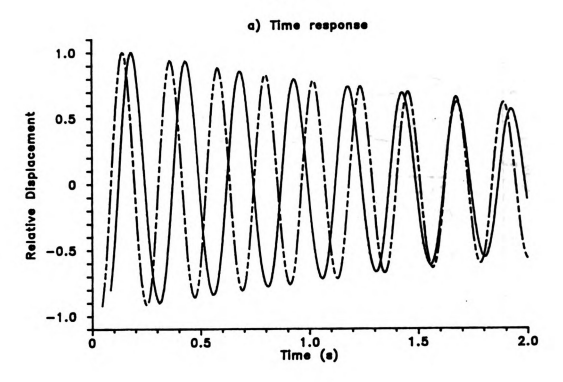


Figure 6.1 Experimental Results of Snap-Back Test, U-Bend Empty, Frequency of Free Bend is 4.4 Hz





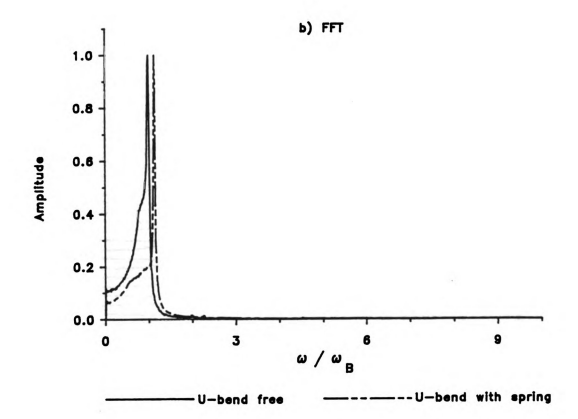
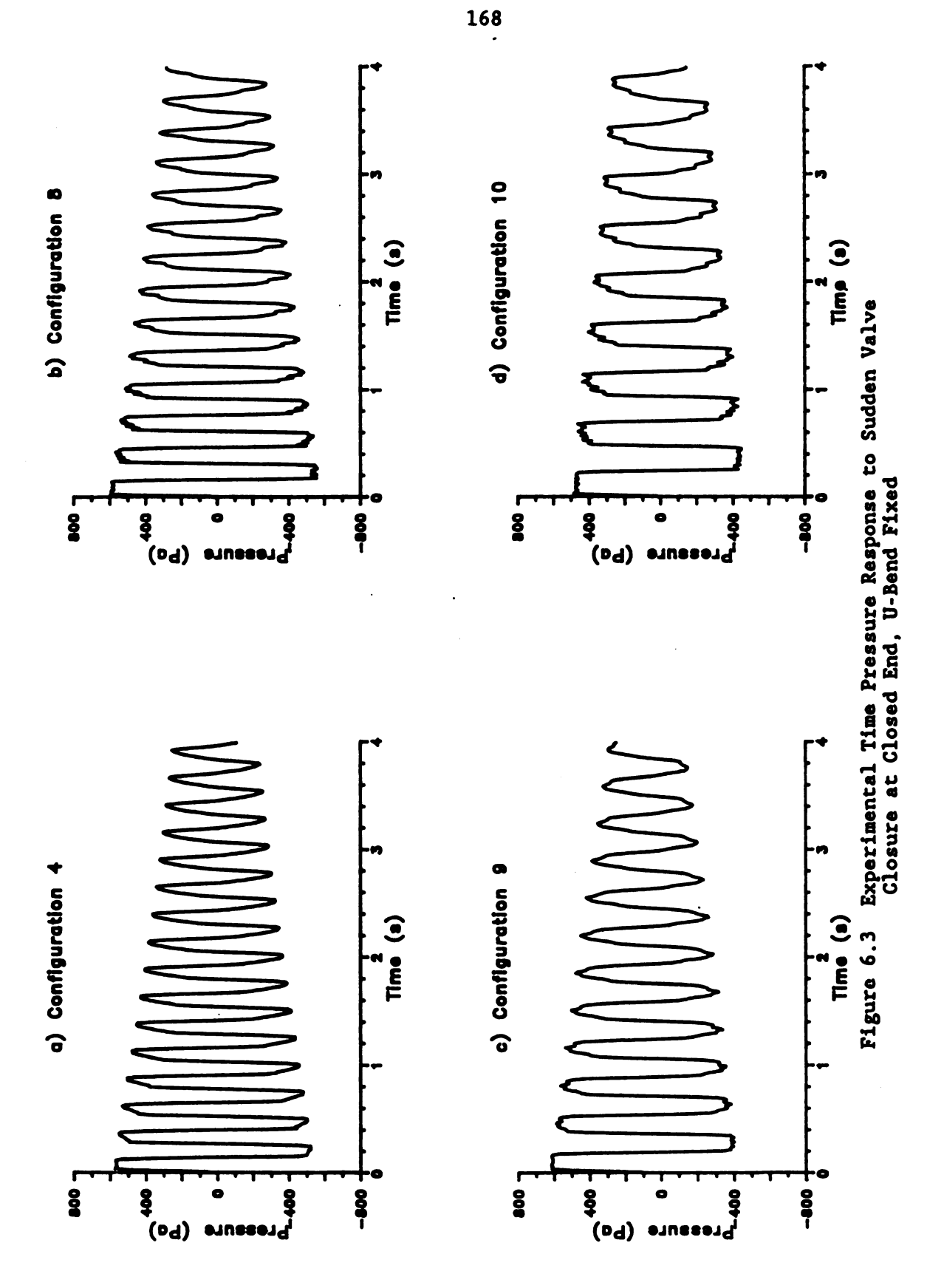
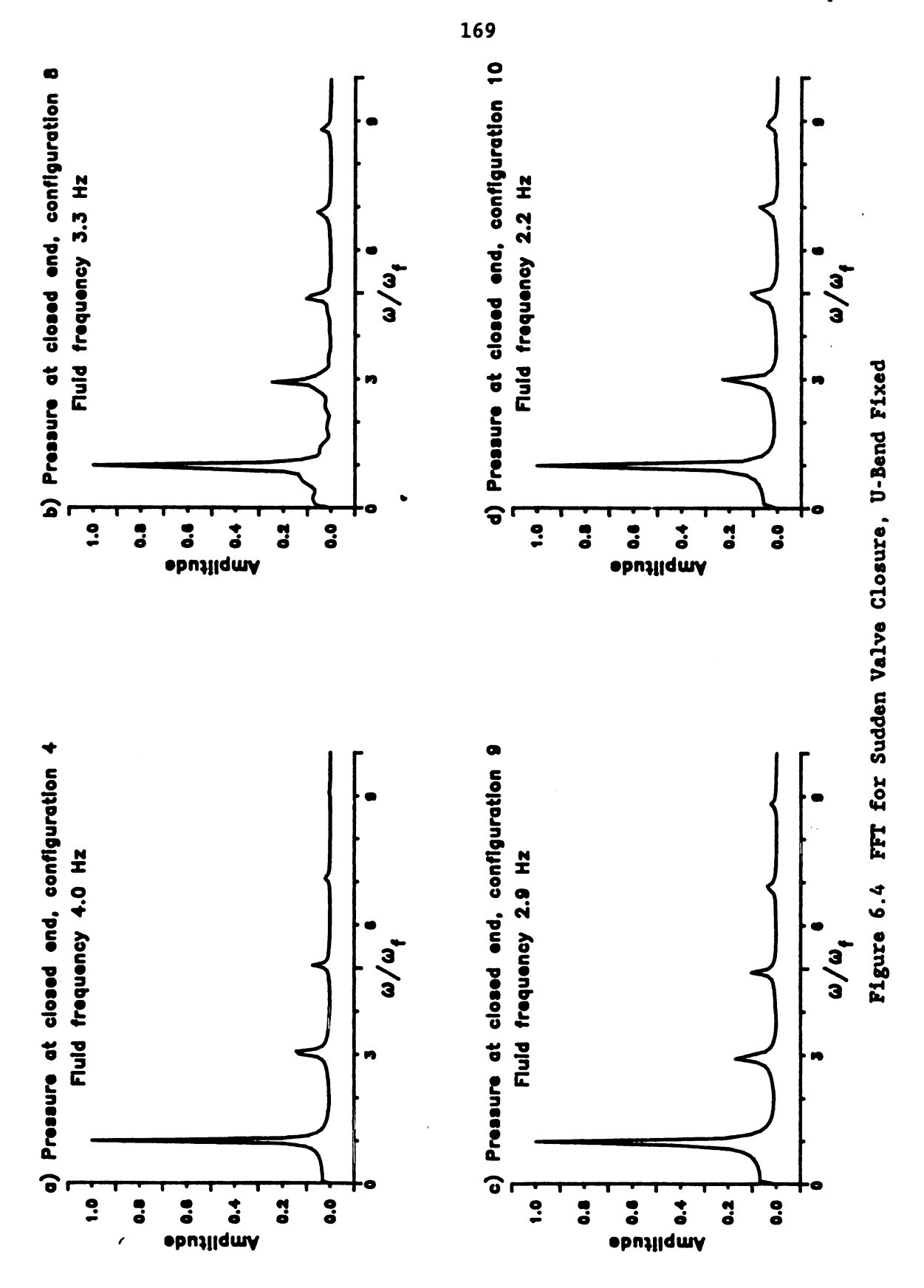
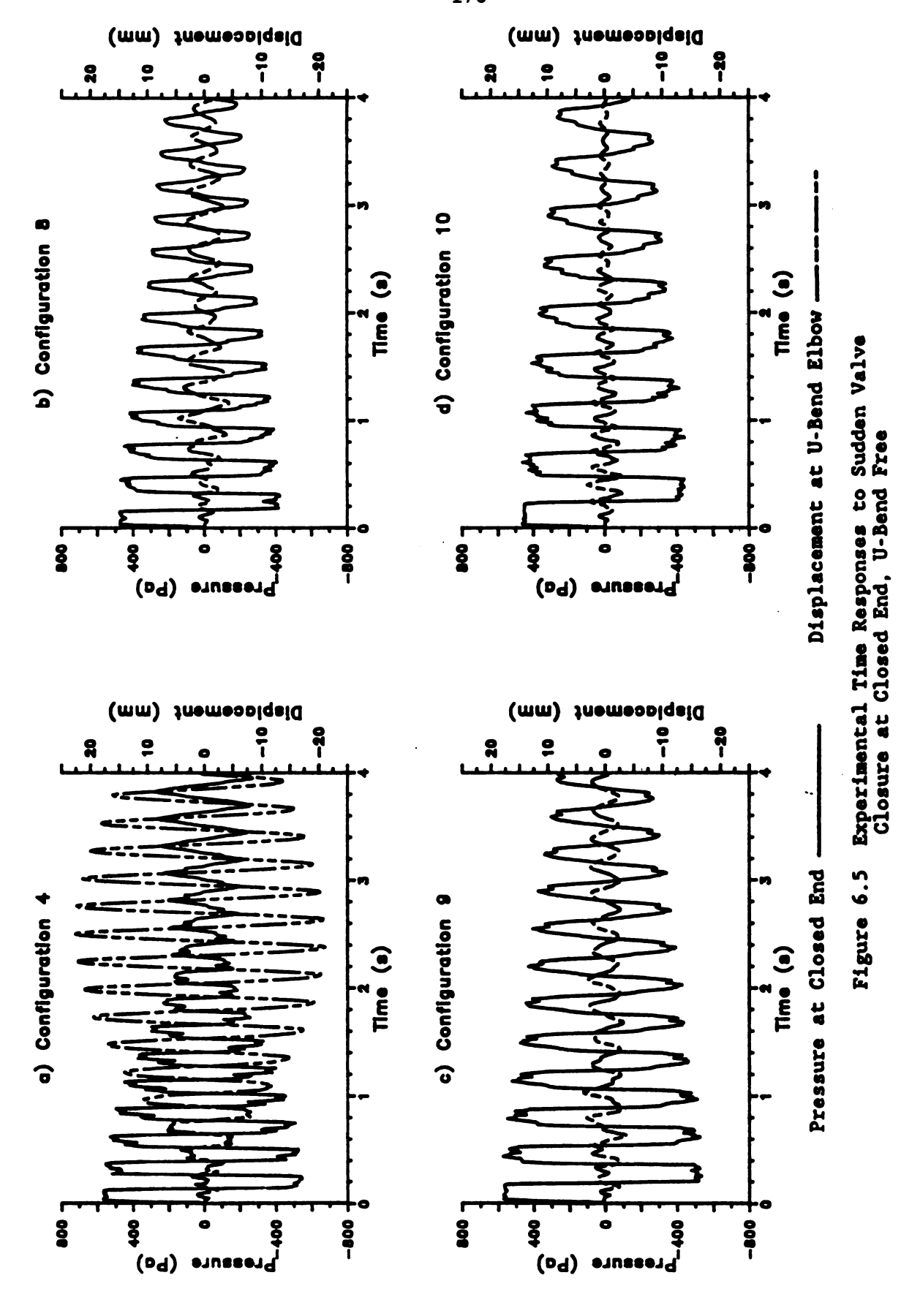


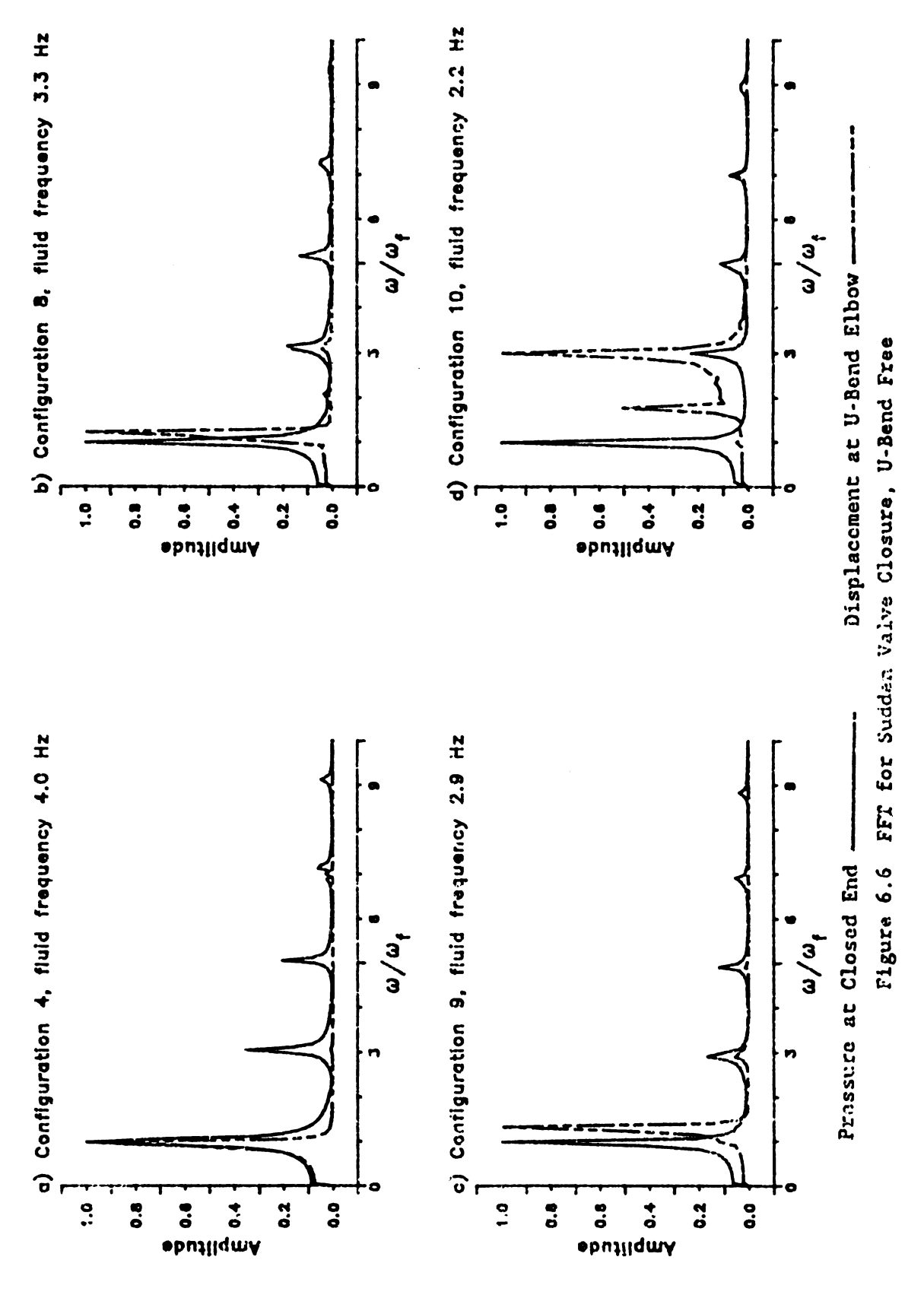
Figure 6.2 Experimental Results of Snap-Back Test, U-Bend Filled, Frequency of Free Bend is 3.9 Hz



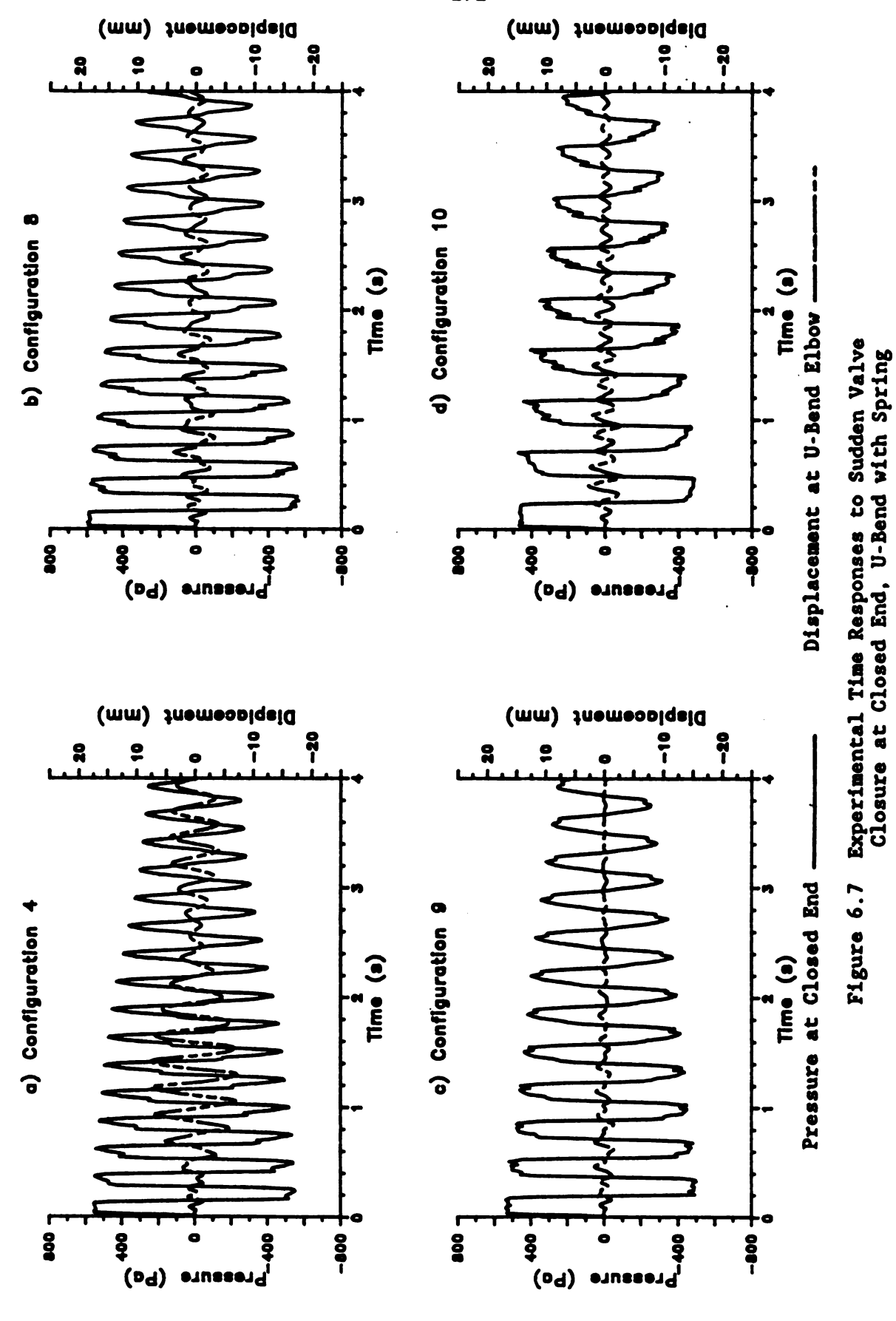


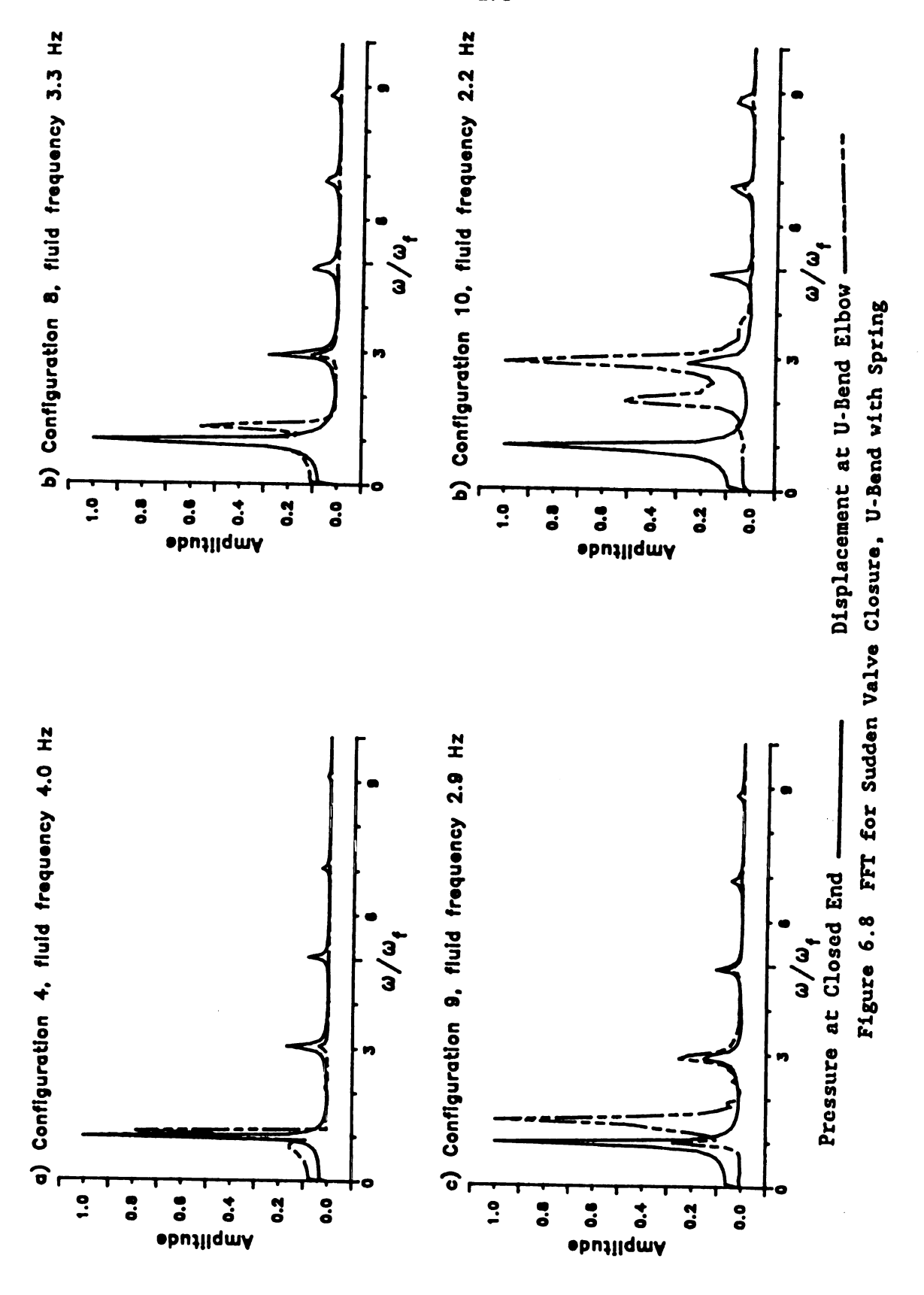












174

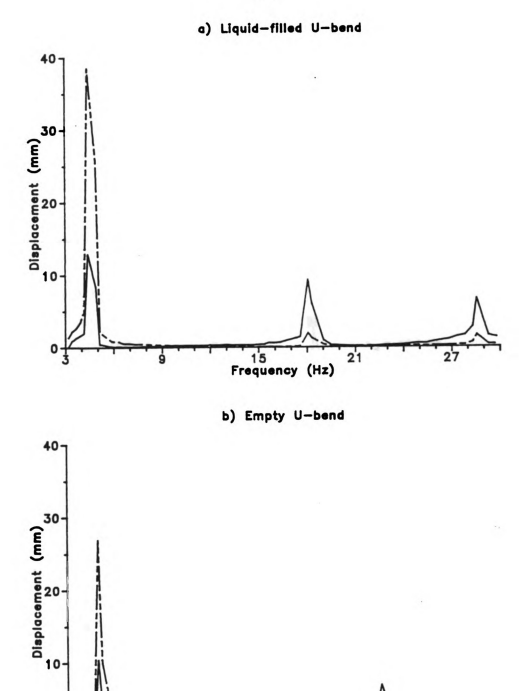


Figure 6.9 Experimental U-Bend Displacements for Harmonic Excitation

-Spring, D 1

15 Frequency (Hz)

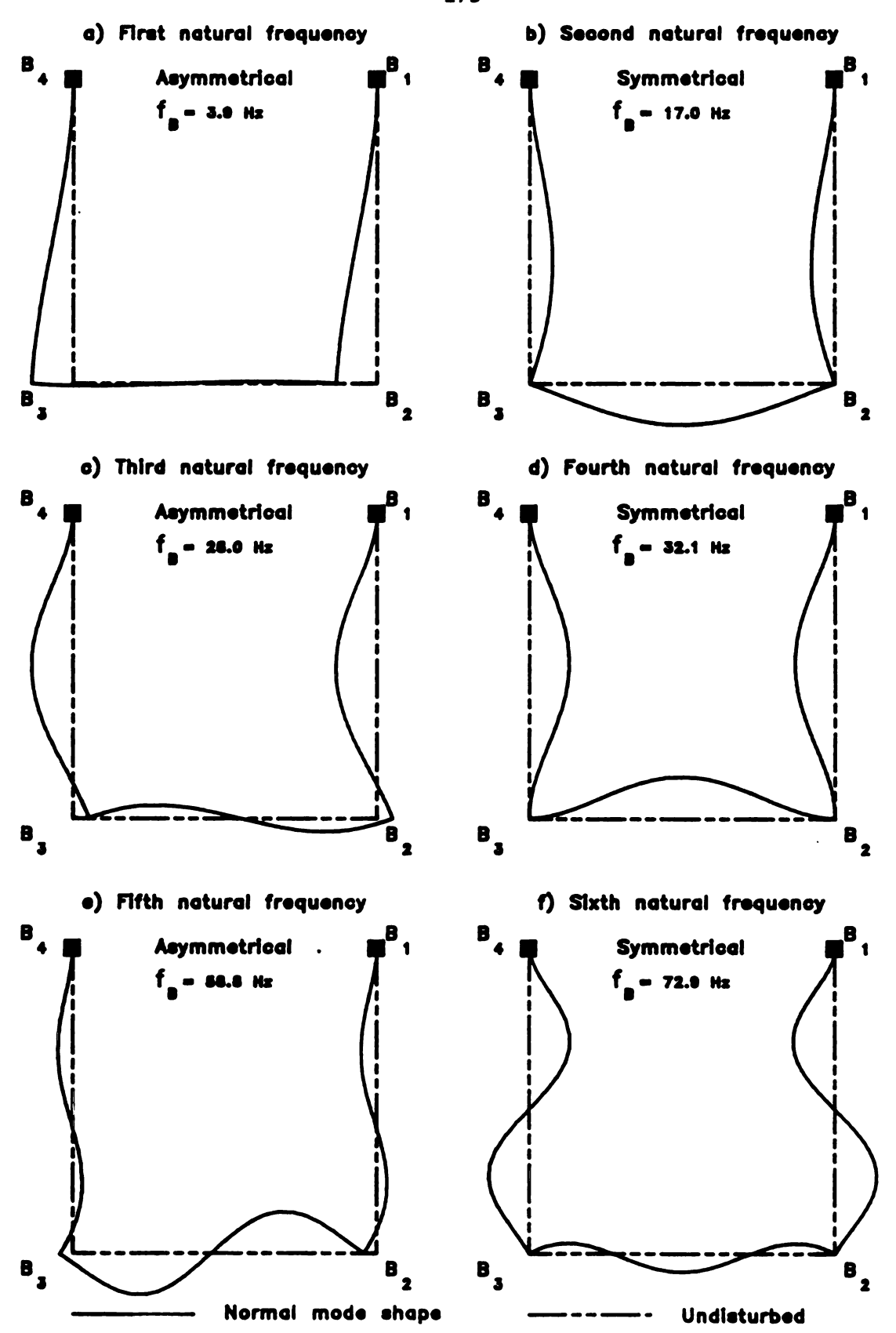


Figure 6.10 Computed U-Bend Mode Shapes, Free Bend

176

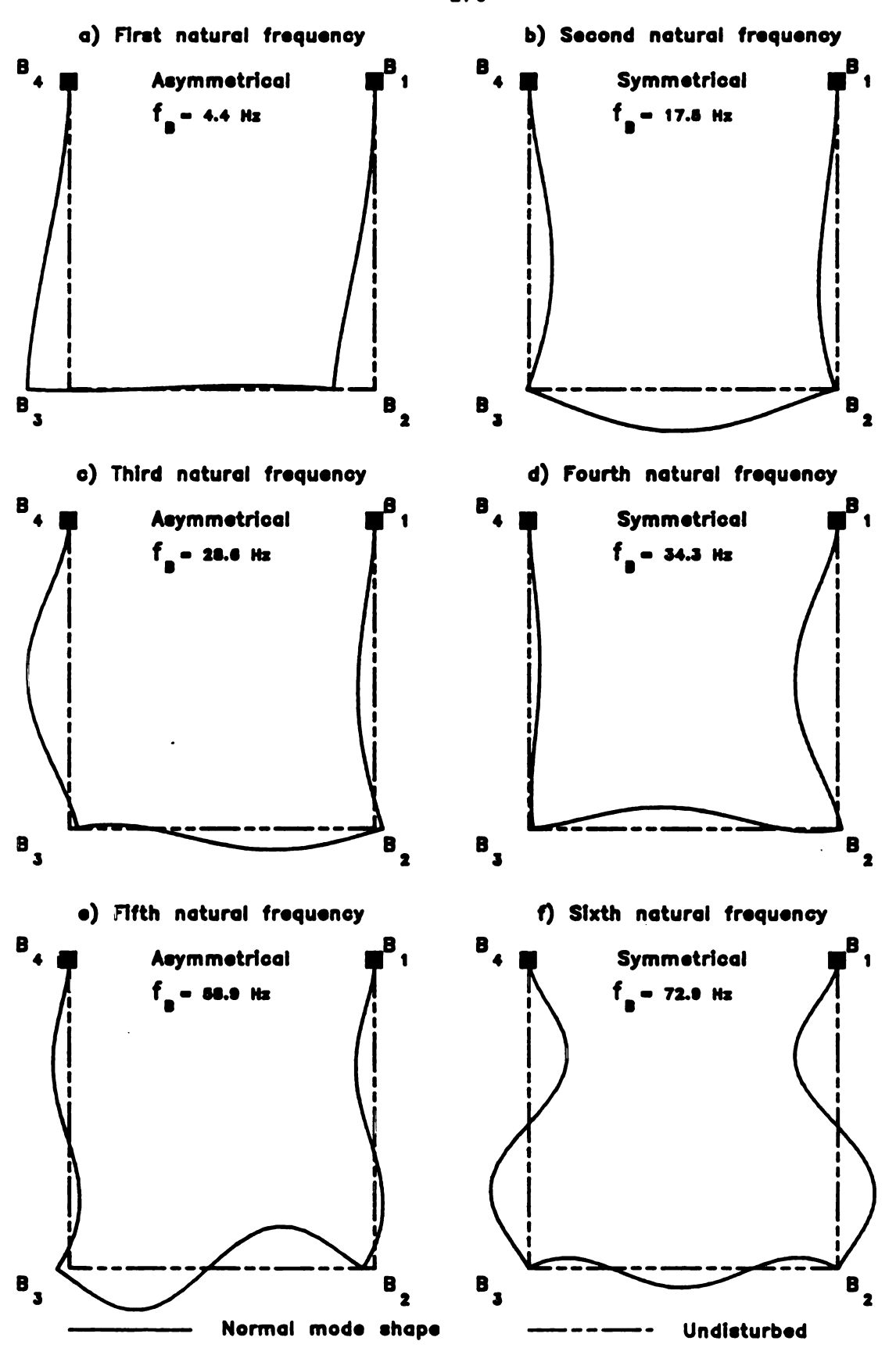


Figure 6.11 Computed U-Bend Mode Shapes, Bend Attached to Spring

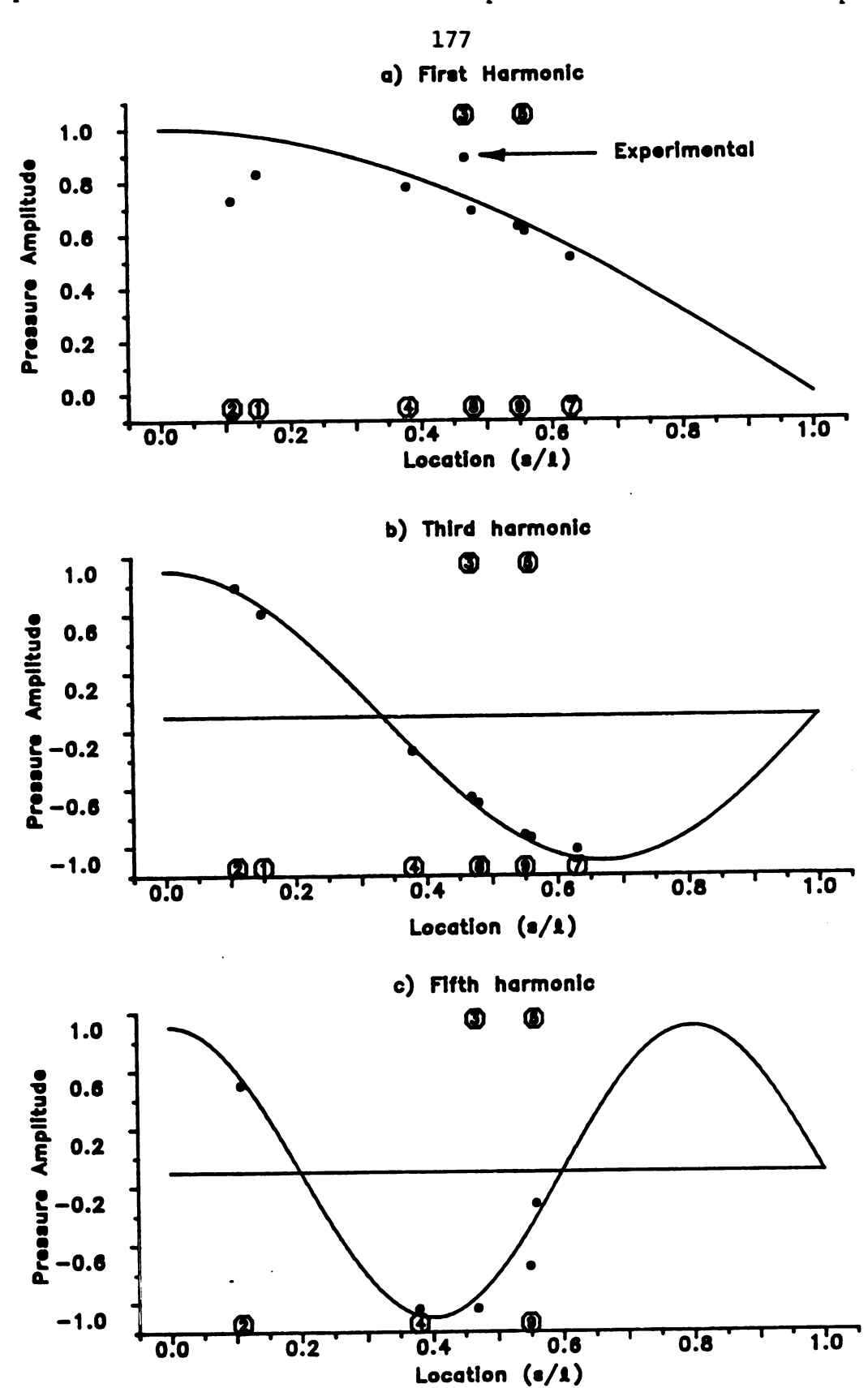


Figure 6.12 Liquid Mode Shapes at Liquid Natural Frequencies

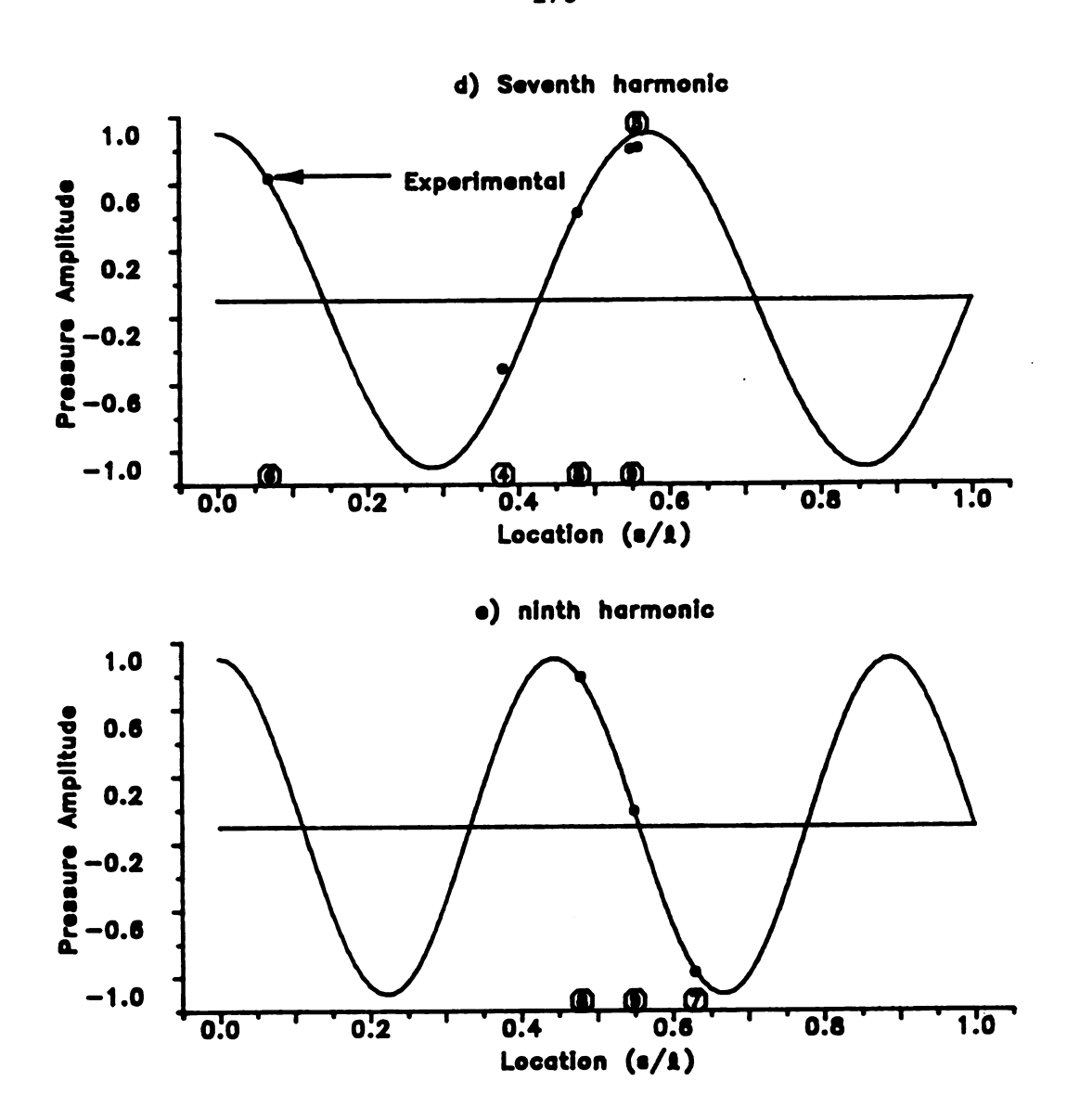
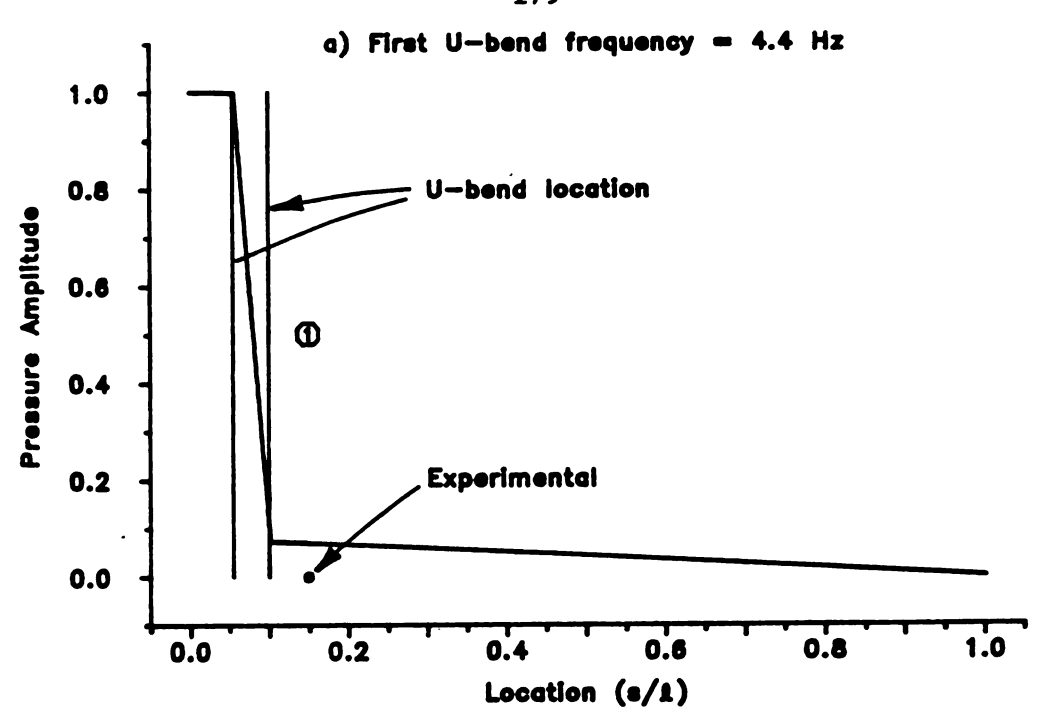


Figure 6.12 (Continuation)





b) Third U-bend frequency = 28.3 Hz

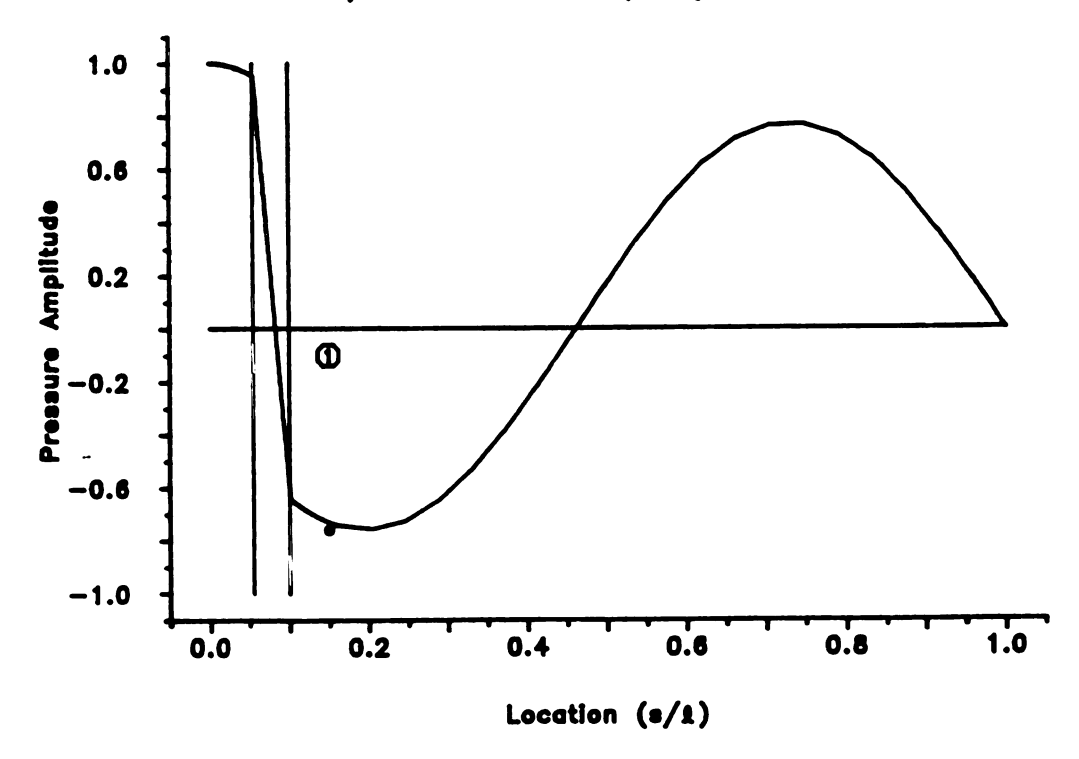
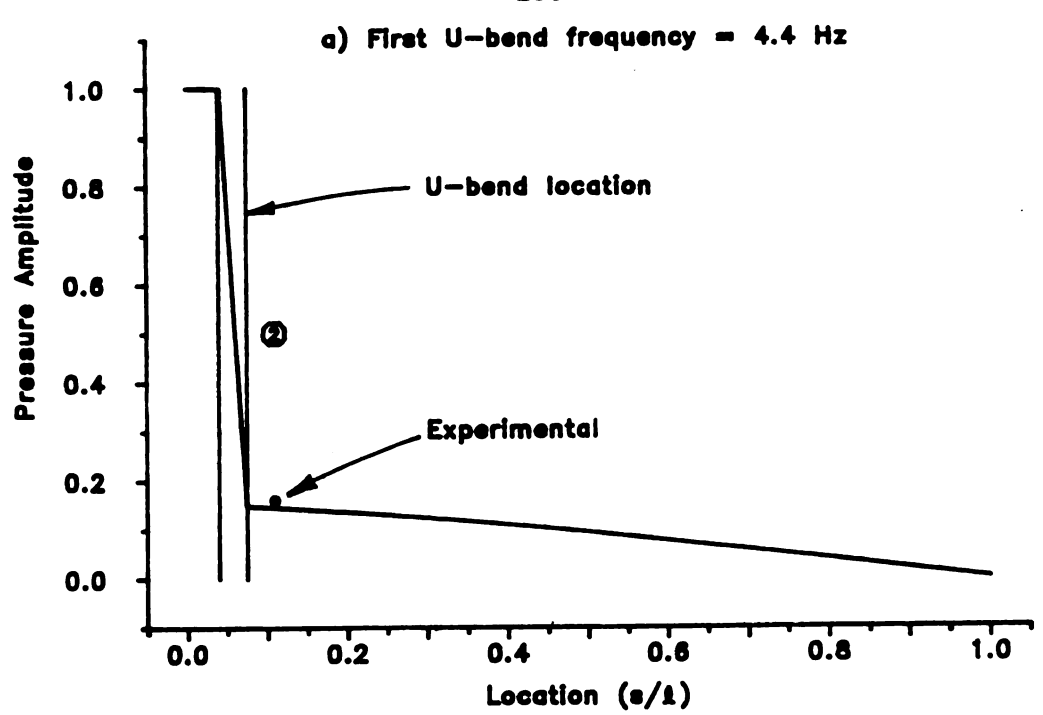


Figure 6.13 Liquid Mode Shapes at U-Bend Natural Frequencies, Configuration 1





b) Third U-bend frequency = 28.3 Hz

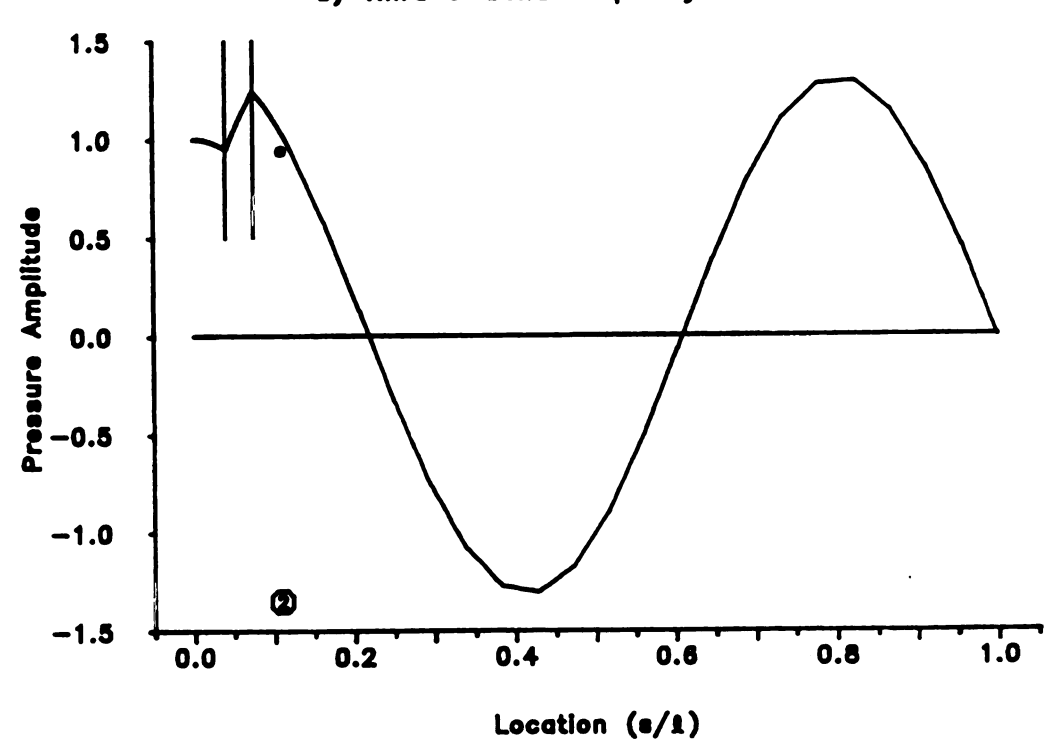
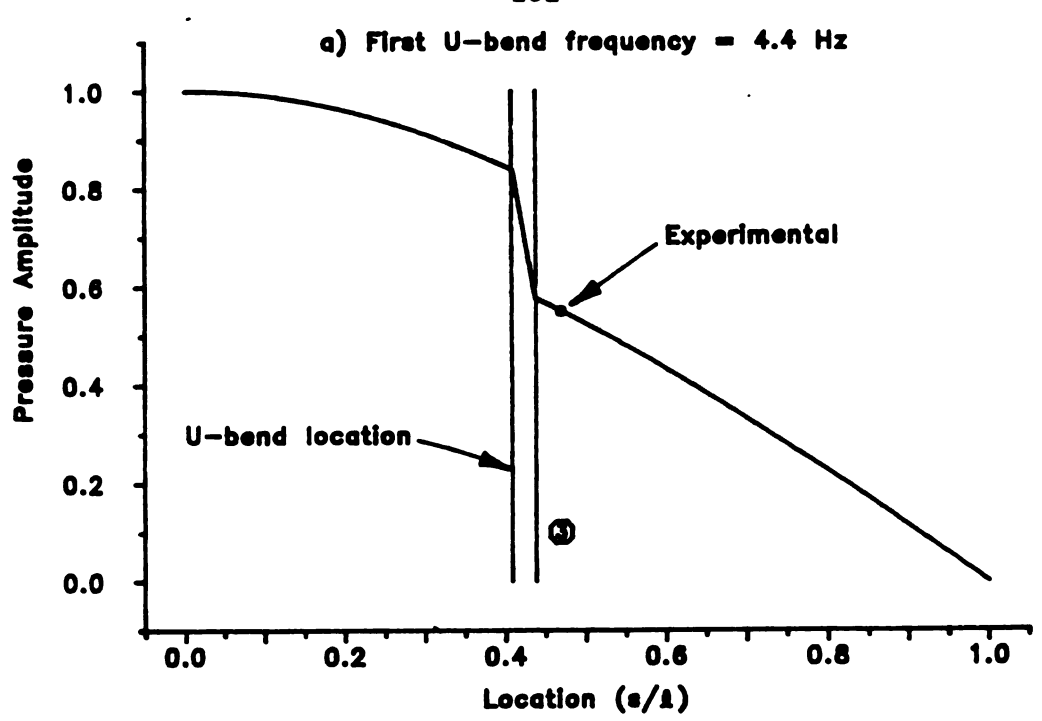


Figure 6.14 Liquid Mode Shapes at U-Bend Natural Frequencies, Configuration 2



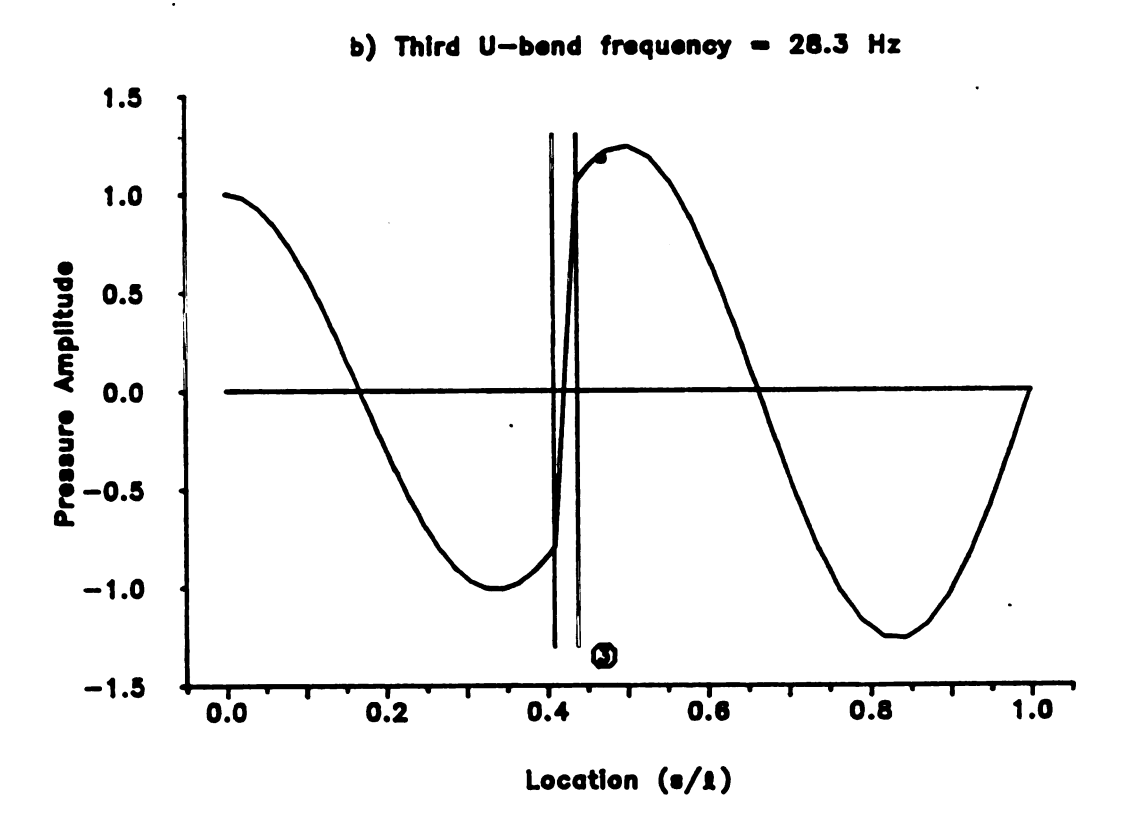
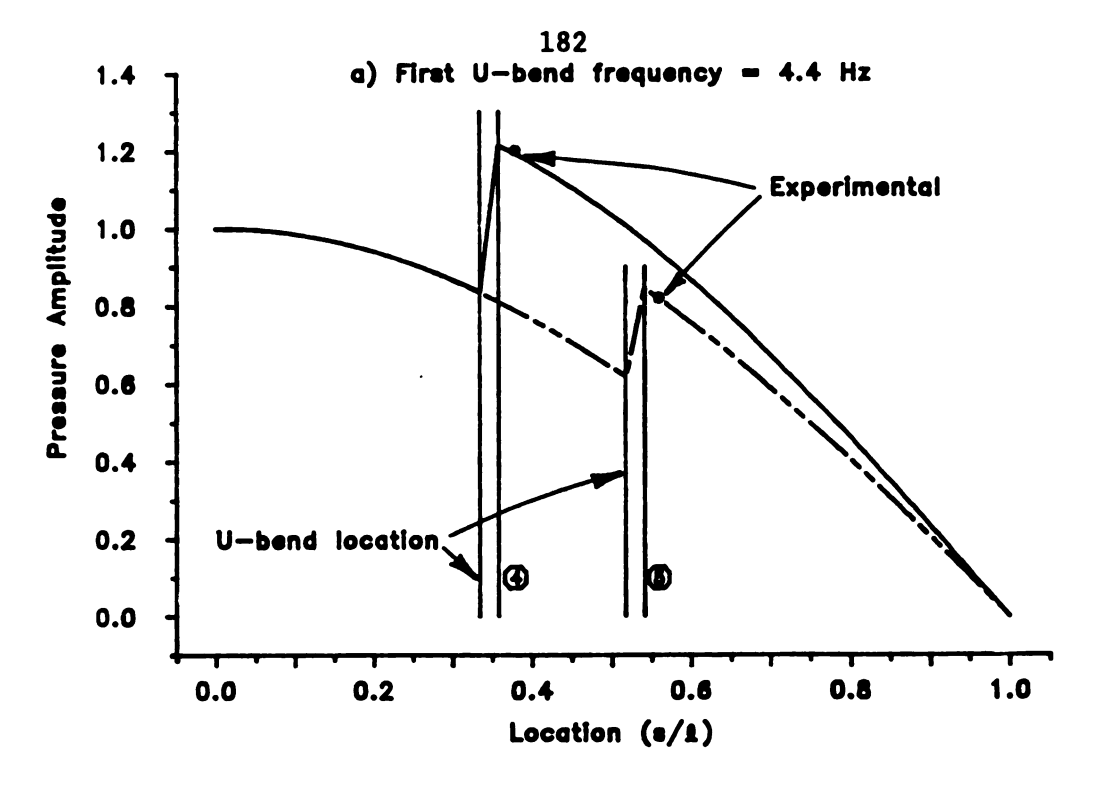


Figure 6.15 Liquid Mode Shapes at U-Bend Natural Frequencies, Configuration 3



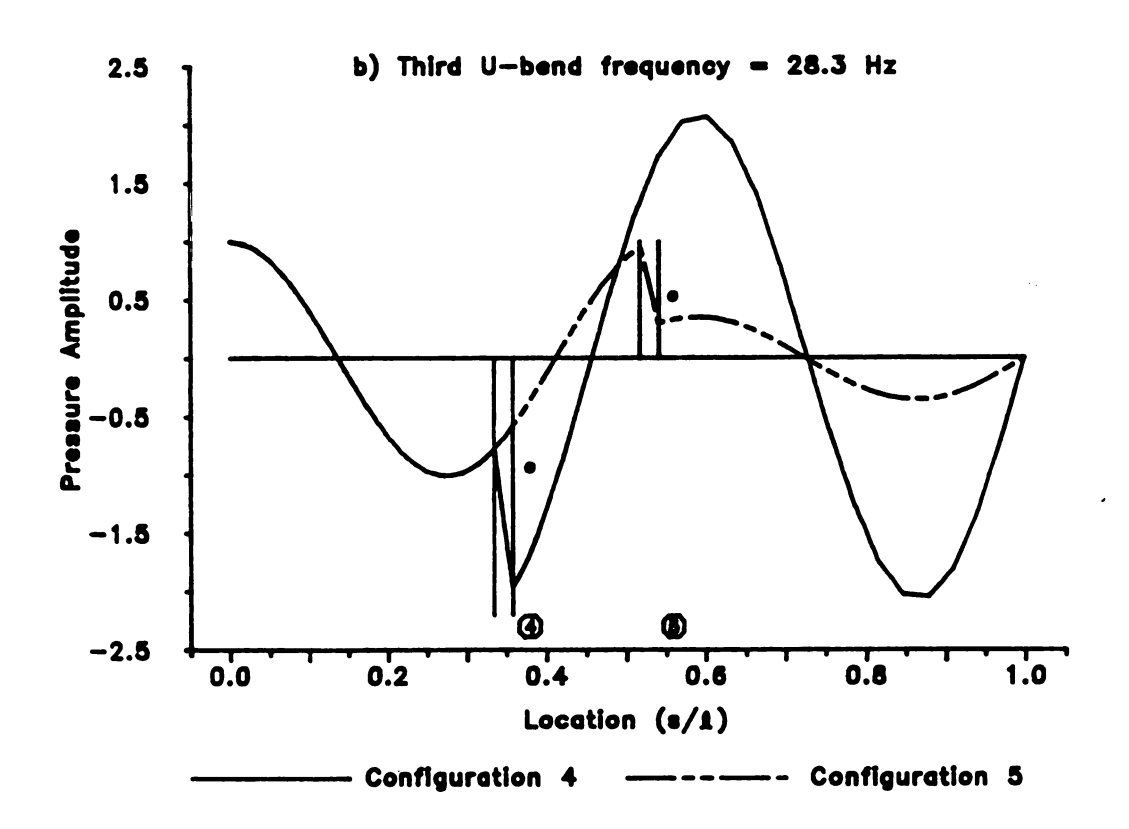
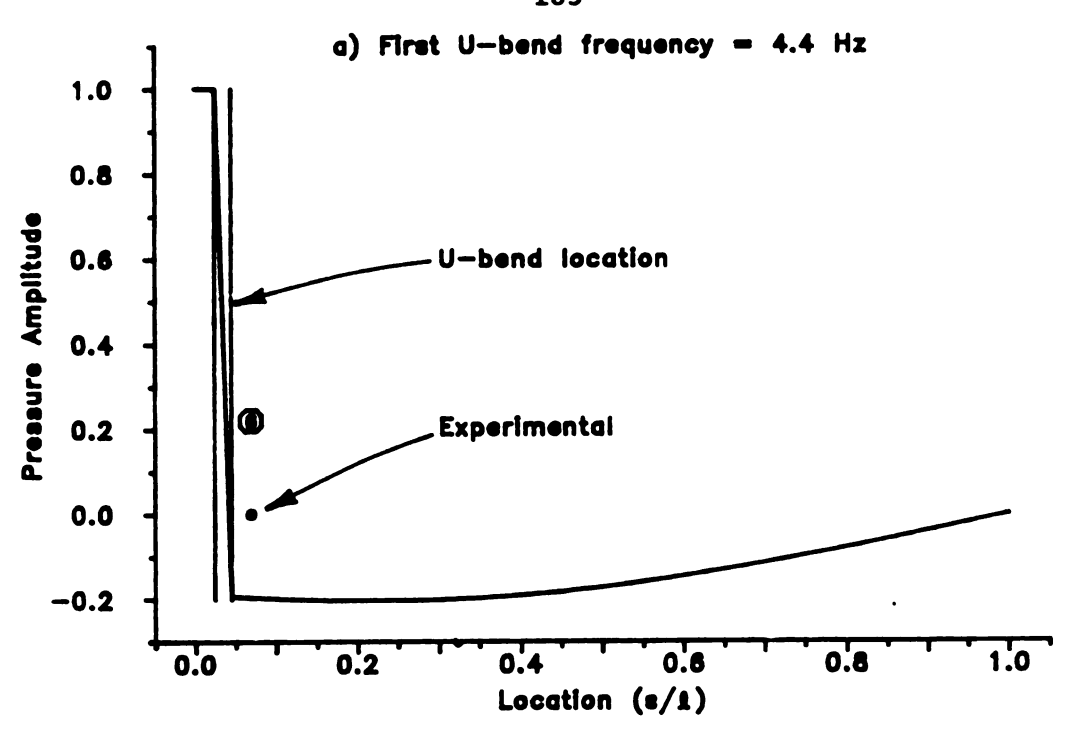


Figure 6.16 Liquid Mode Shapes at U-Bend Natural Frequencies, Configurations 4 and 5





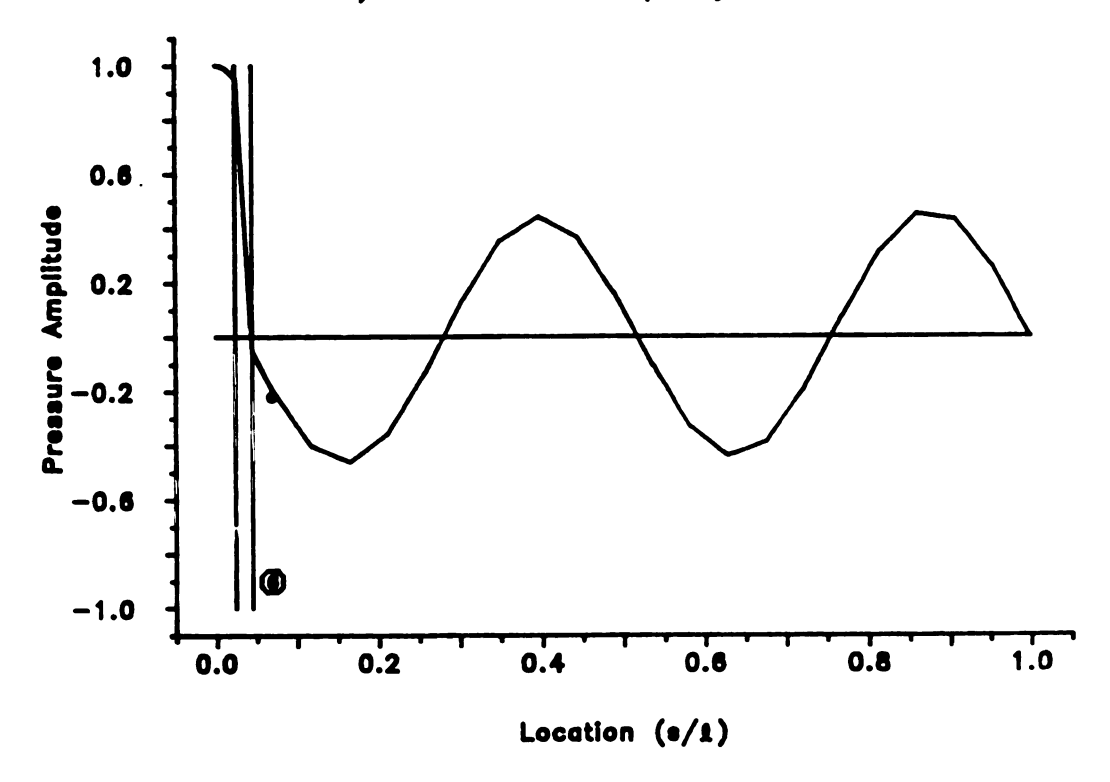
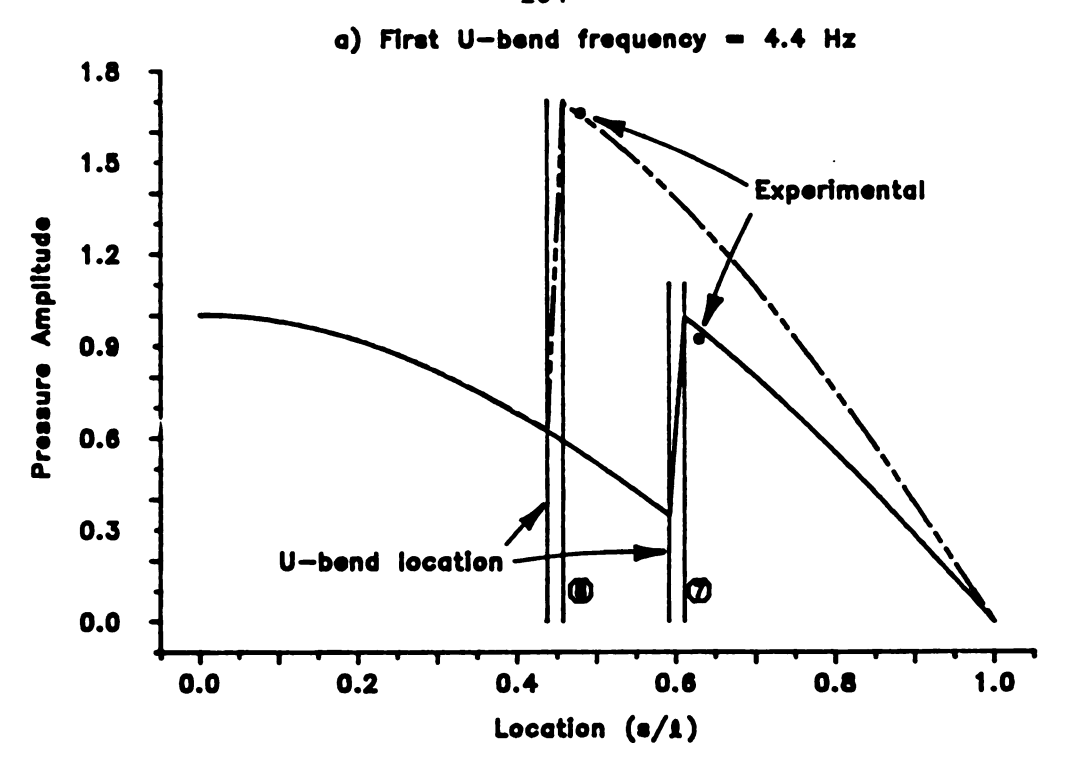


Figure 6.17 Liquid Mode Shapes at U-Bend Natural Frequencies, Configuration 6

184



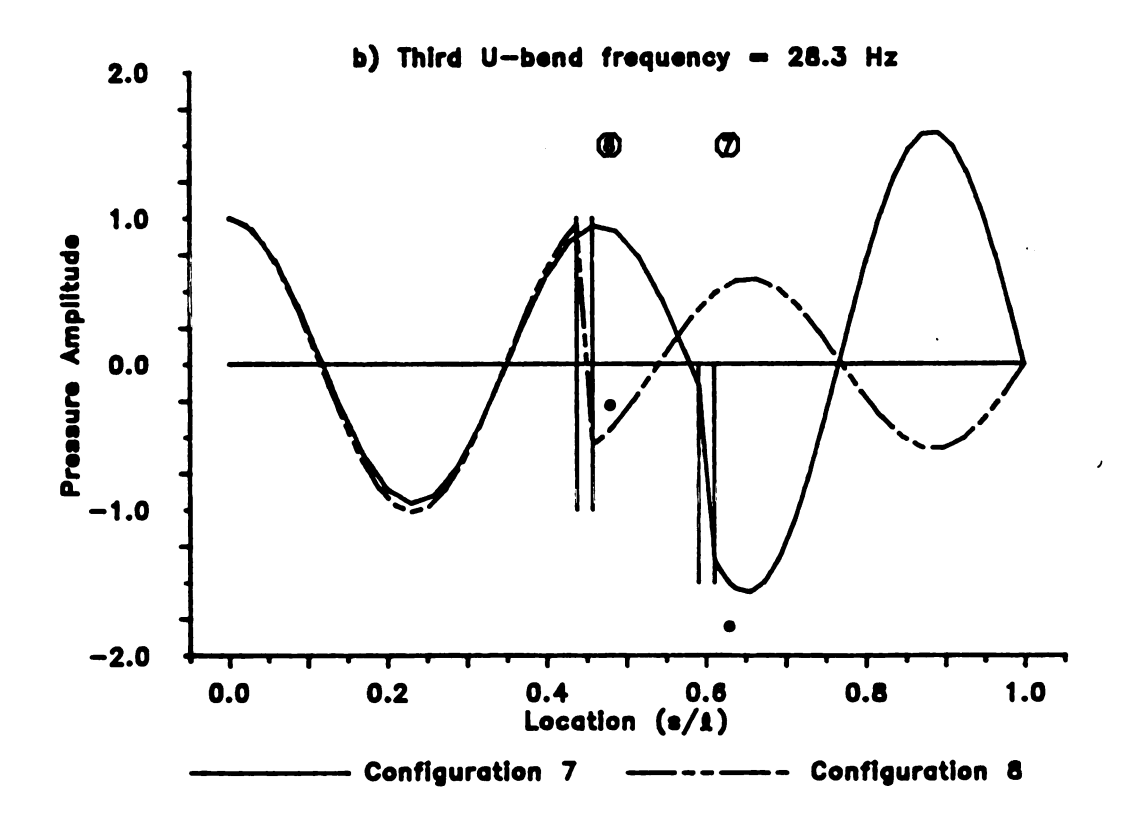
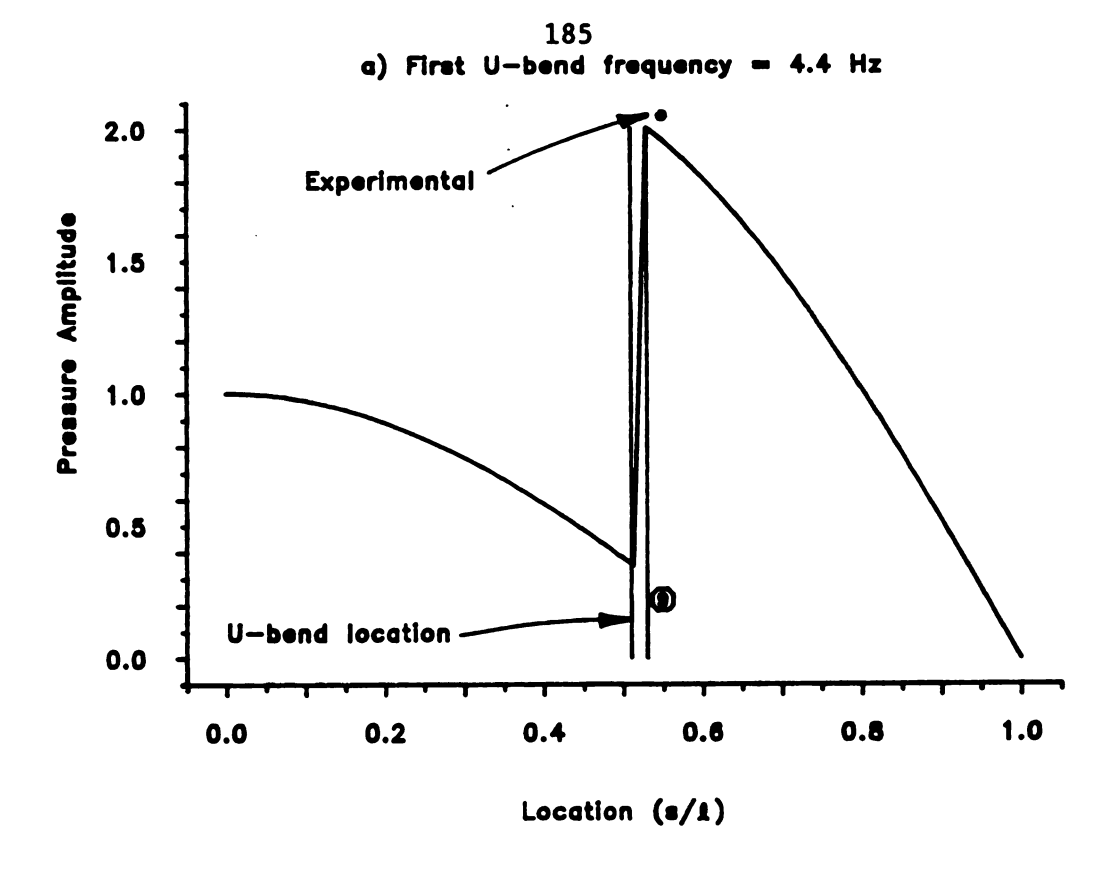


Figure 6.18 Liquid Mode Shapes at U-Bend Natural Frequencies, Configurations 7 and 8



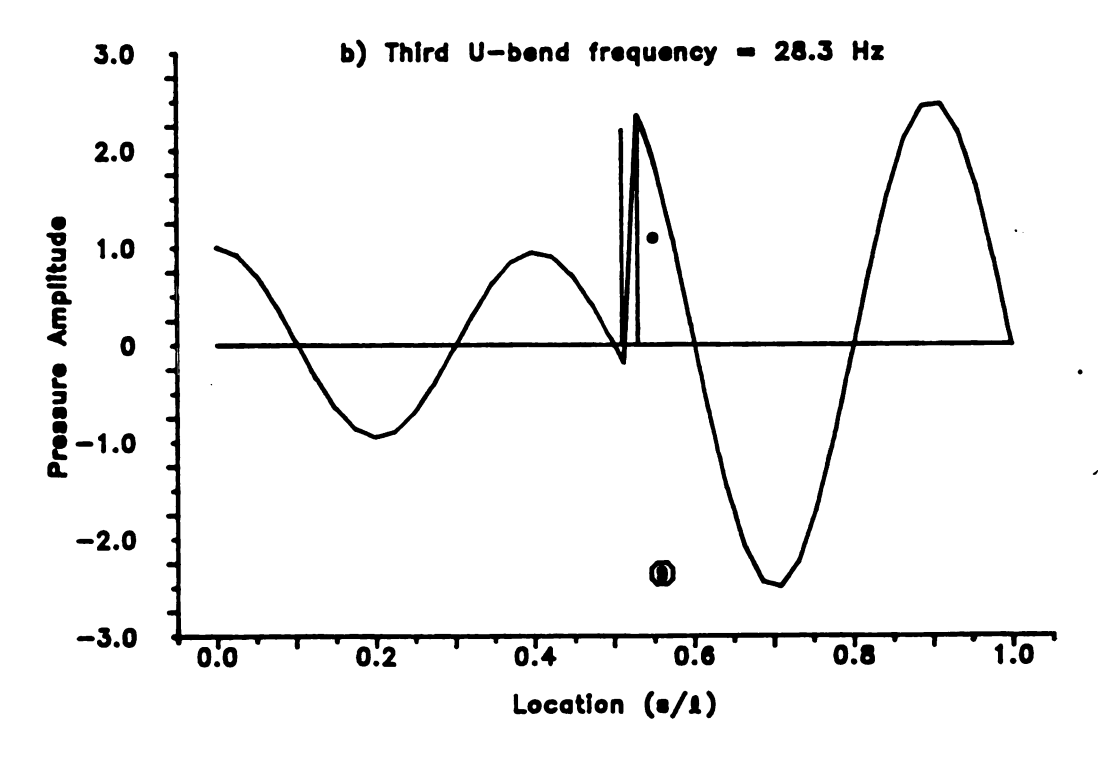


Figure 6.19 Liquid Mode Shapes at U-Bend Natural Frequencies, Configuration 9

CHAPTER 7

SUMMARY AND CONCLUSIONS

The primary objective of this study was to incorporate the flexural and torsional modes of vibration of liquid-filled pipe systems to an existing axially coupled model. The motion of the pipe wall and the contained liquid was represented by using a one-dimensional approximation. This approximation has been proved valid for the first lobar mode of the pipe cross section. A system of fourteen equations and fourteen dependent variables described the motion of the piping. Five families of waves that propagate in the pipe wall and in the liquid were identified. The analytical model incorporated the Poisson and junction coupling mechanisms and included the effect of shear deformation and rotary inertia of the lateral motion of the pipe. The inclusion of these mechanisms represents appropriately the motion of the systems and constitutes an improvement over the previous model by Wilkinson [64].

The transfer matrix method was the numerical model used for the analysis of these systems. The method can predict the pipe wall displacements and forces as well as the pressure and displacement of the liquid. The model provides an alternative to other numerical and analytical methods.

In addition, the Poisson and junction coupling were properly treated. The methodology to incorporate pipe constraints, such as rigid supports, springs, and inertia and external forces, was presented. The inclusion of hydraulic devices, such as orifices and pumps, may be easily accomplished by the use of point matrices.

The field transfer matrices for the flexural modes, developed by Pestel and Leckie [50], were modified to include the mass of the contained liquid. The field transfer matrix for the liquid-axial pipe wall was derived based on the model developed by Wiggert et al. [20]. Four submatrices were identified. The magnitude of the terms of this matrix in the analysis of liquid-filled pipes depends on the frequency at which the system oscillates. The compliance terms may be neglected for high frequency analysis. However, the main diagonal terms of each submatrix are important for low frequency studies.

The results from the transfer matrix method (TMM) were compared with numerical methods such as the method of characteristics (MOC) and the component synthesis method (CSM). The TMM exhibited advantages over the other two methods. The TMM is a one-step computation, whereas the CSM requires two steps for the analysis. In contrast to the MOC, the TMM does not require interpolations for the analysis of systems subjected to harmonic oscillations. Experimental data, available in the literature were also used to provide validation of the transfer matrix method.

An experimental apparatus was designed and built to validate the numerical method. A one-inch, water-filled, copper pipe with a U-type bend was excited with either a transient or harmonic loading to study the response of the system. The experimental tests were conducted on a liquid-filled pipe system with closed-open conditions for the liquid and fixed-fixed conditions for the U-bend. The natural frequencies of the liquid were varied by changing the length of the pipe. The harmonic excitation was applied to a U-bend that was allowed to vibrate in one plane. Numerical analysis results were compared to experimental results. The following conclusions were drawn from the experimental tests:

- 1) The snap-back transient test was used to calibrate the numerical model. The addition of the spring increased the stiffness of the U-bend. This additional stiffness increased the natural frequencies of the bend. Computed results showed that the spring increased by 0.5 Hz the natural frequencies of the U-bend.
- 2) The other transient test used was rapid valve closure. The closure of the valve excited the liquid odd harmonics, but only the first frequency of the U-bend. The time response of the liquid pressure and the displacement of the U-bend were presented. A fast Fourier transform analysis of the time series was performed to obtain the natural frequencies of the system. Good agreement between the experimental liquid harmonics and the corresponding computed results was obtained. The computed frequencies were obtained by assuming no shear or bending for the pipe legs between the valve and U-bend. The same assumption was made for the pipe legs and between the U-bend and the reservoir. Only the axial pipe wall and liquid modes were considered in these pipe

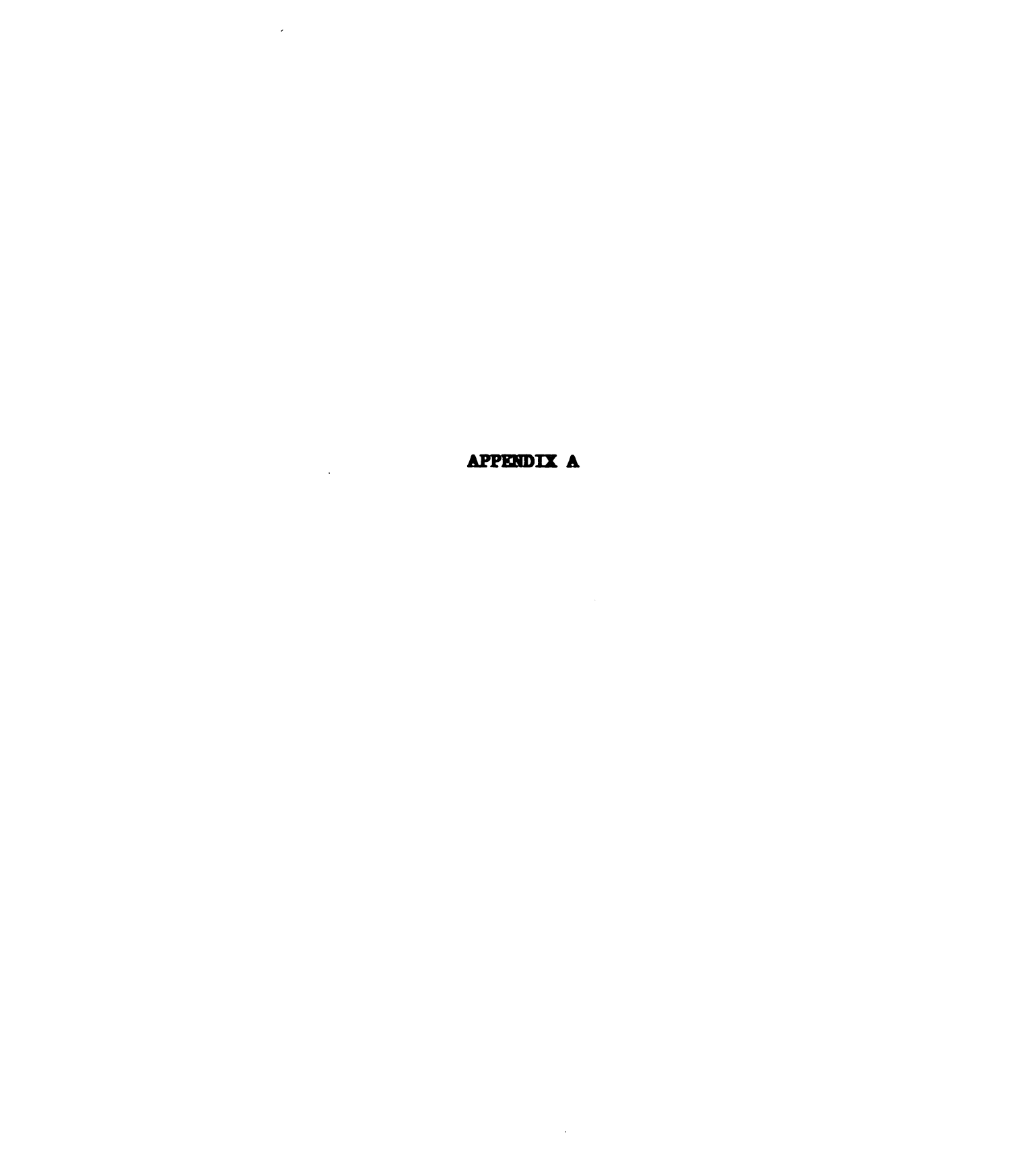
reaches. This test was also used to measure and compare the liquid wave speeds. The experimental results were compared with the wave speed obtained by Budny [22]. The computed results showed that the wave speeds were within 0.5% of the experimental values.

- 3) The harmonic test was used to excite the U-bend, thereby, exciting the liquid. Three U-bend frequencies and nine harmonics of the liquid were excited. Spectral analysis showed that large pressure responses occured at frequencies near the asymmetrical modes of the U-bend. These modes allowed motion of the elbows which generated the junction coupling mechanism. This coupling mechanism was the primary factor to magnify the pressure. The second mode of the U-bend, which corresponds to a symmetrical mode, did not excite the liquid pressure. The computed results predicted the natural frequencies of the system. The magnitude of the pressure response was increased when a liquid frequency was near one of the asymmetrical modes of the U-bend.
- 4) Variations of the pipe length changed the relative location of the U-bend and transducers with respect to the closed-end. A total of nine pipe configurations were studied. This allowed measurement of the liquid pressure mode shapes at discrete points for each pipe configuration. Computed mode shapes showed good correlation with the experimental points. The pressure mode shapes at the natural frequencies of the liquid corresponded to the odd harmonics of a 1/4 sine wave. The mode shapes at the U-bend frequencies show an abrupt change at the horizontal leg of the U-bend. The results showed that at these frequencies the magnitude of the pressure at the bend can increase as

much as 100% from the pressure at the closed end. The magnitudes of the pressure responses at the fluid frequencies are larger than those at the U-bend frequencies.

In summary, the tranfer matrix method is appropriate to predict the natural frequencies of liquid-filled pipes. Poisson and junction coupling are modeled with the use of this method. The experimental results showed that the larger pressure responses occured at higher harmonics and that the responses were magnified when the liquid frequency was near one of the asymmetrical modes of the U-bend. These modes allow motion at the elbows generating the junction coupling. This mechanism amplifies the pressure response of the system. Natural frequencies of complicated piping systems can be estimated by including the flexural, liquid and axial modes at locations where these modes may affect the response of the system. Other reaches can be analyzed by including the appropriate modes, for example only liquid or both liquid and axial.

The model used in this study allowed motion in only one plane. It did not include fluid friction or structural damping. The extension to a three dimensional space can be accomplished by incorporating the torsion mode as well as the flexural mode of the out of plane motion. Experiments are necessary to estimate the influence of these modes on the responses of the system. The incorporation of energy dissipation into the model is necessary to estimate the magnitude of the responses to an excitation.



APPENDIX A

LIOUID-AXIAL PIPE WALL TRANSFER MATRIX

A.1 <u>Introduction</u>

The field transfer matrix $[\mathbf{T}_{\mathrm{fp}}]$ shown in Equation 4.20 will be analyzed for two cases. First, Poisson's ratio is set to zero, thereby decoupling the axial pipe wall and liquid vibration. The results are then compared with those of other authors. Second, Poisson's ratio is taken nonzero; in this case the analysis will focus on the orders of magnitude of the matrix terms when the frequency of oscillation varies.

The analysis is facilitated by arranging the matrix in Equation 4.20 into four submatrices. The arrangement yields:

$$\begin{bmatrix} \sigma C_2 - C_0 & -C_1 + (\sigma + \gamma)C_3 & \frac{\nu b}{h} \tau C_2 & \frac{\nu b}{h} [C_1 - (\sigma + \tau + \gamma)C_3] \\ \sigma (C_1 - \sigma C_3) & \sigma C_2 - C_0 & -\frac{\nu b}{h} \sigma \tau C_3 & -\frac{\nu b}{h} \sigma C_2 \end{bmatrix}$$

$$\begin{bmatrix} T_{fp} \end{bmatrix} = \begin{bmatrix} 2\nu \sigma C_2 & 2\nu [(\sigma + \tau + \gamma)C_3 - C_1] & (\tau + \gamma)C_2 - C_0 & \frac{1}{\tau} [(\tau + \gamma)C_1 - [(\tau + \gamma)^2 + \sigma \gamma]C_3] \\ 2\nu \sigma \tau C_3 & -2\nu \tau C_2 & \tau [(\tau + \gamma)C_3 - C_1] & (\tau + \gamma)C_2 - C_0 \end{bmatrix}$$

$$(A.1)$$

The state vector associated with the above matrix is

$$z - \left\{ \begin{array}{ccc} \frac{U_z}{\ell} & \frac{F_z}{A_p E} & \frac{V}{\ell} & \frac{P}{K^*} \end{array} \right\}^T$$
 (A.2)

The matrix in Equation A.1 can also be written as

$$[\mathbf{T}_{fp}] = \begin{bmatrix} \mathbf{T}_{fp}^{aa} & \mathbf{T}_{fp}^{ab} \\ \hline \mathbf{T}_{fp}^{ba} & \mathbf{T}_{fp}^{bb} \end{bmatrix}$$
(A.3)

Notice that the coupled submatrices $\mathbf{T}_{\mathrm{fp}}^{\mathrm{ab}}$ and $\mathbf{T}_{\mathrm{fp}}^{\mathrm{ba}}$ contain the factors $\frac{\nu \mathrm{b}}{\mathrm{h}}$ and 2ν , respectively. Also, the main diagonal terms of the four submatrices are functions of the cosine of the eigen values λ_1 and λ_2 , whereas the other nondiagonal terms depend on the sine function of the same eigen values. The expressions for these coefficients are given in Equations 4.21g through 4.20j.

A.2 Uncoupled Analysis

Setting Poisson's ratio to zero results in uncoupling the axial pipe wall and liquid variables. The transfer matrix becomes separated into two sub-matrices. The liquid matrix is

$$\begin{cases} \mathbf{P} \\ \mathbf{\rho_f} \mathbf{a_f} \mathbf{\mathring{V}} \\ \mathbf{i} \end{cases} = \begin{bmatrix} \cos(\omega l/\mathbf{a_f}) & -\mathbf{j}\sin(\omega l/\mathbf{a_f}) \\ -\mathbf{j}\sin(\omega l/\mathbf{a_f}) & \cos(\omega l/\mathbf{a_f}) \end{bmatrix} \mathbf{i} \begin{cases} \mathbf{P} \\ \mathbf{\rho_f} \mathbf{a_f} \mathbf{\mathring{V}} \\ \mathbf{i} - 1 \end{cases}$$
(A.4)

193

where \mathring{V} represents the liquid velocity amplitude. This result agrees with that of Wilkinson [64], Chaudhry [7] and Wylie and Streeter [6]. The axial pipe wall matrix is

$$\begin{cases} \sigma_{z} \\ \rho_{f} a_{p} \mathring{U}_{z} \end{cases}_{i} = \begin{bmatrix} \cos(\omega \ell/a_{p}) & j\sin(\omega \ell/a_{p}) \\ j\sin(\omega \ell/a_{p}) & \cos(\omega \ell/a_{p}) \end{bmatrix}_{i} \begin{cases} \sigma_{z} \\ \rho_{f} a_{p} \mathring{U}_{z} \end{cases}_{i-1}$$
(A.5)

where $\mathring{\mathbf{U}}_{\mathbf{Z}}$ represents the axial pipe wall velocity amplitude and $\sigma_{\mathbf{Z}}$ is the axial stress. This matrix agrees with the matrix presented by Wilkinson [64].

A.3 Coupled Analysis

The importance of the coupling terms of the transfer matrix can be studied by using an order of magnitude analysis. An inspection of the matrix terms in Equation A.1 shows that the coefficients and the eigen value parameters σ , τ and γ are function of the frequency in addition to the liquid and pipe material properties. The terms ν , b and h depend on the liquid and pipe material properties. The radius to thickness ratio, b, and the frequency of oscillation, ω , are the parameters varied. The Young's modulus to modified bulk modulus ratio, h, and Poisson's ratio, ν , also affect the order of magnitude of the matrix terms, but they will be kept constant in this analysis. For comparison, a discussion based on numerical evaluations will be presented for pipes of five different

- - -

materials. The liquid is water with K = 2.2 GPa and $\rho_{\rm f}$ = 1000 kg/m³. A similar analysis was performed by Otwell [19] and Stuckenbruck [21]. The physical properties used for the pipe material are shown in Table A.1 [21].

TABLE A.1

PIPE MATERIAL PROPERTIES

Material	Young's Modulus GPa	Density s kg/m	Poisson's Ratio
Steel	210.0	7600	0.27
Cast Iron	80.0	7600	0.25
Copper	115.0	8800	0.34
Aluminum	70.0	2700	0.33
Polyethylene	0.8	1000	0.46

The influence of the pipe cross-section geometry ratio, b, can be facilitated by defining the ratio of coupled wave speeds as

$$c - \frac{c_p}{c_f} \tag{A.6}$$

This ratio can also be defined as the eigen value ratio

$$c = \frac{\lambda_1}{\lambda_2} \tag{A.7}$$

The relations between the coupled wave speed and eigen value for the liquid and axial pipe wall are defined in Equations 3.22 and 3.23. The

variation of c with respect to the pipe cross section ratio is shown in Figure A.la for values of b between 10 and 160. Figures A.lb and A.lc show the coupled wave speeds for both the liquid and pipe in the axial direction for each of the five pipe materials studied and for the same pipe cross section range. The wave speed ratio ranges within one order of magnitude for values of b less than 160 (Figure A.la), except for the polyethylene pipe. For example, for the copper pipe the variation of c is 4 (between 3 and 7), whereas for the polyethylene it is 17 (between 5 and 22). The variation of the wave speed ratio is due to a faster decrease of the liquid speed over the axial speed as b increases (Figure A.lb and A.lc). Therefore, the radius to thickness ratio does not introduce appreciable changes in the order of magnitude of the terms in the transfer matrix.

The variation of the matrix terms with respect to the frequency of oscillation, ω , is analyzed for a copper pipe with b = 10 and liquid natural frequency of 4 Hz. Table A.2 shows the value of the coefficients as the frequency increases. The characteristic parameters σ , τ and γ are also shown. The upper limit frequency is given by the first lobar mode of the pipe cross section, ω_{θ} . As shown by Everstine et al. [86], a one-dimensional analysis is not valid for frequencies greater than ω_{θ} . The frequency expression for the first lobar mode is given in Equation 3.7. This equation may also be written as

$$\omega_{\theta} = \frac{a_{p}}{r} \left[\frac{3}{5b^{2}(1-\nu^{2})(1+b/2d)} \right]^{\frac{1}{2}}$$
 (A.8)

For example, for the copper pipe of Table A.1 with r=0.1 m and b=10 the first lobar mode frequency ω_{g} is 2380 rad/s or 380 Hz.

TABLE A.2

TRANSFER MATRIX PARAMETERS

Coefficient	Equation	Amplitude	Value	Value at $\omega - \omega_{\theta}$
Co	4.20g	$\pm(1+c^2)/(c^2-1)$	1.25	1.3
C_1	4.20h	$\pm(1+c^3)/\lambda_1(c^2-1)$	$3.50/\lambda_1$	0.0
$\mathtt{C_2}$	4.20i	$\pm 2c^2/\lambda_1^2(c^2-1)$	$2.25/\lambda_1^2$	0.0
C _s	4.20j	$\pm c(1+c)/\lambda_1^3(c^2-1)$	$1.50/\lambda_1^2$	0.0
τ	4.20a	$c_{\mathbf{f}}^2 \lambda_1^2 / a_{\mathbf{f}}^2$	$0.96\lambda_1^2$	9075
σ	4.20b	$c_{p}^{2}\lambda_{2}^{2}/a_{p}^{2}$	$1.04\lambda_2^2$	27220
γ	4.20c	$2\nu^2$ b/d c $_{\rm p}^2\lambda_2^2/a_{\rm p}^2$	$0.27\lambda_2^2$	7070

The results given in Table A.2 show that the trigonometric coefficients depend on $1/\lambda_1^n$ where n=0,1,2 or 3 as ω increases, whereas the eigenvalue parameters depend on the square of the eigenvalues. The coefficients are shown in Figure A.2a for the copper water-filled pipe when c is 2.8. Figure A.2b shows the eigen values for the same piping system. The sixteen terms of the transfer matrix are plotted in Figures A.3 through A.6 for varying ratios of oscillation to the liquid natural frequency. Figure A.3 shows the terms for the axial pipe wall submatrix. The coupling submatrices are shown in Figures A.4 and A.5.

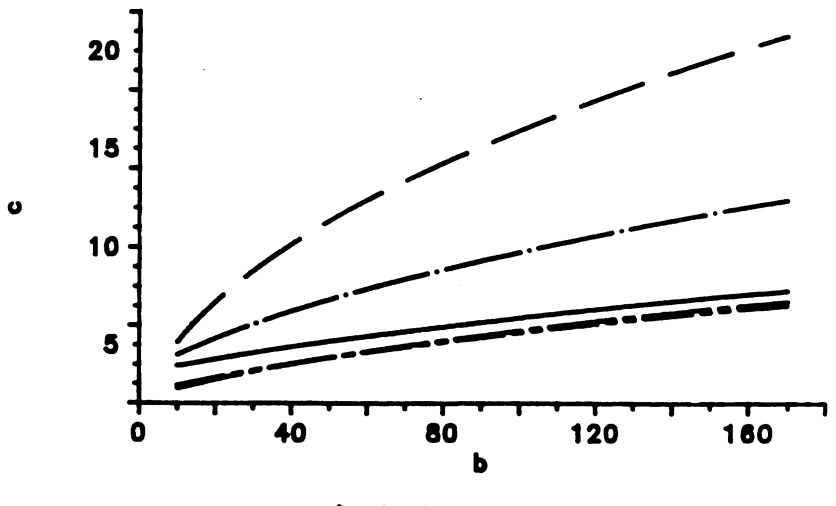
Finally, the liquid submatrix is shown in Figure A.6. The following observations can be made

- 1) The main diagonal terms of the liquid and pipe wall submatrices fluctuate between -1 and 1.
- 2) At low frequencies, the main diagonal terms of the matrix, which depend on C_0 start at a value of 1. The other terms are one order of magnitude lower than the main diagonal terms. This result is also shown in Figure A.2a.
- 3) At high frequencies, the amplitude of the matrix terms (2,1), (2,3), (4,1) and (4,3) increase as the frequency increases. These terms are associated with the apparent stiffness ratio, force or pressure over displacement. The amplitude of the terms (1,2), (1,4), (3,2) and (3,4) decrease as the frequency increases. These terms are associated with the compliance ratio, displacement over force or pressure.

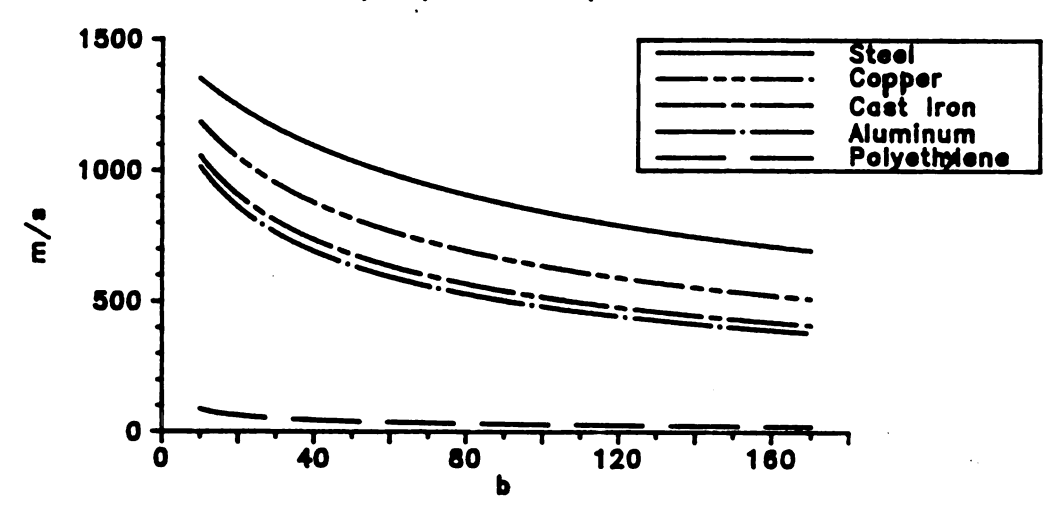
The above observations and the results in Figures A.3 through A.6 show that the compliance terms may be neglected for high frequency analysis. The main diagonal terms can be use for frequencies less than the first liquid frequency and the other terms may be neglected at low frequencies.

198

a) Wave Speed Ratio



b) Liquid Wave Speeds



c) Pipe Wave Speeds

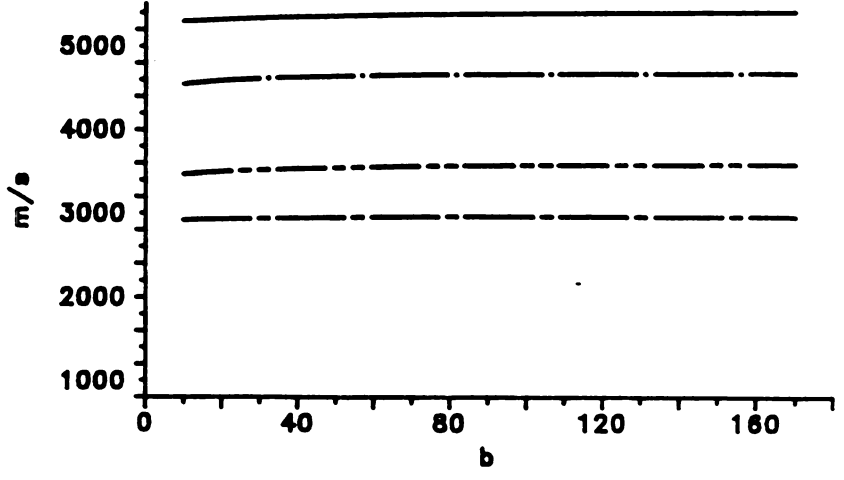
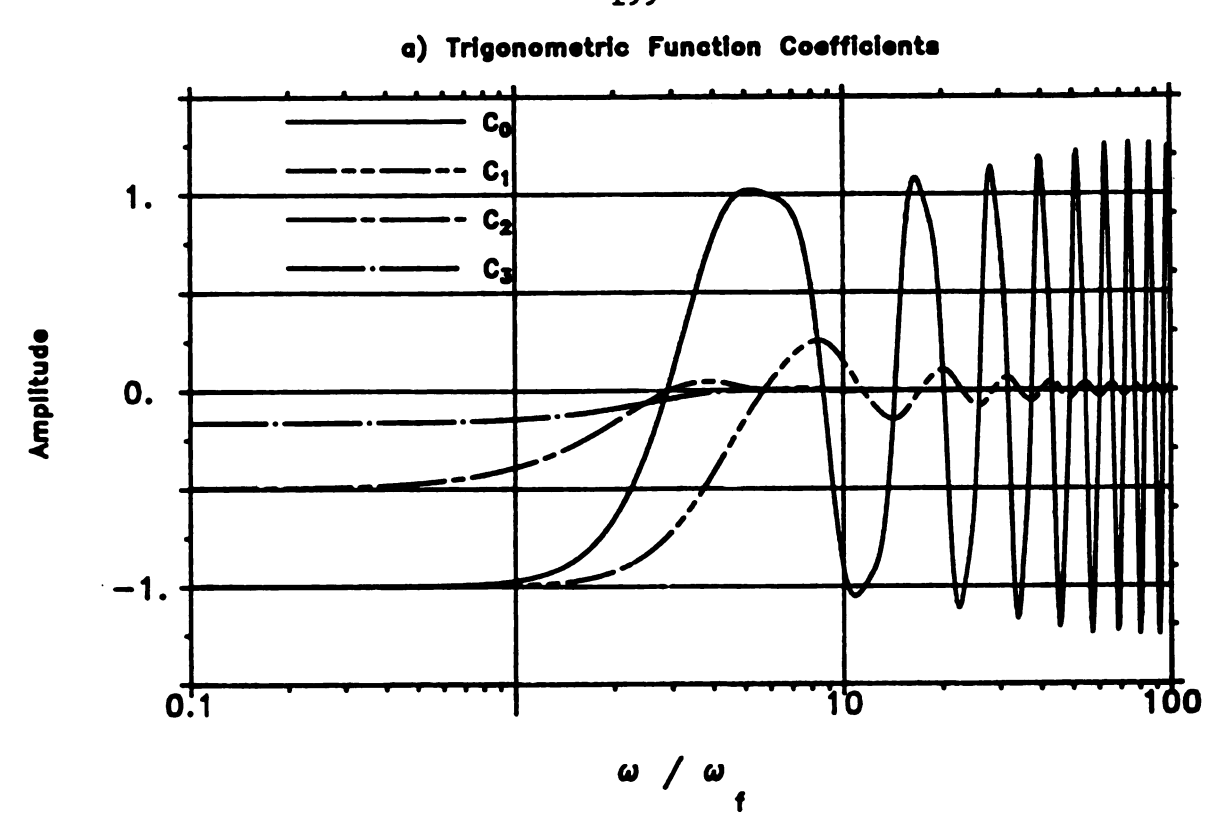


Figure A.1 Liquid and Axial Pipe Wall Wave Speeds Versus
Pipe Cross Sectional Ratio

199



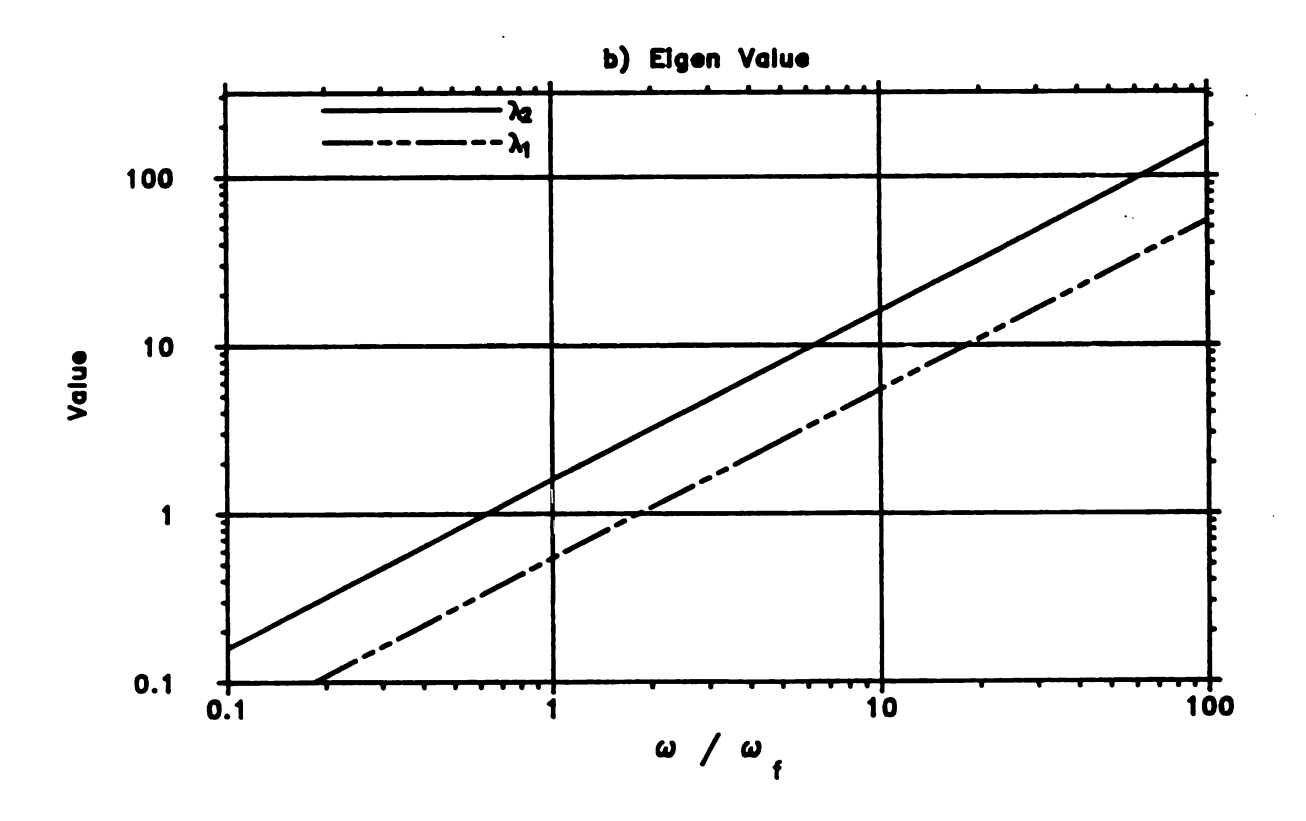
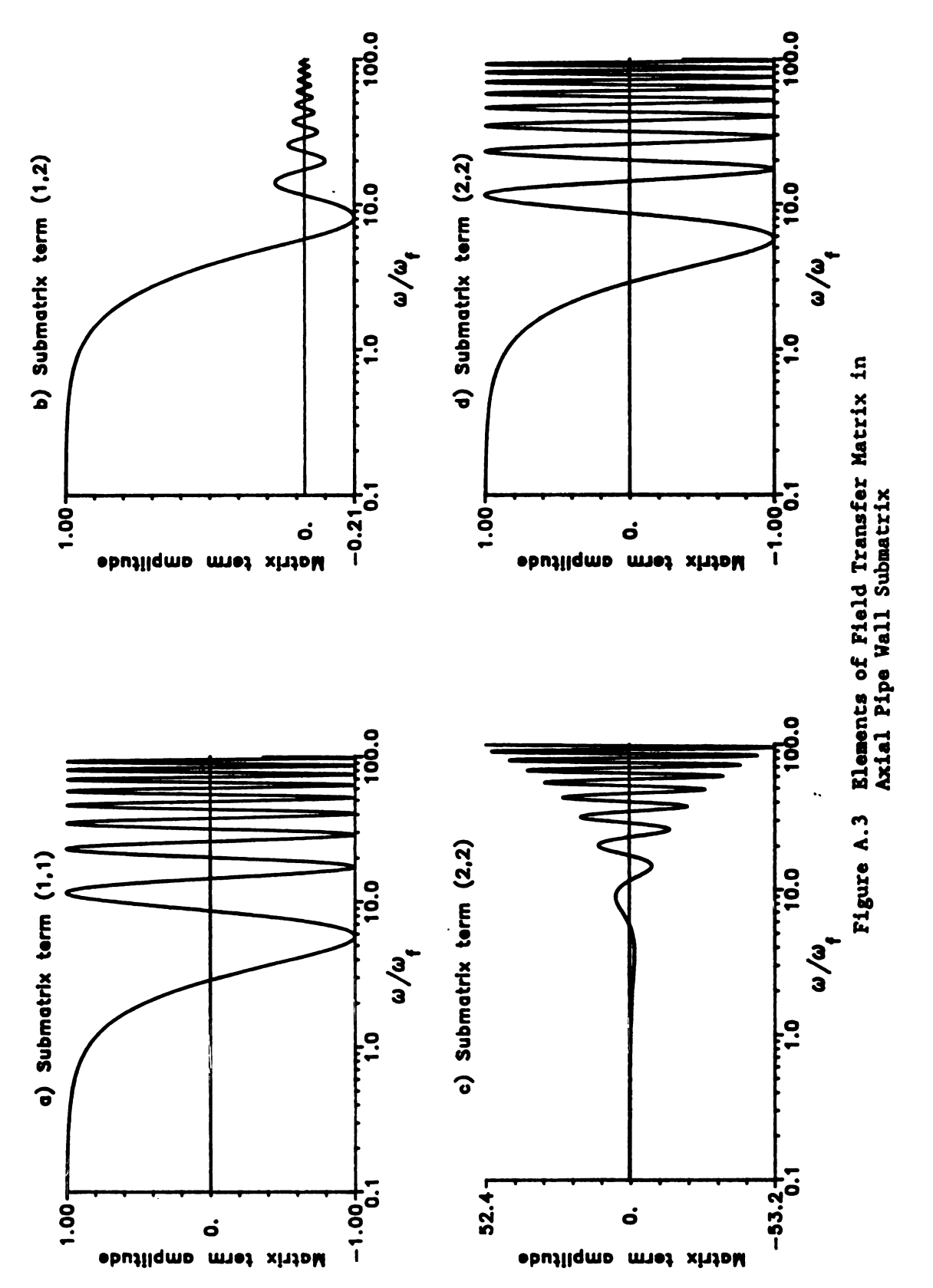
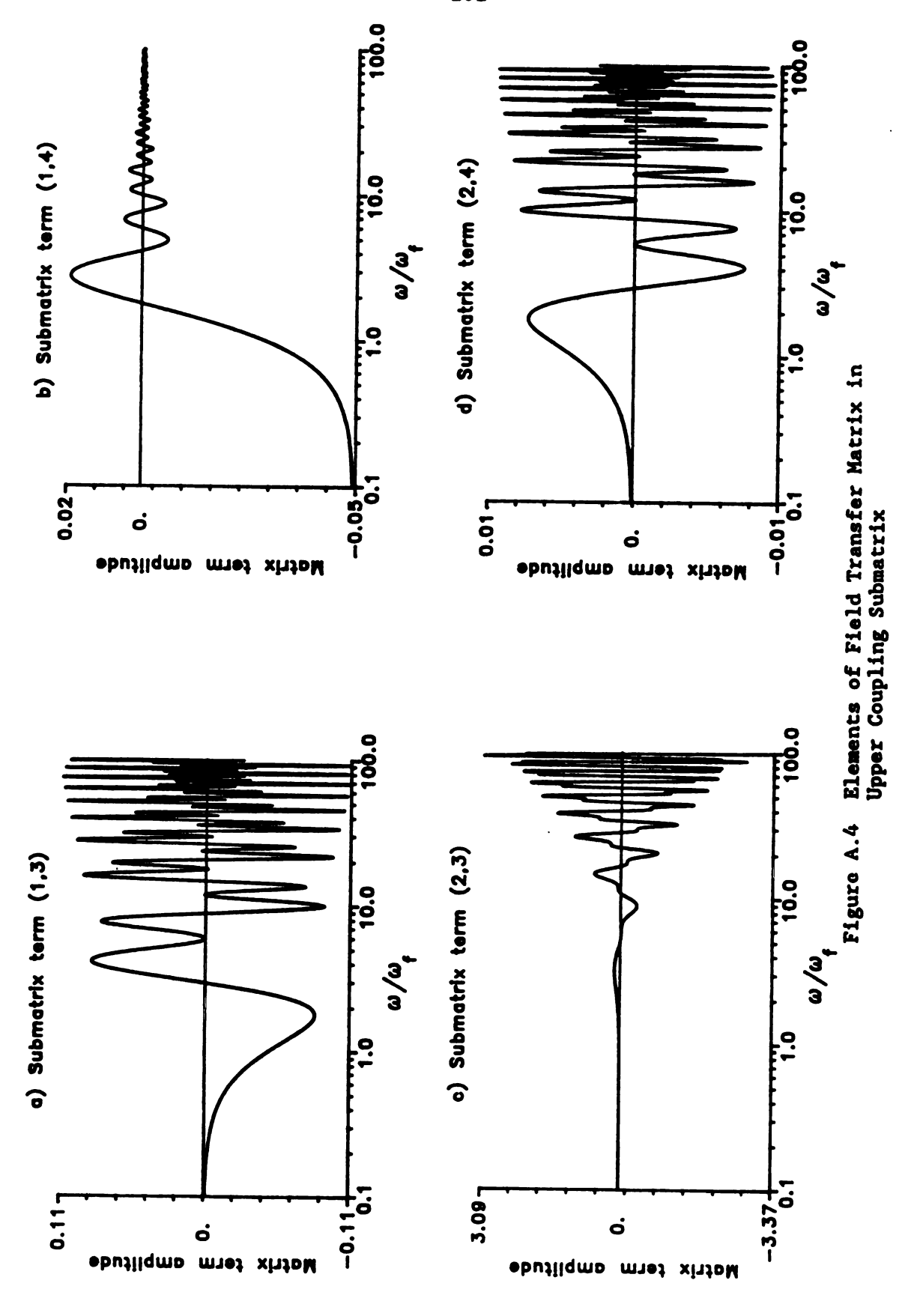
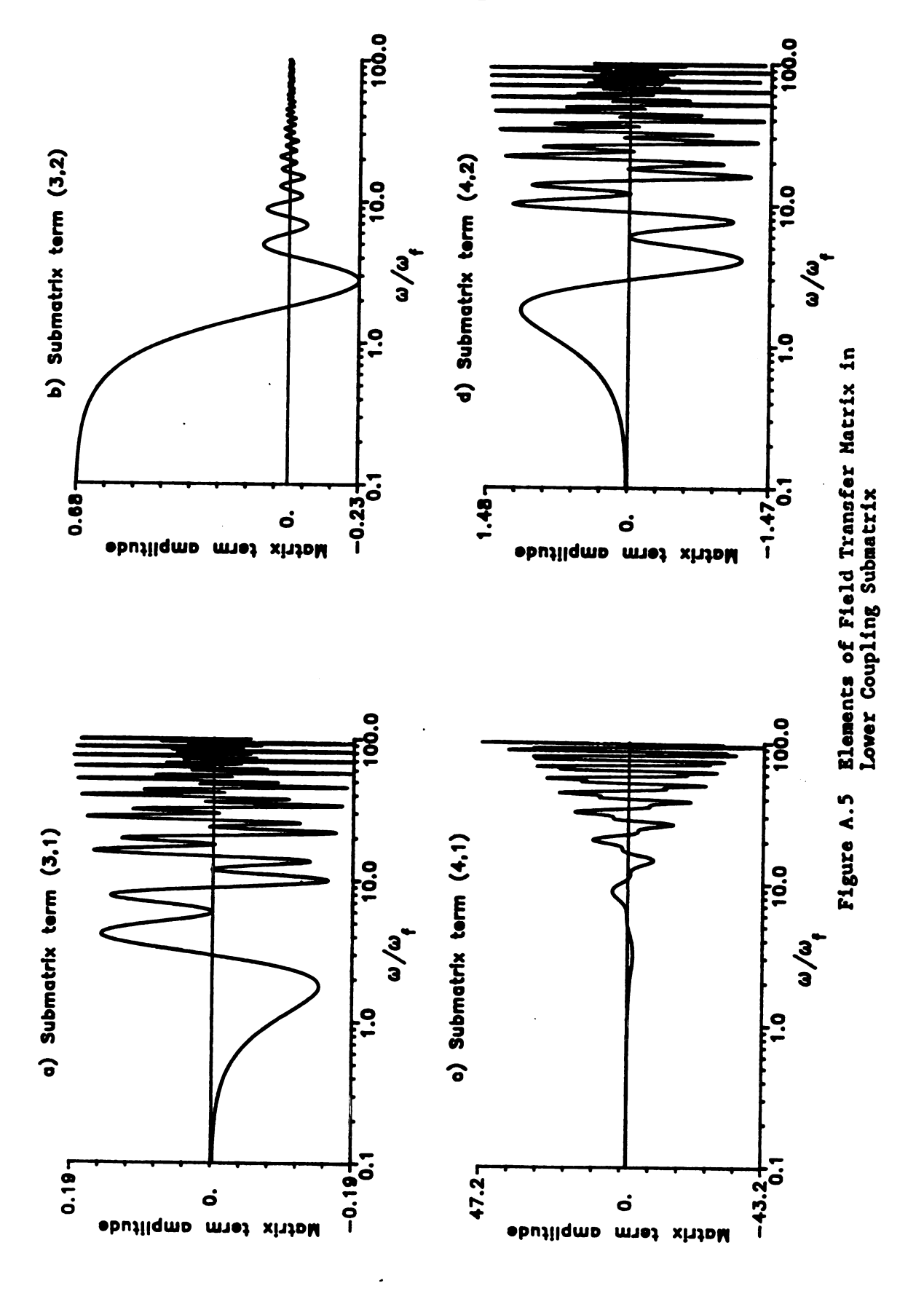
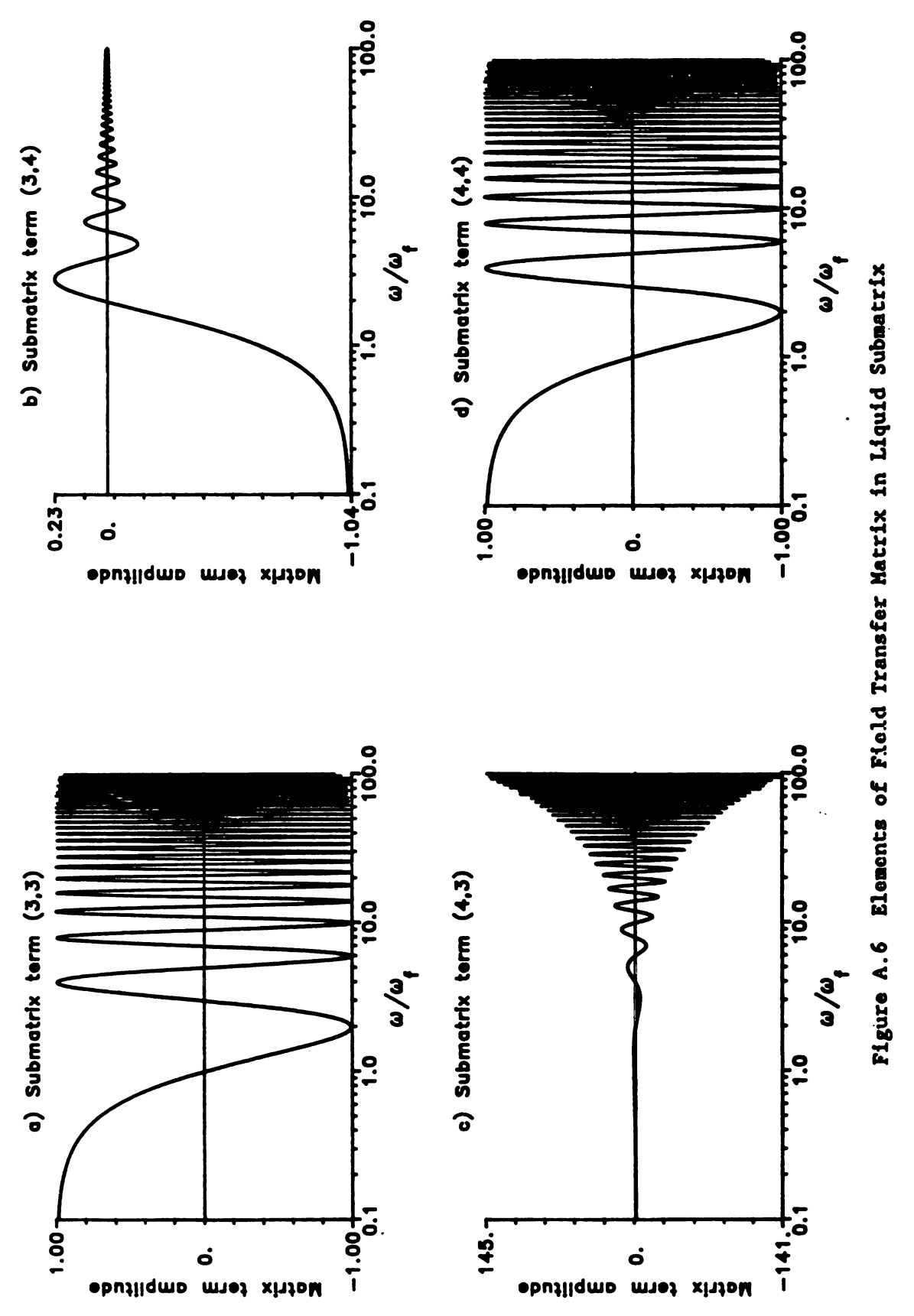


Figure A.2 Parameters for Liquid and Axial Pipe Wall Transfer Matrix









APPENDIX B

APPENDIX B

DATA ACQUISITION

B.1 Introduction

To obtain the required information on harmonic behavior, the dependent variables of liquid pressure and structural displacement must be recorded as a function of time. This was accomplished by using PCB pressure and acceleration transducers interfaced with either a Digital PDP-11/73 computer, or a Tektronix D13 dual beam storage oscilloscope.

B.2 System Components

The analog output signals of the transducers, which are directed to the computer, are converted to a digital format by an analog/digital board, with the sampling rate controlled by a programmable clock board. The software required to perform this conversion and data storage is described below in the Data Acquisition Software section. A schematic of the components of the data acquisition system is shown in Figure 5.7. Each component is described below.

B.2.1 Piezoelectric Pressure Transducers

The principle of a piezoelectric transducer is that a charge is produced across the piezoelectric crystal, which is proportional to the applied pressure. Since this type of transducer is designed to measure dynamic and short term static pressure measurements, all pressure readings taken are dynamic pressure variations about a steady state static pressure. For this study PCB Piezotronics Models 111A26 and 113A24 Dynamic Pressure transducers with built-in unity gain voltage amplifiers were used to measure the liquid pressure within the pipeline at the harmonic and fast acting valve. These units were selected because of their high resonant frequency, acceleration compensated quartz element, and the fact that the signal quality is nearly independent of cable length and motion. Table B.1 lists the published properties and the calibration properties as determined by the manufacturer. The calibration procedure was in compliance with MIL-STD-45662.

TABLE B.1
PROPERTIES OF PRESSURE TRANSDUCERS

Property	Units	Value PCB Serial No.		
		111A26	113A24	
Range (5 volts output)	psi	500.0	1000.0	
_	MPa	3.447	6.894	
Resolution (min. value)	psi	0.1	0.01	
•	Pa	689.4	69.9	
Sensitivity (output)	mV/psi	9.71	5.23	
• • •	mV/kPa	1.41	0.76	
Resonant Frequency	KHz	400.0	425.0	
A/D Error @ Gain of 1	psi	0.97	0.97	
,	kPa	6.73	6.73	
Linearity (error)	%bsl	2.0	2.0	

Connected to each pressure transducer is a PCB Battery Power Unit. The units are PCB Model 480D06 with 1,10, and 100 range signal amplifiers. The function of each battery power unit is to power the transducer electronics, amplify the signal, remove bias from the output signal and indicate normal or faulty system operation. It is a combination power supply and signal amplifier.

The transducers were mounted by tapping a brass block as per PCB specifications. The block was designed so that the end of the transducer would be flush mounted with the inside diameter of the pipeline. Since the end of the transducer is flat and the block was tapped with a circular hole, the mounting is not flush mounted. There is a small deviation due to the curvature of the hole.

B.2.2 Quartz Accelerometers

The principle of a quartz crystal accelerometer is that a charge is produced across the crystal in proportion to the applied acceleration. For this study PCB Piezotronics Model 302A Low Impedance Voltage Mode quartz accelerometers were used to monitor the desired motion. These units were selected because of their ability to measure the acceleration aspect of shock and vibration motion from 1g to 500g, over a wide frequency range. They also offer exceptionally sensitive low frequency response, can follow long duration shock events, and have built-in amplifiers. These types of accelerometers are not linear for frequencies less than 10 Hz. A calibration curve was obtained for each

accelerometer to find the conversion from volts to millimeters. These curves are shown in Figure B.1. A direct displacement measurement technique was used. The accelerometers were attached to the shaker mechanism shown in Figure 5.3 in place of the spring. The circular frequency of the motor was increased and the displacement output from the accelerometers was compared with observed readings from a displacement meter for the same frequency. The range of the displacement meter was one inch, with 1000 divisions per inch. Table B.2 lists the published and calibration properties of the transducers as determined by the manufacturer. The calibration procedure was in compliance with MIL-STD-45662.

The accelerometers were installed by clamping the base of the transducer to the test object with an elastic beryllium-copper threaded stud. To accomplish this, a mounting collar was designed and used to install the transducer at any point along the pipeline. The collar is made of a 63 mm square, 19 mm thick aluminum block. The block is tapped to accept the mounting stud, and a hole is drilled through the center of the block to match the OD of the one inch nominal copper pipe. The block is then cut through the center of the hole and bolt holes are drilled through both sections. Bolts are then used to hold the two pieces together enabling the block to act as a vise squeezing the pipe around its entire circumference.

TABLE B.2

PROPERTIES OF ACCELEROMETER TRANSDUCERS

Property	Units	302 <i>4</i> _5711	Value A Serial 5712	No. _5713
Range FS (5 volt output) Resolution Sensitivity	g mv/g mv/ft/s mv/n/s * mv/mm	500.0 0.01 10.04 0.831 0.253 322.5	500.0 0.01 10.03 0.832 0.253 322.5	500.0 0.01 10.04 0.831 0.253 322.5
Resonant Frequency Frequency Range (±5%) A/D Conversion Error Linearity Integration Error	kHz Hz g %FS	45.0 0.976 1.0 5.0	45.0 L - 5000 0.976 1.0 5.0	45.0 0.976 1.0 5.0

^{*} For frequencies below 10 Hz, the conversion factors for displacement are obtained from Figure B.1

Connected to each transducer is a PCB Dual Integrating Power Unit Model 480A10. The function of this unit is to supply constant current excitation to power ICP sensors over signal lead, eliminate DC bias voltage on output signal by capacitive decoupling, monitor bias voltage on sensor lead for normal or faulty operation by meter indication, and provide either acceleration or velocity output signals. In addition to the above features, it also provides a displacement output signal.

B.2.3 Computer Hardware and Accessories

The computer used for the data collection was a Digital Equipment Corporation DEC PDP-11/73. The installed operating system was RSX-11M-PLUS version 3.0. In addition to the standard equipment present within

a PDP-11/73 system, an analog-to-digital converter and a programmable real-time clock board were installed to facilitate data acquisition. To direct the input and output signals to their appropriate locations, a patch panel was constructed and mounted on the face of the computer cabinet.

B.2.3.1 Analog-to-Digital Converter

The AXVII-C is an LSI-II analog input/output printed circuit board. The board accepts up to sixteen single-ended inputs, or up to eight differential inputs, either unipolar or bipolar. A unipolar input can range from 0 volts to +10 volts DC. The bipolar input range is ±10 volts DC. The analog-to-digital (A/D) output resolution is 12 bit unipolar, or 11 bit bipolar plus sign, with output data notation in octal coding of binary, offset binary, or 2's complement. The A/D converter performance has a system throughput of 25K channel samples per second, with a system accuracy input voltage to digitized value of plus or minus 0.03% full scale. The board also has two separate digital-to-analog converters (DAC). Each DAC has a write-only register that provides 12-bit input data resolution, with an accuracy of plus or minus 0.02% full scale.

By setting the required jumpers on the board, the AXV11-C was configured for bipolar differential inputs with the external trigger set to the I/O connector. The I/O connector was then hardwired to the KWV11-C programmable real-time clock overflow.

B.2.3.2 Programmable Real-Time Clock

The KWV11-C is a sixteen bit resolution programmable real-time clock printed circuit board. It can be programmed to count from one to five crystal-controlled frequencies, from an external input frequency or event, or from the 50/60 Hz line frequency on the LSI-11 bus. The five internal crystal frequencies are 1 MHz, 100 kHz, 10 kHz, 1 kHz, and 100 Hz. The base frequency for the clock is 10 MHz, thus the accuracy of the time measurement is ± 0.1 microseconds.

The clock also has a counter that can be programmed to operate in either a single interval, repeated interval, external event timing, or external event timing from zero base mode. In addition to its clock functions, the KWV11-C also has two Schmitt triggers. The triggers can be set to operate at any level between \pm 12 volts DC on either a positive or negative slope of the external input signal. In response to external events, the Schmitt trigger can start the clock, start A/D conversions in an A/D input board, or generate program interrupts to the processor.

B.2.3.3 Patch Panel

To facilitate use of these data acquisition computer boards, a patch panel was installed on the front of the computer cabinet. It has BNC connectors installed which allow access to the eight differential A/D inputs, the two D/A outputs, and both Schmitt triggers. Switches and potentiometers for each Schmitt trigger were also installed to allow

external control of both the slope and triggering level. In addition, the panel also contains a three volt DC power supply with a connection to the KWV11-C board.

B.2.4 Data Acquisition Software

Digital's K-Series Peripheral Support Routines were used for data acquisition. These machine language routines perform input and output operations through the Connect to Interrupt Vector Executive directive. The routines are highly modular, that is they are designed to perform specific operations. Thus, to complete the sampling, a user program is required to call each routine as various functions are to be performed.

A Fortran computer program was developed to facilitate the data acquisition process. The program accessed the routines for computing and setting the clock rate, setting the A/D channel sampling information, creating and maintaining buffers to store the sampled data, and starting and stopping the sampling. The program was divided into two parts. The first part of the preprocessor is an interactive program. This program allows the user to select the sampling rate, number of channels to be sampled, number of samples per channel, the data acquisition device connected to each channel, and the range of frequencies to be sampled. The second part is the actual sampling routine. This program is designed so that the sampling process is started upon indication of the user. After the sampling process is finished the program requests the user to change the frequency of the motor. At this time the program

allows 30 seconds for the system to reach steady-state conditions. This process continues until all the frequencies of the frequency range have been sampled.

The experimental procedure as well as the hardware and sofware components for rapid valve closure are described by Budny [22].

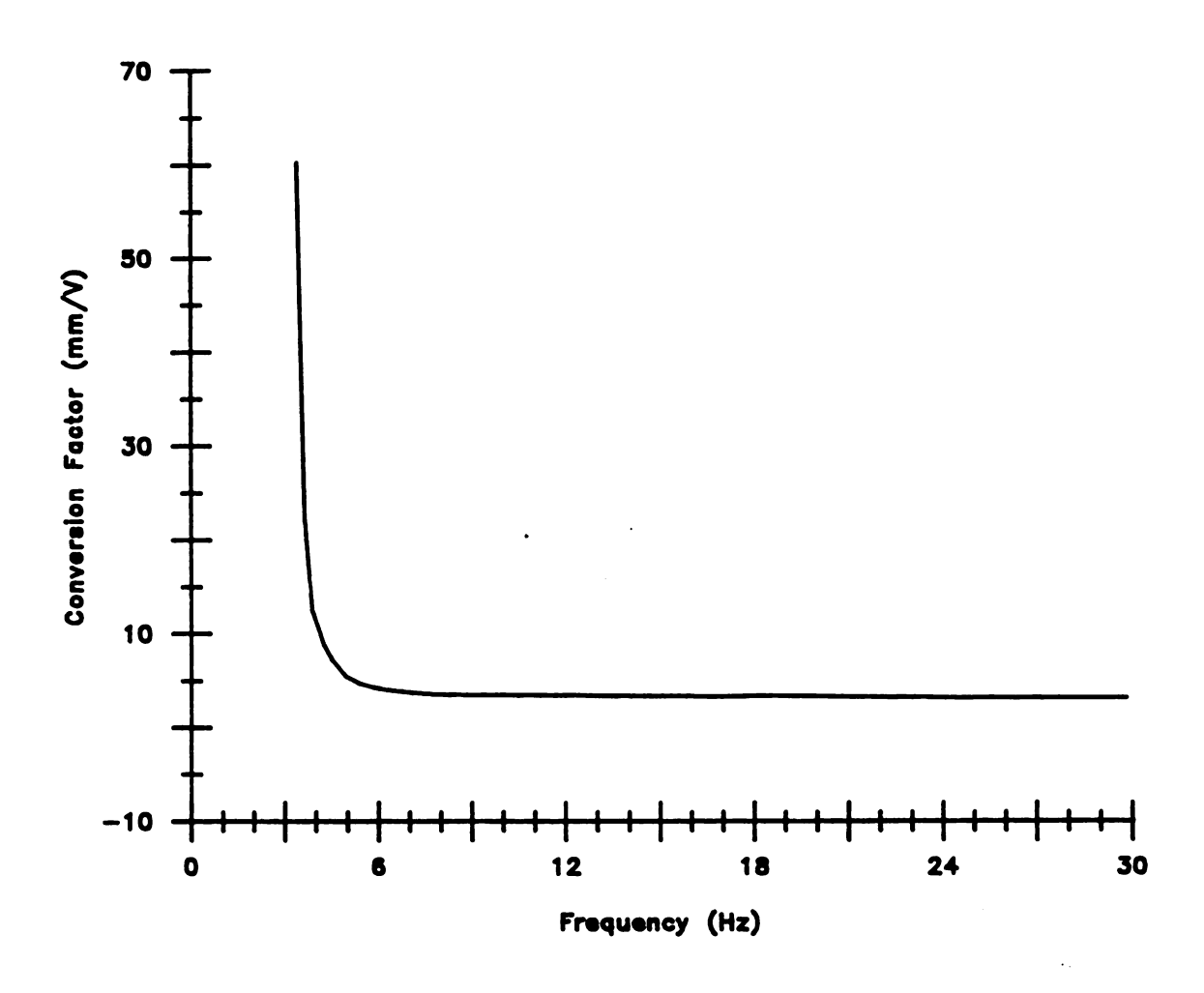


Figure B.1 Displacement Calibration Curve for PCB Accelerometers

LIST OF REFERENCES

LIST OF REFERENCES

- 1) Thorley, A. R. D., "Pressure Transients in Hydraulic Pipelines," ASME Journal of Basic Engineering, Vol. 91, Sept. 1969, pp. 453-461.
- 2) Joukowsky, N. E., translated by O. Simin as "Water Hammer," Proceedings: American Water Works Association, Vol. 24, 1904, pp. 341-424.
- 3) Lamb, H., "On the Velocity of Sound in a Tube, as Affected by the Elasticity of the Walls," <u>Memoires of the Manchester Literary and Philosophical Society</u>, Vol. 42, 1898, p. 1.
- 4) Allievi, L., "Teoria del colpo d'ariete," <u>Atti Collegio Ing. Arch.</u>, 1913 (English translation by E. E. Halmos, "The Theory of Waterhammer," <u>Transactions of American Society of Mechanical Engineers</u>, 1929).
- 5) Jaeger, C., <u>Engineering Fluid Mechanics</u>, translated from German by Wolf, P. O., Blackie & Son Ltd., London, 1956.
- 6) Wylie, E. B., Streeter, V. L., <u>Fluid Transients</u>, FEB Press, Ann Arbor, MI, 1982.
- 7) Chaudhry, M. H., <u>Applied Hydraulic Transients</u>, Van Nostrand Reinhold Company, New York, NY, 1979.
- 8) Wylie, E. B., "Fundamental Equations Of Waterhammer," <u>ASCE Journal of Hydraulic Engineering</u>, Vol. 110, No. 4, April 1984, pp. 539-542.
- 9) Shimada, M., Okushima, S., "New Numerical Model and Technique for Waterhammer," <u>ASCE Journal of Hydraulic Engineering</u>, Vol. 110, No. 6, June 1984, pp. 736-748.
- 10) Liu, W. K., Chang, H. G., "Efficient Computational Procedures for Long-Time Duration Fluid-Structure Interaction Problems," <u>ASME Journal of Pressure Vessel Technology</u>, Vol. 106, Nov. 1984, pp. 317-322.

- 11) Blevins, R. D., Formulas for Natural Frequency and Mode Shape, Van Nostrand Reinhold Company, New York, NY, 1979.
- 12) Leissa, A. W., "Vibration of Shells," NASA Report NASA-SP-288, Ohio State University, 1973.
- 13) Shigley, J. E., Mitchell, L. D., <u>Mechanical Engineering Design</u>, McGraw-Hill Book Co., New York, NY., 4th ed., 1983.
- 14) Skalak, R., "An Extension of the Theory of Water Hammer," Transaction ASME, Vol. 78, No. 1, 1956, pp. 105-116.
- 15) Lin, T. C., Morgan, G. W., "A Study of Axisymmetric Vibrations of Cylindrical Shells as Affected by Rotary Inertia and Transverse Shear," <u>Journal of Applied Mechanics</u>, June 1956, pp. 255-261.
- 16) Lin, T. C., Morgan, G. W., "Wave Propagation through Fluid Contained in a Cylindrical, Elastic Shell," <u>Journal of the Acoustical Society of America</u>, Vol. 28, No. 6, Nov. 1956, pp. 1165-1176.
- 17) Walker, J. S., Phillips, J. W., "Pulse Propagation in Fluid Filled Tubes," <u>Journal of Applied Mechanics</u>, ASME, March 1977, pp. 31-35.
- 18) Wilkinson, D. H., Curtis, E. M., "Water Hammer in a Thin-walled Pipe," <u>Proceedings of the Third International Conference on Pressure Surges</u>, Vol. 1, BHRA Fluid Engineering, Canterbury, England, March 1980, pp. 221-240.
- 19) Otwell, R. S., "The Effect of Elbow Restraint on Pressure Transients," Ph.D. Dissertation, Michigan State University, 1984.
- 20) Wiggert, D. C., Otwell, R. S., Hatfield, F. J., "The Effect of Elbow Restraint on Pressure Transients," <u>ASME Journal of Fluids Engineering</u>, Vol. 107, No. 3, Sept. 1985, pp. 402-406.
- 21) Stuckenbruck, S., Wiggert, D. C., and Otwell, R. S., "The Influence of Pipe Motion on Acoustic Wave Propagation," <u>ASME Journal of Fluids Engineering</u>, Vol. 107, Dec. 1985, pp. 518-522.
- 22) Budny, D. D., "The Influence of Structural Damping on the Internal Fluid Pressure During a Fluid Transient Pipe Flow," Ph.D. Dissertation, Michigan State University, 1988.

- 23) Blade, R. J., Lewis, W., and Goodykoontz, J. H., "Study of a Sinusoidally Perturbed Flow in a Line Including a 90 Degree Elbow with Flexible Supports," NASA Technical Note D-1216, 1962.
- 24) Davidson, L. C., Smith, J. E., "Liquid-Structure Coupling in Curved Pipes I," Shock and Vibration Bulletin, No. 40, Pt. 4, Dec. 1969, pp. 197-207.
- 25) Davidson, L. C., Samsury, D. R., "Liquid-Structure Coupling in Curved Pipes II," Shock and Vibration Bulletin, No. 42, Pt. 1, Jan. 1971, pp. 123-135.
- 26) Wiggert, D. C., Hatfield, F. J., Stuckenbruck, S., "Analysis of Liquid and Structural Transients in Piping by the Method of Characteristics," ASME, FED-Vol. 30, 1985, pp. 97-102.
- 27) Wiggert, D. C., Hatfield, F. J., Lesmez, M. W., "Coupled Transient Flow and Structural Motion in Liquid-Filled Piping Systems," <u>Proceedings of the Fifth International Conference on Pressure Surges</u>, BHRA Fluid Engineering, Hannover, F.R. Germany, Sept., pp. 1-9.
- 28) Joung, I., Shin, Y. S., "A New Model on Transient Wave Propagation in Fluid-Filled Tubes," <u>ASME Proceedings of the Pressure Vessels and Piping Conference</u>, PVP-Vol. 98-7, 1985, pp. 275-281.
- 29) Wood, D. J., "A Study of the Response of Coupled Liquid Flow-Structure Systems Subjected to Periodic Disturbances," <u>ASME Journal of Basic Engineering</u>, Vol. 90, Dec. 1968, pp.532-540.
- 30) Ellis, J., "A Study of Pipe-Liquid Interaction Following Pump Trip and Check-Valve Closure in a Pumping Station," <u>Proceedings of the Third International Conference on Pressure Surges</u>, Vol. 1, BHRA Fluid Engineering, Canterbury, England, March 1980, pp. 203-220.
- 31) Otwell, R. S., "The Effect of Elbow Translations on Pressure Transient Analysis of Piping Systems," <u>ASME Fluid Transients and Fluid-Structure Interaction</u>, PVP-Vol. 64, 1982, pp. 127-136.
- 32) Schwirian, R. E., Karabin, M. E., "Use of Spar Elements to Simulate Fluid-Solid Interaction in the Finite Element Analysis of Piping System Dynamics," <u>Proceedings of the Symposium on Fluid Transients and Structural Interactions in Piping Systems</u>, ASME, June 1981, pp. 1-11.

- 33) Wiggert, D. C., and Hatfield, F. J., "Time Domain Analysis of Fluid-Structure Interaction in Multi-Degree-of-Freedom Piping System," Proceedings of the Fourth International Conference on Pressure Surges, BHRA Fluid Engineering, Bath, England, Sept. 1983.
- 34) Hatfield, F. J., Wiggert, D. C., and Otwell, R. S., "Fluid Structure Interaction in Piping by Component Synthesis," <u>ASME Journal of Fluids Engineering</u>, Vol. 104, No. 4, Sept. 1982, pp. 318-325.
- 35) Hurty, W. C., "Dynamic Analysis of Structural Systems Using Component Modes," <u>AIAA Journal</u>, Vol. 3, No. 4, April 1965, pp. 678-685.
- 36) Wolf, J. A., Jr., "Modal Synthesis for Combined Structural-Acoustic Systems," <u>AIAA Journal</u>, Vol. 15, 1977, pp. 743-745.
- 37) Hatfield, F. J., Davidson, L. C., and Wiggert, D. C., "Acoustic Analysis of Liquid-Filled Piping by Component Synthesis: Experimental Validation and Examination of Assumptions," <u>ASME Fluid Transients and Fluid-Structure Interaction</u>, Vol. PVP 64, 1982, pp. 106-115.
- 38) Quezon, A. J., and Everstine, G. C., <u>Stress Indices and Flexibility Factors for 90-Degree Piping Elbows with Straight Pipe Extensions</u>, David W. Taylor Naval Ship Research and Development Center, Vol. CMLD-82/05, Feb. 1982.
- 39) Wiggert, D. C., "Coupled Transient Flow and Structural Motion in Liquid-Filled Piping Systems: A Survey," <u>ASME Proceedings of the Pressure Vessels and Piping Conference</u>, Vol. 86-PVP-4, July 1986.
- 40) Rothe, P. H., Wiggert, D. C., "Fluid-Structure Considerations in Power Plant Piping," <u>ASME Proceedings of the Pressure Vessels and Piping Conference</u>, 1987.
- 41) Jaeger, C., "The Theory of Resonance in Hydropower Systems. Discussion of Incidents and Accidents Ocurring in Pressure Systems," ASME Journal of Basic Engineering, Vol. 85, Dec. 1963, pp. 631-640.
- 42) Hatfield, F. J., Wiggert, D. C., "Response of Pipelines to Seismic Motion in the Axial Direction," <u>ASME Proceedings of the Pressure Vessels and Piping Conference</u>, June, 1987.
- 43) Hatfield, F. J., Wiggert, D. C., "Seismic Time-Response of Liquid-Filled Piping," ASME Proceedings of the Pressure Vessels and Piping Conference, June, 1988.

- 44) Ogawa, N., "A Vibration Test of Earthquake Induced Hydraulic Transients of Liquid-Filled Pipelines," <u>ASME Proceedings of the Pressure Vessels and Piping Conference</u>, 1984, pp. 189-195.
- 45) Wylie, E. B., Streeter, V. L., "Resonance in Bersimis No. 2 Piping System," <u>ASME Journal of Basic Engineering</u>, Vol. 87, No. 4, Dec. 1965, pp. 925-931.
- 46) Fashbaugh, R. H., Streeter, V. L., "Resonance in Liquid Rocket Engine Systems," <u>ASME Journal of Basic Engineering</u>, Vol. 87, No. 4, Dec. 1965, pp. 1011-1017.
- 47) Zielke, W., Wylie, E. B., Keller, R. B., "Forced and Self-Excited Oscillations in Propellant Lines," <u>ASME Journal of Basic Engineering</u>, Vol. 91, Ser. D., No. 4, Dec. 1969, pp. 671-677.
- 48) Wylie, E. B., "Resonance in Pressurized Piping Systems," ASME Journal of Basic Engineering, Vol. 87, No. 4, Dec. 1965, pp. 960-966.
- 49) Zielke, W., Hack, H. P., "Resonance Frequencies and Associated Mode Shapes of Pressurized Piping Systems," <u>BHRA International Conference on Pressure Surges</u>, 1972.
- 50) Pestel, E. C., Leckie, F. A., <u>Matrix Methods in Elastomechanics</u>, McGraw-Hill Book Co., New York, 1963.
- 51) Molloy, C. T., "Use of Four-Pole Parameters in Vibration Calculations," <u>Journal of the Acoustical Society of America</u>, Vol. 29, No. 7, July 1957, pp. 842-853.
- 52) Clough, R. W., Penzien, J., <u>Dynamics of Structures</u>, McGraw-Hill Book Co., New York, 1975.
- 53) Thomson, W. T., <u>Theory of Vibration with Applications</u>, 2nd ed., Prentice Hall, Englewood Cliffs, NJ, 1981.
- 54) Meirovitch, L., <u>Analytical Methods in Vibrations</u>, MacMillan, London, England, 1967.
- 55) Reed, M.B., <u>Electrical Network Synthesis</u>, Prentice Hall, New York, 1955.

- 56) Dawson, B., Davies, M., "An Improved Transfer Matrix Procedure," International Journal for Numerical Methods in Engineering, Vol. 8, 1974, pp. 111-117.
- 57) Chaudhry, M. H., "Resonance in Pressurized Piping Systems," <u>ASCE Journal of the Hydraulic Division</u>, Vol. 96, No. HY9, Sept. 1970, pp. 1819-1837.
- 58) Chaudhry, M. H., "Resonance in Pipes Having Variable Characteristics," <u>ASCE Journal of the Hydraulic Division</u>, Vol. 98, No. HY2, Feb. 1972, pp. 325-332.
- 59) To, C. W. S., "The Acoustic Simulation and Analysis of Complicated Reciprocating Compressor Piping Systems, I: Analysis Technique and Parameter Matrices of Acoustic Elements," <u>Journal of Sound and Vibration</u>, Vol. 96, No. 2, 1984, pp. 175-194.
- 60) To, C. W. S., "The Acoustic Simulation and Analysis of Complicated Reciprocating Compressor Piping Systems, II: Program Structure and Applications," <u>Journal of Sound and Vibration</u>, Vol. 96, No. 2, 1984, pp. 195-205.
- 61) Keskinen, R., "Vibration of Three-Dimensional Piping Subject to Pump Pulsation," <u>International Conference on Structural Mechanics and Reactor Technology</u>, August 13-17, 1979, Transactions Part F 4.3.
- 62) To, C. W. S., Kaladi, V., "Vibration of Piping Systems Containing a Moving Medium," <u>ASME Journal of Pressure Vessel Technology</u>, Vol. 107, Nov. 1985, pp. 344-349.
- 63) Dupuis, C., Rousselet, J., "Application of the Transfer Matrix Method to Non-Conservative Systems Involving Fluid Flow in Curved Pipes," <u>Journal of Sound and Vibration</u>, Vol. 98, No. 3, 1985, pp. 415-429.
- 64) Wilkinson, D. H., "Acoustic and Mechanical Vibrations in Liquid-Filled Pipework Systems," <u>Proceedings of the Vibration in Nuclear Plant Conference</u>, British Nuclear Engineering Society, May 1978.
- 65) Wiggert, D. C., Lesmez, M. W., Hatfield, F. J., "Modal Analysis of Vibrations in Liquid-Filled Piping Systems," <u>ASME Proceedings Fluid Transients in Fluid-Structure Interaction</u>, FED-Vol. 56, Dec. 1987, pp. 107-113.

- 66) Lesmez, M. W., Wiggert, D. C., Hatfield, F. J., "Experimental Modal Analysis of Vibrations in Liquid-Filled Piping Systems," <u>ASME Proceedings of the Pressure Vessels and Piping and Nuclear Engineering Divisions</u>, Vol. 4, Dec. 1988, pp. 25-36.
- 67) Goodson, R. E., Leonard, R. G., "A Survey of Modeling Techniques for Fluid Line Transients," <u>ASME Journal of Basic Engineering</u>, June 1972, pp. 474-482.
- 68) Timoshenko, S., Young, D. H., <u>Vibration Problems in Engineering</u>, 3rd ed., D. Van Nostrand Company, NY, 1955.
- 69) Grant, D. A., "The Effect of Rotary Inertia and Shear Deformation on the Frequency and Normal Mode Equations of Uniform Beams Carrying a Concentrated Mass," <u>Journal of Sound and Vibration</u>, Vol. 57, No. 3, 1978, pp. 357-365.
- 70) Rayleigh, L., The Theory of Sound, Dover Publications, 2nd ed., New York, 1945, Art. 339.
- 71) Timoshenko, S. P., "On the Correction for Shear of the Differential Equation for Transverse Vibration of Prismatic Bars," <u>Philosophical Magazine</u>, Ser. 6, Vol. 41, 1921, pp. 744-746.
- 72) Timoshenko, S. P., "On the Transverse Vibration of Bars of Uniform Cross Sections," <u>Philosophical Magazine</u>, Ser. 6, Vol. 43, 1922, pp. 125-131.
- 73) Mindlin, R. D., Deresiewicz, H., "Timoshenko's Shear Coefficient for Flexural Vibrations of Beams," Technical Report No. 10, ONR Project NR064-388, Department of Civil Engineering, Columbia University, New York, 1953.
- 74) Cowper, G. R., "The Shear Coefficient in Timoshenko's Beam Theory," ASME Journal of Applied Mechanics, June 1966, pp. 335-340.
- 75) Vardy, A. E., Fan, D., "Water Hammer in a Closed Tube," <u>Proceedings of the Fifth International Conference on Pressure Surges</u>, BHRA Fluid Engineering, Hannover, F.R. Germany, Sept. 1986, pp. 123-137.
- 76) Wylie, C. R., Barrett, L. C., <u>Advanced Engineering Mathematics</u>, 5th ed., McGraw-Hill Book Co., New York, 1982.

- 77) Abbot, H. F., Gibson, W. L., McCaig, I. W., "Measurements of Auto-Oscillations in a Hydroelectric Supply Tunnel and Penstock Systems," Transactions of ASME, Vol. 85, Dec. 1963, pp. 625-630.
- 78) Weast, R. C., <u>CRC Handbook of Chemistry and Physics</u>, 60th ed., CRC Press, Boca Raton, Florida, 1980, pp. D187, E47, F5, F51.
- 79) Streeter, V. L., Wylie, E. B., <u>Fluid Mechanics</u>, 7th ed., McGraw-Hill Book Co., New York, 1979, pp. 534-535.
- 80) Westaway, C. R., Loomis, A. W., <u>Cameron Hydraulic Data</u>, Ingersoll-Rand, Woodcliff Lake, N.J., 1977, pp. 3-36, 4-3.
- 81) Wilkins, R. A., Bunn, E. S., <u>Copper and Copper Base Alloys</u>, McGraw-Hill Book Co., New York, 1943, pp. 1-26.
- 82) Thomson Industries, Linear Motion Technology Guide, 1986.
- 83) Chang, C. H., "Vibrations of Frames With Inclined Members," <u>Journal of Sound and Vibration</u>, Vol. 56, No. 2, Jan., 1978, pp. 201-214.
- 84) Shigley, J. E., Uicker, J. J. Jr., <u>Theory of Machines and Mechanisms</u>, McGraw-Hill Book Co., New York, 1980, pp. 451-470.
- 85) Williams, D. J., "Waterhammer in Non-Rigid Pipes: Precursor Waves and Mechanical Damping," <u>Journal of Mechanical Engineering Science</u>. <u>Institute of Mechanical Engineers</u>, Vol. 19, No. 6, 1977, pp. 237-242.
- 86) Everstine, G. C., Marcus, M. S., Quezon A. J., <u>Finite Element Prediction Methods for Dynamic Response of Fluid-Filled Elastic 3-D Piping Systems</u>, David W. Taylor Naval Ship Research and Development Center, DTNSRDC-82/100, Jan. 1983.
- 87) Radabaugh, E. C., George, H. H., "Effect of Internal Pressure on Flexibility and Stress-Intensification Factors of Curved Pipe or Welding Elbows," <u>Transactions of ASME</u>, Vol. 79, 1957, pp. 939-948.
- 88) von Karman, T., "Uber die Formanderung dunnwandiger Rohre, insbesondere federnder Ausgleichrohre," Z. Vereines Dtsch. Ing., Vol. 55, 1911, pp. 1889-1895.

- 89) Leonard, R. W., Budiansky, B., "Report 1173 On Traveling Waves in Beams," National Advisory Committee for Aeronautics, 1954.
- 90) Goldberg, D.E., Wylie, E.B., "Characteristics Method Using Time-Line Interpolations," <u>ASCE Journal of Hydraulic Engineering</u>, May 1983, pp. 670-683.
- 91) Boyce, W. E., DiPrima, R. C., <u>Introduction to Differential Equations</u>, John Wiley & Sons., New York, 1970.
- 92) Bhattacharyya G. K., Johnson, G. K., <u>Statistical Concepts and Methods</u>, John Wiley & Sons, New York, NY, 1977.
- 93) Malmstadt, H. V., Enke, C. G., Crounch, S. R., <u>Electronics and Instrumentation for Scientists</u>, The Benjamin/Cummings Publishing Company, Inc., Menlo Park, CA, 1981.

		•
•		
		1

AICHIGAN STATE UNIV. LIBRARIES
31293005740042